Hybrid Control for Performance Improvement of Linear Systems

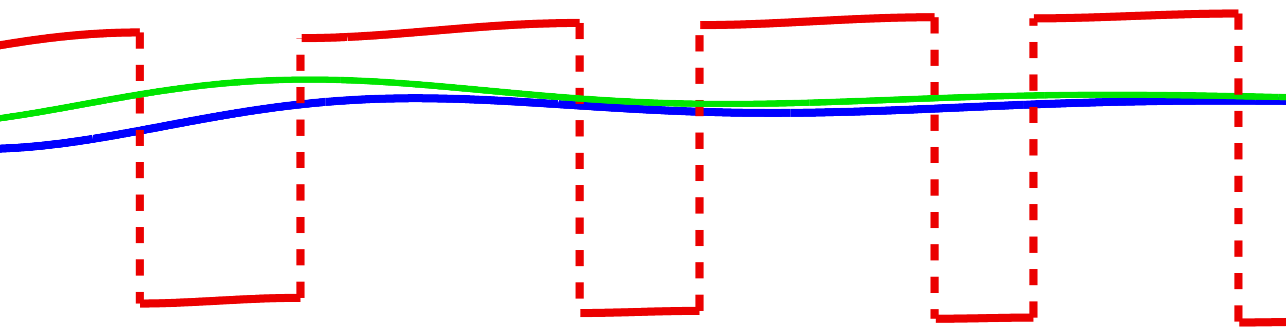

Bas van Loon

Hybrid control for performance improvement of linear systems

Bas van Loon

This research is supported by the Dutch Technology Foundation STW, which is part of the Netherlands Organisation for Scientific Research (NWO) and partly funded by the Ministry of Economic Affairs (project number 10953).

A catalogue record is available from the Eindhoven University of Technology Library.
ISBN: 978-90-386-4002-0

Typeset by the author using LaTeX

Cover design: Tom van der Sande and Bas van Loon
Reproduction: CPI - Koninklijke Wöhrman, Zutphen, the Netherlands

Hybrid control for performance improvement of linear systems

PROEFSCHRIFT

ter verkrijging van de graad van doctor aan de
Technische Universiteit Eindhoven, op gezag van de
rector magnificus, prof.dr.ir. F.P.T. Baaijens, voor een
commissie aangewezen door het College voor
Promoties, in het openbaar te verdedigen
op dinsdag 26 januari 2016 om 16.00 uur

door

Sebastiaan Johannes Leonardus Maria van Loon

geboren te Tilburg

Dit proefschrift is goedgekeurd door de promotoren en de samenstelling van de promotiecommissie is als volgt:

voorzitter:	prof.dr. L.P.H. de Goey
1^{e} promotor:	prof.dr.ir. W.P.M.H. Heemels
2^{e} promotor:	prof.dr.ir. N. van de Wouw
co-promotor:	dr.ir. M.F. Heertjes
leden:	prof.dr. S. Weiland
	prof.dr. L. Zaccarian (LAAS-CNRS & University of Trento)
	prof.dr. A.J. van der Schaft (University of Groningen)

Het onderzoek dat in dit proefschrift wordt beschreven is uitgevoerd in overeenstemming met de TU/e Gedragscode Wetenschapsbeoefening.

Contents

1 Introduction **1**

1.1 Linear control of linear motion systems 1

1.2 Hybrid control for linear (motion) systems 5

1.3 Objectives and contributions 7

1.3.1 Contributions of the thesis 8

1.3.2 Contributions of the individual chapters 10

1.4 Outline of this thesis 12

2 Scheduled controller design for systems with two switching sensor configurations **13**

2.1 Introduction 13

2.2 Problem formulation and system description 15

2.2.1 Introduction to the problem 16

2.2.2 Switched system formulation 19

2.2.3 Industrial state-of-the-art control design 20

2.3 Scheduled controller design 21

2.4 Stability analysis 24

2.5 Experimental results on a wafer stage 25

2.5.1 Design of the proposed scheduled controller 25

2.5.2 Experimental results 27

2.6 Conclusions 29

3 Bandwidth-on-demand motion control with a nano-positioning application **31**

3.1 Introduction 31

3.1.1 Nomenclature 34

3.2 Reference-dependent variable-gain control: a ‘bandwidth-on-demand’ approach 35

3.2.1 Motivation for a ‘bandwidth-on-demand’ controller 35

3.2.2 Description of the control configuration . . . 37
3.3 Stability conditions and design guidelines . . . 38
3.3.1 Stability and convergence . . . 39
3.3.2 Design and tuning guidelines . . . 41
3.4 Case-study on an industrial nano-positioning motion system . . . 46
3.4.1 Nano-positioning motion stage . . . 47
3.4.2 Design of a reference-dependent variable-gain controller . . . 47
3.4.3 Experimental results . . . 53
3.5 Conclusions . . . 57

4 Frequency-domain tools for stability analysis of reset control systems 59
4.1 Introduction . . . 59
4.1.1 Nomenclature . . . 61
4.2 System description and problem formulation . . . 61
4.2.1 Hybrid closed-loop model . . . 61
4.2.2 Problem formulation . . . 64
4.3 Frequency-domain tools for stability analysis . . . 64
4.4 Case-study on an industrial piezo-actuated motion system . . . 66
4.4.1 Problem setting . . . 66
4.4.2 Controller design . . . 67
4.4.3 Experimental verification . . . 69
4.5 Conclusions . . . 71

5 Split-path nonlinear integral control for transient performance improvement 73
5.1 Introduction . . . 73
5.1.1 Nomenclature . . . 75
5.2 Split-path nonlinear integrator . . . 76
5.2.1 Introduction and motivation of the SPANI filter . . . 76
5.2.2 Description of the control system . . . 77
5.3 Hybrid system modeling . . . 79
5.4 Stability analysis . . . 81
5.5 Case study on a pick-and-place machine . . . 83
5.5.1 Simulation model . . . 83
5.5.2 Transient performance comparison with $\tau_D = 0$ . . . 85
5.5.3 Transient performance comparison with $\tau_D > 0$ . . . 87
5.5.4 Final note . . . 89
5.6 Conclusions . . . 90

6 Improved $\mathcal{L}_2$-gain analysis for a class of hybrid systems 91
6.1 Introduction . . . 91
6.1.1 Nomenclature . . . 93
6.2 Hybrid model class and problem formulation . . . 93
6.3 Unified modeling framework . . . 94
6.3.1 Periodic event-triggered control systems . . . 95
6.3.2 Reset control systems . . . 96
6.3.3 Networked control systems . . . 98
6.4 Stability and $\mathcal{L}_2$-gain analysis of the hybrid system . . . 100
6.4.1 Riccati-based analysis . . . 100
6.4.2 Main result on novel $\mathcal{L}_2$-gain conditions . . . 102
6.5 Reset control example . . . 105
6.6 Conclusions . . . 106

7 Conclusions and recommendations 107
7.1 Conclusions . . . 107
7.2 Recommendations . . . 110

A Proofs and technical results 113
A.1 Appendices of Chapter 2 . . . 114
A.1.1 Proof of Proposition 2.1 . . . 114
A.1.2 Proof of Theorem 2.2 . . . 115
A.2 Appendix of Chapter 3 . . . 119
A.2.1 Proof of Theorem 3.1 . . . 119
A.3 Appendix of Chapter 4 . . . 120
A.3.1 Hybrid systems notation . . . 120
A.3.2 Proof of Theorem 4.1 . . . 120
A.4 Appendices of Chapter 5 . . . 125
A.4.1 Hybrid systems notation . . . 125
A.4.2 Proof of statement Remark 5.1 . . . 125
A.4.3 Proof of Theorem 5.1 . . . 126
A.5 Appendix of Chapter 6 . . . 129
A.5.1 Proof of Theorem 6.2 . . . 129

Summary 139

Societal summary 143

Samenvatting 145

Dankwoord 149

List of publications 153

Curriculum vitae 155

Chapter 1

Introduction

Abstract – In this introductory chapter, the research of this thesis is motivated. In particular, a different perspective on high performance control of linear (motion) systems is proposed by exploiting *hybrid* controllers instead of linear controllers. To motivate this paradigm shift towards hybrid control, linear control of linear (motion) systems together with its advantages and disadvantages will be (briefly) discussed in Section 1.1. In Section 1.2, the use of hybrid control for linear (motion) systems will be discussed along with the potential advantages that hybrid control can offer compared to linear control. The objectives and contributions of this thesis are presented in Section 1.3, followed by the outline of this thesis in Section 1.4.

1.1 Linear control of linear motion systems

High-tech mechatronic systems, such as wafer scanners, printers, pick-and-place machines, electron microscopes, etc., have to perform their (motion) tasks with increasingly high performance demands on precision, throughput, etc., thereby requiring the utmost of the current mechatronic designs. In order to meet these stringent performance requirements, feedback/feedforward controllers are essential in any of these high-tech applications. To allow for a good interaction with feedback/feedforward controllers, the (mechanical) design of these systems is highly optimized such that their dynamic behavior can be regarded as approximately linear. Hence, in the scope of such applications *linear* (motion) systems form an important class of (motion) systems, which motivates the focus on this type of systems in this thesis.

The vast majority of linear (motion) systems are being controlled by linear proportional-integral-derivative (PID) type controllers, which are based on the present (P), past (I) and future (D) control error, see, e.g., Åström and Hägglund (2001), and can easily be designed using data-based frequency-domain loop-shaping techniques, see Franklin et al. (2006); Skogestad and Postlethwaite (2005); Steinbuch and Norg (1998). In fact, in industry there is a strong demand for such data-based techniques for controller design and analysis, i.e., employing measured signals instead of parametric models, see, e.g., Steinbuch et al. (2005). It is therefore that loop-shaping techniques are widely used in industry as they allow the control engineer to design linear controllers for both stability and performance using the (measured) frequency response of the open-loop transfer function (by means of a Nyquist diagram), or via closed-loop frequency response functions such as the sensitivity function $\mathcal{S}$ and the complementary sensitivity function $\mathcal{T}$. Although linear controllers can be easily designed using loop-shaping techniques and the linear plant models can be rather easily obtained from experiments, the resulting linear (PID-like) controllers have the drawback that they suffer from inherent fundamental limitations leading to inevitable control design trade-offs, see Freudenberg et al. (2000); Seron et al. (1997). For instance, it is well-known that $|\mathcal{S}|$ and $|\mathcal{T}|$ cannot both be small at the same frequency, which leads to trade-offs between desirable control properties such as disturbance attenuation ($\mathcal{S}$ small) and noise reduction ($\mathcal{T}$ small) at each frequency. This is closely related to one of the most well-known fundamental limitations in classical linear control theory, namely the 'waterbed-effect'. The waterbed-effect states that increasing the bandwidth of an linear time-invariant (LTI) control system will improve the low-frequency (frequencies below the bandwidth) tracking and disturbance attenuation properties, but it will also increase the sensitivity to high-frequency (frequencies above the bandwidth) disturbances and measurement noise. In linear systems, the waterbed-effect is inevitable and holds irrespective of which method is used to design the LTI controller, be it via classical loop-shaping techniques or using a systematic LTI controller synthesis like an $\mathcal{H}_\infty$-design, see, e.g., Zhou et al. (1996).

A second fundamental limitation is imposed by Bode's gain-phase relationship, see, e.g., Freudenberg et al. (2000); Seron et al. (1997), which states that for an LTI stable minimum phase transfer function, the phase of its frequency response function (FRF) is uniquely determined by the magnitude of the frequency response and vice versa. As a result, the gain and phase properties of a closed-loop control system cannot be designed independently from each other, which often results in inevitable design conflicts based on the desired performance specifications set by the control engineer. For example, it is impossible to add integral action to a feedback control system, typically included to achieve zero steady-state errors, without introducing the negative effect of phase lag as well. Another fundamental limitation, which applies to the majority of motion systems, is given by the fact that for a stable closed-loop system, the error step response necessarily overshoots if the open-loop transfer function of the linear plant with LTI controller contains a double integrator, see, e.g., (Seron et al., 1997, Theorem 1.3.2).

Due to the ever increasing performance demands on speed and accuracy of

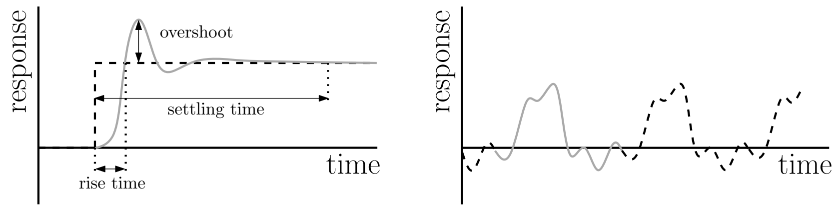

(a) Transient performance (b) Steady-state performance

Fig. 1.1. Schematic representation of two different performance viewpoints: (a) transient performance and (b) steady-state performance.

high-tech mechatronic systems, the fundamental limitations in LTI control, associated with the inevitable design trade-offs mentioned above, are becoming serious barriers for the design of controllers meeting future performance specifications. Therefore, this thesis proposes a paradigm shift towards a larger class of controllers, namely hybrid/nonlinear controllers, in order to achieve performance goals that are not achievable by LTI control. In Section 1.2, this controller class will be introduced.

Let us first briefly discuss two different viewpoints on performance that are taken in this thesis: Steady-state performance and transient performance. The latter is often expressed in terms of performance measures such as overshoot, rise-time and settling-time, and quantified in terms of the time-domain response to step-inputs (or step-disturbances) acting on the system, see Fig. 1.1(a). Steady-state performance is quantified based on the steady-state response of the system due to external perturbations acting on the system, after transient effects have vanished, see Fig. 1.1(b). In the linear context, steady-state performance can easily be assessed analytically through frequency response functions, such as, for example, the sensitivity and complementary sensitivity functions. However, this result relies on the superposition principle and the property that a linear stable system exhibits, for each bounded disturbance, a unique bounded globally asymptotically stable solution, to which all solutions converge, irrespective of the initial condition. Unfortunately, such favorable properties do not extend to the hybrid/nonlinear domain in general. In fact, for arbitrary disturbances nonlinear systems generally exhibit multiple steady-state solutions, which hampers an accurate and unique performance assessment. As a result, one often resorts to use performance measures in terms of bounds on norms of the state/output evolution, such as the ones based on the ISS-gain, see Sontag and Wang (1995) and the $\mathcal{L}_2$-gain, see van der Schaft (1999). In this respect, note that both these performance measures apply to linear systems as well (in the linear context the $\mathcal{L}_2$-gain is equal to the so-called $\mathcal{H}_\infty$-norm).

In optimal control for linear (motion) systems, one is interested in finding a controller that results in minimizing a particular norm, e.g., $\mathcal{H}_2$-, $\mathcal{H}_\infty$- and $\mathcal{L}_1$

are commonly used, of a transfer function from a certain input signal to a certain output signal. In Stoorvogel (1995), the $\mathcal{L}_1$ optimal control problem is considered for linear systems in which the author shows that a nonlinear controller can outperform a linear controller when minimizing the $\mathcal{L}_1$-norm. However, for $\mathcal{H}_\infty$-based techniques (targeting the worst-case $\mathcal{L}_2$-gain from inputs to outputs) for LTI systems, it is known that there exists no nonlinear (possibly time-varying) controller which yields a lower $\mathcal{L}_2$-gain than the optimal linear controller, see Khargonekar and Poolla (1986). Moreover, an $\mathcal{H}_\infty$-design guarantees that the $\mathcal{L}_2$-gain of a system is smaller than a certain value for whole classes of disturbance and reference signals, which may be a too conservative view on performance for the particular disturbance and reference signals acting on the system under study. In addition, disturbance characteristics or performance specifications may be non-stationary, e.g., during different phases of a motion task or different modes of operation of a positioning system, undermining the optimality of a linear control solution. Hence, it is therefore highly important to formulate appropriate (and specific) performance measures that can discriminate between linear and hybrid controllers based on the practical control design problem at hand.

The following example considers the working principle of an industrial pick-and-place machine in order to motivate that fundamental limitations in LTI control may lead to several controller design trade-offs.

Example 1.1. *Pick-and-place machines are used to place electrical components, such as resistors, capacitors, integrated circuits etc., with a high speed and high precision on a printed circuit board (PCB). These PCBs are, in turn, used in a large variety of applications, such as, high-end consumer electronics, computers, medical equipment, etc. After the pick-and-place machine has placed the PCB within the working area of the placement head, the working principle of the placement head can be separated into three main steps. In the first step the placement head picks up an electrical component using, for instance, a vacuum pipette. In the second step, the placement head is navigated to a pre-described position on the PCB, where it should place the component. Finally, in the third step, the component is placed on the PCB as soon as all positioning tolerances are met. Based on the working principle, the following design tradeoffs for control can be formulated.*

- ***Steady-state performance versus (fast) convergence to an error bound.*** *In order to achieve an optimal machine throughput, it is important to start the third step as soon as possible. Namely, the actual placement of the electrical component on the PCB in the third step can only be finalized when the closed-loop error, related to transients induced in step two, has converged within a pre-described error bound. Due to the presence of external disturbances, integral action in the controller is necessary in order to achieve zero steady-state errors. However, this comes inevitably at the* *cost of a decrease in transient performance (in terms of overshoot to step inputs, and, hence, a slower convergence to the specified error bound).*

- ***Different modes of operation.*** *The modes of operation can roughly be divided into two categories: A standstill mode (step one and three) requiring a high accuracy, and a fast-motion mode (step two) requiring a high velocity (throughput). During standstill, a low bandwidth controller is preferable in order not to amplify high-frequency disturbances; however, during fast movements, a high-bandwidth controller is preferable to achieve good tracking performance.*

Example 1.1 pinpoints/indicates two relevant situations in which LTI feedback control inevitably results in a compromise, and thus a suboptimal control solution. This calls for allowing a larger class of controllers beyond the LTI strategies to provide improved control solutions that meet the future specifications. Therefore, in this thesis we consider a larger class of controllers being *hybrid/nonlinear controllers.* The main objective of this thesis is to explore how such controllers can offer the desired performance improvements (compared to LTI control).

1.2 Hybrid control for linear (motion) systems

Hybrid controllers consist of a dynamical system with interacting continuous and discrete (or non-smooth) components. To a control engineer accustomed to linear techniques, it might be counterintuitive to introduce nonlinearities into an otherwise smooth (and linear) feedback control system. However, the desire to push the performance of a linear control system beyond the achievable boundaries, and thus relieving the the fundamental limitations imposed by LTI feedback control motivate non-conventional and hybrid control solution. Indeed, the use of nonlinear controller components (that are intentionally designed by us as control engineers), offers the necessary design freedom to overcome these fundamental limitations.

In literature, numerous results have been presented that show the potential of a hybrid/nonlinear controller to outperform LTI feedback controllers for linear (motion) systems. This is highlighted in the concise literature overview below.

One of the most well-known hybrid control strategies to improve the transient performance of linear (motion) systems is reset control. A reset controller is an LTI control system of which the state, or a subset of the state is reset to a certain value (usually zero) whenever appropriate algebraic conditions on its input and output are satisfied. Reset control has its origin in 1958 by the introduction of the so-called Clegg integrator, see Clegg (1958). The Clegg integrator was proposed to overcome the inherent performance limitation in LTI control related to a balance between settling time and overshoot. Despite its potential, reset control was not considered further until the mid-70s by the work of Horowitz et al., see Horowitz and Rosenbaum (1975); Krishnan and Horowitz (1974). Especially in the last two decades, it has regained attention in both theoretically oriented research, see e.g., Aangenent et al. (2010); Baños and Barreiro (2012); Beker et al. (2004); Loquen et al. (2008); Nešić et al. (2011); Prieur et al. (2013), as well as in application-oriented research, see, e.g., Baños and Barreiro (2012); Panni et al. (2014); Zheng et al. (2000).

Another hybrid control strategy that focusses on the integral action of the controller in order to improve the transient performance is given in Feuer et al. (1997), in which a switched integral controller is proposed for an LTI plant consisting of an integrator. In Heertjes and Vardar (2013), a sliding mode controller with a saturated integrator is studied, which essentially switches between proportional-derivative (PD) control and proportional-integral-derivative (PID) control in order to limit the overshoot while still achieving a zero steady-state error. In a similar context, the concept of composite nonlinear feedback in Lin et al. (1998) combines two linear control laws with a nonlinear tuning function to improve the transient response of second-order LTI systems. The split-path nonlinear (SPAN) filter has been introduced in 1966 by Foster et al. (1966), and was designed as a phase lead filter that does not cause magnitude amplification. In Aangenent et al. (2005); Fong and Szeto (1980); Foster et al. (1966); Zoss et al. (1968), it was experimentally demonstrated that a controller with such a nonlinear SPAN filter can outperform its linear counterpart with respect to overshoot to a step response, and hence, can improve the transient performance of linear (motion) systems. In Hespanha and Morse (2002), the authors propose a switched controller to a similar problem as mentioned before in Example 1.1, i.e., the control of a complex system where conflicting requirements make a single LTI controller less desirable. In Narendra and Balakrishnan (1997), the authors focus on improving the transient performance of adaptive systems, while Eker and Malmborg (1999) considers a switched controller that is able to improve both the transient performance as well as the steady-state performance of linear systems.

As opposed to linear controllers, the design and tuning of hybrid controllers is often rather complex and requires additional expertise of the control engineer. In this context, it is important to mention that control engineers (in industry) are often used to analyze performance, and to design stabilizing controllers, based on 'linear' frequency-domain characteristics of a closed-loop control system, such as the sensitivity function and complementary sensitivity function, as already mentioned shortly before. In fact, all previously mentioned hybrid/nonlinear control strategies have in common that closed-loop stability cannot be verified anymore using 'linear' tools such as the Nyquist stability theorem, see, e.g., Franklin et al. (2006); Skogestad and Postlethwaite (2005). Often, their design and analysis requires accurate parametric models and solving linear matrix inequalities (LMIs), which, from an industrial point-of-view, introduces considerable design complexity and is not easily embraced as it does not connect to the state-of-the-art of industrial design tools.

An exception is found in the use of variable-gain control (VGC), see Heertjes and Steinbuch (2004). In VGC, the design and analysis can be based on easy-to-obtain measured frequency response functions (FRFs) characterizing the system dynamics. The concept of VGC has already been successfully applied in numerous industrial applications to improve the (transient and/or steady-state) performance of linear (motion) systems, see, e.g., Armstrong et al. (2001); Heertjes and Nijmeijer (2012); Heertjes et al. (2013, 2009); Hunnekens et al. (2015a); van de Wouw et al. (2008); Zheng et al. (2005). The acceptance of VGC in industry hinges on the fact that these controllers are fairly intuitive for (motion) control engineers as their design has strong connections to techniques they are accustomed to. Indeed, the linear part of these controllers can be designed using frequency-domain loop-shaping techniques, the add-on nonlinear part often relates in a clear way to the underlying linear controllers, and closed-loop stability can be verified using (measured) frequency response data. As an example, the use of VGC has been used to overcome similar LTI control design trade-offs as those considered in Example 1.1. For instance, the work in Heertjes and Nijmeijer (2012); Heertjes et al. (2009); van de Wouw et al. (2008) deals with balancing trade-offs between low-frequency tracking properties and sensitivity to high-frequency disturbances. In this respect, VGC offers the possibility to provide additional control gain in case of large servo errors (typically stemming from low-frequency disturbances), while for small servo errors (typically stemming from high-frequency disturbances and measurement noise) less (or no) additional gain is applied. The other control design trade-off in Example 1.1, i.e., deteriorating the transient response of a (motion) system by including integral action in the controller, is considered in Hunnekens et al. (2015b). In that paper, the authors propose a variable-gain integral controller (VGIC) that limits the integral action if the error exceeds a certain threshold, thereby limiting, in turn, the amount of overshoot.

1.3 Objectives and contributions

The concise literature overview in Section 1.2 suggests that hybrid controllers offer opportunities to improve the performance of linear (motion) systems compared to LTI controllers. For the design of such hybrid controllers, it is a known fact that ‘classical’ steady-state performance measures, such as the $\mathcal{L}_2$-gain and ISS-gain, in a controller design criterion for a linear (motion) system will not likely favor hybrid controllers over linear ones (although the *characterization* of these measures given a hybrid/nonlinear controlled system remains to be important). It is therefore important to formulate appropriate (and hence, specific) performance measures that can discriminate between linear and hybrid controllers based on the practical control design problem at hand. In addition, in order to enhance their (industrial) acceptance, there is a need for design and analysis tools for hybrid controllers that bridge the gap between hybrid systems theory (with formal stability guarantees) and industrial control practice, commonly exploiting frequency-domain design tools and non-parametric models, e.g., easy-to-obtain measured FRF descriptions of the (motion) system dynamics. Summarizing, the general objectives of this thesis can be stated as follows:

(I) *The development of novel hybrid/nonlinear controllers to improve the transient and/or steady-state performance of linear motion systems which are applicable to industrial high-tech systems;*

(II) *The development of novel techniques to analyze stability and performance of hybrid systems, preferably by exploiting frequency-domain design tools and non-parametric models;*

(III) *Experimental and industrial validation of the proposed controllers and techniques.*

1.3.1 Contributions of the thesis

The main contributions of this thesis can be summarized in terms of contributions on these three general objectives, which will be further detailed below.

Objective (I): Novel hybrid controller designs that connect to the industrial practice and result in an improved performance.

In this thesis, several novel hybrid controllers are proposed of which the associated design is intuitive for (motion) control engineers in industrial practice. In Chapter 2, a switched controller architecture is presented for motion systems that exhibit, from a control point-of-view, position-dependent dynamics as a result of varying sensor configurations. All individual components (except the time-varying gain) of the resulting controller can be designed using classical frequency-domain loop-shaping techniques. Compared to the current linear control solution, an improved transient and steady-state performance is realized.

In Chapter 3, a novel 'bandwidth-on-demand' variable-gain control strategy is proposed that allows for a varying 'bandwidth' of the feedback controller. Easy-to-use tuning guidelines are presented for the design of such a 'bandwidth-on-demand' controller, which are intuitive for (motion) control engineers because all linear components can be designed using frequency-domain loop-shaping and a guideline to design the time-varying gain is provided. The ability to vary the 'bandwidth' online is advantageous if the motion system is subject to time-varying, and reference-dependent, performance requirements as this feature allows to balance trade-offs between low-frequency tracking performance and sensitivity to higher-frequency disturbances in a favorable manner compared to LTI control solutions.

Chapter 5, revisits the concept of the split-path nonlinear filter and introduces a novel variant: The split-path nonlinear integrator (SPANI). This nonlinear control strategy focuses on improving the transient performance in terms or reducing overshoot, while still ensuring a zero steady-state error in the presence of constant external disturbances. The SPANI is easy to design as it allows the control engineer to design a linear integrator in parallel to a nominal linear controller, which can be done using classical frequency-domain loop-shaping techniques, and then simply replace the linear integrator by a SPANI with the same gain.

Objective (II): Novel techniques to analyze stability and performance of hybrid systems.

The contributions on this topic are twofold and can be categorized by 'data-based' conditions and 'LMI-based' conditions.

Three of the five chapters of this thesis present (novel) conditions to verify stability and performance of hybrid systems, and are based on easy-to-obtain measured frequency response data. In particular, the stability conditions for the switched controller architecture in Chapter 2, for the 'bandwidth-on-demand' controller in Chapter 3, and for reset controllers in Chapter 4, are all graphically verifiable based on measured frequency response data.

In Chapter 5, a formal stability analysis is presented for the feedback control configuration with SPANI based on a hybrid dynamical system model for the closed-loop dynamics. Based on this hybrid modeling formalism, sufficient Lyapunov-based stability conditions are provided in terms of linear matrix inequalities, which also prove to be useful in the design of the SPANI.

Chapter 6 focusses on a particular hybrid system class that is useful for the modeling and analysis of more recent popular control application domains, such as event-triggered control (ETC) systems, see, e.g., Heemels et al. (2012) for a recent overview, reset control systems (RCS) and networked control systems (NCS), see, e.g., Bemporad et al. (2010); Hespanha et al. (2007). This chapter also provides novel LMI-based conditions to analyze the stability and the $\mathcal{L}_2$-performance of the hybrid systems under study using trajectory-dependent Lyapunov/storage functions as a technical novelty.

Objective (III): Validation on industrial benchmark systems.

Several industrial benchmark systems are considered in this thesis in order to validate the proposed hybrid controllers and/or analysis techniques. In Chapter 2, the proposed switched controller is experimentally validated on a motion system used in the lithographic industry. In Chapter 3, the effectiveness of the proposed controller with 'bandwidth-on-demand' characteristics is experimentally demonstrated using an industrial nano-positioning motion system. The practical applicability of the data-based stability conditions for reset control systems is demonstrated through experiments on an industrial piezo-actuated motion system used in the lithography industry. Finally, Chapter 5 considers a model-based case study of a positioning operation of an industrial pick-and-place machine to validate the proposed split-path nonlinear integrator (SPANI).

1.3.2 Contributions of the individual chapters

Chapter 2 presents a novel scheduled controller design that allows to switch between two LTI controllers based on the actual position of the system. The motivation for such a switched controller architecture stems from a case study of a motion stage used in the lithography industry that exhibits, from a control point-of-view, position-dependent dynamics as a result of varying sensor configurations. An important feature of the proposed architecture is the fact that all individual filters (LTI controllers) can be designed using classical frequency-domain loop-shaping techniques. Moreover, graphical conditions based on (measured) frequency-domain data are provided under which closed-loop stability can be guaranteed irrespective of how the switching between the two LTI controllers occurs in time. The effectiveness of the proposed scheduling technique, as a way to improve both transient and steady-state performance compared to the state-of-the-art industrial LTI control solution, is demonstrated by means of experiments on a high-precision industrial motion stage.

Chapter 3 introduces a novel variable-gain control strategy that allows to vary the 'bandwidth' of the feedback controller online. The ability to vary the 'bandwidth' of the resulting controller online is advantageous in case the motion system is subject to time-varying, and reference-dependent, performance requirements. In fact, this feature allows us to balance between low-frequency tracking performance and sensitivity to higher-frequency disturbances in a much better way than LTI controller design, which typically requires a compromise between these conflicting design goals thereby limiting the overall performance. The variable-gain controller consists of frequency-domain loop-shaped linear filters and a variable-gain element. The gain of this element depends on reference information and determines the desired reference-dependent 'bandwidth' of the resulting controller. Controller design guidelines and data-based frequency-domain conditions to verify stability and convergence of the closed-loop system are presented. These guidelines and conditions result in an overall design and tuning of the 'bandwidth-on-demand' variable-gain control strategy that is intuitive for control engineers. The intuitive design and the ability of the 'bandwidth-on-demand' controller to outperform LTI controllers are emphasized through experiments on an industrial nano-positioning motion system.

Chapter 4 presents new (sufficient) stability conditions for reset control systems based on measured frequency response data. These results are the first data-based stability conditions for reset control systems, which can contribute to the industrial acceptance of these high-potential nonlinear controllers. The applicability of these novel conditions and the effectiveness of the reset control strategy are illustrated by experiments on an industrial piezo-actuated motion system.

Chapter 5 revisits an 'old' hybrid control concept consisting of a so-called split-path nonlinear filter (SPAN filter). The SPAN filter incorporates non-smooth (and thus nonlinear) elements, such as the absolute value function and the sign function, into an otherwise linear control loop. This filter was first introduced in 1966, see Foster et al. (1966), in which the authors aimed to circumvent the classical Bode gain-phase relationship in linear control. The goal in Foster et al. (1966) has been to design a filter which could add phase to a control system (such as a lead filter) without the negative effect of an increased high-frequency gain. In Chapter 5, a different goal is pursued by focussing on the trade-off induced by including integral action in the control loop, namely, it is impossible to add integral action to a feedback control system, typically included to achieve zero steady-state errors, without introducing the negative effect of phase lag. In this chapter, a novel variant of the SPAN filter is introduced, namely, the split-path nonlinear integrator (the SPANI), with the aim to reduce the amount of overshoot in a transient response (by appropriately modulating magnitude and sign information of the integral action in the hybrid controller), while still allowing to remove the effect of constant disturbances acting on the system. A hybrid switched dynamical system framework is used to model the SPANI control configuration, in closed loop with a linear plant, which allows for a formal stability analysis of the closed-loop system in terms of linear matrix inequalities (LMIs). The effectiveness of the SPANI is investigated through a model-based study of positioning operations in an industrial pick-and-place machine.

In *Chapter 6*, a particular class of hybrid systems with periodic time-triggered jump conditions is considered in which the jump map has a piecewise linear character. The unifying modeling capabilities, and hence the relevance, of this hybrid systems class is demonstrated by modeling control systems arising in three relevant application domains being: Event-triggered control (ETC) systems, see, e.g., Heemels et al. (2012), reset control systems (RCS) and networked control systems (NCS), see, e.g., Bemporad et al. (2010); Hespanha et al. (2007), in this hybrid framework. In fact, the unifying modeling character of this chapter is instrumental in enabling the transfer of results between the diverse application domains. Moreover, new tools are presented for the analysis of stability and the $\mathcal{L}_2$-gain properties of these hybrid systems. The effectiveness of the proposed modeling and analysis techniques is illustrated by means of a RCS example.

1.4 Outline of this thesis

The outline of this thesis is as follows. Next to the main chapters (2-6) that contain the new contributions of this work and were outlined above, the conclusions and recommendations for future work are presented in *Chapter 7*. Finally, the mathematical proofs and some additional technical notation are reported in *Appendix A*. The main chapters (2-6) in this thesis are based on research papers. Therefore, they are self contained and can be read independently from one another.

Chapter 2

Scheduled controller design for systems with two switching sensor configurations

Abstract – In this chapter, we consider a hybrid system consisting of a motion stage that exhibits, from a control point-of-view, position-dependent dynamics as a result of varying sensor configurations. A scheduled controller design is proposed that is intuitive for control engineers as all individual filters can be obtained using classical frequency-domain loop-shaping techniques thereby connecting to the industrial motion control practice. Moreover, data-based graphical conditions are provided in the frequency-domain under which closed-loop stability can be verified irrespective of how the switching between the controllers occurs in time. The effectiveness of the proposed scheduling technique, as a way to improve both transient and steady-state performance compared to the current state-of-the-art industrial control solution, is demonstrated by means of experiments on a high-precision industrial motion stage.

2.1 Introduction

High-precision motion stages, such as positioning devices used in the semi-conductor industry, are subject to ever increasing requirements on stage acceleration (throughput) and positioning accuracy (imaging quality), see, e.g., Butler (2011). As a result, the influence of structural mode deformation in these stages cannot be neglected. The sensor configuration, i.e., the amount and location of the sensors used in the measurement system, yields a specific characterization of these structural dynamics and is therefore essential for control. In many practical situations, the availability of sensors depends on the position of the motion stage

This chapter is based on van Loon et al. (2015d).

as individual sensors can become 'out of range' as a result of physical limitations on their operating ranges. As a result, the sensor configuration may vary as a function of the stage position, which essentially makes the stage, from a control point-of-view, a switched system, see Liberzon (2003), or a position-dependent dynamical system. This complicates the overall design significantly, certainly if the design techniques have to connect to the state-of-the-art industrial control context. In fact, an important open problem is the design of control systems for dynamical systems with switching sensor configurations based on, for industry important, tools such as frequency-domain loop-shaping techniques, see, e.g., Skogestad and Postlethwaite (2005); Steinbuch and Norg (1998). The major advantage of these tools is that they do not necessarily require parametric models but can be based on easy-to-obtain (and accurate) measured frequency response functions (FRFs) characterizing the motion stage dynamics. In the context of switched systems, this forms a tremendous challenge for which many existing approaches do not meet the desired design requirements.

In industry, the problem of position-dependent dynamics is often dealt with by means of robust control design, see e.g., van de Wal et al. (2002), in which the authors propose an $\mathcal{H}_\infty$-controller for this purpose. Although such an approach meets the desired industrial design requirements, it often results in conservatism because (a) one single linear time-invariant (LTI) controller is active within the whole range of operation, and (b) due to the inherent classical performance trade-offs in LTI feedback control systems, see, e.g., Freudenberg et al. (2000); Seron et al. (1997). To overcome these limitations, several (nonlinear) control techniques exist in the literature that can adapt the controller dynamics according to the on-line measured actual position of the system. One such technique is referred to as gain scheduling, see, e.g., Leith and Leithead (2000); Rugh and Shamma (2000). In gain scheduling, the designer typically selects a finite grid of operating points within the whole range of operation. For each of these operating points FRFs are identified, and based on these FRFs, dedicated local LTI controllers are designed which are implemented by interpolation. Although the design and implementation is intuitive for control engineers, no constructive results exist to formally and systematically guarantee stability and performance of the closed-loop gain-scheduled system, especially under fast parameter variations. Another technique is linear parameter varying (LPV) control, see, e.g., Dinh et al. (2005); Groot Wassink et al. (2005); Scherer (2001); Shamma and Athans (1991), which yields parameter-dependent controllers. This technique typically requires a parametric model that describes how the dynamics of a system varies as a function of the position. Compared to our approach, in which the design relies on easy-to-measure FRFs of the motion system, obtaining such parametric models is time-consuming and often they are still not accurate enough to properly describe the system dynamics. Opposed to gain scheduling, the synthesis of LPV controllers yields a priori guaranteed stability and performance properties of the LPV controlled system. However, contrary to our proposed graphical data-based conditions to verify closed-loop stability, LPV control requires solving linear matrix inequalities (LMIs), which from an industrial point-of-view is not easy to adopt as it does not connect to the state-of-the-art industrial design. Also many designs for the control of switched systems, see, e.g., Deaecto et al. (2011); Heemels et al. (2010); Liberzon (2003) require accurate parametric models and LMI-based designs that are not so easily embraced by control engineers in industry. As a consequence, there is often a need for design tools for switched systems, such as the class of dynamical systems with position-dependent switching of sensor configurations studied in this chapter, that bridge the gap between hybrid systems theory (with formal stability guarantees) and industrial control practice, commonly exploiting frequency-domain design tools and non-parametric models, e.g., measured FRF descriptions of the motion system dynamics.

In this chapter, we provide a solution for such an exemplary problem in the context of an industrial motion stage for the lithography industry. In particular, we will adopt a scheduled controller architecture that, based on the on-line measured actual position of the system, switches between two dedicated (local) LTI controllers. Moreover, we will show that the overall design of the proposed controller is intuitive for control engineers because, (a) all individual LTI controllers can be designed using classical frequency-domain loop-shaping techniques based on measured FRFs, (b) graphical data-based conditions are provided to verify closed-loop stability under arbitrary switching, and (c) the control architecture allows for implementation of all components in a standard motion control software environment. The practical feasibility of the proposed approach is emphasized by means of a case study on an industrial wafer motion stage, which is also used to demonstrate the potential of the proposed scheduled controller by experimental results, including the improvements it provides with respect to the state-of-the-art industrial control solution.

The remainder of the chapter is organized as follows. In Section 2.2, we provide the problem formulation and introduce the plant model in the form of a switched system. In Section 2.3, the proposed control design is introduced and in Section 2.4 conditions for stability are provided. Finally, experimental results are given in Section 2.5 and we will end with conclusions in Section 2.6.

2.2 Problem formulation and system description

In this chapter, we consider the problem of high-performance control of linear time-invariant (LTI) systems subject to position-dependent switching of sensor configurations as a result of physical limitations of sensor operating ranges. The problem itself is described in Section 2.2.1 and is inspired by an industrial wafer stage system. The modeling of such a system is discussed in Section 2.2.2, and the current industrial solution to deal with this problem is discussed in Section 2.2.3.

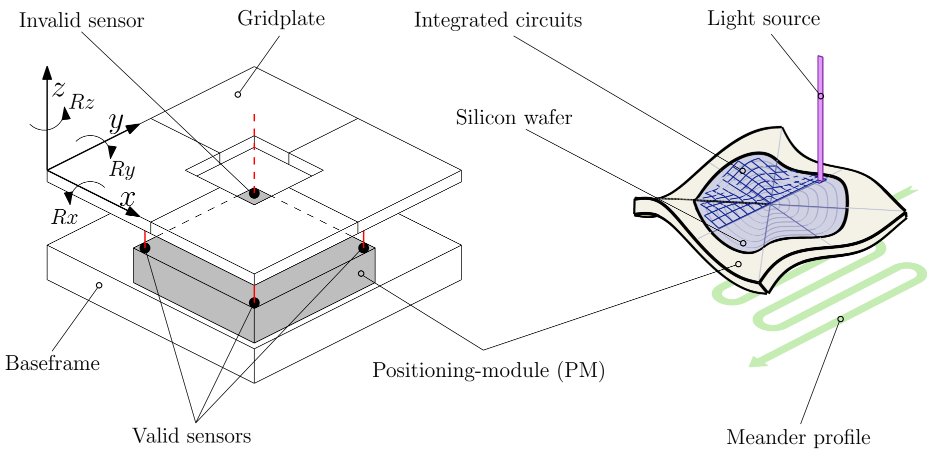

Fig. 2.1. Schematic representation of a wafer stage (right picture taken from van Herpen (2014)).

2.2.1 Introduction to the problem

In this section, we consider a wafer stage system that is schematically depicted in Fig. 2.1 and Fig. 2.2. A wafer stage is a module of a wafer scanner, which is a device used to expose silicon wafers to a light source from an optical column as part of the production process of integrated circuits (ICs), see, e.g., Butler (2011); Martinez and Edgar (2006). The positioning-module (PM) supports a wafer and positions this wafer with respect to the light source in both scanning (x, y) and focus (z) direction. The light path enters the stage in negative z-direction at a fixed (x, y)-position (typically the center of the depicted stage). In this respect, the so-called point-of-interest (POI) is defined as the intersection between the light path with the surface of the wafer, see Fig. 2.2. This POI is time-varying because the wafer is subject to exposure via a meander-like pattern in the (x, y)-plane.

Our goal is to control the POI such that it tracks the meander-like reference setpoint, see Fig. 2.1, with a high accuracy. However, the true position of the POI is *not* directly measurable and can only be estimated based on sensor information. The estimation of the POI is called the point-of-control (POC) and will be used for closed-loop servo control, which makes that the availability of actual sensor information, provided by the measurement system, is crucial for feedback control. For the considered wafer stage, the measurement system consists of four gridplates and four sensors. These sensors are mounted on the PM (indicated by the black dots in Fig. 2.1 and Fig. 2.2) and provide two measurements each (the 2D encoders measure a horizontal and vertical displacement, see Fig. 2.2). The square hole surrounded by the gridplates is to enable exposure of the wafer to the light source. However, due to this hole, each of the four sensors can enter

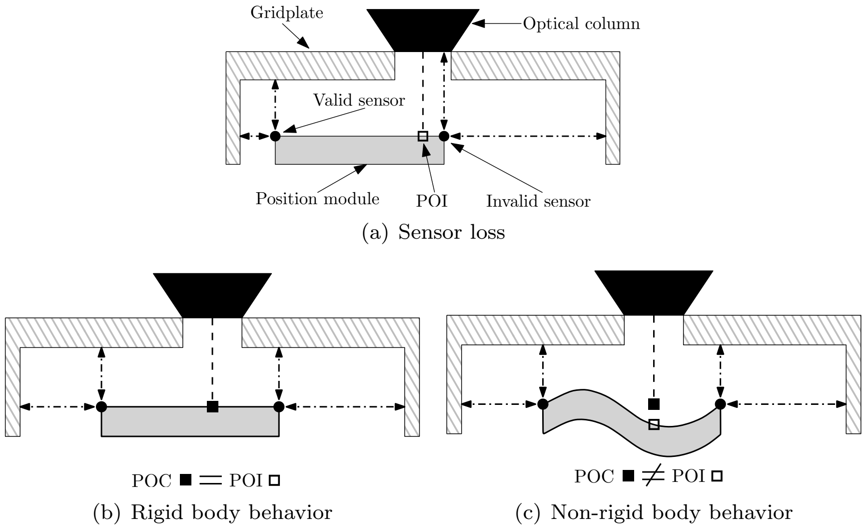

Fig. 2.2. Schematic representation of a wafer stage in 2D. In this figure, (a) represents the situation where a sensor is out-of-range, and (b) and (c) represent rigid body behavior and non-rigid body behavior, respectively.

an 'out-of-range' state depending on the position of the PM with respect to the gridplates, see Fig. 2.1 and Fig. 2.2. As a result, the measurement system has five local sensor configurations, namely, one that uses all four sensors, while the other four use a (different) set of three sensors. To make this more precise, we define the range of operation $\Theta \subset \mathbb{R}^2$, i.e., the region in the (x, y)-plane where the wafer stage can operate, and a position vector $\theta(t) \in \Theta$, denoting the actual position of the PM at time $t \in \mathbb{R}_{\geq 0}$. We define regions $\Lambda_i \subseteq \Theta$, $i = 1, 2, \ldots, n$, where each of the sensor configurations is available. Moreover, it holds that $\cup_{i=1}^{n} \Lambda_i = \Theta$, and these regions might be overlapping. In fact, in our case with $n = 5$, they are schematically depicted in Fig. 2.3(a). In this figure, the subset in which all four sensors are available is denoted by Λ_2, and the subsets in which only three sensors are available are Λ_i, $i \in \{1, 3, 4, 5\}$.

Remark 2.1. *All four sensors are available in region Λ_2, which implies that also the other configurations are available.*

Based on the outcome of all available sensors, which each provide two measurements, the displacement of the PM along the orthogonal coordinate system as in Fig. 2.1, in which the six DOFs of motion are defined, is obtained using coordinate transformations. In this coordinate system, the dynamics along each axis, reconstructed by the measurement system, consists of a rigid body mode

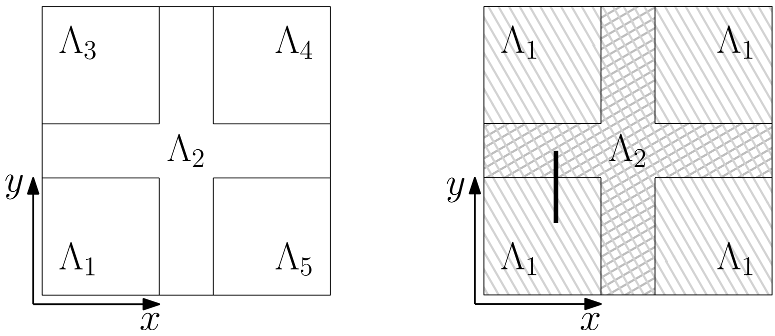

(a) $n = 5$ (b) $n = 2$

Fig. 2.3. Schematic representation of the subdivision of the range of operation Θ into regions $\Lambda_1, \Lambda_2, \ldots, \Lambda_n$, with (a) $n = 5$, and (b) $n = 2$, in the (x, y)-plane. The thick black line in Fig. 2(b) represents the location of the setpoint, as considered in Section 2.5.2, in the (x, y)-plane.

and a number of structural modes. In the ideal case, this structural mode behavior should be suppressed by the control system as these structural dynamics complicate the estimation of the exact position of the POI, i.e., when the stage behaves as a rigid body mode we typically have POC = POI, see Fig. 2.2(b), and non-rigid body behavior usually causes POC $\neq$ POI, see Fig. 2.2(c). However, due to the limited amount of actuators (six actuators for six modes), feedback control is limited to the control of the rigid body modes only, which is common practice in industrial motion control, see also Butler (2011); van de Wal et al. (2002). To this extent, the measurement system should provide a good six DOF rigid body position estimate as this enables us to achieve an as high as possible controller bandwidth and, as a result, the POC can better track the meander-like reference setpoint. When $\theta \in \Lambda_2$, all four sensors are available and, hence, the measurement system provides eight measurements while only the six rigid body modes are estimated. This is referred to as over-sensing and enables the 'removal' of structural mode behavior in the output, i.e., the appearance of some structural modes are *unobservable* in the output used for controlling the system. When transferring from region Λ_2 to region Λ_i, $i \in \{1, 3, 4, 5\}$, one of the 4 sensors becomes invalid, and as a result, the effect of these structural mode deformations becomes visible in the output, thereby making the rigid body position estimate worse compared to the situation in which all four sensors are available.

2.2.2 Switched system formulation

In this chapter, we focus on controlling the POC in z-direction only, in which the loss of sensor information results in a less accurate rigid body position estimate, as described above. In fact, because the input to the controller is observed by a switched set of sensors depending on the position of the stage in the (x, y)-plane, the z-dynamics exhibits, from *a control (input-output) point-of-view*, position dependent dynamics[1]. As a result, a switched system representation is obtained, which can be modeled by means of different output matrices $C_{\mathcal{P}_i}$, $i = 1, 2, \ldots, 5$. To be precise, the z-dynamics of the motion stage can be represented by a single-input-multi-output (SIMO) switched system of the form

$$\Sigma_{sw} : \begin{cases} \dot{x}_{\mathcal{P}} &= A_{\mathcal{P}} x_{\mathcal{P}} + B_{\mathcal{P}} u_{\mathcal{P}} \\ y_{\mathcal{P}_i} &= \begin{cases} C_{\mathcal{P}_i} x_{\mathcal{P}} & \text{when } \theta \in \Lambda_i \\ \varnothing & \text{when } \theta \notin \Lambda_i, \end{cases} \end{cases} \tag{2.1}$$

with input $u_{\mathcal{P}} \in \mathbb{R}$, state vector $x_{\mathcal{P}} \in \mathbb{R}^{n_{\mathcal{P}}}$ with $n_{\mathcal{P}}$ the number of states, and output $y_{\mathcal{P}_i} \in \mathbb{R}$, $i = 1, 2, \ldots, 5$, indicating the i-th measured output that is active in its corresponding region Λ_i. When $\theta \notin \Lambda_i$ the output $y_{\mathcal{P}_i}$ is not available, which is indicated by $y_{\mathcal{P}_i} = \varnothing$.

Due to to (2.1), we can associate[2] 5 local LTI systems to their corresponding regions Λ_i, $i \in \{1, 2, \ldots, 5\}$, which can also be described by the corresponding single-input-single-output (SISO) transfer functions

$$\mathcal{P}_i(s) = \frac{y_{\mathcal{P}_i}(s)}{u_{\mathcal{P}}(s)} \tag{2.2}$$

with $i = 1, 2, \ldots, 5$ and $s \in \mathbb{C}$. Note that all $\mathcal{P}_i(s)$, $i = 1, 2, \ldots, 5$, share at least two poles at $s = 0$ (because we consider a motion system) and possibly some other dynamics. This allows us to express (2.2) as

$$\mathcal{P}_i(s) = \mathcal{F}(s)\Delta_{\mathcal{P}_i}(s), \tag{2.3}$$

in which the shared plant dynamics are represented by $\mathcal{F}(s)$ and the remaining dynamics by $\Delta_{\mathcal{P}_i}(s)$, $i \in \{1, 2, \ldots, 5\}$. Note that for the (motion) systems that we consider, $\Delta_{\mathcal{P}_i}(s)$, $i \in \{1, 2, \ldots, 5\}$ contains stable dynamics only.

To illustrate the possible differences in observed dynamic behavior, consider the regions Λ_i, $i = 1, 2$, in Fig. 2.3(a), for which FRF measurements of the local plants $\mathcal{P}_i(j\omega)$, $\omega \in \mathbb{R}$, $i = 1, 2$, are given in Fig. 2.4. Recall that, for $\theta \in \Lambda_2$, some structural modes are unobservable in the output due to over-sensing, and

[1] In this respect, it is important to note that the z-dynamics itself does not depend on the position.

[2] Due to the fact that the sensors/encoders are placed at fixed locations on the PM, the local LTI plant descriptions $\mathcal{P}_i(s)$, $s \in \mathbb{C}$, corresponding to each fixed sensor set do not depend on the position θ within its corresponding region Λ_i, $i \in \{1, 2, \ldots, 5\}$.

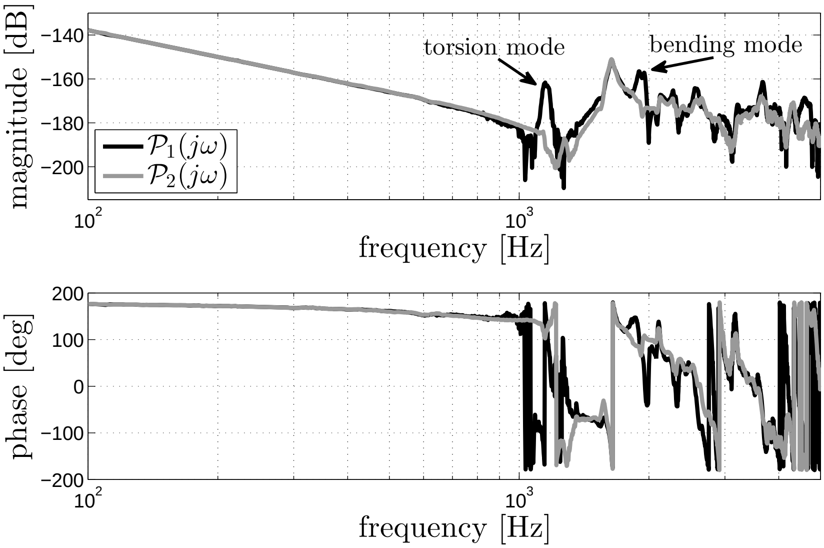

Fig. 2.4. FRF measurements of the local plants $\mathcal{P}_i(j\omega)$, $\omega \in \mathbb{R}$, $i = 1, 2$.

as a result, two structural modes, which appear in $\mathcal{P}_1(j\omega)$, are absent in $\mathcal{P}_2(j\omega)$. To be precise, these modes are the torsion mode at ± 1150 Hz, and a bending mode at ± 1900 Hz, see Fig. 2.4.

2.2.3 Industrial state-of-the-art control design

In industry, control design for systems described by (2.1) often consists of two steps. First, a single LTI controller $\mathcal{C}(s)$, $s \in \mathbb{C}$, which results in an asymptotically stable closed-loop system for all 5 *individual* local LTI plants $\mathcal{P}_1, \ldots, \mathcal{P}_5$, is designed based on 5 local FRFs using frequency-domain loop-shaping techniques. Subsequently, in order to use this SISO LTI controller $\mathcal{C}(s)$ with (2.1), based on the switching outputs $y_{\mathcal{P}_1}, y_{\mathcal{P}_2}, \ldots, y_{\mathcal{P}_5}$, an output scheduling law is introduced, such that from (2.1) the following SISO LPV system results

$$\dot{x}_{\mathcal{P}} = A_{\mathcal{P}} x_{\mathcal{P}} + B_{\mathcal{P}} u_{\mathcal{P}} \tag{2.4a}$$

$$y_{\mathcal{P}} = \sum_{i=1}^{n} \phi_i(\theta) C_{\mathcal{P}_i} x_{\mathcal{P}}, \tag{2.4b}$$

with $y_{\mathcal{P}} \in \mathbb{R}$, and $\phi_i(\theta) \in [0, 1]$, $i = 1, 2, \ldots, 5$, position-dependent output scheduling parameters that satisfy $\sum_{i=1}^{5} \phi_i(\theta) = 1$, and $\phi_i(\theta) = 0$ when $\theta \notin \Lambda_i$ for $i = 1, 2, \ldots, 5$. Although appealing for industry, this control solution has two significant drawbacks:

(1) There is no a priori guarantee for stability of the closed-loop connection of plant (2.4) with LTI controller $\mathcal{C}(s)$ for all $\theta(t) \in \Theta$ varying over time;

(2) The control of all local plants with one robust LTI controller $\mathcal{C}(s)$ potentially limits performance.

In the remainder of this chapter, we assume that $\mathcal{P}_1$ can be used to describe the plants $\mathcal{P}_i$, $i = 1, 3, 4, 5$ in Fig. 2.3(a), and hence, $i = 1, 2$ in (2.1) (see Fig. 2.3(b)). A scheduled controller design for $i = 1, 2, \ldots, 5$ is a topic of ongoing research, for which the design presented here forms a first important and fundamental step.

Remark 2.2. *In the special case of $i = 1, 2$, the regions Λ_i, $i = 1, 2$, are described by $\Lambda_1 := \Theta$ and $\Lambda_2 \subset \Theta$, see Remark 2.1, and depicted schematically in Fig. 2.3(b). Hence, for $i = 1, 2$, one can take $\phi_1(\theta) = 1$ and $\phi_2(\theta) = 0$, $\theta \in \Theta$, (as $y_{\mathcal{P}_1}$ is available for all $\theta \in \Theta$, i.e., $\Lambda_1 = \Theta$) in* (2.4) *and design one LTI controller $\mathcal{C}(s)$, $s \in \mathbb{C}$, based on the plant $\mathcal{P}_1(s)$. This would remove the previously mentioned drawback (1), still leaving drawback (2).*

2.3 Scheduled controller design

In this section, we present a scheduled controller architecture with the aim to switch between two LTI controllers $\mathcal{C}_i(s)$, $i = 1, 2$, based on the actual position $\theta \in \Theta$. The proposed scheduled controller architecture, which is schematically depicted in Fig. 2.5, results in an effective controller $\mathcal{C}_2(s)$ (designed based on $\mathcal{P}_2(j\omega)$) when $\theta \in \Lambda_2$, and results in $\mathcal{C}_1(s)$ (designed based on $\mathcal{P}_1(j\omega)$) otherwise. Consider Fig. 2.5, in which $r \in \mathbb{R}$ denotes the reference signal, $d \in \mathbb{R}$ an unknown but bounded disturbance, and Σ_{sw} is given by (2.1) with $n = 2$, $\Lambda_1 = \Theta$, and $\Lambda_2 \subset \Theta$. The position-dependent scheduling gain is denoted by $\alpha(\theta)$ and can take values in $[0, 1]$. Moreover, the (non)availability of $y_{\mathcal{P}_2}$ in (2.1), and Fig. 2.5 is modeled via the position-dependent indicator function

$$\beta(\theta) = \begin{cases} 1 & \text{when} \quad \theta \in \Lambda_2 \\ 0 & \text{when} \quad \theta \notin \Lambda_2. \end{cases} \tag{2.5}$$

The to-be-designed filters $\mathcal{C}_\Delta(s)$ and $\mathcal{C}_2(s)$ in Fig. 2.5 are both LTI and can be designed using classical frequency-domain loop-shaping techniques. The procedure to do so is as follows. The first step in designing these filters is to design dedicated LTI controllers $\mathcal{C}_1(s)$ and $\mathcal{C}_2(s)$, $s \in \mathbb{C}$, based on measured FRF data of the local plants $\mathcal{P}_1(j\omega)$ and $\mathcal{P}_2(j\omega)$, $\omega \in \mathbb{R}$, respectively. These LTI controllers typically consist of the following linear filters: A PID-type filter, a second-order low pass filter, and a number of notch filters. Because both $\mathcal{C}_i(s)$, $i = 1, 2$, contain a PID-type filter, they share at least one pole at $s = 0$ (due to the

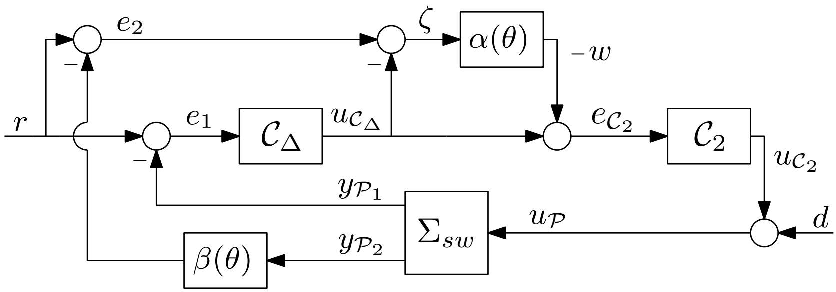

Fig. 2.5. Schematic representation of the feedback loop with SIMO plant Σ_{sw}, as in (2.1), and the proposed scheduled controller.

integrator) and possibly some other dynamics. In the second step, the shared dynamics are collected in an LTI filter $\mathcal{H}(s)$ such that

$$\mathcal{C}_i(s) = \mathcal{H}(s)\Delta_{\mathcal{C}_i}(s), \tag{2.6}$$

in which $\Delta_{\mathcal{C}_i}(s)$, $i = 1, 2$, contain the remaining controller dynamics. This allows us to design the LTI filter $\mathcal{C}_\Delta(s)$ in Fig. 2.5 as

$$\mathcal{C}_\Delta(s) = \Delta_{\mathcal{C}_2}^{-1}(s)\Delta_{\mathcal{C}_1}(s). \tag{2.7}$$

Design criterion 1. *The LTI controllers $\mathcal{C}_i(s)$, $i = 1, 2$, are designed such that they do not contain non-minimum phase zeros and have an equal relative degree, although their state dimensions may vary. The filter $\mathcal{H}(s)$ is designed such that no pole-zero cancelations take place in* (2.6)*, and as a result, in* (2.7)*.*

Note that by Design criterion 1, $\mathcal{C}_\Delta(s)$ as in (2.7) is a proper filter, i.e., its relative degree is zero. This follows from the fact that $\mathcal{C}_i(s)$, $i = 1, 2$, have an equal relative degree and, consequently, so do $\Delta_{\mathcal{C}_i}(s)$, $i = 1, 2$.

Remark 2.3. *The series connection*

$$\begin{aligned} \mathcal{C}_2(s)\mathcal{C}_\Delta(s) &= \mathcal{H}(s)\Delta_{\mathcal{C}_2}(s)\Delta_{\mathcal{C}_2}^{-1}(s)\Delta_{\mathcal{C}_1}(s) \\ &= \mathcal{C}_1(s) \end{aligned} \tag{2.8}$$

has pole-zero cancelations if $\mathcal{C}_2(s) \neq \mathcal{H}(s)$, i.e., the poles/zeros of $\Delta_{\mathcal{C}_2}(s)$ are canceled. However, by Design criterion 1, $\Delta_{\mathcal{C}_2}(s)\Delta_{\mathcal{C}_2}^{-1}(s)$ involves no unstable pole-zero cancelations, i.e., the filter $\Delta_{\mathcal{C}_2}(s)$ does not contain any unstable poles, nor non-minimum phase zeros.

The proposed controller structure in Fig. 2.5 has all the shared controller dynamics $\mathcal{H}(s)$ active irrespective of the value of the switching function $\alpha(\theta)$, which is advantageous for bumpless transfer and integrator windup, see Zaccarian and Teel (2002). Moreover, by designing

$$\alpha(\theta) = 0 \quad \text{when } \theta \notin \Lambda_2, \tag{2.9}$$

we have that $\beta(\theta) = 1$ if $\alpha(\theta) \neq 0$, and thus

$$e_{\mathcal{C}_2}(t) = \alpha(\theta(t))r(t) - \alpha(\theta(t))y_{\mathcal{P}_2}(t) + (1 - \alpha(\theta(t)))u_{\mathcal{C}_\Delta}(t). \tag{2.10}$$

As a result, the closed-loop system of Fig. 2.5 can be treated as a feedback connection between an LTI system and a (to be designed) variable gain $\alpha : \theta \to [0, 1]$, and hence belongs to the class of Lur'e-type systems, see e.g., Khalil (2000). The linear dynamical part of the Lur'e-type system description of the closed-loop system is given by

$$\mathcal{G}(s) = \frac{\mathcal{P}_2(s)\mathcal{C}_2(s) - \mathcal{P}_1(s)\mathcal{C}_1(s)}{1 + \mathcal{P}_1(s)\mathcal{C}_1(s)}, \tag{2.11}$$

denoting the transfer function between 'input' w and 'output' ζ, in feedback with a variable gain element $\alpha : \theta \to [0, 1]$. In order to derive a state-space description of the closed-loop dynamics, we introduce the state-space realization of $\mathcal{C}_2$, given by

$$\mathcal{C}_2 : \begin{cases} \dot{x}_{\mathcal{C}_2} = A_{\mathcal{C}_2} x_{\mathcal{C}_2} + B_{\mathcal{C}_2} e_{\mathcal{C}_2} \\ u_{\mathcal{C}_2} = C_{\mathcal{C}_2} x_{\mathcal{C}_2}, \end{cases} \tag{2.12}$$

in which $x_{\mathcal{C}_2} \in \mathbb{R}^{n_{\mathcal{C}_2}}$ with $n_{\mathcal{C}_2}$ the number of states, and e_1, $e_{\mathcal{C}_2}$, $u_{\mathcal{C}_2} \in \mathbb{R}$, and the state-space realization of $\mathcal{C}_\Delta$, given by

$$\mathcal{C}_\Delta : \begin{cases} \dot{x}_{\mathcal{C}_\Delta} = A_{\mathcal{C}_\Delta} x_{\mathcal{C}_\Delta} + B_{\mathcal{C}_\Delta} e_1 \\ u_{\mathcal{C}_\Delta} = C_{\mathcal{C}_\Delta} x_{\mathcal{C}_\Delta} + D_{\mathcal{C}_\Delta} e_1, \end{cases} \tag{2.13}$$

in which $x_{\mathcal{C}_\Delta} \in \mathbb{R}^{n_{\mathcal{C}_\Delta}}$ with $n_{\mathcal{C}_\Delta}$ the number of states, and $u_{\mathcal{C}_\Delta} \in \mathbb{R}$. A realization of the closed-loop dynamics in state-space form can be obtained by collecting the individual state-space models of Σ_{sw} as in (2.1), (2.12) and (2.13) in one overall model given as follows

$$\dot{x} = Ax + Bw + Fv \tag{2.14a}$$
$$\zeta = Cx + D_v v \tag{2.14b}$$
$$w = -\alpha(\theta)\zeta, \tag{2.14c}$$

with $x := [x_{\mathcal{P}}^\top \; x_{\mathcal{C}_2}^\top \; x_{\mathcal{C}_\Delta}^\top]^\top \in \mathbb{R}^n$, external inputs $v = [r \;\; d]^\top \in \mathbb{R}^{n_v}$, and matrices given by

$$\left[\begin{array}{c|c|c} A & B & F \\ \hline C & & D_v \end{array}\right] = \left[\begin{array}{ccc|c|cc} A_{\mathcal{P}} & B_{\mathcal{P}} C_{\mathcal{C}_2} & 0 & 0 & 0 & B_{\mathcal{P}} \\ -B_{\mathcal{C}_2} D_{\mathcal{C}_\Delta} C_{\mathcal{P}_1} & A_{\mathcal{C}_2} & B_{\mathcal{C}_2} C_{\mathcal{C}_\Delta} & -B_{\mathcal{C}_2} & B_{\mathcal{C}_2} D_{\mathcal{C}_\Delta} & 0 \\ -B_{\mathcal{C}_\Delta} C_{\mathcal{P}_1} & 0 & A_{\mathcal{C}_\Delta} & 0 & B_{\mathcal{C}_\Delta} & 0 \\ \hline D_{\mathcal{C}_\Delta} C_{\mathcal{P}_1} - C_{\mathcal{P}_2} & 0 & -C_{\mathcal{C}_\Delta} & & 1 - D_{\mathcal{C}_\Delta} & 0 \end{array}\right]. \tag{2.15}$$

Note that the state-space model (2.14) can be a non-minimal realization for the transfer-function (2.11) due to possible pole-zero cancelations, see Remark 2.3.

2.4 Stability analysis

In this section, we present graphical data-based conditions to verify input-to-state stability (ISS), see Arcak and Teel (2002); Sontag and Wang (1995), of the closed-loop system as in Fig. 2.5 for every $\alpha : \theta \to [0, 1]$ independent of how $\alpha(\theta(t))$ depends on time $t \in \mathbb{R}_{\geq 0}$. But first, we want to emphasize that the system matrix A of the system (2.14) is Hurwitz by proper controller design.

Proposition 2.1. *The system matrix A of the system* (2.14) *is Hurwitz under the following conditions:*

(i) The open-loop $\mathcal{O}_1(j\omega) = \mathcal{P}_1(j\omega)\mathcal{C}_1(j\omega)$ satisfies the Nyquist stability criterion, see Skogestad and Postlethwaite (2005), for all $\omega \in \mathbb{R}$;

(ii) Design criterion 1 holds;

(iii) The controller $\mathcal{C}_1(s)$ does not cancel any unstable dynamics (if present) in $\mathcal{P}_1(s)$, i.e., $\mathcal{P}_1(s)\mathcal{C}_1(s)$ has no unstable pole-zero cancelation.

Proof. The proof can be found in A.1.1. □

The following theorem poses sufficient conditions under which global exponential stability (GES) of the equilibrium $x^* = 0$ is guaranteed for zero inputs. Moreover, the same conditions guarantee that the system (2.14) is ISS with respect to r and d. See Sontag and Wang (1995) for the exact definition of ISS.

Theorem 2.2. *Consider the system* (2.14) *with variable gain $\alpha(\theta(t)) \in [0, 1]$, $t \in \mathbb{R}_{\geq 0}$. Suppose that*

(I) The system matrix A is Hurwitz;

(II) There exist a constant $\rho > 1$ such that the transfer function $\mathcal{G}(j\omega)$ satisfies

$$\frac{1}{\rho} + Re(\mathcal{G}(j\infty)) > 0, \tag{2.16}$$

and

$$\frac{1}{\rho} + Re(\mathcal{G}(j\omega)) > 0 \quad \textit{for all } \omega \in \mathbb{R}. \tag{2.17}$$

Then the equilibrium point $x^* = 0$ of the system (2.14) *is GES (when $r = 0$ and $d = 0$), and the system* (2.14) *is ISS with respect to r and d.*

Proof. The proof can be found in Appendix A.1.2. □

Theorem 2.2 is based on the circle criterion, see, e.g., Khalil (2000), which offers data-based graphical frequency-domain conditions to assess closed-loop stability of systems of the form (2.14), see, e.g., Heertjes and Steinbuch (2004); Heertjes et al. (2009); Hunnekens et al. (2015b). The circle criterion in its standard form, see Khalil (2000), requires minimality of the system (2.14). However, due to our proposed controller structure minimality of the system (2.14) is lost, see Remark 2.3. Nevertheless, under the mild Design criterion 1, we obtain that A is Hurwitz (according to Proposition 2.1), which together with the circle criterion condition in (II) leads to GES and ISS even though the minimality condition is not satisfied. Although there exist some literature on the circle criterion for non-minimal systems, see Brogliato et al. (2007) and references therein, none of them could directly be applied to our case. Still, the circle condition presented in Yakubovich et al. (2004) seems related to our result in Theorem 2.2, since no explicit requirement regarding minimality is stated. Unfortunately, no formal proof was found in Yakubovich et al. (2004) showing that minimality is not necessary. Therefore, we provided a formal proof of the circle criterion in case of non-minimal systems based on the additional requirement in hypothesis (I).

2.5 Experimental results on a wafer stage

In this section, the proposed scheduled controller approach is applied to control the z-axis of the motion stage as introduced in Section 2.2.1.

2.5.1 Design of the proposed scheduled controller

The scheduled controller is *exactly* implemented as represented in the block-scheme given in Fig. 2.5, in which the switching of $\alpha : \theta \to [0, 1]$ is currently implemented by a discontinuous switch given by

$$\alpha(\theta) = \begin{cases} 1 & \text{when } \theta \in \Lambda_2 \\ 0 & \text{when } \theta \notin \Lambda_2. \end{cases} \tag{2.18}$$

The LTI controllers $\mathcal{C}_i(s)$, $i = 1, 2$, are loop-shaped based on the corresponding plant FRFs $\mathcal{P}_i(j\omega)$, $i = 1, 2$, see Fig. 2.4. Both controllers consist of a PID filter, a second-order low pass filter, and a limited number of notch filters. Bode plots of $\mathcal{C}_i(s)$, $i = 1, 2$, are depicted in Fig. 2.6. In this case study, the structure of both controllers is almost identical except for one additional notch filter in $\mathcal{C}_1(s)$, necessary to compensate for the structural mode around ± 1150 Hz in $\mathcal{P}_1(j\omega)$ (which is absent in $\mathcal{P}_2(j\omega)$), see Fig. 2.4. Without the phase lag introduced by this additional notch filter, $\mathcal{C}_2(s)$ can have a higher gain for frequencies below the bandwidth, thereby increasing the tracking performance. Stability of each

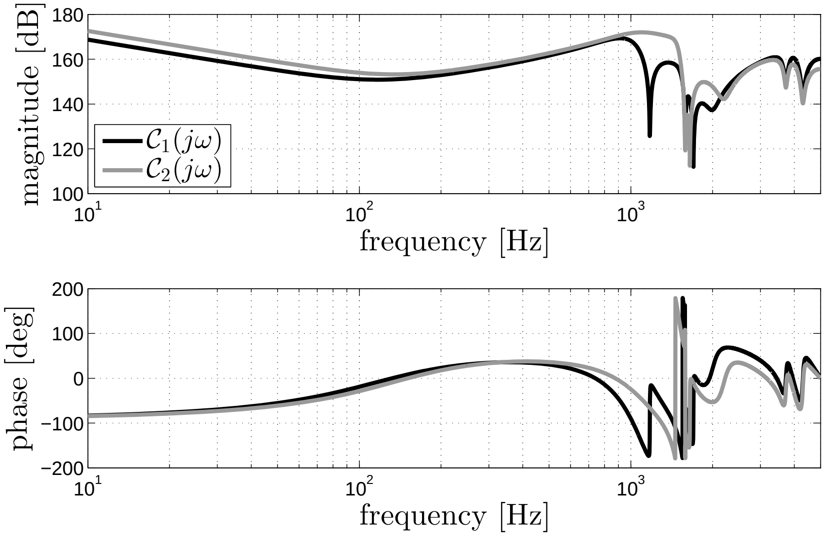

Fig. 2.6. Bode plots of the controllers $\mathcal{C}_i(j\omega)$, $i = 1, 2$.

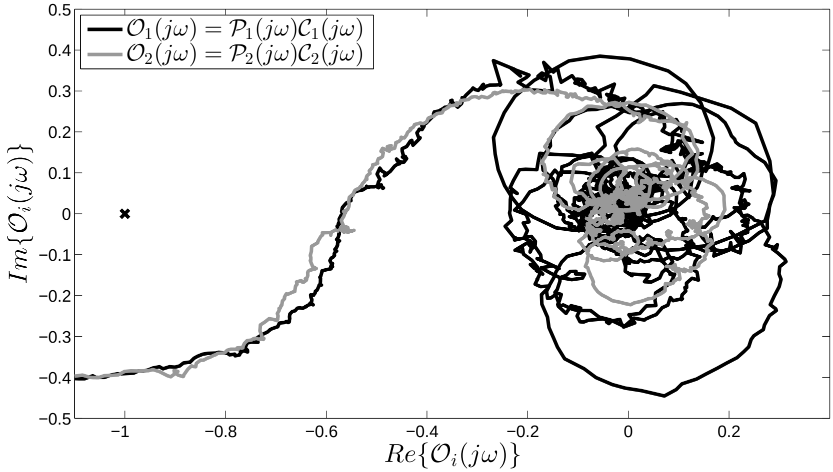

Fig. 2.7. Nyquist diagrams of $\mathcal{O}_i(j\omega) = \mathcal{P}_i(j\omega)\mathcal{C}_i(j\omega)$, $i = 1, 2$.

individual/local closed loop is verified by means of the Nyquist criterion, see Skogestad and Postlethwaite (2005) and Fig. 2.7, which shows robust stability given a modulus margin of approximately 8 dB. Consequently, the conditions of Proposition 2.1 are met, thereby satisfying condition (I) of Theorem 2.2. The final step in the design is to verify the circle criterion condition (II) in Theorem

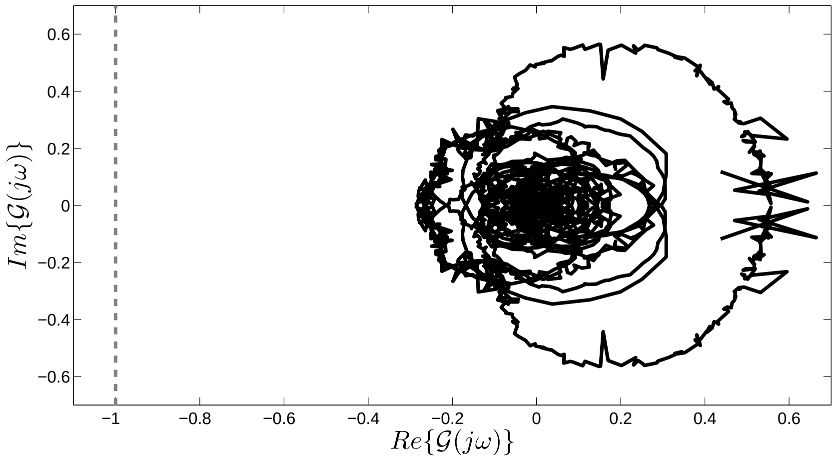

Fig. 2.8. Nyquist diagram of $\mathcal{G}(j\omega)$ as in (2.11) in which the dashed line represents -1.

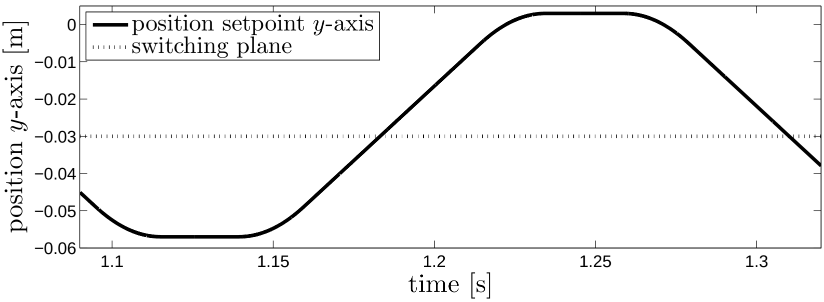

Fig. 2.9. Position setpoint trajecory of y-axis and scheduling borders.

2.2. Let us first note that condition (2.16) is trivial for many motion systems, since $\mathcal{G}(j\omega) \to 0$ for $\omega \to \infty$. The second condition (2.17) is verified by means of Fig. 2.8, which represents the Nyquist diagram of $\mathcal{G}(j\omega)$ as in (2.11), showing that $Re(\mathcal{G}(j\omega)) > -\frac{1}{\rho}$, for some $\rho > 1$ is met for all $\omega \in \mathbb{R}$. In this respect, note that the user can influence $Re(\mathcal{G}(j\omega))$ by means of the design of $\mathcal{C}_i(s)$, $i = 1, 2$, and thus the circle criterion condition (II).

2.5.2 Experimental results

In this section, the proposed scheduled controller approach is applied to control the z-axis of the motion stage as introduced in Section 2.2.1. Moreover, we compare the obtained results with those using a SISO LTI controller $\mathcal{C}(s)$ as described in Section 2.2.3, which is selected as $\mathcal{C}(s) = \mathcal{C}_1(s)$. The setpoint used during the experiments consists of a trajectory in y-direction, depicted schematically in the (x, y)-plane by the thick black line in Fig. 2.3(b), and is given in Fig. 2.9.

In the lithographic industry, the accuracy of the wafer stage is often expressed in terms of overlay and imaging quality, see Butler (2011). Let us first consider overlay, which is the ability of the wafer stage to expose two images exactly on top of each other. In this respect, the moving average (MA) performance measure is of central interest as this forms a measure of the average position error of the wafer stage during exposure, which, in turn determines the location where the image is placed on the wafer. The MA represents the lower-frequency part of the error, and is defined as

$$\mathrm{MA} := \frac{1}{T_e} \int_{-\frac{T_e}{2}}^{\frac{T_e}{2}} e(t)dt, \tag{2.19}$$

in which T_e represents the exposure time, and $e(t)$ represents the position error of the z-axis as a function of time t. The second quality measure is the imaging quality, which is directly affected by the accuracy of the positioning of the wafer stage, i.e., position errors reduce the contrast. In this respect, the moving standard deviation (MSD) performance measure is of central interest, which is defined as

$$\mathrm{MSD} := \sqrt{\frac{1}{T_e} \int_{-\frac{T_e}{2}}^{\frac{T_e}{2}} \left(e(t) - \mathrm{MA}\right)^2 dt}, \tag{2.20}$$

and represents the higher-frequency part of the positioning error. Therefore, is a direct measure of high frequency noise suppression. The MA and MSD of the positioning error are depicted in Fig. 2.10 and Fig. 2.11, respectively. In both figures, the yellow surface represents the situation in which $\alpha(\theta) = 1$, whereas $\alpha(\theta) = 0$ elsewhere. Clearly, both the MA as well as the MSD are reduced using our proposed scheduled controller. This can be further clarified by considering Fig. 2.12, which shows the cumulative power spectral density (CPSD) of the tracking error response of the z-axis for both control strategies. In this figure, we see a performance increase over the complete frequency range which, intuitively, can be explained as follows. For frequencies below the closed-loop bandwidth (± 300 Hz), this is a result of the higher feedback gain of $\mathcal{C}_2(s)$. For frequencies above the bandwidth, this is due to the absence of two structural modes that appear in $\mathcal{P}_1(j\omega)$, at ± 1150 Hz and at ± 1900 Hz, which do not appear in $\mathcal{P}_2(j\omega)$, see Fig. 2.4.

Remark 2.4. *Note that the discontinuous switching might excite high frequency plant dynamics, and therefore, changing $\alpha(\theta(t))$ in a smooth manner could perhaps improve the results even further.*

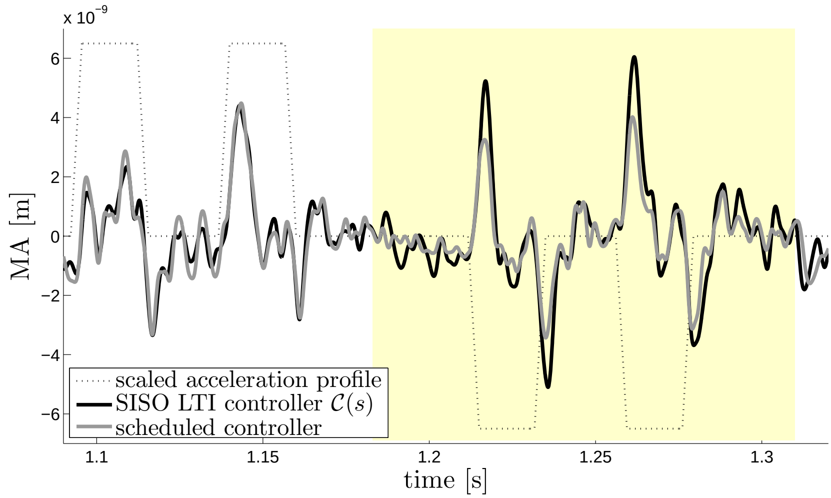

Fig. 2.10. MA of the z-axis error. In this figure, $\alpha(\theta) = 1$ in the yellow surface and $\alpha(\theta) = 0$ elsewhere.

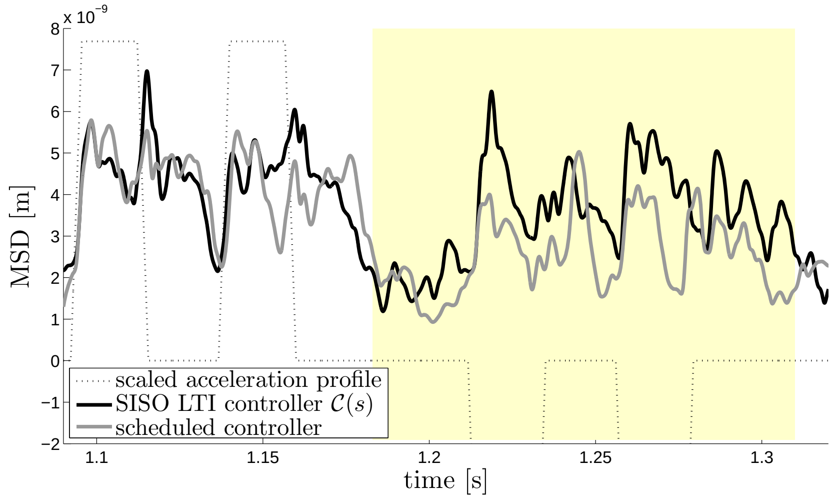

Fig. 2.11. MSD of the z-axis error. In this figure, $\alpha = 1$ in the yellow surface and $\alpha = 0$ elsewhere.

2.6 Conclusions

In this chapter, we proposed a novel scheduling controller architecture for dynamical systems with position-dependent switching sensor configurations in the

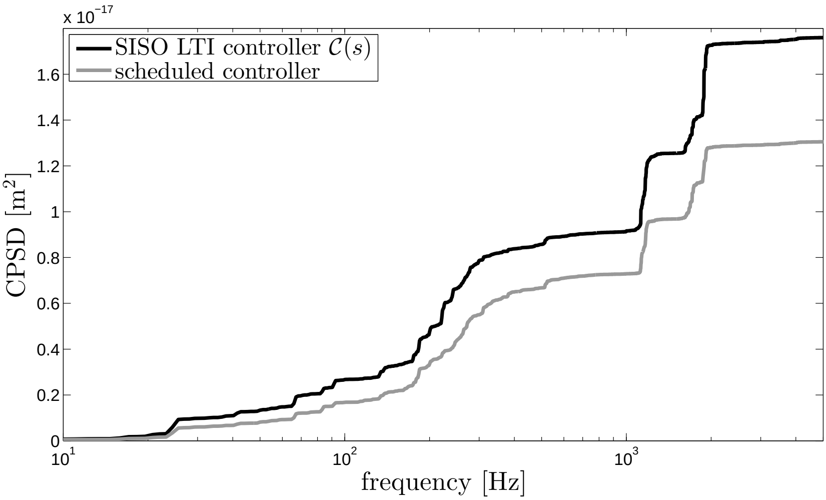

Fig. 2.12. CPSD of z-axis error.

context of an industrial wafer stage. Based on the actual measured position of the motion system, dedicated (local) linear time-invariant (LTI) controllers are switched on or off. To meet the requirements from industry, these LTI controllers are designed using classical frequency-domain loop-shaping techniques based on measured frequency response functions (FRFs), and are implementable in a standard software environment. Moreover, easy-to-handle data-based conditions are presented that allow the user to verify whether the scheduled feedback control system is input-to-state stable with respect to external disturbances, measurement noise and reference signals, irrespective of how the switching between the controllers occurs in time. In fact, these frequency-domain conditions are based on a generalized form of the circle criterion for which minimality of the underlying system is not required. The practical feasibility of the proposed controller scheduling architecture, as well as the ability to outperform the state-of-the-art industrial control solution, has been experimentally demonstrated on an industrial wafer stage system.

Chapter 3

Bandwidth-on-demand motion control with a nano-positioning application

Abstract – In this chapter we introduce a 'bandwidth-on-demand' variable-gain control strategy that allows for a varying bandwidth of the feedback controller. The proposed controller architecture can achieve improved performance given time-varying, reference-dependent performance requirements compared to linear time-invariant control suffering from design trade-offs between low-frequency tracking performance and sensitivity to higher-frequency disturbances. The variable-gain controller consists of frequency-domain loop-shaped linear filters and a variable-gain element. The gain of this element depends on reference information and determines the desired reference-dependent bandwidth of the resulting controller. Controller design guidelines and data-based frequency-domain conditions to verify stability and convergence of the closed-loop system are presented. These guidelines and conditions render the overall design and tuning of the 'bandwidth-on-demand' variable-gain control strategy intuitive for control engineers. This fact, together with the ability of the 'bandwidth-on-demand' controller to outperform linear time-invariant controllers, is emphasized through experiments on an industrial nano-positioning motion system.

3.1 Introduction

The increasing performance demands on speed, accuracy, throughput, etc., of today's high-precision motion systems require them to operate under diverse modes of operation, each having their own specific set of performance requirements. If this comes with the presence of multiple disturbance sources, active

This chapter is based on van Loon et al. (2015c).

in various frequency ranges, this poses a challenging control design task. This is due to the fact that the vast majority of controller designs techniques generally relies on classical linear control theory in which fundamental design trade-offs are inherently present. Namely, increasing the bandwidth of the controlled system improves the low-frequency disturbance rejection properties, and, hence, the tracking-performance, but due to the waterbed effect, this also results in a larger sensitivity to higher-frequency disturbances (i.e., around and/or above the bandwidth), see, e.g., Freudenberg et al. (2000); Seron et al. (1997). This fundamental trade-off can already be challenging when just one mode of operation is considered, but this is severely aggravated when high performance is required in multiple modes of operation because this generally means that the control objectives vary over time, e.g., depend on the reference. As an example, consider Fig. 3.1, which depicts a typical reference trajectory applied in many industrial positioning systems, such as pick-and-place machinery, metrology stages, lithographic systems, copiers, etc. During standstill (the reference is constant), high-frequency disturbance sources are often dominant over low-frequency disturbance sources, such that a low bandwidth of the controlled system is desired in order not to amplify these high-frequency disturbances. On the other hand, when the reference is changing low-frequency disturbances play a dominant role in the closed-loop error, and, hence, a high bandwidth is preferred to achieve good tracking performance. Due to fundamental limitations in linear time-invariant (LTI) feedback control, the design of one LTI controller typically requires a compromise between these conflicting design goals thereby limiting the overall performance achievements of the controlled system.

In this chapter, we propose a variable-gain control strategy that allows for a reference-dependent, and thus time-varying, 'bandwidth' of the feedback controller. By taking on-line reference information into account, this feature allows to 'anticipate' on the required 'bandwidth' for each mode of operation. This allows, contrary to LTI control, to deal with the conflicting control objectives induced by reference-dependent dominance of multiple disturbance sources that are acting in various frequency ranges. The proposed controller consists of frequency-domain loop-shaped linear filters and a variable-gain element, with its gain depending on reference information and inducing the desired 'bandwidth' of the resulting controller. The proposed controller structure supports the design of all the linear components of the variable-gain controller configuration using well-known (frequency-domain) loop-shaping techniques, see, e.g., Steinbuch and Norg (1998). It therefore connects to the state-of-the-art industrial motion control setting, in which easy-to-measure frequency response functions (FRFs) play an important role in the controller design, e.g., by using frequency-domain loop-shaping techniques.

The concept of variable-gain control has already been successfully applied in numerous industrial applications to improve the performance of (linear) motion systems, see, e.g., Armstrong et al. (2001); Heertjes and Nijmeijer (2012); Heert-

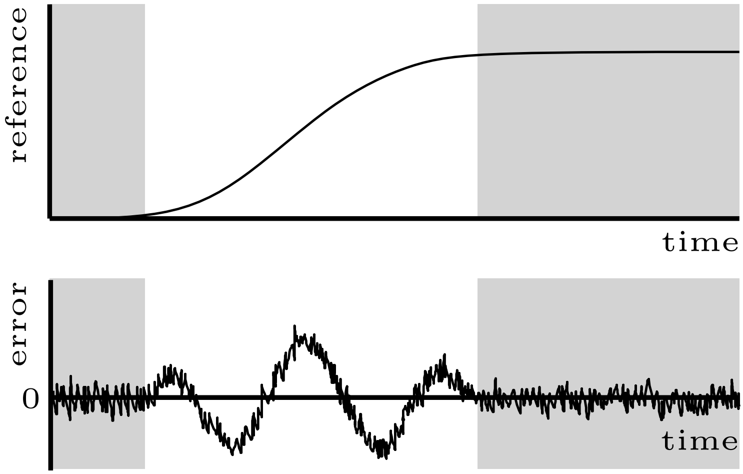

Fig. 3.1. Schematic representation of a possible controller design trade-off. The upper figure shows a typical reference trajectory versus time, the lower figure a possible corresponding error profile corrupted by multiple (high/low frequency) disturbance sources. In the shaded gray areas, high frequency disturbances are dominant, thereby requiring a low bandwidth of the controlled system. However, during movements (corresponding to the white area) low frequency disturbances are dominant and a high bandwidth is preferred in order to improve the tracking performance.

jes et al. (2009); Hunnekens et al. (2015a); van de Wouw et al. (2008); Zheng et al. (2005). In fact, the use of variable-gain control to target similar LTI control design trade-offs as considered in this chapter, i.e., balancing trade-offs between low-frequency tracking properties and sensitivity to higher-frequency disturbances, has been considered in e.g., Heertjes and Nijmeijer (2012); Heertjes et al. (2009); van de Wouw et al. (2008). The novelty in our approach lies in the fact that we couple this fundamental trade-off to time-varying control objectives depending on on-line reference information, which makes it possible to design a time-varying controller with a 'bandwidth-on-demand' characteristic.

Other techniques that can deal with the considered trade-off are, e.g., linear parameter varying (LPV) control, see, e.g., Dinh et al. (2005); Groot Wassink et al. (2005); Scherer (2001); Shamma and Athans (1991) and switched controller design, see, e.g., Deaecto et al. (2011); Hespanha and Morse (2002); Liberzon (2003); Narendra and Balakrishnan (1997). LPV control allows to construct parameter-dependent controllers with a similar 'bandwidth-on-demand' characteristic as our proposed variable-gain controller. This can be done by constructing the LPV controller such that it can vary its controller parameters as a function of the on-line reference information. The downside of such an approach, compared to the control design proposed in this chapter, is that it requires a parametric plant model and the synthesis of these LPV controllers requires solving linear matrix inequalities (LMIs), which both are less desirable from a practical point-of view. Switched controllers are designed such that they are able to switch between several LTI controllers, depending on some switching function which may depend on reference information. However, this approach has several disadvantages compared to the variable-gain controller proposed here. For instance, one has to prevent undesired large transients at the moment of switching, the so-called bumpless transfer problem, see, e.g., Zaccarian and Teel (2002) and references therein. Moreover, many designs for the synthesis and control of switched systems, see, e.g., Deaecto et al. (2011); Heemels et al. (2010); Liberzon (2003), require, similar to LPV control, accurate parametric models and LMI-based designs that are not so easily embraced by control engineers in industry.

Summarizing, the main contributions of this chapter are as follows. Firstly, a novel reference-dependent variable-gain control strategy is introduced that has a 'bandwidth-on-demand' characteristic. Secondly, easy-to-use design guidelines are presented as well as graphical data-based conditions to verify stability and convergence of the variable-gain controlled closed-loop system. Thirdly, the entire design process and its potential to outperform LTI controllers are experimentally demonstrated on an industrial case study of a nano-positioning motion stage.

The outline of this chapter is as follows. Section 3.2 considers the motivation of this work and presents the proposed control architecture. In Section 3.3, data-based conditions to assess stability and convergence of the closed-loop system are provided together with design guidelines. In Section 3.4, we discuss an industrial case study of a nano-positioning motion stage and show how the analysis and design guidelines presented in Section 3.3 can be applied in practice. Moreover, the ability of the 'bandwidth-on-demand' strategy to outperform LTI controllers (with a fixed bandwidth) is demonstrated by means of experimental results on a nano-positioning motion stage. Finally, in Section 3.5, we end with conclusions.

3.1.1 Nomenclature

The following notational conventions will be used. Let $\mathbb{N}$, $\mathbb{R}$, $\mathbb{R}_{\geq 0}$, $\mathbb{C}$ denote the set of non-negative integers, real numbers, nonnegative real numbers and complex numbers, respectively, and $\mathbb{R}^n$ denote the space of n-dimensional vectors with the standard Euclidean norm denoted by $\|\cdot\|$. The real part of a complex variable z is denoted by $Re(z)$. The Laplace transform of a signal $x : \mathbb{R}_{\geq 0} \to \mathbb{R}^n$ is denoted by $\mathfrak{L}\{x\}$ and $s \in \mathbb{C}$ denotes the Laplace variable.

3.2 Reference-dependent variable-gain control: a 'bandwidth-on-demand' approach

In this section, a reference-dependent variable-gain control strategy will be proposed that enables a 'bandwidth-on-demand' characteristic of the resulting feedback controller. In Section 3.2.1, we provide a further motivation for such a hybrid controller. A description of a generic motion control system including the proposed add-on reference-dependent variable-gain controller will be given in Section 3.2.2.

Let us first make precise what is meant by bandwidth given its prominent role in this chapter. Consider therefore the linear feedback control configuration in Fig. 3.2 with linear plant $\mathcal{P}(s)$, $s \in \mathbb{C}$, and a linear controller $\mathcal{C}(s)$. The bandwidth ω_b is defined as the frequency $\omega \in \mathbb{R}$ where the magnitude of the open-loop $|\mathcal{P}(j\omega)\mathcal{C}(j\omega)|$ crosses 1 from above for the first time, see, e.g., Skogestad and Postlethwaite (2005). By definition, bandwidth is a linear time-invariant (LTI) concept and, hence, does not apply to our proposed time-varying control strategy. Nevertheless, with abuse of definition, we will use the term 'bandwidth' in this chapter but use quotation marks to avoid confusion with the LTI case. Moreover, from this point onward we sometimes use the terms 'low-bandwidth/high-bandwidth' controller to denote a controller that results in a low/high bandwidth, respectively.

3.2.1 Motivation for a 'bandwidth-on-demand' controller

Consider Fig. 3.2, which represents a classical LTI feedback controlled system. In this figure, $e := r - y - \eta$ denotes the tracking error between the reference signal r, the output y of the single-input-single-output (SISO) linear time-invariant (LTI) plant $\mathcal{P}(s)$, $s \in \mathbb{C}$, and the measurement noise η. The SISO LTI controller is given by $\mathcal{C}(s)$, and d_i and d_o denote unknown, bounded input/output disturbances, respectively.

Let us for now only focus on the closed-loop error e, and by doing so, two transfer functions are of central interest. The first one is the sensitivity function

$$\mathcal{S}(s) := \frac{1}{1 + \mathcal{P}(s)\mathcal{C}(s)}, \tag{3.1}$$

which represents the closed-loop transfer from (i) the reference signal r, (ii) the output disturbance d_o, and (iii) the measurement noise η, to the error signal e. As such, it reflects the ability of the controller to reduce the servo error e under the external inputs r, d_o and η and, therefore, forms a key qualifier in assessing closed-loop performance. The second function of interest is the process sensitivity function

$$\mathcal{S}_p(s) := -\frac{\mathcal{P}(s)}{1 + \mathcal{P}(s)\mathcal{C}(s)}, \tag{3.2}$$

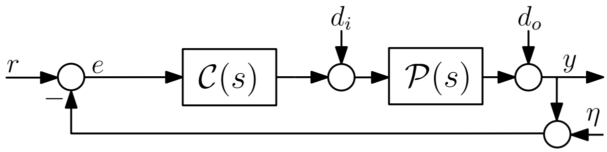

Fig. 3.2. Schematic representation of a classical LTI feedback controlled system.

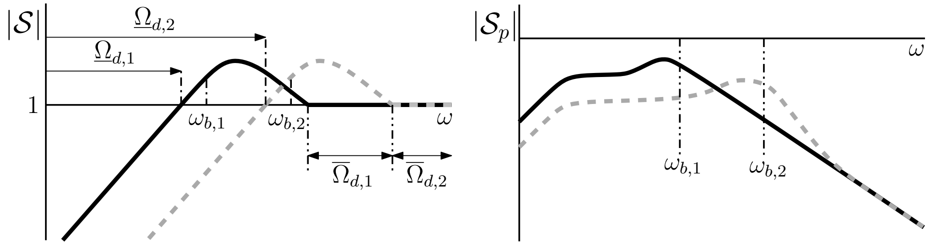

Fig. 3.3. Schematic representation of the Bode magnitude plot for the sensitivity function $\mathcal{S}(j\omega)$ and process sensitivity function $\mathcal{S}_p(j\omega)$, for both a low-bandwidth $\underline{\omega}_b$ (solid) as well as a high-bandwidth $\overline{\omega}_b$ (dashed) situation.

which represents the closed-loop transfer between the input disturbance d_i to the error signal e. Fig. 3.3 shows a schematic representation of the Bode magnitude plot for the sensitivity function $\mathcal{S}(j\omega)$ and the process sensitivity function $\mathcal{S}_p(j\omega)$ for a typical motion control setting, $\omega \in \mathbb{R}$. By using loop-shaping techniques, see, e.g., Steinbuch and Norg (1998), the design of the LTI feedback controller $\mathcal{C}_{lbw}(j\omega)$ in the frequency domain aims to attain the desired shape for the frequency response of $\mathcal{S}(j\omega)$ and $\mathcal{S}_p(j\omega)$, such that sufficient robustness margins, reference tracking, disturbance rejection properties, etc., are obtained.

In classical (motion) control, the bandwidth ω_b is normally chosen as high as possible for performance reasons. Indeed, a high bandwidth is advantageous for low-frequency (frequencies below the bandwidth) disturbance rejection and, hence, results in a good tracking performance. This is illustrated in Fig. 3.3. For a bandwidth $\omega_{b,1}$, disturbances with a frequency content that is contained in the frequency range $\underline{\Omega}_{d,1}$ are suppressed, while for a higher bandwidth $\omega_{b,2}$ this frequency range is obviously much broader and given by $\underline{\Omega}_{d,2}$. By the waterbed-effect, it is known that the area of sensitivity suppression is compensated by an area of sensitivity increase at higher frequencies. In particular, a higher bandwidth will result in a peak ($|\mathcal{S}(j\omega)| >> 1$) at higher frequencies, see Fig. 3.3. High frequency disturbances such as sensor noise η and actuator noise $d_{i,act}$ have a frequency content that is typically contained in $\overline{\Omega}_{d,2}$ in Fig. 3.3. In case of bandwidth's $\omega_{b,1}$ and $\omega_{b,2}$, such disturbances will likely have a

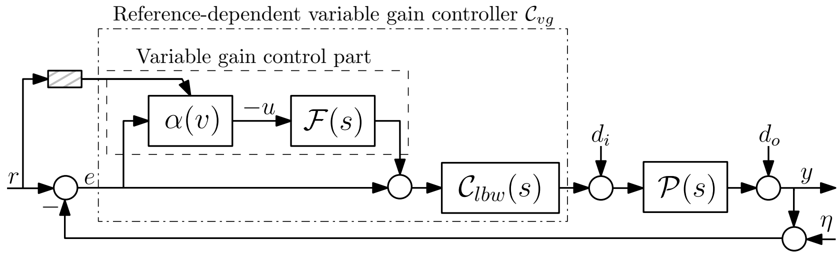

Fig. 3.4. Schematic representation of the reference-dependent variable-gain controlled system.

similar effect on the closed-loop error e, see Fig. 3.3. However, in case ‘high-frequency’ disturbances have frequency content that is not much higher than the bandwidth, e.g., if the frequency content of these disturbances is contained in the frequency range $\overline{\Omega}_{d,1}$, this will inevitably result in control design trade-offs. During time-varying reference motion, the low-frequency disturbances will likely be dominant over the high-frequency disturbances, and, as a result, the bandwidth $\omega_{b,2}$ is still preferable. However, what if accuracy is not only required during movements (i.e., reference tracking), but *also* at standstill/low reference velocities? At standstill/low-velocities, it is clearly advantageous to have a bandwidth $\omega_{b,1}$ because disturbances in the frequency range $\overline{\Omega}_{d,1}$ will not be amplified. In practice, this trade-off results in the design of an LTI feedback controller that achieves at best a compromise among these conflicting design goals such that a reasonable performance is obtained given these inherent system design limitations.

As we will demonstrate in this chapter, the proposed reference-dependent variable-gain control method, that will be formally introduced in the following section, allows for a reference-dependent ‘bandwidth’ of the feedback controller, i.e., the ‘bandwidth’ (and thereby the controller) is varied on-line based on a relation between the preferred bandwidth and the actual reference characteristics.

3.2.2 Description of the control configuration

The overall reference-dependent feedback control configuration as proposed in this chapter is shown in Fig. 3.4. It consists of a standard LTI feedback controlled system, similar as in Fig. 3.2 with $\mathcal{C}(s) = \mathcal{C}_{lbw}(s)$, augmented with an add-on variable gain control part. This variable gain part of the total controller $\mathcal{C}_{vg}$ consists of an LTI shaping filter $\mathcal{F}(s)$, and a time-varying variable gain $\alpha(v(t))$ depending on a *scheduling variable* $v(t)$, $t \in \mathbb{R}_{\geq 0}$, which is related to characteristics of the reference signal. In this chapter, and in particular in Section 3.4, we will use the reference velocity as scheduling variable, i.e., $v(t) = \dot{r}(t)$, although other options are imaginable as well. For instance, the variable gain could depend on the reference position, i.e., $v(t) = r(t)$, on the acceleration, i.e., $v(t) = \ddot{r}(t)$, etc. The process of extracting the relevant information, e.g., $v(t) = \dot{r}(t)$, from the reference signal r is indicated by the dashed box in Fig. 3.4. Note that for the particular choices mentioned, the reference information is not required to be known in advance. The variable gain element is given by a mapping $\alpha : \mathbb{R} \to [0, \bar{\alpha}]$, where $\bar{\alpha} \in \mathbb{R}_{>0}$ denotes the maximum value. Let us first consider the situation where $\alpha \in [0, \bar{\alpha}]$ is a *fixed* gain, and study the following cases ($\alpha = 0$ and $\alpha \in (0, \bar{\alpha}]$):

1. If $\alpha = 0$, we have a linear control scheme with linear controller $\mathcal{C}^f_{vg}(s) = \mathcal{C}_{lbw}(s)$;

2. For a *fixed* $\alpha \in (0, \bar{\alpha}]$, we have a linear control scheme with controller

$$\mathcal{C}^f_{vg}(s) = (1 + \alpha\mathcal{F}(s))\mathcal{C}_{lbw}(s). \tag{3.3}$$

Remark 3.1. *The reference-dependent variable-gain controller reduces only to an LTI controller for fixed values of α. Therefore, we denote it by $\mathcal{C}^f_{vg}(s)$ only when α is fixed, and use $\mathcal{C}_{vg}$ with $\alpha(v(t))$ varying over time otherwise.*

The introduction of this variable gain allows us to deal with the conflicting design criteria as described in the introduction and discussed in detail in Section 3.2.1, i.e., preferring a controller that results in a low bandwidth $\underline{\omega}_b$ over a controller that results in a higher bandwidth $\underline{\omega}_b < \omega_b \leq \overline{\omega}_b$, or vise versa, *depending on actual reference information.* In fact, by assigning $\alpha(v(t)) = 0$ to the situation where a low bandwidth is preferable, the user can loop-shape the controller $\mathcal{C}_{lbw}(s)$ such that the best possible performance is obtained for this particular situation. On the other hand, the proposed structure of the reference-dependent variable-gain controller $\mathcal{C}_{vg}$ allows that, by proper design of the variable gain element $\alpha : \mathbb{R} \to [0, \bar{\alpha}]$ and the linear filter $\mathcal{F}(s)$ (see below in Section 3.3.2), the 'bandwidth' ω_b of the variable-gain controller $\mathcal{C}^f_{vg}(s)$ (for fixed values of α) will gradually increase (and can take values in $[\underline{\omega}_b, \overline{\omega}_b]$) for increasing values of $\alpha \in [0, \bar{\alpha}]$.

3.3 Stability conditions and design guidelines

In this section, we present data-based graphical conditions to verify stability and convergence (Demidovich (1961); Pavlov et al. (2006)) of the closed-loop system as in Fig. 3.4 for every $\alpha : \mathbb{R} \to [0, \bar{\alpha}]$ and any choice of scheduling variable v. Hence, the stability will be guaranteed independent of how $\alpha(v(t))$ depends on time as long as it takes values in $[0, \bar{\alpha}]$. Moreover, general design guidelines are provided in section 3.3.2.

3.3.1 Stability and convergence

The system as in Fig. 3.4 belongs to the class of Lur'e-type systems, see, e.g., Khalil (2000), as depicted schematically in Fig. 3.5. Such systems consist of a linear dynamical part in feedback with with a time-varying, but memoryless, variable gain element given (in this case) by $\varphi(v(t), e)$. Consider therefore Fig. 3.5, in which the linear part is given by

$$\mathfrak{L}\{e\} = \mathcal{G}_{eu}(s)\mathfrak{L}\{u\} + \mathcal{G}_{ew}(s)\mathfrak{L}\{w\}, \tag{3.4}$$

where the external inputs are denoted by $w = [r \;\; d^\top]^\top \in \mathbb{R}^{n_w}$, with reference input $r \in \mathbb{R}$ and a vector $d = [d_i^\top \;\; d_o^\top \;\; \eta]^\top \in \mathbb{R}^{n_d}$ containing the external disturbances. In (3.4), the transfer function between 'input' u and 'output' e, see Fig. 3.5, is given by

$$\mathcal{G}_{eu}(s) = \mathcal{F}(s)\underbrace{\frac{\mathcal{P}(s)\mathcal{C}_{lbw}(s)}{1 + \mathcal{P}(s)\mathcal{C}_{lbw}(s)}}_{=:\mathcal{T}(s)}, \tag{3.5}$$

in which $\mathcal{T}(s)$ represents the complementary sensitivity function, and the transfer function between the external inputs w and e is given by

$$\mathcal{G}_{ew}(s) = \left[\mathcal{S}(s) \;\; -\mathcal{S}_p(s) \;\; -\mathcal{S}(s) \;\; -\mathcal{S}(s)\right], \tag{3.6}$$

in which $\mathcal{S}(s)$ and $\mathcal{S}_p(s)$ are given in (3.1) and (3.2), respectively, with $\mathcal{C}(s) = \mathcal{C}_{lbw}(s)$. The closed-loop dynamics can be represented in state-space form as

$$\dot{x} = Ax + Bu + B_w w \tag{3.7a}$$
$$e = Cx + D_w w \tag{3.7b}$$
$$u = -\varphi(v, e) \tag{3.7c}$$

with state $x \in \mathbb{R}^{n_x}$, (A, B, C) minimal such that $\mathcal{G}_{eu}(s) = C(sI - A)^{-1}B$, and $\mathcal{G}_{ew}(s) = C(sI - A)^{-1}B_w + D_w$ with I an identity matrix of appropriate dimensions. Finally, the variable gain in Fig. 3.5 depends on the reference via

$$\varphi(v, e) = \alpha(v)e, \tag{3.8}$$

for all $v \in \mathbb{R}$ and $e \in \mathbb{R}$.

If (the origin of the) the system (3.7), (3.8) is asymptotically stable for a *fixed* value of α (in absence of external disturbances, i.e., $w = 0$), it is known (via linear system theory) that it exhibits a unique, bounded, and globally asymptotically stable steady-state solution (irrespective of the initial condition) for any bounded external variables, see, e.g., Hespanha (2009). Clearly, such a property does not hold in general for nonlinear systems such as the closed-loop system with the variable gain as studied here. However, here we establish conditions such that

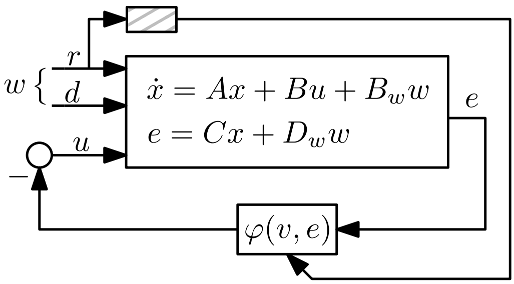

Fig. 3.5. Schematic representation of a Lur'e-type description of the reference-dependent variable-gain controlled system.

these favorable properties can be guaranteed for systems with time-varying gains $\alpha(v(t))$, independent of the particular reference r (recall that $v(t) = \dot{r}(t)$). In the literature, such a property is called convergence, see Demidovich (1961); Pavlov et al. (2006). Before we provide conditions to ensure that our proposed variable-gain control design renders the closed-loop system (3.7), (3.8) convergent, we first provide a formal definition of a convergent system. Therefore, consider a general nonlinear system description of the form

$$\dot{x} = f(x, w, t) \tag{3.9}$$

with state $x \in \mathbb{R}^{n_x}$ and input $w \in \mathbb{R}^{n_w}$. The function $f(x, w, t)$ is locally Lipschitz in x, continuous in w and piecewise continuous in t. Moreover, the inputs $w(t)$ are assumed to be piecewise continuous functions of time defined for all $t \in \mathbb{R}$.

Definition 3.1. *Demidovich (1961); Pavlov et al. (2006) System* (3.9) *is said to be*

- *convergent if there exists a solution $\bar{x}_w(t)$ such that*
  - *(i) $\bar{x}_w(t)$ is defined for all $t \in \mathbb{R}$ and bounded for all $t \in \mathbb{R}$,*
  - *(ii) $\bar{x}_w(t)$ is globally asymptotically stable;*
- *exponentially convergent if it is convergent and $\bar{x}_w(t)$ is globally exponentially stable.*

In Definition 3.1, the solution $\bar{x}_w(t)$ (which depends on the input $w(t)$) denotes the steady-state solution of the system (3.9). It states that any solution of a convergent system converges to a bounded steady-state solution, independent of its initial conditions. For exponentially convergent systems, this steady-state solution is also unique, see Pavlov et al. (2006). Being able to ensure convergence of the variable-gain controlled system (3.7), (3.8) is advantageous from a stability, a performance and a design point-of-view. Namely, convergence implies firstly, stability for any reference and disturbance realization, and secondly, the existence of a unique steady-state solution. The latter property allows for a unique steady-state performance evaluation in the face of disturbances, and, as such, it also results in an easier design and tuning of the variable-gain controller $\mathcal{C}_{vg}$. The following conditions are sufficient to establish that a system of the form (3.7), (3.8) is exponentially convergent.

Theorem 3.1. *Consider system* (3.7) *with* $\varphi(v, e)$ *given by* (3.8), *in which* $\alpha : \mathbb{R} \to [0, \bar{\alpha}]$ *for some* $\bar{\alpha} \in \mathbb{R}_{>0}$. *Suppose that*

(I) The system matrix A is Hurwitz;

(II) The frequency response function $\mathcal{G}_{eu}(j\omega)$ *as in* (3.6) *satisfies*

$$\frac{1}{\bar{\alpha}} + Re(\mathcal{G}_{eu}(j\infty)) > 0, \tag{3.10}$$

and

$$\frac{1}{\bar{\alpha}} + Re(\mathcal{G}_{eu}(j\omega)) > 0 \quad \text{for all} \;\; \omega \in \mathbb{R}. \tag{3.11}$$

Then, system (3.7), (3.8) *is exponentially convergent.*

Proof. The proof can be found in Appendix A.2.1. □

Remark 3.2. *Condition (I) of Theorem 3.1 will be satisfied by proper controller design of* $\mathcal{C}_{lbw}(s)$. *This is due to the fact that if the open-loop* $\mathcal{P}(s)\mathcal{C}_{lbw}(s)$ *satisfies the Nyquist stability criterion, see, e.g., Skogestad and Postlethwaite (2005), the complementary sensitivity function* $\mathcal{T}(s)$ *has all its poles located in the complex left half plane (LHP). In addition, if the shaping filter* $\mathcal{F}(s)$ *is designed such that it has no unstable poles, the transfer function* $\mathcal{G}_{eu}(s)$ *as in* (3.6) *will have all its poles located in the LHP as well. As a result, the system matrix A of* (3.7) *will be a Hurwitz matrix. Moreover, note that for many motion systems* $\mathcal{G}_{eu}(j\omega) \to 0$ *for* $\omega \to \infty$, *resulting in condition* (3.10) *being satisfied automatically.*

3.3.2 Design and tuning guidelines

In this section, we present a systematic design approach of a reference-dependent variable-gain controller $\mathcal{C}_{vg}$ as in Fig. 3.4, where we assume that a plant model $\mathcal{P}(s)$ is available, e.g., identified based on measured frequency response data. This approach consists of four steps.

Step 1: *Study the control trade-off.*

The first step consists of studying the control design trade-off in greater detail, which can be done in a model-based environment as well as by means of experiments. The following knowledge is required to perform this study:

- The minimum and maximum scheduling variable under which the system needs to operate, i.e., determine $\underline{v}$ and $\overline{v}$ such that $v(t) \in [\underline{v}, \overline{v}]$ for all $t \in \mathbb{R}_{\geq 0}$;

- A performance measure $J(v, \omega_b)$ depending on the scheduling variable v and the bandwidth ω_b, typically related to the application at hand (in this chapter, we assume that a low J corresponds to a good performance);

- [In case of a model-based study] A (rough) estimation of the types, and the corresponding frequency ranges, of the disturbances acting on the system, i.e., d_i, d_o and η in Fig. 3.2.

Consider the model structure as in Fig. 3.2 in which (in case of a model-based study) we use the estimated plant model $\mathcal{P}(s)$. First, we define a grid of constant scheduling variables $v_{c,i}$, $i = 1, 2, \ldots, n$, satisfying $v_{c,i} \in [\underline{v}, \overline{v}]$ with $\underline{v} = v_{c,1} < v_{c,2} < \ldots < v_{c,n-1} < v_{c,n} = \overline{v}$. Moreover, we design m LTI controllers $\mathcal{C}_j(s)$ (see Fig. 3.2) with each a different bandwidth $\omega_{b,j}$, $j = 1, 2, \ldots, m$. Then, for *each* of these constant scheduling variables $v_{c,i}$, $i = 1, 2, \ldots, n$, we evaluate the performance for *each* of these LTI controllers $\mathcal{C}_j(s)$, $j = 1, 2, \ldots, m$. This allows us to (approximately) characterize the performance as a function of the bandwidth for each $v_{c,i}$, $i = 1, 2, \ldots, n$. This results in 'performance' curves as schematically depicted in Fig. 3.6. This figure represents the control design trade-off because each particular value $v_{c,i}$ for the scheduling variable will typically show optimal performance (minima in Fig. 3.6, indicated by the black dots) for a different bandwidth ω_b. We denote this 'optimal bandwidth' by $\omega_{b,opt,i}$ for the corresponding scheduling variable $v_{c,i}$, and is given by

$$\omega_{b,opt,i} = \arg\min_{\omega_b} J(v_{c,i}, \omega_b), \tag{3.12}$$

for $i = 1, 2, \ldots, n$.

Step 2: *Design of a low-bandwidth and high-bandwidth controller $\mathcal{C}_{lbw}(s)$ and $\mathcal{C}_{hbw}(s)$, respectively.*
Based on **Step 1**, we select the desired low bandwidth $\underline{\omega}_b$ as

$$\underline{\omega}_b = \min_{i=1,2,\ldots,n} \omega_{b,opt,i}, \tag{3.13}$$

and design the corresponding LTI controller $\mathcal{C}_{lbw}(s)$. In **Step 4**, we will ensure that the variable-gain controller $\mathcal{C}^f_{vg}(s)$ represents $\mathcal{C}_{lbw}(s)$ if $\alpha(\underline{v}) = 0$. The LTI controller $\mathcal{C}_{hbw}(s)$ is designed[1] such that the highest achievable bandwidth $\overline{\omega}_b$ is obtained under sufficient robustness margins[2], such as gain margin, modulus margin, phase margin etc., see, e.g., Skogestad and Postlethwaite (2005). This

[1]Note that both $\mathcal{C}_{lbw}(s)$ and $\mathcal{C}_{hbw}(s)$ can be designed using well-known frequency-domain loop-shaping techniques, see, e.g., Steinbuch and Norg (1998).

[2]In this respect, note that (in general) $\overline{\omega}_b \neq \max_{i=1,2,\ldots,n} \omega_{b,opt,i}$.

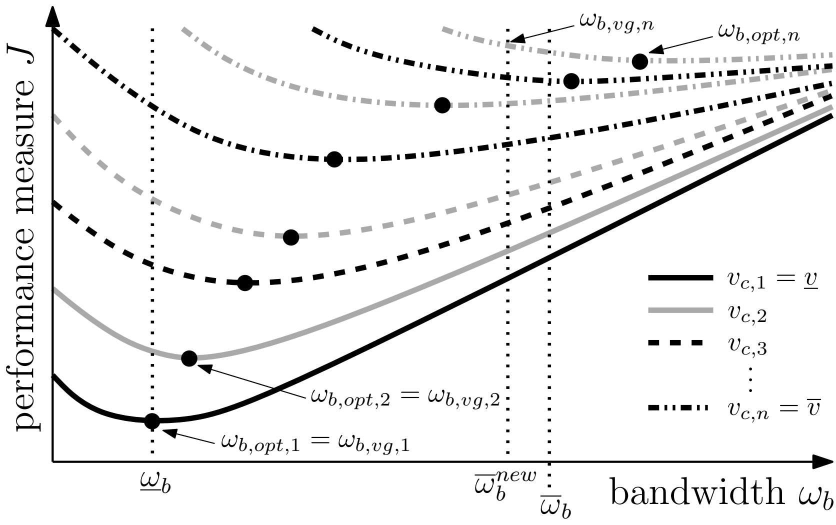

Fig. 3.6. Schematic representation of a possible control trade-off for a range of constant scheduling variables $v_{c,i}$, $i = 1, 2 \ldots, n$, in the set $v_{c,i} \in [\underline{v}, \overline{v}]$ with $v_{c,1} = \underline{v}$ and $v_{c,n} = \overline{v}$.

high-bandwidth controller $\mathcal{C}_{hbw}(s)$ is the 'target' controller for the high gain situation, i.e., when $\alpha(\overline{v}) = \bar{\alpha}$ we aim to approximate $\mathcal{C}_{hbw}(s)$ with our variable gain controller $\mathcal{C}_{vg}^{f}(s)$. How to achieve this will be discussed in the next step.

Step 3: *Design the linear filter $\mathcal{F}(s)$ and determine the maximum allowable gain $\bar{\alpha}$.*
Once $\underline{\omega}_b$ and $\overline{\omega}_b$ have been determined in **Step 2**, we will design $\mathcal{F}(s)$ and $\bar{\alpha}$ with the aim to vary the 'bandwidth' ω_b of the resulting controller $\mathcal{C}_{vg}$ on-line in the set $[\underline{\omega}_b, \overline{\omega}_b]$, depending on the scheduling variables v. The control architecture of the proposed variable-gain controller as in Fig. 3.4 results in $\mathcal{C}_{vg}^{f}(s) = \mathcal{C}_{lbw}(s)$ for the limit case $\alpha = 0$. For the other limit case, $\alpha = \bar{\alpha}$, we aim to design $\mathcal{F}(s)$, and determine $\bar{\alpha}$, such that

$$(1 + \bar{\alpha}\mathcal{F}(s))\mathcal{C}_{lbw}(s) = \mathcal{C}_{hbw}(s). \tag{3.14}$$

When satisfying (3.14) *exactly*, we obtain values of $\bar{\alpha}$ and $\mathcal{F}(s)$ (which is normalized to gain 1 when $j\omega = 0$) corresponding to an 'optimal high-gain situation', satisfying

$$\bar{\alpha}_{opt}\mathcal{F}_{opt}(s) = \frac{\mathcal{C}_{hbw}(s)}{\mathcal{C}_{lbw}(s)} - 1. \tag{3.15}$$

From (3.15) and the normalization $\mathcal{F}_{opt}(j\omega) = 1$ when $j\omega = 0$, $\bar{\alpha}_{opt}$ and $\mathcal{F}_{opt}(s)$

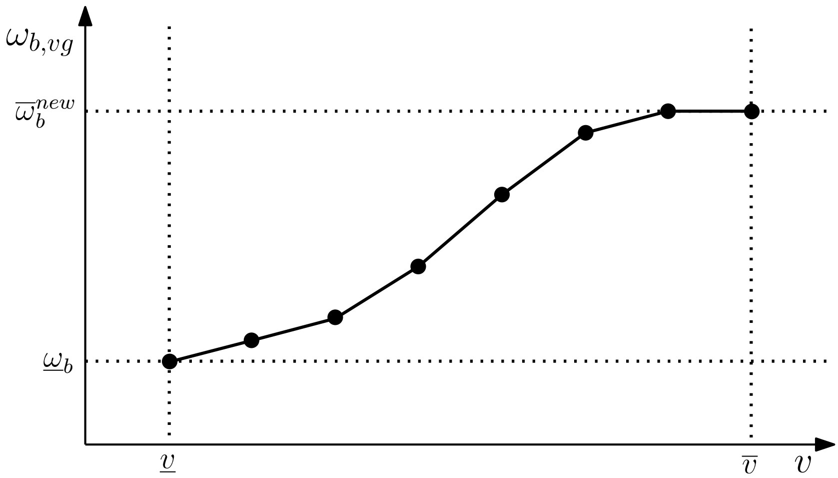

Fig. 3.7. Schematic representation of a possible relation between the scheduling variables $v_c \in [\underline{v}, \overline{v}]$, and the desired bandwidth $\omega_{b,vg} \in [\underline{\omega}_b, \overline{\omega}_b^{new}]$ of the variable gain controller $\mathcal{C}_{vg}$.

can be determined uniquely. However, this optimal choice might not always be practically feasible due to the following reasons:

1. This approach does *not* guarantee a priori the closed-loop stability of (3.7), (3.8), for the obtained $\bar{\alpha}_{opt}$ and $\mathcal{F}_{opt}(s)$;

2. This approach of fixing $\bar{\alpha}$ and $\mathcal{F}(s)$ leaves the designer with no possibilities to influence the shape of $\mathcal{G}_{eu}(j\omega)$ as in (3.6), e.g., through the manual shaping of $\mathcal{F}(s)$, in order to satisfy the circle criterion condition (3.11) leading to stability and convergence guarantees, see, e.g., Heertjes et al. (2005); van de Wouw et al. (2008);

3. If the difference between the low-bandwidth $\underline{\omega}_b$ and high-bandwidth $\overline{\omega}_b$ is large, this approach might yield a high gain $\bar{\alpha}_{opt}$. Consequently, for such high values of $\bar{\alpha}_{opt}$, we have that $\frac{1}{\bar{\alpha}_{opt}} \rightarrow 0$. Therefore, in such cases, the frequency response function $\mathcal{G}_{eu}(j\omega)$ as in (3.6), with $\bar{\alpha} = \bar{\alpha}_{opt}$ and $\mathcal{F}(s) = \mathcal{F}_{opt}(s)$, is required to be (almost) positive real in order to satisfy the conditions of Theorem 3.1, which in many (motion control) cases is a too strict requirement.

Therefore, it is often better to design the filter $\mathcal{F}(s)$ manually by loop-shaping techniques, in which $\mathcal{F}_{opt}(s)$ resulting from (3.15) can be used as a target design. In this respect, if (3.14) is not exactly satisfied for the resulting $\mathcal{F}(s)$ and $\bar{\alpha}$, the target bandwidth $\overline{\omega}_b$ can most probably not be attained anymore. Therefore, from this point onward, the bandwidth of the resulting controller $\mathcal{C}_{vg}^f(s) = (1+$

$\bar{\alpha}\mathcal{F}(s))\mathcal{C}_{lbw}(s)$ is denoted by $\overline{\omega}_b^{new}$, for which it typically holds that $\overline{\omega}_b^{new} \leq \overline{\omega}_b$. How to apply this approach will be demonstrated in Section 3.4.2.

Step 4: *Design the 'reference-to-gain' mapping* $\alpha : [\underline{v}, \overline{v}] \to [0, \bar{\alpha}]$.
The last step in the design of a reference-dependent variable-gain controller $\mathcal{C}_{vg}$ is to design the mapping $\alpha : [\underline{v}, \overline{v}] \to [0, \bar{\alpha}]$. We start by establishing a relation between the 'bandwidth' ω_b of $\mathcal{C}_{vg}$ as a function of $\alpha \in [0, \bar{\alpha}]$. Note that, for fixed values of α, the controller $\mathcal{C}_{vg}^f(s)$ as in (3.3) (in which the shaping filter $\mathcal{F}(s)$ and maximal gain $\bar{\alpha}$ follow from **Step 3**) is linear and that the resulting bandwidth can be straightforwardly assessed. In particular, for each $\alpha_i \in [0, \bar{\alpha}]$, $i = 1, 2, \ldots, n$, on a discrete grid, we assess the corresponding bandwidth $\omega_{b,i}$, $i = 1, 2, \ldots, n$. By interpolation, the relation

$$\omega_b = H_{bw}(\alpha) \tag{3.16}$$

can be approximately determined for all $\alpha \in [0, \bar{\alpha}]$. Here we assume that the map $H_{bw} : [0, \bar{\alpha}] \to [\underline{\omega}_b, \overline{\omega}_b^{new}]$ is strictly monotone (although one can also deal with other situations). Then, the desired 'reference-to-gain' mapping $\alpha : [\underline{v}, \overline{v}] \to [0, \bar{\alpha}]$ is given by

$$\alpha(v) = \arg \min_{0 \leq \alpha \leq \bar{\alpha}} J(v, H_{bw}(\alpha)). \tag{3.17}$$

Remark 3.3. *An alternative (perhaps more intuitive but less general) approach to design the mapping* $\alpha : [\underline{v}, \overline{v}] \to [0, \bar{\alpha}]$ *comprises three steps:*

1. *First, we establish a relation between the scheduling variable* $v \in [\underline{v}, \overline{v}]$ *and the 'desired bandwidth'* $\omega_{b,vg} \in [\underline{\omega}_b, \overline{\omega}_b^{new}]$*, of the variable-gain controller* $\mathcal{C}_{vg}$*. Based on the analysis in **Step 1** (resulting in an optimal bandwidth* $\omega_{b,opt}$ *as a function of the scheduling variable* v_c*), **Step 2** (resulting in a minimum and maximum attainable bandwidth* $\underline{\omega}_b$, $\overline{\omega}_b$*, respectively), and **Step 3** (resulting in a new maximum attainable bandwidth* $\overline{\omega}_b^{new}$*), this relation is given by*

$$\omega_{b,vg}(v) = arg \min_{\underline{\omega}_b \leq \omega_b \leq \overline{\omega}_b^{new}} J(v, \omega_b). \tag{3.18}$$

Note that the values in (3.18) *for* $v = v_{c_1}, v_{c_2}, \ldots, v_{c_n}$ *are determined based on the curves computed in **Step 1**, see Fig. 3.6, while interpolation is used to obtain the values for* $w_{b,vg}(v)$ *in between. This is schematically depicted in Fig. 3.7. Note that, for those* $\omega_{b,opt,i} > \overline{\omega}_b^{new}$, $i \in \{1, 2, \ldots, n\}$*, we typically take* $\overline{\omega}_b^{new}$ *(see Fig. 3.6 and Fig. 3.7), and thus* $\omega_{b,vg}(v_i) = \min(\omega_{b,opt,i}, \overline{\omega}_b^{new})$, $i \in \{1, 2, \ldots, n\}$*, because a higher bandwidth cannot be obtained due to robust stability reasons;*

2. *In the second step, we establish a relation between the 'bandwidth'* ω_b *of* $\mathcal{C}_{vg}$ *as a function of* $\alpha \in [0, \bar{\alpha}]$*. This has been detailed above in **Step 4**, and resulted in the expression* (3.16)*, in which* H_{bw} *is required to be strictly monotone;*

3. *The third part consists of combining both relations (constructed in parts 1) and 2) above), which yields the desired 'reference-to-gain' mapping* $\alpha : [\underline{v}, \overline{v}] \to [0, \bar{\alpha}]$, *and is given by*

$$\alpha(v) = H_{bw}^{-1}(\omega_{b,vg}(v)). \tag{3.19}$$

In this respect, (3.17) *is more general and does not even require the strict monotonicity of* H_{bw} *as in* (3.16).

Remark 3.4. *The proposed first part in* ***Step 4*** *(i.e., establishing a relation between the scheduling variable* v *and the 'desired bandwidth'* $\omega_{b,vg}$*) is a 'guideline' of a possible design procedure. Especially when a model-based study is performed in* ***Step 1****, it depends on the accuracy of the obtained model and the disturbance identification. Nevertheless, it provides the user with valuable insights on how the 'bandwidth'* $\omega_{b,vg}$ *of the variable-gain controller* $\mathcal{C}_{vg}$ *should vary as a function of the scheduling variable* v*. Of course, the user can re-design (parts of) this relation, e.g., based on experimental knowledge, if desirable. Note that this will not jeopardize stability and convergence of the system* (3.7), (3.8) *as long as* $\alpha(v(t)) \in [0, \bar{\alpha}]$, $t \in \mathbb{R}_{\geq 0}$ *due to the stability and convergence guarantees obtained in* ***Step 3***.

3.4 Case-study on an industrial nano-positioning motion system

The nano-positioning motion system considered in this chapter is an experimental setup of a high-precision motion system that requires movements with velocities ranging from standstill, to nanometers per second (nm/s), to even millimeters per second (mm/s), all with (sub)nanometer resolution. The nano-positioning motion system has several key modes of operation, namely: (i) standstill, (ii) constant velocities in a broad range, and (iii) fast (user-operated) point-to-point movements. Due to the presence of multiple disturbance sources in various frequency ranges (depending also on the mode of operation), this results in conflicting control design trade-offs. As such, this nano-positioning motion system forms a relevant case-study to validate the practical feasibility of the proposed 'bandwidth-on-demand' variable-gain control strategy, see also Section 3.2.1.

The experimental setup will be discussed in Section 3.4.1. The design[3] of a reference-dependent variable-gain controller, using the guidelines presented in Section 3.3.2, will be discussed in Section 3.4.2, after which we present the experimental results in Section 3.4.3.

[3] To protect the interests of the manufacturer, we can not provide concrete information about the reference velocities (and thus scheduling variables v) and the disturbance modeling. For the same reason, all figures in this section have either been scaled or use blank axes in terms of units.

3.4.1 Nano-positioning motion stage

The nano-positioning motion system is driven by piezoelectric actuators and controlled by an xPC Target system coupled to a host computer, which allows us to execute Matlab/Simulink controller implementations in real-time. The experimental setup is positioned on a vibration isolation table, and equipped with a 1^{st}-order 100 Hz low-pass actuation filter $\mathcal{P}_{act}(s)$ in the hardware to filter off high-frequency actuator noise. This low-pass actuation filter $P_{act}(s)$ is given by the transfer function

$$\mathcal{P}_{act}(s) = \frac{1}{\frac{1}{2\pi 100}s + 1}. \tag{3.20}$$

The measured frequency response functions of the plant $\mathcal{P}_n(j\omega)$ with and without the additional low-pass filter, i.e., $\mathcal{P}_n(j\omega)\mathcal{P}_{act}(j\omega)$ and $\mathcal{P}_n(j\omega)$, respectively, are depicted in Fig. 3.8. This shows that the plant $\mathcal{P}_n(j\omega)$ behaves as a rigid-body system in the frequency range of interest. Moreover, Fig. 3.8 reveals the presence of a significant, and thus bandwidth-limiting, delay.

The experimental nano-positioning motion setup operates in a lab-environment instead of in its dedicated application. Therefore, additional disturbances are emulated to recover the real situation in the application as much as possible. Based on measurement data, an output disturbance $d_{o,add} = \mathcal{H}(s)\varepsilon$ has been identified, where the magnitude of $\mathcal{H}(j\omega)$ is depicted in Fig. 3.9 and ε is normally distributed white noise with zero mean and variance $\lambda_\varepsilon^2 = (2\cdot 10^{-9})^2$. As a result, a controlled experiment is created that allows us to analyze the influence of the bandwidth ω_b on the performance measure as realistically as possible.

3.4.2 Design of a reference-dependent variable-gain controller

To illustrate the intuitive design of a reference-dependent variable-gain controller, we follow the design process using the guidelines presented in Section 3.3.2, in which, from this point onward, the scheduling variable is taken as the reference velocity, i.e., $v(t) = \dot{r}(t)$, $t \in \mathbb{R}_{\geq 0}$.

Step 1 in the design: In this step, we study the control design trade-off in a model-based environment. Consider therefore Fig. 3.2, in which the plant is given by $\mathcal{P}(s) = \mathcal{P}_n(s)\mathcal{P}_{act}(s)$, with $\mathcal{P}_n(s)$ a 2^{nd}-order LTI model identified on measured FRF data, see Fig. 3.8, and $\mathcal{P}_{act}(s)$ as in (3.20).

Next, the following information is employed:

- The minimum reference velocity is $\underline{v} = 0$;
- The following disturbances are acting on the system:
  - Sensor noise η, modeled as white noise with zero mean and variance $\lambda_\eta^2 = (10^{-9})^2$;

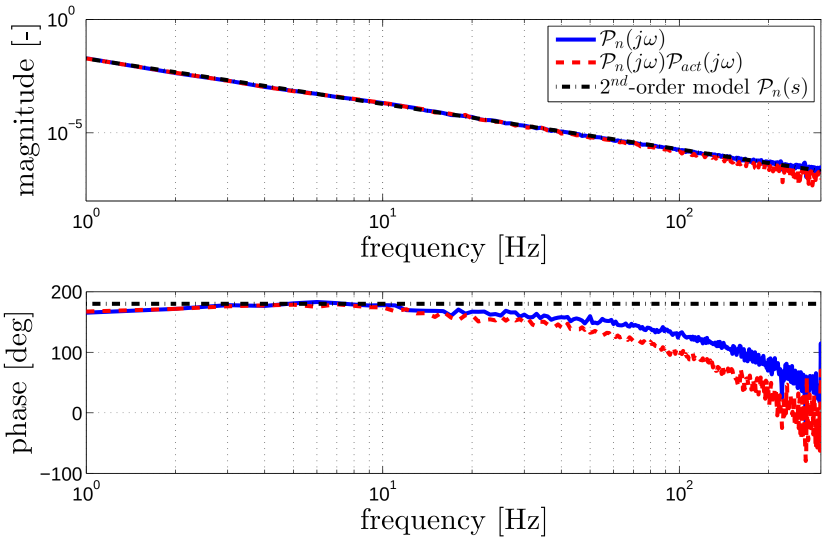

Fig. 3.8. Measured frequency response functions of: the nano-motion stage $\mathcal{P}_n(j\omega)$ (solid blue), the nano-motion stage with additional hardware actuation filter $\mathcal{P}_n(j\omega)\mathcal{P}_{act}(j\omega)$ (dashed red) and of the identified 2^{nd}-order plant model (dash-dotted black).

– Actuator noise $d_{i,act}$ modeled as white noise with zero mean and variance $\lambda^2_{d_{i,act}} = (\sqrt{10^{-19}})^2$;

– Periodic impact disturbances $d_{i,p}$ that depend on the reference velocity v, which are induced by piezoelectric actuators;

– Environmental disturbances $d_{o,add} = \mathcal{H}(s)\varepsilon$, where $\mathcal{H}(s)$ is depicted in Fig. 3.9 and ε is normally distributed white noise with zero mean and variance $\lambda^2_\varepsilon = (2 \cdot 10^{-9})^2$.

- The performance measure is taken as the mean square of the error, which is given for a $N \times 1$ vector e by

$$e_{MS} := \frac{1}{N}\sum_{i=1}^{N} |e_i|^2. \tag{3.21}$$

Next, a range of constant velocities $v_{c,i}$, $i = 1, 2, \ldots, 11$, are created in the set $v_{c,i} \in [0, \overline{v}]$, and 21 LTI controllers $\mathcal{C}_j(s)$ are designed each having a different bandwidth, $j = 1, 2, \ldots, 21$. These controllers all consist of the same types of linear filters, namely a lead filter, integrator and 2^{nd}-order low-pass filter, and

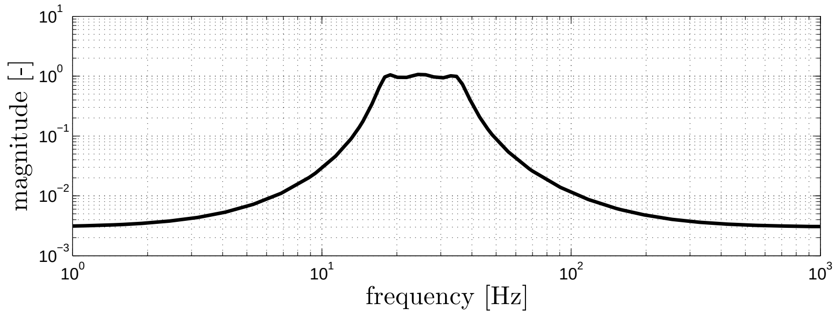

Fig. 3.9. Bode magnitude plot of the disturbance filter $\mathcal{H}(j\omega)$.

Table 3.1. Variables of the individual LTI controllers $\mathcal{C}_j(s)$ as function of the bandwidth $\omega_{b,j}$ (in Hz), $j = 1, 2, \ldots, m$.

Component	**Variables**
Lead	$f_{le1,j} = \frac{1}{4}\omega_{b,j}$, $f_{le2,j} = 4\omega_{b,j}$
Integrator	$f_{I,j} = \frac{1}{9}\omega_{b,j}$
2^{nd}-order low-pass	$f_{l,j} = 6\omega_{b,j}$

are given by

$$\mathcal{C}_j(s) = k_{p,j} \left\{ \frac{s + 2\pi f_{I,j}}{s} \right\} \left\{ \frac{\frac{1}{2\pi f_{le1,j}} s + 1}{\frac{1}{2\pi f_{le2,j}} s + 1} \right\} \left\{ \frac{1}{\frac{1}{(2\pi f_{l,j})^2} s^2 + \frac{1}{2\pi f_{l,j}} s + 1} \right\}, \tag{3.22}$$

where the parameters, which depend on the bandwidth $\omega_{b,j}$, are given in Table 3.1, with $j = 1, 2, \ldots, 21$. By shaping the gains $k_{p,j}$ to the appropriate value, 21 controllers with a different bandwidth $\omega_{b,j} \in [5, 25]$ Hz, $j = 1, 2, \ldots, 21$ have been designed. Then, following the procedure of **Step 1**, the performance as a function of the bandwidth for each $v_{c,i}$, $i = 1, 2, \ldots, 11$, is characterized and depicted in Fig. 3.10. This shows us that indeed the 'optimal bandwidth' $\omega_{b,opt,i}$ increases for increasing reference velocities $v_{c,i}$, $i = 1, 2, \ldots, 11$.

Step 2 in the design: The low-bandwidth is chosen as $\underline{\omega}_b = 5$ Hz. The controller design of $\mathcal{C}_{lbw}(s)$ is based on the plant $\mathcal{P}_n(s)\mathcal{P}_{act}(s)$, thereby explicitly taking the hardware actuation filter $\mathcal{P}_{act}(s)$ into account. The hardware actuation filter has a cut-off frequency of 100 Hz, which does not pose limitations on achieving a bandwidth of $\underline{\omega}_b = 5$ Hz. However, $\mathcal{P}_{act}(s)$ does poses severe limitations on the maximum achievable bandwidth. Therefore, $\mathcal{P}_{act}(s)$ was *removed* from the setup and thus not included in the controller design of $\mathcal{C}_{hbw}(s)$, i.e., this is based on the plant $\mathcal{P}_n(s)$ only. In order to make a fair compar-

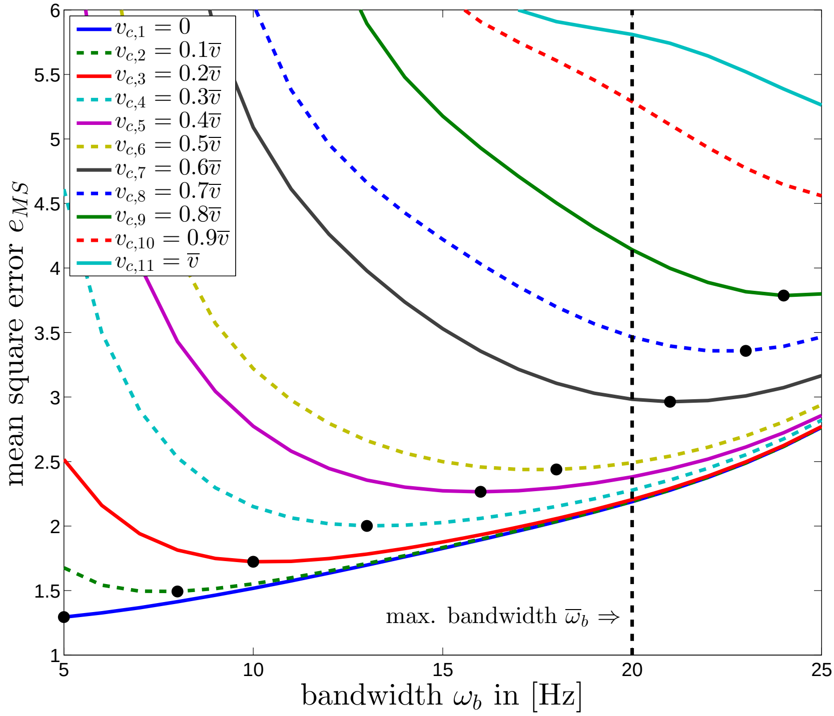

Fig. 3.10. Mean square of the closed-loop error e_{MS}, at various constant reference velocities $v_{c,i}$ as a function of the bandwidth ω_b. The black dots denote the minima of each curve, and thus the optimal bandwidth $\omega_{b,opt,i}$ for each particular reference velocity, $i = 1, 2, \ldots, 11$.

ison with the low-bandwidth situation, an additional 1^{st}-order low-pass filter $\mathcal{P}_{act,hbw}(s)$ is *digitally* included in the design of $\mathcal{C}_{hbw}(s)$. This filter $\mathcal{P}_{act,hbw}(s)$ is designed with cut-off frequency $20\overline{\omega}_b$ Hz, i.e., with the same ratio compared to the low-bandwidth (5 Hz) situation ($20\underline{\omega}_b = 100$ Hz). This finally results in a high-bandwidth controller $\mathcal{C}_{hbw}(s)$ that achieves a bandwidth of $\overline{\omega}_b = 20$ Hz. Fig. 3.11 depicts the resulting open-loop frequency response functions of $\mathcal{P}_n(j\omega)\mathcal{P}_{act}(j\omega)\mathcal{C}_{lbw}(j\omega)$ and $\mathcal{P}_n(j\omega)\mathcal{P}_{act,hbw}(j\omega)\mathcal{C}_{hbw}(j\omega)$, showing that a bandwidth of 5 Hz and 20 Hz is achieved, respectively.

In this respect, it is important to emphasize that the hardware actuation filter $\mathcal{P}_{act}(s)$ will be included during the experiments with the variable-gain controller. In **Step 3**, we will explicitly taking this into account during the design of the shaping filter $\mathcal{F}(s)$.

Step 3 in the design: In this step, we will first determine the shaping filter

$\mathcal{F}_{opt}(s)$ and maximal gain $\bar{\alpha}_{opt}$ for the 'optimal high-gain situation'. Because the actuation filter $\mathcal{P}_{act}(s)$ will be present in the hardware during the experiments with the reference-dependent variable-gain controller $\mathcal{C}_{vg}$, we take this explicitly into account in the design of the shaping filter $\mathcal{F}_{opt}(s)$ (and later in $\mathcal{F}(s)$) in order to make a fair comparison with $\mathcal{C}_{hbw}(s)$ for high values of α. By doing so, the optimal gain $\bar{\alpha}_{opt}$ and optimal shaping filter $\mathcal{F}_{opt}(s)$ follow from

$$\bar{\alpha}_{opt}\mathcal{F}_{opt}(s) = \frac{\mathcal{P}_{act,hbw}(s)\mathcal{C}_{hbw}(s)}{\mathcal{P}_{act}(s)\mathcal{C}_{lbw}(s)} - 1. \tag{3.23}$$

This results in a gain $\bar{\alpha}_{opt} = 129$ and a shaping filter $\mathcal{F}_{opt}(s)$ (which is normalized to gain 1 when $j\omega = 0$) as depicted in Fig. 3.12. It was already argued in Section 3.3.2 that this approach might result in a (too) high gain $\bar{\alpha}_{opt}$ such that satisfying the circle criterion condition of Theorem 3.1 is hard. Indeed, as indicated in Fig. 3.13, the solid green line intersects the dashed-green line and, hence, we do not satisfy $Re(\mathcal{F}_{opt}(j\omega)\mathcal{T}(j\omega)) > -\frac{1}{129}$ for all $\omega \in \mathbb{R}$, for $\mathcal{T}(j\omega)$ as in (3.6) with $\mathcal{P}(j\omega) = \mathcal{P}_n(j\omega)\mathcal{P}_{act}(j\omega)$. Nevertheless, $\mathcal{F}_{opt}(s)$ forms a good starting point for the manual design of $\mathcal{F}(s)$. Closer inspection of Fig. 3.12 shows that the filter $\mathcal{F}(s)$ should have a -1 slope in the frequency range $\sim [0.7, 6]$ Hz, which basically represents the shift of the integrator to higher frequencies, which is realized by designing an appropriate lag filter. In the frequency range $\sim [30, 105]$ Hz we observe a $+3$ slope in Fig. 3.12, which is realized by adding three lead filters. These create phase lead around the high bandwidth by 'canceling' the 2^{nd}-order low-pass filter in $\mathcal{C}_{lbw}(s)$ and the 1^{st}-order low-pass actuation filter $\mathcal{P}_{act}(s)$ around those frequencies. Finally, in order to satisfy the circle criterion condition (3.11), a notch filter is added to fine-tune the shape of $Re(\mathcal{G}_{eu}(j\omega))$. This can be done graphically by means of a Nyquist diagram of $\mathcal{G}_{eu}(j\omega)$ as in (3.6), with $\mathcal{P}(j\omega) = \mathcal{P}_n(j\omega)\mathcal{P}_{act}(j\omega)$. This tuning/loop-shaping procedure results in the shaping filter $\mathcal{F}(s)$ as depicted by the dashed line in Fig. 3.12, and which is given by the following transfer function:

$$\begin{aligned}\mathcal{F}(s) = &\left\{\frac{\frac{1}{2\pi 26}s+1}{\frac{1}{2\pi 105}s+1}\right\}\left\{\frac{\frac{1}{2\pi 30}s+1}{\frac{1}{2\pi 110}s+1}\right\}^2\left\{\frac{\frac{1}{2\pi 6}s+1}{\frac{1}{2\pi 0.5}s+1}\right\}\\ &\times\left\{\frac{\frac{1}{(2\pi 26.5)^2}s^2+\frac{2\cdot 0.85}{2\pi 26.5}s+1}{\frac{1}{(2\pi 80)^2}s^2+\frac{2\cdot 1.3}{2\pi 80}s+1}\right\}.\end{aligned} \tag{3.24}$$

Based on the circle criterion condition (3.11), the maximal gain is selected as $\bar{\alpha} = 29$, thereby allowing for some robustness margin, see Fig. 3.13, which shows that the solid red line stays on the right of the dashed-red line with some margin. Once the circle criterion condition (3.11) has been verified, i.e., $Re(\mathcal{G}_{eu}(j\omega)) > -\frac{1}{29}$ for all $\omega \in \mathbb{R}$, and realizing that $\mathcal{G}_{eu}(j\omega) \to 0$ for $\omega \to \infty$, condition (II) of Theorem 3.1 is satisfied. In order to verify condition (I), note that the low-bandwidth controller $\mathcal{C}_{lbw}(s)$ is designed such that the open-loop

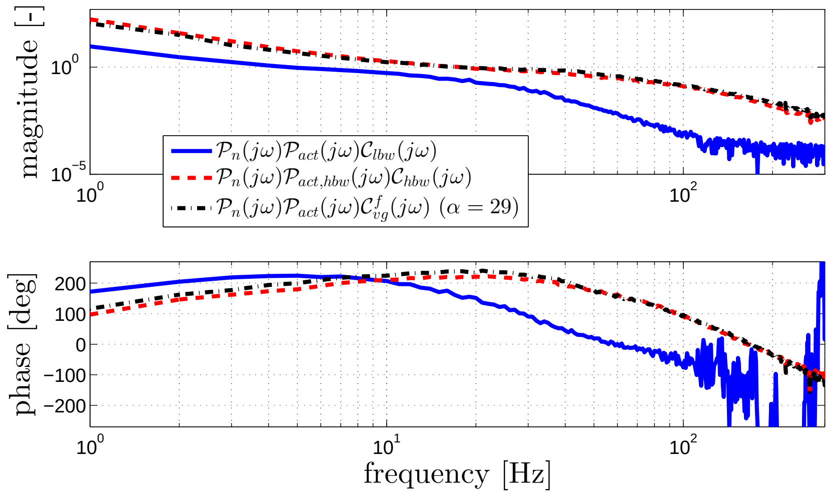

Fig. 3.11. Measured open-loop frequency response functions using the low bandwidth controller, i.e., $\mathcal{P}_n(j\omega)\mathcal{P}_{act}(j\omega)\mathcal{C}_{lbw}(j\omega)$, the high bandwidth controller, i.e., $\mathcal{P}_n(j\omega)\mathcal{P}_{act,hbw}(j\omega)\mathcal{C}_{hbw}(j\omega)$, and the reference-dependent variable-gain controller i.e., $\mathcal{P}_n(j\omega)\mathcal{P}_{act}(j\omega)\mathcal{C}^f_{vg}(j\omega)$, for fixed $\alpha = 29$ (note that for $\alpha = 0$ we obtain $\mathcal{P}_n(j\omega)\mathcal{P}_{act}(j\omega)\mathcal{C}_{lbw}(j\omega)$).

$\mathcal{P}_n(s)\mathcal{P}_{act}(s)\mathcal{C}_{lbw}(s)$ satisfies the Nyquist stability criterion, see, e.g., Skogestad and Postlethwaite (2005). Since the shaping filter $\mathcal{F}(s)$ as in (3.24) has no unstable poles, we also satisfy condition (I) of Theorem 3.1, see Remark 3.2. Hence, we can conclude that all conditions of Theorem 3.1 are being satisfied, which guarantees that the designed reference-dependent variable-gain controlled system is exponentially convergent, independent of how the gain $\alpha(v(t)) \in [0, 29]$, $t \in \mathbb{R}_{\geq 0}$, varies over time.

Due to the proposed design of $\mathcal{C}_{vg}$, the open-loop frequency response of $\mathcal{P}_n(s)\mathcal{P}_{act}(s)\mathcal{C}^f_{vg}(s)$ (for $\alpha = 0$) is exactly equal to $\mathcal{P}_n(s)\mathcal{P}_{act}(s)\mathcal{C}_{lbw}(s)$. However, this does not apply to the high-gain case, i.e., $\mathcal{P}_n(s)\mathcal{P}_{act}(s)\mathcal{C}^f_{vg}(s)$ for $\alpha = 29$ is not equal to $\mathcal{P}_n(s)\mathcal{P}_{act,hbw}(s)\mathcal{C}_{hbw}(s)$, see Fig. 3.11. This is because the shaping filter $\mathcal{F}(s) \neq \mathcal{F}_{opt}(s)$, but was shaped manually to satisfy the closed-loop stability and convergence conditions of Theorem 3.1. In fact, for $\alpha = \bar{\alpha} = 29$, the reference-dependent variable-gain controller is able to achieve a bandwidth of 18 Hz, which is sufficiently close to the desired bandwidth of 20 Hz using $\mathcal{C}_{hbw}(s)$ (see Fig. 3.10).

Step 4 in the design: The 'reference-to-gain' mapping $\alpha : [0, \overline{v}] \to [0, 29]$ is obtained[4] by following the three design parts listed in **Step 4**. The 'reference-to-

[4]The resulting mapping from **Step 4** is slightly adjusted on the basis of some experiments.

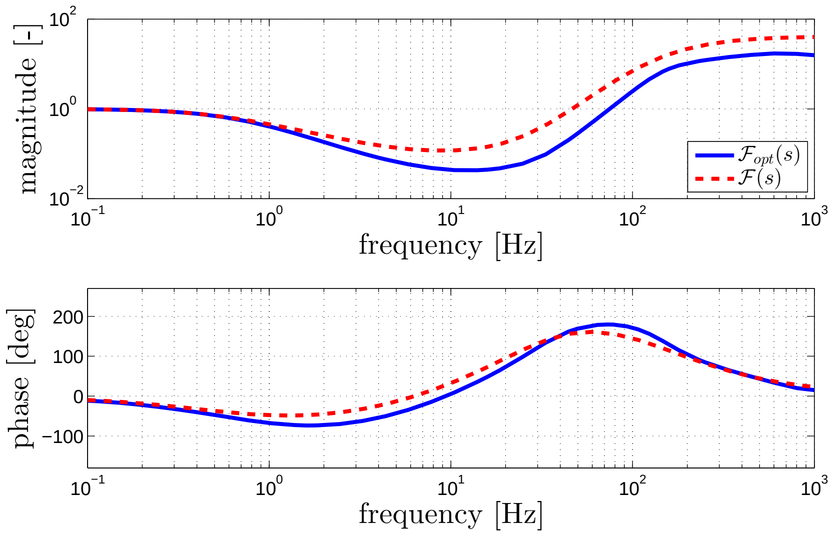

Fig. 3.12. Bode plot of the shaping filters $\mathcal{F}(s)$ and $\mathcal{F}_{opt}(s)$.

gain' mapping $\alpha : [0, \overline{v}] \to [0, 29]$ that is used during the experiments is depicted in Fig. 3.14.

3.4.3 Experimental results

Let us start with presenting the results of the performance analysis of the measured steady-state error e, depicted in Fig. 3.15. The analysis is performed for constant reference velocities $v(t) = v_c$, for all $t \in \mathbb{R}_{\geq 0}$, using the two linear controllers $\mathcal{C}_{lbw}(s)$ and $\mathcal{C}_{hbw}(s)$ and the reference-dependent variable-gain controller $\mathcal{C}_{vg}^{f}(s)$ as in (3.3) for different *fixed* values of $\alpha \in [0, 29]$. Note that for each velocity v_c there exists a corresponding $\alpha \in [0, 29]$, see Fig. 3.14. Let us first focus on low velocities v_c in the range $[0, 0.1 \cdot \overline{v}]$, see the zoom plot in Fig. 3.15. Clearly, in this range both the low-bandwidth controller $\mathcal{C}_{lbw}(s)$ as well as the reference-dependent variable-gain controller $\mathcal{C}_{vg}^{f}(s)$ perform better than the high-bandwidth controller $\mathcal{C}_{hbw}(s)$ as their mean square error e_{MS} is significantly lower (at $v_c = 0$) or, at worst, (approximately) equal (at $v_c = 0.1 \cdot \overline{v}$). At standstill, we achieve (approximately) the same performance with the variable-gain controller $\mathcal{C}_{vg}^{f}(s)$ (with $\alpha = 0$) as for $\mathcal{C}_{lbw}(s)$, while compared to $\mathcal{C}_{hbw}(s)$, the performance is increased by $\sim 66\%$. This is due to the fact that for this case, the disturbances $d_{o,add}$, $d_{i,a}$ and η are being dominant, which are more ampli-

This is due to the fact that a model-based study in **Step 1** might not result in the most optimal relation between the reference velocity and the 'optimal bandwidth', see Remark 3.4, requiring some additional fine-tuning.

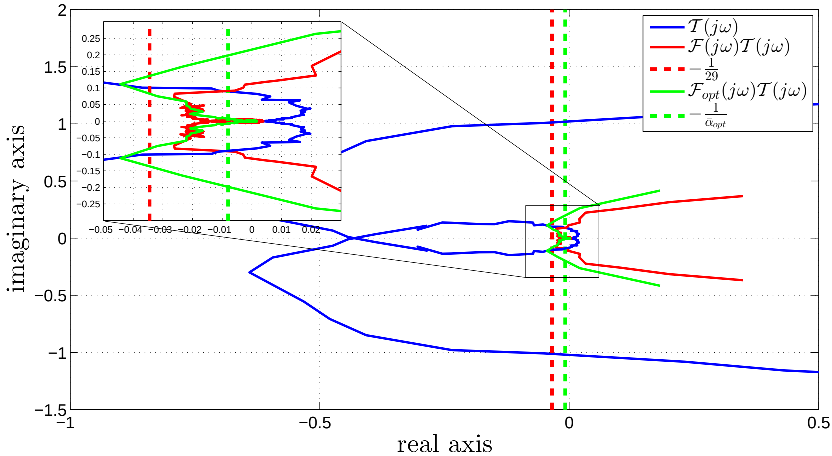

Fig. 3.13. Nyquist diagram for $\mathcal{G}_{eu}(j\omega)$ as in (3.6) for three cases: No shaping filter $\mathcal{F}(s)$ (solid blue), with shaping filter $\mathcal{F}(s)$ as in (3.24) (solid red) and with the optimal shaping filter $\mathcal{F}_{opt}(s)$ (solid green). The circle criterion condition $Re(\mathcal{F}(j\omega)\mathcal{T}(j\omega)) > -\frac{1}{\bar{\alpha}}$, is met for all $\omega \in \mathbb{R}$ with $\mathcal{F}(s)$ as in (3.24) and $\bar{\alpha} = 29$.

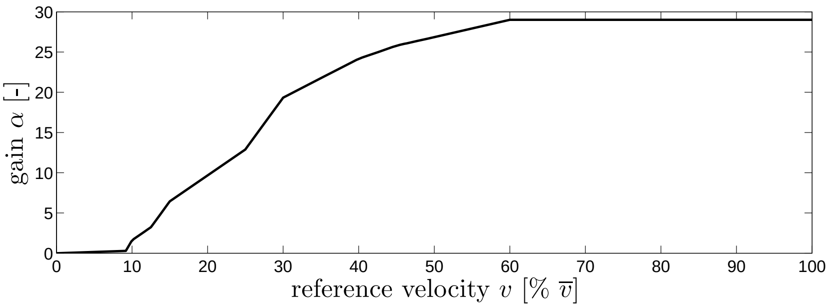

Fig. 3.14. The relationship between the reference velocity v (represented in % of $\overline{v}$) and α.

fied in the high-bandwidth situation. The increase in performance compared to the high-bandwidth situation is also clearly visible in the time-domain, see Fig. 3.16, which shows the measured steady-state error at standstill.

Fig. 3.15 also demonstrates that the higher the reference velocity v_c, the more beneficial it is to have a higher bandwidth controller. This is due to the fact that for increasing reference velocities the periodic disturbance d_p due to the piezo-electric actuator becomes more influential and eventually dominant over $d_{o,add}$,

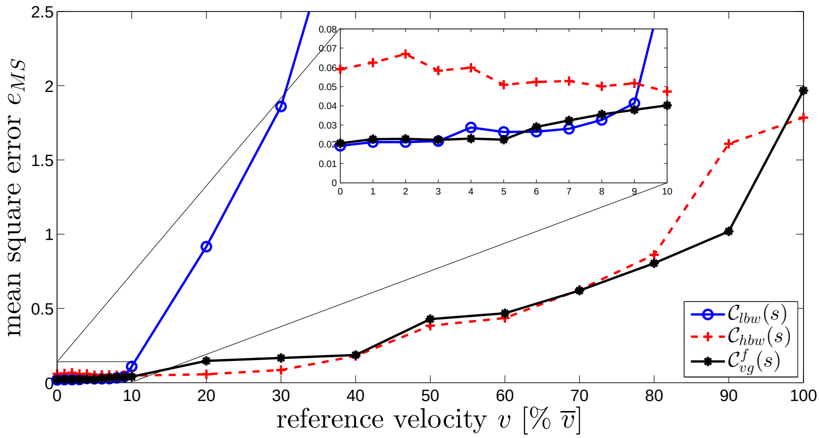

Fig. 3.15. Performance measure of the measured steady-state error e of the nano-motion system during 20 constant velocities v_c in the range $[0, \overline{v}]$ (represented in % of $\overline{v}$).

$d_{i,a}$ and η. The effect of this disturbance is suppressed by increasing the gain α, and as a result, the 'bandwidth' ω_b of the variable-gain controller $\mathcal{C}_{vg}$. With this in mind, let us now focus in Fig. 3.15 on the velocities v_c in the range $[0.1 \cdot \overline{v}, \overline{v}]$. As expected, the low-bandwidth controller $\mathcal{C}_{lbw}(s)$ performs worst, since its bandwidth of 5 Hz is too low to suppress the periodic impact disturbances d_p caused by the piezo actuators. The high-bandwidth controller $\mathcal{C}_{hbw}(s)$ and our reference-dependent variable-gain controller $\mathcal{C}_{vg}^f(s)$ show an approximately similar performance, which is superior compared to that of $\mathcal{C}_{lbw}(s)$.

Fig. 3.17 shows the measured steady-state error at a high constant velocity of $\overline{v}$ for which the low-frequency periodic disturbance d_p is dominant. The performance of the high-bandwidth controller $\mathcal{C}_{hbw}(s)$ and the variable-gain controller $\mathcal{C}_{vg}^f(s)$ are comparable, as was already indicated in Fig. 3.15. It is clear that the periodic impact disturbances d_p are much better suppressed by $\mathcal{C}_{hbw}(s)$ and $\mathcal{C}_{vg}^f(s)$ than using the low-bandwidth controller $\mathcal{C}_{lbw}(s)$.

The previous results were obtained for constant reference velocities, resulting in fixed values of α and, hence, a comparison between $\mathcal{C}_{lbw}(s)$ and $\mathcal{C}_{hbw}(s)$ with a linear controller $\mathcal{C}_{vg}^f(s)$. However, it is (also) important to compare the behavior for *time-varying* velocity profiles, which is depicted in Fig. 3.18. This figure shows the time-domain error behavior for a constant acceleration, starting from $v(t) = 0$ until we move at $v(t) = \overline{v}$ for approximately 5 sec, and then moving back to $v(t) = 0$. Indeed, as indicated in Fig. 3.18, the performance using $\mathcal{C}_{vg}$ for low velocities is comparable with using $\mathcal{C}_{lbw}(s)$, while for high velocities the performance of $\mathcal{C}_{vg}$ is similar to $\mathcal{C}_{hbw}(s)$. This demonstrates that the

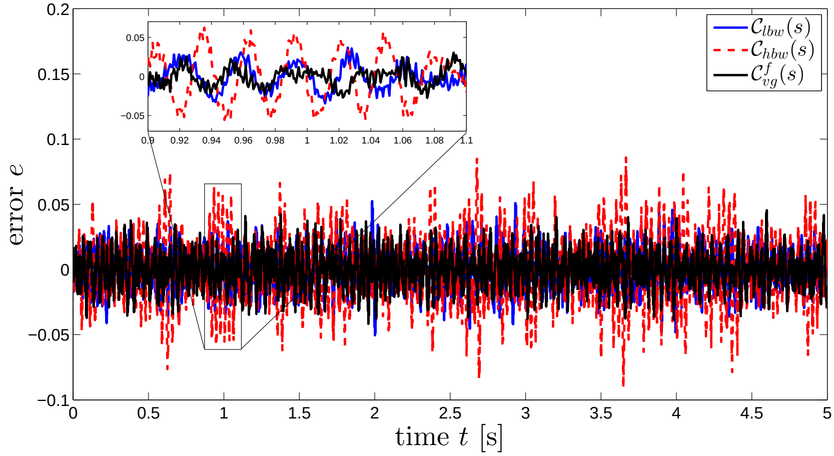

Fig. 3.16. Measured steady-state error e of the nano-motion system during standstill, i.e., velocity $v_c = 0$.

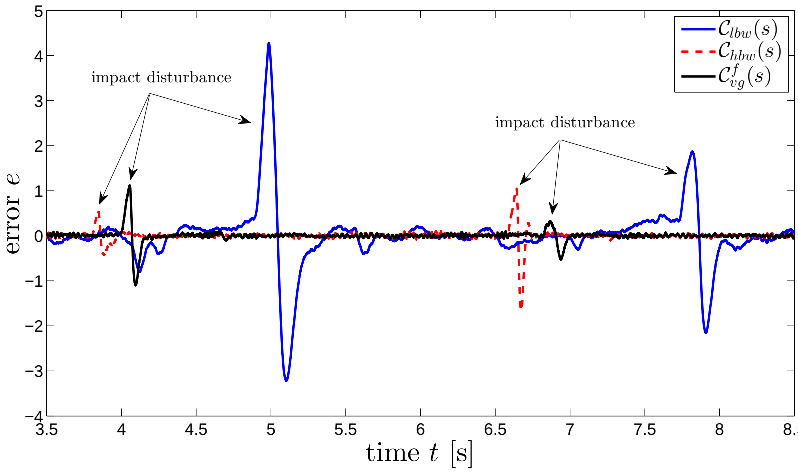

Fig. 3.17. Measured steady-state error e of the nano-motion system during a constant velocity $v_c = \overline{v}$.

proposed reference-dependent variable-gain controller $\mathcal{C}_{vg}$ is able to deal with reference-dependent conflicting control design trade-offs. In fact, the experiments show that the variable-gain controller $\mathcal{C}_{vg}$ can achieve 'the best of both worlds', referring to preferring a controller that results in a low bandwidth $\underline{\omega}_b$

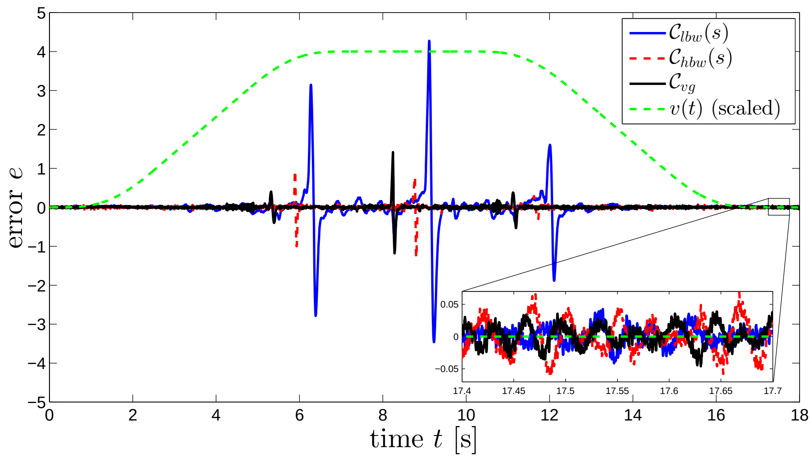

Fig. 3.18. Time-domain performance analysis, moving from $v(t) = 0$ to $v(t) = \overline{v}$ with a constant acceleration, and back to $v(t) = 0$.

over a controller that results in a high bandwidth $\overline{\omega}_b$, or vise versa, depending on the actual reference information.

3.5 Conclusions

In this chapter, we proposed a novel reference-dependent variable-gain control strategy that allows for a varying 'bandwidth' of the feedback controller in order to deal with reference-dependent conflicting control design trade-offs between low-frequency tracking and high-frequency noise suppression. A complete design framework for such reference-dependent variable-gain controllers has been presented, in which most of the design steps involve the usage of state-of-practice frequency-domain loop-shaping tools. This design feature, together with graphical data-based conditions to verify stability and convergence of the variable gain controlled closed-loop system, makes the analysis and design intuitive for control engineers and, as such, connects to the industrial control engineering practice. The design framework has been applied to an industrial nano-positioning motion system with diverse modes of operation, characterized by particular reference velocities, and all having their own specific performance requirement. Despite the challenging and conflicting control goals, it has been experimentally demonstrated that the proposed reference-dependent variable-gain controller indeed has the ability to outperform (fixed bandwidth) linear time-invariant controllers.

Chapter 4

Frequency-domain tools for stability analysis of reset control systems

Abstract – The potential of reset controllers to improve the transient performance of linear (motion) systems has been extensively demonstrated in the literature. The design and stability analysis of these reset controllers generally rely on the availability of parametric models and on the numerical solution of linear matrix inequalities. Both these aspects may hamper the application of reset control in industrial settings. To remove these hurdles and stimulate broader application of reset control techniques in practice, we present new sufficient conditions, based on measured frequency response data on the system to be controlled, to verify input-to-state stability of closed-loop reset control systems. The effectiveness of these conditions is demonstrated through experiments on an industrial piezo-actuated motion system.

4.1 Introduction

A reset controller is a linear time-invariant (LTI) control system of which the state, or a part of the state is reset to a certain value (usually zero) whenever appropriate algebraic conditions on its input and output are satisfied. Reset controllers were proposed in 1958, see Clegg (1958), in order to overcome the inherent performance limitations of linear feedback controllers imposed by Bode's gain-phase relationship. Especially in the last two decades, reset control has regained attention from the control community in both theoretically oriented research, see e.g., Aangenent et al. (2010); Baños and Barreiro (2012); Beker et al. (2004); Nešić et al. (2008); Prieur et al. (2013), as well as in applications

This chapter is based on van Loon et al. (2015a).

Baños and Barreiro (2012); Heertjes et al. (2015); Panni et al. (2014); Zheng et al. (2000). However, despite the potential of a reset controller to improve the transient performance of linear systems, reset controllers are often not so easily embraced by (motion) control engineers in industry. To a large extent, this is caused by the fact that the vast majority of existing tools for the stability analysis and the design of reset controllers rely on parametric models and on solving linear matrix inequalities using those models. As such, they do not interface well with the current industrial (motion) control design practice, in which typically frequency-domain tools and non-parametric models are exploited, see, e.g., Butler (2011). Therefore, an important open problem is to obtain easy-to-use, 'industry-friendly' design tools for reset control systems using frequency-domain techniques as a basis.

In this chapter, we contribute to solving this important open problem and focus, in particular, on deriving stability conditions that are graphically verifiable on the basis of *measured* frequency response data concerning the system dynamics. These conditions apply, amongst others, to the reset condition employed in Aangenent et al. (2010); Forni et al. (2011); Nešić et al. (2008); Zaccarian et al. (2011), and have some connections to recent developments in variable gain control (VGC), see, e.g., Heertjes and Steinbuch (2004); Hunnekens et al. (2015b); van de Wouw et al. (2008). In VGC, the use of the circle criterion, see, e.g., Khalil (2000), is central in obtaining stability conditions based on frequency-domain system models. A key step in this approach for VGC is to write the closed-loop system as a so-called Lur'e-type system, i.e., a feedback interconnection of an LTI dynamical system and a static memoryless nonlinearity, see Khalil (2000). Unfortunately, such an approach it not directly applicable to reset controllers as the closed-loop system would be an interconnection of an LTI dynamical system and a reset controller. This is not a (true) Lur'e-type system as the reset controller (as opposed to the VGC element) consists of a *dynamical* system that exhibits discontinuities (jumps) in the state variables rather than a static memoryless element. As such, applying Lur'e-type stability arguments calls for a new perspective on reset control systems which we will provide in this chapter by abstracting away from the internal dynamics of the reset controller and focusing instead on its input/output behavior, that can be confined to a certain sector bound, see Khalil (2000). This sector bound can subsequently be employed in a circle criterion-like condition. We will formally prove that this will yield sufficient conditions to assess input-to-state stability (ISS), see Cai and Teel (2009); Sontag and Wang (1995), of reset control systems (including the internal dynamics) by evaluating (measured) frequency response data.

The outline of this chapter is as follows. In Section 4.2, we present the control architecture. In Section 4.3, we present our main results. In Section 4.4, we discuss an industrial case study and demonstrate the applicability of the presented results in practice. Finally in Section 4.5, we provide the conclusions.

4.1.1 Nomenclature

The following notational conventions will be used. Let $\mathbb{N}$, $\mathbb{R}$, $\mathbb{R}_{\geq 0}$, $\mathbb{C}$ denote the set of non-negative integers, real numbers, nonnegative real numbers and complex numbers, respectively. The Laplace transform of a signal $x : \mathbb{R}_{\geq 0} \to \mathbb{R}^n$, is denoted by $\mathfrak{L}\{x\}$ and $s \in \mathbb{C}$ denotes the Laplace variable. A function $\gamma : \mathbb{R}_{\geq 0} \to \mathbb{R}_{\geq 0}$ belongs to class-$\mathcal{K}$ if it is continuous, zero at zero, and strictly increasing. A function $\beta : \mathbb{R}_{\geq 0} \times \mathbb{R}_{\geq 0} \to \mathbb{R}_{\geq 0}$ belongs to class-$\mathcal{KL}$ if $\beta(\cdot, t)$ is of class-$\mathcal{K}$ for each $t \geq 0$, and, $\beta(s, \cdot)$ is decreasing and satisfies $\lim_{t\to 0} \beta(s, t) = 0$ for each $s \geq 0$.

4.2 System description and problem formulation

4.2.1 Hybrid closed-loop model

We will mainly focus on the single-input-single-output (SISO) control architecture as depicted in Fig. 4.1, although our results are applicable to other configurations as well, see Remark 4.5 below. The closed-loop system in Fig. 4.1 consists of a linear time-invariant (LTI) plant given by the transfer function $\mathcal{P}(s)$, $s \in \mathbb{C}$, a nominal LTI controller with transfer function $\mathcal{C}(s)$, reference $r \in \mathbb{R}$, output $y_p \in \mathbb{R}$, tracking error $e := r - y_p \in \mathbb{R}$ and external disturbances $d \in \mathbb{R}^{n_d}$. In this figure, $\mathcal{R}$ denotes a reset controller, which is modeled in terms of the hybrid system formalism of Goebel et al. (2012) as

$$\mathcal{R} : \begin{cases} \dot{x}_r = f(x_r, e) & \text{if } (e, -u) \in \mathcal{F} \\ x_r^+ = g(x_r) & \text{if } (e, -u) \in \mathcal{J} \\ u = -C_r x_r \end{cases} \tag{4.1a}$$

with state $x_r \in \mathbb{R}^{n_r}$, controller output $u \in \mathbb{R}$, and where the flow map f in (4.1a) is given for $x_r \in \mathbb{R}^{n_r}$ and $e \in \mathbb{R}$ by

$$f(x_r, e) = A_r x_r + B_r e, \tag{4.1b}$$

and the jump map g in (4.1a) is given for $x_r \in \mathbb{R}^{n_r}$ by

$$g(x_r) = 0. \tag{4.1c}$$

Here, A_r, B_r, C_r are constant real matrices of appropriate dimensions. In (4.1), flow of the reset controller state x_r occurs when the input/output pair $(e, -u)$ is in the flow set $\mathcal{F}$ given by

$$\mathcal{F} := \{(e, -u) \in \mathbb{R}^2 \mid eu \leq -\tfrac{1}{\alpha} u^2\} \tag{4.2a}$$

with $\alpha \in (0, \infty]$, and state resets occur when the input/output pair $(e, -u)$ is in the jump set $\mathcal{J}$ given by

$$\mathcal{J} := \{(e, -u) \in \mathbb{R}^2 \mid eu \geq -\tfrac{1}{\alpha} u^2\}. \tag{4.2b}$$

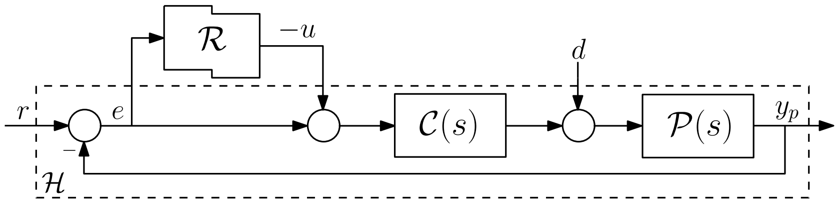

Fig. 4.1. Schematic representation of a reset control scheme.

For a schematically representation of the flow set $\mathcal{F}$ and jump set $\mathcal{J}$, see Fig. 4.2(a). In this respect, note that for $\alpha = \infty$, the flow set $\mathcal{F}$ is the region corresponding to $eu \leq 0$. Later, the concept of hybrid time domains and solutions (solution pairs) of hybrid systems of the form (4.1), (4.2) will be used, which are defined for a general class of hybrid systems with inputs in Appendix A.3.1 for convenience of the reader. For more details on this hybrid modeling framework we refer the reader to Cai and Teel (2009); Goebel et al. (2012).

Remark 4.1. *The general class of reset controllers in* (4.1), (4.2) *encompasses two of the most well-known reset controllers in the literature, i.e., the Clegg integrator and the First-Order-Reset-Element (FORE). Namely, these can be can be modeled as in* (4.1) *using*

$$\textit{Clegg integrator}: \ (A_r, B_r, C_r) = (0, \omega_i, 1), \tag{4.3}$$

$$\textit{FORE}: \ (A_r, B_r, C_r) = (\beta, \omega_i, 1), \tag{4.4}$$

in which $n_r = 1$, $\omega_i \in \mathbb{R}_{\geq 0}$ *represents the integrator gain, and* $\beta \in \mathbb{R}$ *denotes the single pole of the FORE, see, e.g., Zaccarian et al. (2005) and the references therein. By selecting* $\alpha = \infty$, *the reset condition applied in Aangenent et al. (2010); Forni et al. (2011); Nešić et al. (2008); Zaccarian et al. (2005) can be modeled in* (4.2).

Let us adopt the following assumption on the reset controller (4.1), (4.2).

Assumption 4.1. *The pair* (A_r, C_r) *is detectable.*

Remark 4.2. *Note that Assumption 4.1 is trivially satisfied for the Clegg integrator and the FORE because they are both one dimensional systems* ($n_r = 1$), *see Remark 4.1.*

The closed-loop system in Fig. 4.1 can be written as a feedback interconnection between an LTI dynamical system $\mathcal{H}$ and the reset controller $\mathcal{R}$, as depicted in Fig. 4.2(b). In Fig. 4.2(b), the LTI dynamical system $\mathcal{H}$ is given by

$$\mathcal{H}: \begin{cases} \dot{\xi} = A\xi + Bu + B_w w & \text{(4.5a)} \\ e = C\xi + D_w w & \text{(4.5b)} \end{cases}$$

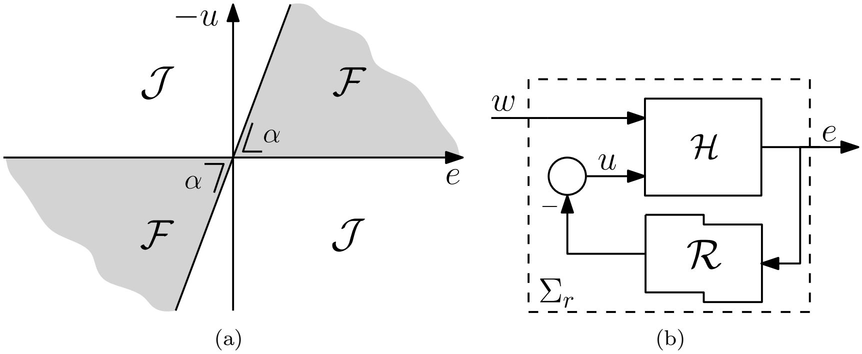

Fig. 4.2. (a) Schematic representation of the flow set $\mathcal{F}$ and jump set $\mathcal{J}$, (b) Feedback interconnection between an LTI dynamical system $\mathcal{H}$ as in (4.5) and $\mathcal{R}$ as in (4.1), (4.2).

with state $\xi \in \mathbb{R}^{n_\xi}$ containing the states of both the plant $\mathcal{P}(s)$ as well as those of the nominal LTI controller $\mathcal{C}(s)$, and the external inputs are denoted by $w = [r \;\; d^\top]^\top \in \mathbb{R}^{n_w}$. Moreover, it is assumed that (A, B, C) is minimal such that

$$\mathfrak{L}\{e\} = \mathcal{G}_{eu}(s)\mathfrak{L}\{u\} + \mathcal{G}_{ew}(s)\mathfrak{L}\{w\}, \tag{4.6}$$

in which the transfer function between 'input' u and 'output' e, see Fig. 4.2(b), is given by

$$\mathcal{G}_{eu}(s) = C(sI - A)^{-1}B = \frac{\mathcal{P}(s)\mathcal{C}(s)}{1 + \mathcal{P}(s)\mathcal{C}(s)}, \tag{4.7}$$

and the transfer function between the external inputs w and e is given by

$$\begin{aligned} \mathcal{G}_{ew}(s) &= C(sI - A)^{-1}B_w + D_w \\ &= \left[\tfrac{1}{1+\mathcal{P}(s)\mathcal{C}(s)} \;\; \tfrac{-\mathcal{P}(s)}{1+\mathcal{P}(s)\mathcal{C}(s)} \right]. \end{aligned} \tag{4.8}$$

The closed-loop system in Fig. 4.2(b) with $\mathcal{H}$ as in (4.5), and $\mathcal{R}$ as in (4.1), (4.2), can be written as the hybrid model

$$\Sigma_r : \begin{cases} \dot{x} \;\;= \bar{A}x + \bar{B}w, & \text{if } (e, -u) \in \mathcal{F}, \quad (4.9\text{a}) \\ x^+ = \bar{A}_r x, & \text{if } (e, -u) \in \mathcal{J}, \quad (4.9\text{b}) \\ u \;\;= -\bar{C}_r x & (4.9\text{c}) \\ e \;\;= \bar{C}x + D_w w & (4.9\text{d}) \end{cases}$$

with augmented state vector $x := [\xi^\top \ \ x_r^\top]^\top \in \mathbb{R}^{n_\xi + n_r}$ and

$$\bar{A} = \begin{bmatrix} A & -BC_r \\ B_rC & A_r \end{bmatrix}, \ \bar{B} = \begin{bmatrix} B_w \\ B_rD_w \end{bmatrix}, \ \bar{A}_r = \begin{bmatrix} I_{n_\xi} & 0 \\ 0 & 0 \end{bmatrix}, \ \bar{C}_r = \begin{bmatrix} 0 \ C_r \end{bmatrix},$$
$$\text{and } \ \bar{C} = \begin{bmatrix} C \ 0 \end{bmatrix}. \tag{4.9e}$$

4.2.2 Problem formulation

The objective of this chapter is to derive sufficient conditions to assess (input-to-state) stability of the hybrid system (4.9) with (4.2), based on (measured) frequency response data of the linear part $\mathcal{G}_{eu}(j\omega)$, $\omega \in \mathbb{R}$, of the closed-loop system dynamics.

4.3 Frequency-domain tools for stability analysis

In this section, we present our main result consisting of novel data-based conditions guaranteeing input-to-state stability (ISS), see Cai and Teel (2009); Sontag and Wang (1995), for reset control systems described by (4.9) with (4.2). Therefore, we employ the following definition of ISS.

Definition 4.1. *The closed-loop hybrid system Σ_r as in* (4.9) *with* (4.2)*, is said to be input-to-state stable (ISS), if for any solution x to* (4.9), (4.2) *for disturbance w, with $\sup_t \operatorname{dom} x = \infty$, it holds that for all $(t, j) \in \operatorname{dom} x$ there exist a $\mathcal{KL}$ function β and $\mathcal{K}$ function γ such that*

$$\|x(t,j)\| \le \beta(\|x(0,0)\|, t) + \gamma\left(\|w_{[0,t]}\|_\infty\right) \tag{4.10}$$

for all $t \in \mathbb{R}_{\ge 0}$.

Remark 4.3. *Our definition of ISS differs from the definition of ISS for hybrid systems as in Cai and Teel (2009). First, we are primarily interested in the evolution of the state x over continuous time t only, and less at 'reset/jump' instances, see Cai and Teel (2009); Goebel et al. (2012). Second, Definition 4.1 only applies to a solution x to* (4.9) *with* (4.2) *for a disturbance w, that is unbounded in the t direction, i.e., $\sup_t \operatorname{dom} x = \infty$. Unfortunately, we cannot formally guarantee that the hybrid system* (4.9) *with* (4.2) *is persistently flowing, i.e., meaning that all maximal solution pairs (x, w) have unbounded domains in the t direction. However, this can be guaranteed by including temporal regularization, see, e.g., Forni et al. (2011); Nešić et al. (2008); Zaccarian et al. (2011) in* (4.1), (4.2)*. Including such time-regularized condition might be natural in our proposed approach, as, the results in Forni et al. (2011); Nešić et al. (2008), indicate that the input/output pair $(e, -u)$ of $\mathcal{R}$ as in* (4.1), (4.2) *might be still* *confined to a (slightly) larger sector* $[0, \bar{\alpha}]$, *with* $\bar{\alpha} \geq \alpha$ *(depending on the disturbances). However, additional research is required to confirm the validity of the above line of thoughts, and to transform it into a systematic design procedure.*

Our main result is presented next in the form of a theorem.

Theorem 4.1. *Consider the system* (4.9) *with* (4.2) *and fixed* $\alpha \in (0, \infty]$, *and let Assumption 4.1 hold. Then, system the* (4.9) *with* (4.2) *is ISS according to Definition 4.1 if the following conditions are satisfied:*

(I) The system matrix A *of* (4.5) *is Hurwitz;*

(II) The transfer function $\mathcal{G}_{eu}$ *as in* (4.8) *satisfies*

$$\frac{1}{\alpha} + Re(\mathcal{G}_{eu}(j\infty)) > 0 \tag{4.11}$$

and

$$\frac{1}{\alpha} + Re(\mathcal{G}_{eu}(j\omega)) > 0 \quad \text{for all} \;\; \omega \in \mathbb{R}. \tag{4.12}$$

Proof. The proof can be found in Appendix A.3.2. □

Remark 4.4. *Considering the conditions in Theorem 4.1, the following remarks are in place:*

1. *Condition (I) will be satisfied by design of a stabilizing feedback controller* $\mathcal{C}(s)$. *This is due to the fact that if the open-loop* $\mathcal{P}(s)\mathcal{C}(s)$ *satisfies the Nyquist stability criterion, see, e.g., Skogestad and Postlethwaite (2005),* $\mathcal{G}_{eu}(s)$ *as in* (4.8) *(which represents the complementary sensitivity function) has all its poles located in the complex left half plane (LHP) and the system matrix* A *of* (4.5) *will be Hurwitz;*
2. *For many (motion) systems* $\mathcal{G}_{eu}(j\omega) \to 0$ *for* $\omega \to \infty$, *resulting in condition* (4.11) *being satisfied automatically;*
3. *The frequency-domain circle-criterion condition* (4.12) *can be verified graphically in a Nyquist diagram using (measured) frequency response data. We care to stress that this represents the power of the conditions in Theorem 4.1 in terms of practical applicability, which will be illustrated using an industrial case study in Section 4.4.*

Remark 4.5. *Note that our conditions are not limited to control configurations as depicted in Fig. 4.1. Consider for instance the configuration as in Fig. 4.3, which is commonly used in the literature, see, e.g., Aangenent et al. (2010); Beker et al. (2004); Nešić et al. (2008); Zaccarian et al. (2011). In such a case, the conditions of Theorem 4.1 still apply for* $\mathcal{G}_{eu}(s) = \mathcal{P}(s)\mathcal{C}(s)$. *However, for many (motion) systems, the conditions in Theorem 4.1 will not yield feasible results in case* $\mathcal{G}_{eu}(s) = \mathcal{P}(s)\mathcal{C}(s)$ *since, e.g., the open-loop* $\mathcal{P}(s)\mathcal{C}(s)$ *is not allowed to contain any integrators.*

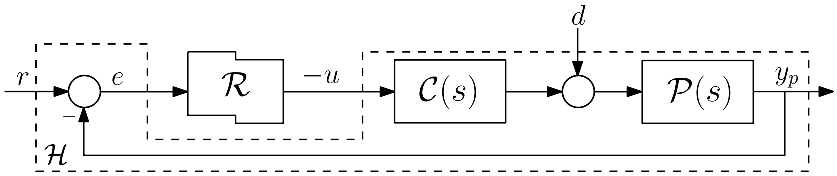

Fig. 4.3. Schematic representation of a reset control scheme.

Remark 4.6. *Our results in Theorem 4.1 show some analogies with the results in Carrasco et al. (2010). In Carrasco et al. (2010), the concept of passivity has been used to analyze stability of reset systems. Key in their work is the fact that a (full) reset system retains the passivity properties of its underlying base system, i.e., the system without the reset part. As a result, $\mathcal{L}_2$-stability conditions are posed which can be verified in the frequency domain.*

4.4 Case-study on an industrial piezo-actuated motion system

In this section, we demonstrate the effectiveness of our newly proposed stability conditions by considering an industrial case study of the control of the z-axis of a piezo-actuated motion system that is used in the lithography industry.

4.4.1 Problem setting

During the process of wafer scanning, light from an (extreme) ultra-violate source travels through an optical path, see, e.g., Butler (2011). This optical path includes a reticle, containing a blueprint of the integrated circuits to be processed, and a lens system. The lens system consists of several lens elements that are individually controlled by piezo actuators during the scanning process. Due to the limited stroke of the piezo actuators, a calibration, or so-called 'shuffle motion', needs to be performed whenever stroke limitations occur (which may happen more than once during a full wafer exposure). The duration of such a shuffle motion should be kept as small as possible because it compromises machine throughput, i.e., the amount of wafers that can be processed per unit of time is decreased because the scanning process is interrupted during a shuffle motion. Moreover, also from a control point-of-view the occurrence of a shuffle motion poses potential problems. Namely, during a shuffle motion the piezo-actuated system operates in an open-loop mode such that after the shuffle, i.e., when closing the loop again, the motion system (which then operates in scanning mode) suffers from an initial value problem. This problem becomes even

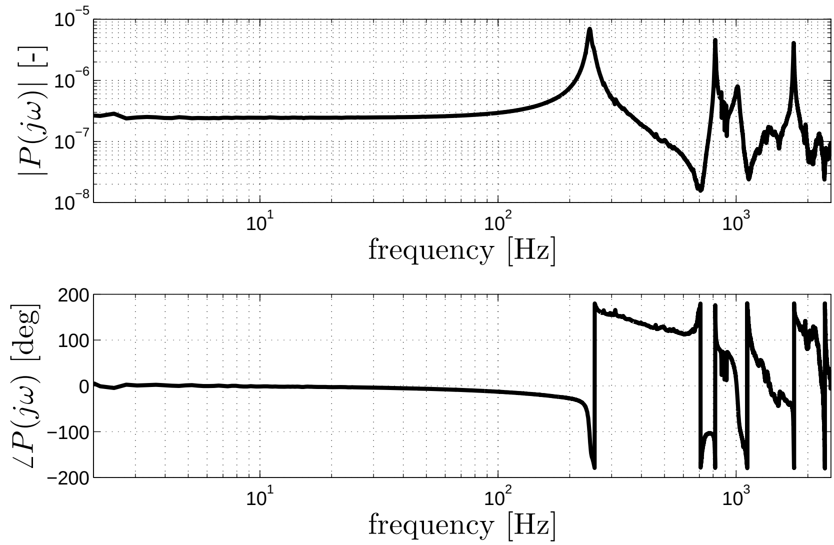

Fig. 4.4. Measured frequency response function of the lens system in z-direction.

more pronounced in view of the disturbance rejection properties required during scanning mode, for which a proportional (double) integral controller (PI^{2}D), i.e., a controller with two integrators, is preferred over PID control with one integrator, while (additional) integral action deteriorates the transient performance to errors induced by the shuffle motion.

4.4.2 Controller design

In this section, we will design a reset controller of the form (4.1), (4.2), which consists of an LTI controller with integral action combined with an additional Clegg integrator. The motivation for such a reset controller stems from the problem setting, i.e., due to the double integral action it is expected that good disturbance attenuation properties are maintained during a scanning motion, while the transient behavior is expected to be improved compared to a PI^{2}D controller because one of the two integrators is allowed to reset its buffer. In order to compare the obtained results, also two LTI controllers are designed, namely, a PID and a PI^{2}D controller. All three controllers can be implemented in the control architecture as in Fig. 4.1, while the design process (of all three considered controllers) will be entirely based on measured frequency-domain data.

Consider Fig. 4.4, which depicts the measured frequency response function

(FRF) of the plant $\mathcal{P}(j\omega)$, $\omega \in \mathbb{R}$. Based on this plant FRF, the nominal controller $\mathcal{C}(s)$, $s \in \mathbb{C}$, of Fig. 4.1 is designed using classical loop-shaping techniques, see, e.g., Skogestad and Postlethwaite (2005); Steinbuch and Norg (1998), and is given by

$$\mathcal{C}(s) = \mathcal{C}_{pid}(s)\mathcal{C}_{n,1}(s)\mathcal{C}_{n,2}(s)\mathcal{C}_{lp}(s), \tag{4.13}$$

which consists of a series connection between a PID controller $\mathcal{C}_{pid}(s)$, two notch filters $\mathcal{C}_{n,i}(s)$, $i = 1, 2$, and a second-order low-pass filter $\mathcal{C}_{lp}(s)$. We consider the following three controllers:

1. An LTI PID-type controller $\mathcal{C}_{\mathrm{PID}}(s) := \mathcal{C}(s)$, with $\mathcal{C}(s)$ as in (4.13). This results in the control architecture as in Fig. 4.1 in which $\mathcal{R}$ is absent;

2. An LTI PI^{2}D-type controller $\mathcal{C}_{\mathrm{PI^2D}}(s) := \mathcal{C}_i(s)\mathcal{C}(s)$, with $\mathcal{C}(s)$ as in (4.13) designed in series with an additional lag filter

$$\mathcal{C}_i(s) = \frac{s + \omega_i}{s} = \frac{\omega_i}{s} + 1, \tag{4.14}$$

   in which $\omega_i \in \mathbb{R}_{>0}$ denotes the integrator cut-off frequency. This results in the control architecture as in Fig. 4.1 in which $\mathcal{R} = \frac{\omega_i}{s}$ (and thus represents an LTI integrator);

3. A reset controller $\mathcal{C}_{\mathcal{R}}$. In its basis, this controller is similar to the $\mathcal{C}_{\mathrm{PI^2D}}(s)$ controller (thus with the same $\omega_i \in \mathbb{R}_{>0}$ and $\mathcal{C}(s)$ as in (4.13)), with the essential difference that $\mathcal{R}$ is not LTI but represents a *Clegg integrator*. This yields the control architecture as in Fig. 4.1 with $\mathcal{R}$ given by (4.1), (4.2), in which $\alpha \in (0, \infty]$ is yet to be determined and $(A_r, B_r, C_r) = (0, \omega_i, 1)$, see, e.g., (4.3).

Closed-loop stability using both LTI controllers, i.e., the $\mathcal{C}_{\mathrm{PID}}(s)$ and $\mathcal{C}_{\mathrm{PI^2D}}(s)$ controller, can be verified using standard linear arguments, e.g., using the Nyquist stability criterion, see Skogestad and Postlethwaite (2005). Here, we will only discuss how our newly proposed conditions in Theorem 4.1 can help in assessing closed-loop stability for the controller $\mathcal{C}_{\mathcal{R}}$. These conditions are verified as follows: the satisfaction of Assumption 4.1 is rather trivial, since the Clegg integrator is a one-dimensional system. Condition (I) will be satisfied by design of a stabilizing feedback controller $\mathcal{C}(s)$ as in (4.13), see also Remark 4.4. The first requirement of condition (II), i.e., (4.11), is satisfied as $\mathcal{G}_{eu}(j\omega) \to 0$ for $\omega \to \infty$. Finally, the circle criterion condition (4.12), which is verified by means of the Nyquist diagram of $\mathcal{G}_{eu}(j\omega)$ in Fig. 4.5. This figure shows that $Re(\mathcal{G}_{eu}(j\omega)) > -\frac{1}{\alpha}$, for $\alpha \in (0, 2.17]$ is met for all $\omega \in \mathbb{R}$. In the remainder of this case study, we take $\alpha = 2.17$ resulting that the input/output pair (e, u) of $\mathcal{R}$ as in (4.1), (4.2) is confined to the sector $[0, 2.17]$.

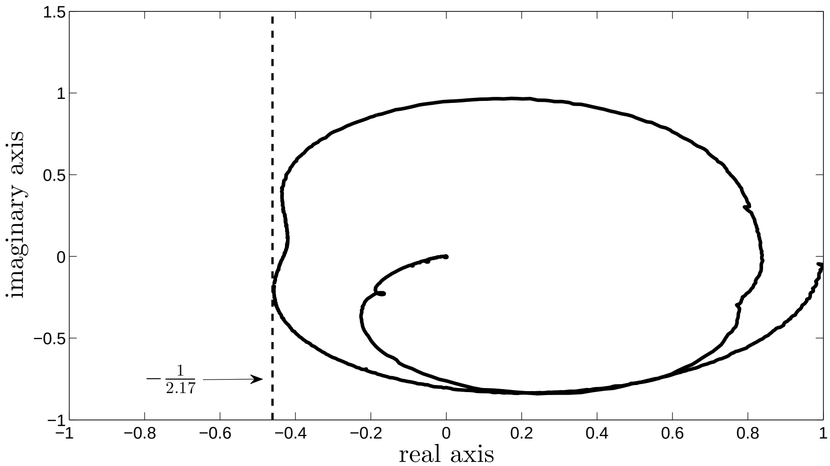

Fig. 4.5. Nyquist diagram of $\mathcal{G}_{eu}(j\omega)$ showing that the circle criterion condition $Re(\mathcal{G}_{eu}(j\omega)) > -\frac{1}{\alpha}$, is met for all $\omega \in \mathbb{R}$ with $\alpha = 2.17$.

4.4.3 Experimental verification

In this section, we present experimental results in the form of the moving average (MA) filtered error response[1], which is defined as follows:

$$\text{MA} := \frac{1}{T_e} \int_{-\frac{T_e}{2}}^{\frac{T_e}{2}} e(t)dt, \tag{4.15}$$

in which T_e represents the exposure time, and $e(t)$ represents the position error of the z-axis as a function of time t.

Remark 4.7. *Note that time-regularization, see Remark 4.3, occurs naturally in most practical (sampled-data) implementations of systems of the form* (4.9) *with* (4.2)*, see, e.g., Chapter 6 of this thesis.*

Consider Figs. 4.6 and 4.7 in which the measurement results are depicted during scanning motion and shuffle motion, respectively. Both figures show the MA filtered error responses for four different controller configurations, namely: $\mathcal{C}_{\text{PID}}(s)$, $\mathcal{C}_{\text{PI}^2\text{D}}(s)$, and $\mathcal{C}_{\mathcal{R}}$ with $\alpha \in \{2.17, \infty\}$.

Let us first focus on the resulting error responses using both linear controllers. During scanning motion $\mathcal{C}_{\text{PI}^2\text{D}}(s)$ clearly shows favorable disturbance rejection properties as it forces the MA filtered error response towards zero during the

[1] The use of MA filtered error responses is common practice in the lithography industry, see, e.g., Butler (2011). Note, however, that the actual time instances of reset are not immediately detectable from these *filtered* error responses.

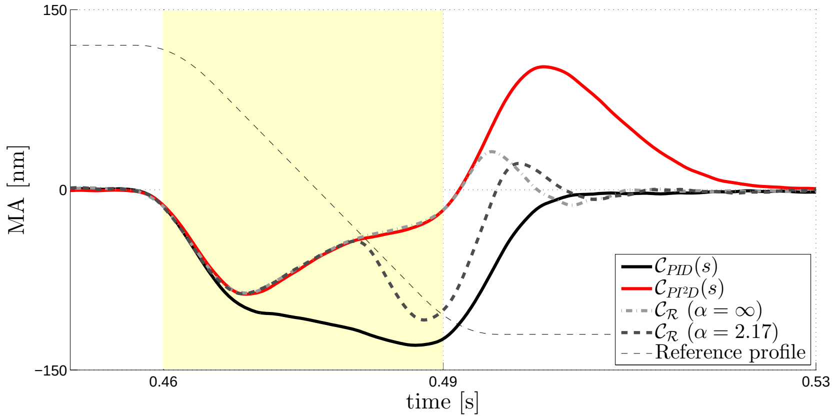

Fig. 4.6. Moving average (MA) filtered error responses during a scanning motion under different controller configurations.

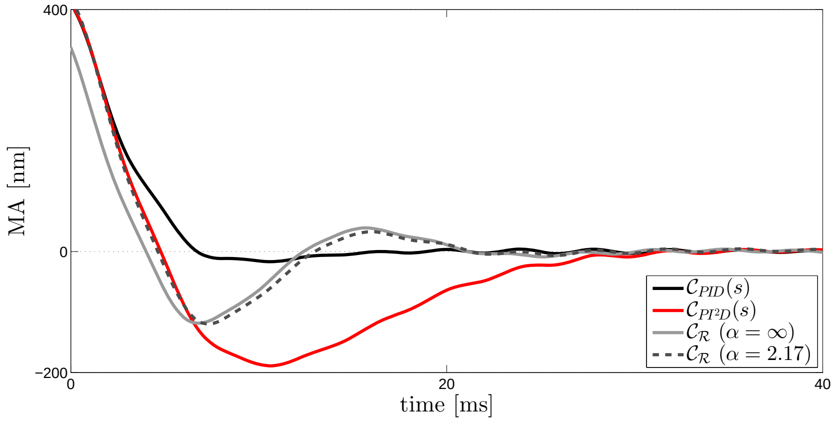

Fig. 4.7. Moving average (MA) filtered error responses during a shuffle motion under different controller configurations.

critical interval, which indicated by the yellow surface in Fig. 4.6. However, during a shuffle motion, the $\mathcal{C}_{\mathrm{PI^2D}}(s)$ controller induces significantly more overshoot and a larger settling time compared to the $\mathcal{C}_{\mathrm{PID}}(s)$ controller.

These results exemplary one of the most well-known linear control design trade-offs, i.e., adding integral action to a feedback control system improves the disturbance rejection properties at a cost of a decrease in transient performance (in terms of an increase in overshoot and settling time), see, e.g., Seron et al.

(1997). By considering $\mathcal{C}_{\mathcal{R}}$ instead, and hence, allowing one of the integrators to reset its buffer whenever $eu \geq -\frac{1}{\alpha}u^2$, we aim to achieve 'the best of both worlds', i.e., maintaining the disturbance rejection properties associated with a double integrator, while the transient response is comparable to a controller with a single integrator. Consider therefore again Figs. 4.6 and 4.7. These figures reveal that $\mathcal{C}_{\mathcal{R}}$ with $\alpha = \infty$ results in comparable disturbance rejection properties as $\mathcal{C}_{\mathrm{PI^2D}}(s)$, while its overshoot and settling behavior is much better. However, closed-loop stability is only guaranteed for all $\alpha \in (0, 2.17]$. So let us focus on the MA filtered error responses of $\mathcal{C}_{\mathcal{R}}$ with $\alpha = 2.17$. Fig. 4.7 shows that the overshoot and settling is comparable to $\mathcal{C}_{\mathcal{R}}$ with $\alpha = \infty$, but its disturbance rejection properties are worse. This can be explained by the fact that the smaller the value of α, the sooner the reset controller resets its buffer, while this buffer (integral action) is actually necessary to suppress the effect of the disturbance. Nevertheless, the disturbance rejection properties are still better compared to the $\mathcal{C}_{\mathrm{PID}}(s)$ controller.

4.5 Conclusions

In this chapter, we presented novel conditions for the input-to-state stability of reset control systems that allow for verification based on (measured) frequency response data of the linear part of the closed-loop system. An industrial piezo-actuated motion system has been used to demonstrate the effectiveness *and* user-friendliness of these conditions. This is because we have shown that closed-loop stability of the reset control system was verified using easy-to-obtain frequency response data, and hence, without the necessity of an (accurate) parametric system model and numerically solving LMIs. As such, these new results may contribute to the industrial acceptance of reset controllers, which in itself provide great opportunities in increasing the performance of linear (motion) systems.

Chapter 5

Split-path nonlinear integral control for transient performance improvement

Abstract – In this chapter, we introduce the split-path nonlinear integrator (SPANI) as a novel nonlinear filter designed to improve the *transient* performance of linear systems in terms of overshoot, while preserving good rise-time and settling behavior. In particular, this nonlinear controller targets the well-known trade-off induced by integral action, which removes steady-state errors due to constant external disturbances, but deteriorates transient performance in terms of increased overshoot. The rationale behind the proposed SPANI filter is to ensure that the integral action has, at all times, the same sign as the closed-loop error signal, which, as we will show, enables a reduction in overshoot thereby leading to an overall improved transient performance. The resulting closed-loop dynamics is modeled by a hybrid dynamical system, and provide sufficient Lyapunov-based conditions for stability. Furthermore, we illustrate the effectiveness, the design and the tuning of the proposed controller in a benchmark simulation study of an industrial pick-and-place machine.

5.1 Introduction

In classical linear control theory, it is well-known that Bode's gain-phase relationship causes a hard limitation on achievable performance trade-offs in linear time-invariant (LTI) feedback control systems, see, e.g., Freudenberg et al. (2000); Seron et al. (1997). The related interdependence between gain and phase is often in conflict with the desired performance specification set by the control

This chapter is based on van Loon et al. (2015b) and has been published as a preliminary version in Hunnekens (2014).

engineer. For example, it is impossible to add integral action to a feedback control system, typically included to achieve zero steady-state errors, without introducing the negative effect of phase lag. It was the fundamental gain-phase relationship for LTI systems that motivated W.C. Foster and co-workers in 1966 to develop the split-path nonlinear (SPAN) filter, in which they intended to design the gain and phase characteristics separately Foster et al. (1966). Another fundamental limitation is given by the fact that for a stable closed-loop system, the error step response necessarily overshoots if the open-loop transfer function of the linear plant with LTI controller contains a double integrator, see, e.g., (Seron et al., 1997, Theorem 1.3.2). The latter fundamental limitation applies to the majority of motion systems (of which the industrial benchmark study in this chapter is an example).

In Aangenent et al. (2005); Fong and Szeto (1980); Foster et al. (1966); Steinbuch et al. (2005); Zoss et al. (1968), the SPAN filter was designed as a phase lead filter that does not cause magnitude amplification. It was shown that a controller with such a nonlinear SPAN filter can outperform its linear counterpart with respect to overshoot to a step response. In this chapter, we also aim to achieve the same objective, namely, enhancing *transient* performance of linear (motion) systems in terms of overshoot, but we will propose a variant/extension to the SPAN filter, which we will call the split-path nonlinear integrator (SPANI). In contrast to the SPAN filter as in Aangenent et al. (2005); Fong and Szeto (1980); Foster et al. (1966); Steinbuch et al. (2005); Zoss et al. (1968), the SPANI is a *nonlinear integrator* that enforces the integral action to take the same sign as the closed-loop error signal, thereby limiting the amount of overshoot and, as a result, improving the transient performance while still guaranteeing a zero steady-state error in the presence of a constant reference and disturbance signal.

Several other hybrid/nonlinear control strategies for improving the transient performance for linear systems have been proposed in the literature, see Hunnekens (2014) for a recent overview. In this respect, we would like to mention reset control because it exhibits interesting analogies with the SPANI controller proposed in this chapter. Firstly, reset control has also been introduced quite some time ago in 1958 Clegg (1958), but especially in the last two decades, it has regained attention in both theoretically oriented research, see e.g., Aangenent et al. (2010); Baños and Barreiro (2012); Beker et al. (2004); Nešić et al. (2011); Prieur et al. (2013), as well as in applications Baños and Barreiro (2012); Panni et al. (2014); Zheng et al. (2000). Secondly, both strategies have the common feature of using a switching surface (or region) to trigger a change in the control signal, which leads to the injection of discontinuous control signals into an otherwise smooth (and linear) feedback system. Distinctively, reset control employs the same (linear) control law on both sides of the switching surface and a state reset takes place on the switching surface, whereas we will show that due to the construction of the SPANI filter, the dynamics changes after a switch and no state reset takes place. Another important difference is that a reset controller is not capable of achieving a zero-steady state error in the presence of constant reference and disturbance signals, see, e.g., Baños and Barreiro (2012), while the SPANI comes with such guarantees. We will furthermore demonstrate that the proposed (output feedback) controller structure supports the design of all the linear components of the SPANI controlled system using well-known (frequency-domain) loop-shaping techniques. Consequently, the specifically chosen control structure enhances the applicability to industrial control practice since it allows the control engineer to loop-shape the (linear part of the) controller such that it has favorable disturbance attenuation properties, while the SPANI serves as a hybrid *add-on* element that improves the transient performance.

It is well-known that many nonlinear control strategies have in common that closed-loop stability cannot be verified anymore using 'linear' tools such as the Nyquist stability theorem (except in specific cases, see Hunnekens (2014)). Hence, the importance of the development of other testable stability conditions is evident. Despite this fact, none of the works that considered SPAN filters, e.g., Aangenent et al. (2005); Fong and Szeto (1980); Foster et al. (1966); Steinbuch et al. (2005); Zoss et al. (1968), provided such results thus far. In this chapter, we propose, therefore, the first testable Lyapunov-based stability conditions for a feedback control system including the newly proposed SPANI controller.

The chapter is organized as follows. In Section 5.2, we introduce and motivate the proposed SPANI filter. Subsequently, in Section 5.3, we model the resulting closed-loop system as a hybrid system, for which in Section 5.4 stability conditions are provided. In Section 5.5, we illustrate the potential of the proposed nonlinear control strategy using a model-based benchmark example of an industrial pick-and-place machine. Finally, we end with conclusions in Section 5.6.

5.1.1 Nomenclature

The following notational conventions will be used. Let $\mathbb{R}$ denote the set of real numbers and $\mathbb{R}^n$ the n-fold Cartesian product $\mathbb{R} \times \ldots \times \mathbb{R}$ with the standard Euclidean norm denoted by $\|\cdot\|$. We use $\wedge$, $\vee$ to denote the logical 'and', 'or' operator, respectively. For a matrix $S \in \mathbb{R}^{n\times m}$, we denote by $\text{im}S := \{Sv \mid v \in \mathbb{R}^m\}$ the image of S, and by $\text{ker}S := \{x \in \mathbb{R}^m \mid Sx = 0\}$ its kernel. For two subspaces V, W of $\mathbb{R}^n$, we use $V + W = \{v + w \mid v \in V,\ w \in W\}$ to denote the direct sum, and write $V \oplus W = \mathbb{R}^n$ when $V + W = \mathbb{R}^n$ and $V \cap W = \{0\}$. We call a matrix $P \in \mathbb{R}^{n\times n}$ positive definite and write $P \succ 0$, if P is symmetric (i.e., $P = P^\top$) and $x^\top P x > 0$ for all $x \neq 0$. Similarly, we call $P \prec 0$ negative definite when $-P$ is positive definite. For brevity, we write symmetric matrices of the form $\begin{bmatrix} A & B \\ B^\top & C \end{bmatrix}$ as $\begin{bmatrix} A & B \\ \star & C \end{bmatrix}$. An $n \times n$ identity matrix is denoted by $I_{n\times n}$, and $O_{k\times l}$ denotes a $k \times l$ matrix with all zero entries. The distance of a vector $x \in \mathbb{R}^n$ to a set $\mathcal{A} \subset \mathbb{R}^n$ is defined by $\|x\|_{\mathcal{A}} := \inf_{y\in\mathcal{A}} \|x - y\|$.

5.2 Split-path nonlinear integrator

In Section 5.2.1, we will briefly revisit the original SPAN filter, and, based on these historical developments, propose a new variation/extension to this filter called/being the SPANI filter. Additionally, in Section 5.2.2, a description of the complete feedback control system will be given.

5.2.1 Introduction and motivation of the SPANI filter

Originally, the key motivation behind the development of the SPAN filter was to obtain a filter in which the gain and phase could be designed independently Foster et al. (1966). To achieve such favorable properties, the input signal of the filter, being the closed-loop error e, is divided into two separate branches of which the outputs are multiplied in order to form the control signal u_s, as schematically depicted in Fig. 5.1. The lower branch contains a sign element, which removes all magnitude information as its output is either ± 1, thereby retaining the *phase* information. The opposite holds for the upper branch as it contains an absolute value element thereby removing all sign information and retaining only the *magnitude* information. Moreover, both branches contain a linear filter $\mathcal{H}_i(s)$, $i \in \{1, 2\}$, $s \in \mathbb{C}$. In Aangenent et al. (2005); Fong and Szeto (1980); Foster et al. (1966); Zoss et al. (1968), the authors use filters of the form $\mathcal{H}_1(s) = 1/(s + \tau_1)$ (lag filter) and $\mathcal{H}_2(s) = (s + \tau_2)/(s + \tau_3)$ (lead filter), with the aim to add phase lead without magnitude amplification.

In this chapter, we use the concept of the SPAN filter to propose a new nonlinear controller with the goal to improve the *transient* performance of linear (motion) systems, which is quantified in terms of overshoot to step responses of the closed-loop system, while still guaranteeing a zero steady-state error in the presence of a constant reference and disturbance signal. For that purpose, we select a linear integrator for $\mathcal{H}_1(s)$, i.e., $\mathcal{H}_1(s) = \omega_i/s$, and take $\mathcal{H}_2(s) = 1$. We call this nonlinear filter the *split-path nonlinear integrator* (SPANI), which is schematically represented in the dashed rectangle in Fig. 5.2, with $\epsilon = 0$. The rationale behind the design of this SPANI filter can be best understood by considering a step response (or the response to a step disturbance) of a system containing integral control. In order to achieve a zero steady-state error, the integrator integrates the error e over time resulting in build-up of the integral buffer. As soon as the error e becomes zero, i.e., $e = 0$, the integrator still has the integrated error stored in its state. Due to the phase lag introduced by the integrator, it takes some time to empty this buffer, causing the error to overshoot. In contrast to a linear integrator, the SPANI enforces the integral action to take the same sign as the error signal, due to the presence of the absolute value and the sign element, see Fig. 5.2. This results in non-smooth behavior at the time instant when $e = 0$, i.e., an instantaneous switch of the sign of the integral action takes place, thereby inducing a reduction in overshoot.

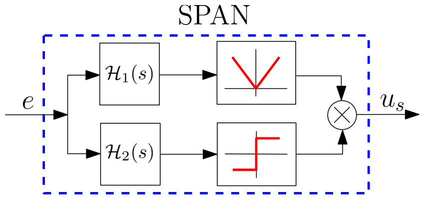

Fig. 5.1. Schematic representation of the SPAN filter.

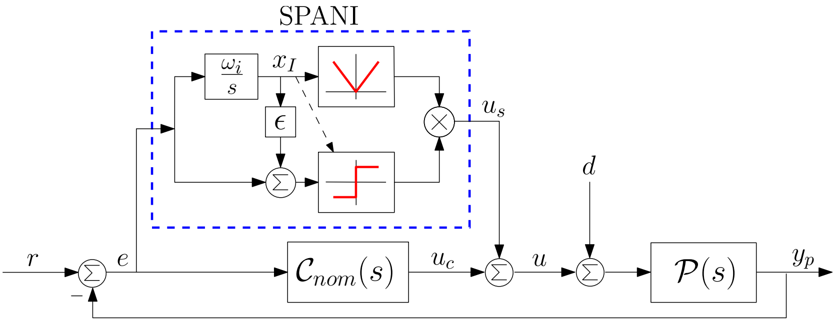

Fig. 5.2. Feedback loop with plant $\mathcal{P}(s)$, linear controller $\mathcal{C}_{nom}(s)$ and the proposed SPANI controller.

5.2.2 Description of the control system

The overall feedback configuration used in this chapter is shown in Fig. 5.2. In this figure, $e := r - y_p$ is the tracking error between the reference signal r and the output y_p of the plant with transfer function $\mathcal{P}(s)$, $s \in \mathbb{C}$. Moreover, d denotes an unknown, bounded input disturbance and $u := u_c + u_s$ the total control input, which consists of the control input u_c produced by the linear controller with transfer function $\mathcal{C}_{nom}(s)$ and the control input u_s of the SPANI. The linear part of the closed-loop system consists of a single-input-single-output (SISO) LTI plant

$$\mathcal{P} : \begin{cases} \dot{x}_p = A_p x_p + B_p u + B_p d \\ y_p = C_p x_p \end{cases} \tag{5.1}$$

with state $x_p \in \mathbb{R}^{n_p}$, and a SISO LTI nominal controller

$$\mathcal{C}_{nom} : \begin{cases} \dot{x}_c = A_c x_c + B_c e \\ u_c = C_c x_c + D_c e \end{cases} \tag{5.2}$$

with state $x_c \in \mathbb{R}^{n_c}$. The state (and output) of the integrator $\mathcal{C}_I(s) = \omega_i/s$, with gain $\omega_i \in \mathbb{R}_{>0}$, is defined by $x_I \in \mathbb{R}$. The *sign*-function in the lower branch of

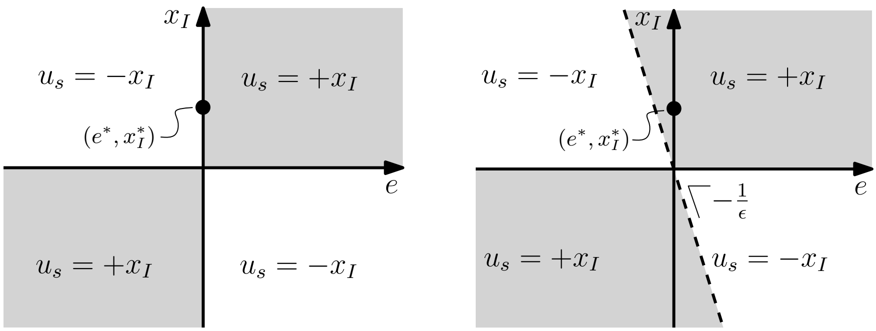

(a) SPANI with $\epsilon = 0$ (b) SPANI with $\epsilon > 0$

Fig. 5.3. Schematic representation of the control action of the SPANI in the (e, x_I)-plane.

the SPANI, see Fig. 5.2, is formally defined as

$$sign(e, x_I) = \begin{cases} 1 & \text{if } e > 0, \\ 1 & \text{if } e = 0 \text{ and } x_I \geq 0, \\ -1 & \text{if } e = 0 \text{ and } x_I < 0, \\ -1 & \text{if } e < 0, \end{cases} \tag{5.3}$$

which shows that when $e = 0$, we have $u_s = +x_I$ (the dependence of the sign-function on x_I is denoted by the dashed arrow in Fig. 5.2). The SPANI controller as in Fig. 5.2 can be modeled as a switched system with dynamics

$$\text{SPANI}: \begin{cases} \dot{x}_I = \omega_i e \\ u_s = \begin{cases} +x_I & \text{if } x_I(\epsilon x_I + e) \geq 0 \\ -x_I & \text{if } x_I(\epsilon x_I + e) < 0, \end{cases} \end{cases} \tag{5.4}$$

in which $x_I \in \mathbb{R}$ denotes the state of the integrator in the SPANI controller and $\epsilon \in \mathbb{R}_{\geq 0}$. For $\epsilon = 0$, we recover the situation as considered in Section 5.2.1, i.e., a filter that enforces the integral action to take the *exact* same sign as the error signal. For such a case, the situation where the 'default' integrator is active ($u_s = +x_I$) corresponds to $ex_I \geq 0$ and the situation where the integrator has negative sign ($u_s = -x_I$) corresponds to $ex_I < 0$, see Fig. 5.3(a) for a representation in the (e, x_I)-plane. The SPANI as in (5.4) therefore represents a more general class of SPANI controllers, in which the (typically small) parameter ϵ is associated with tilting of one of the switching boundaries, see Fig. 5.3(b), and is included to create a SPANI controller with favorable robustness properties compared to the

SPANI with $\epsilon = 0$ (which is closer to the classical SPAN filter). The latter claim can be intuitively explained as follows. Consider Fig. 5.3 and focus first on the SPANI with $\epsilon = 0$, i.e., Fig. 5.3(a). Note that the desired equilibrium point, with x_I having the equilibrium value x_I^* and e having the equilibrium value $e^* = 0$, i.e., $(e, x_I) = (e^*, x_I^*)$, is located exactly on the switching plane, see Fig 5.3(a). Note in this respect that since $e^* = 0$ is enforced by the integral action, it typically requires integral action ($x_I^* \neq 0$) to achieve such zero steady-state error, e.g., if constant disturbances are present. Given the fact that the desired equilibrium is on a switching boundary, small perturbations around this equilibrium may cause the dynamics to switch, resulting in an instantaneous change of sign of u_s. This might result in a large number of consecutive switches, which is highly undesired in many applications. By introducing the tilting parameter ϵ, we ensure that the equilibrium is located strictly inside the set where $x_I(\epsilon x_I + e) \geq 0$, see Fig. 5.3(b). As a consequence, we ensure that, locally around the equilibrium, no switching occurs. In Section 5.4, we present conditions that can help in making an appropriate choice for ϵ.

Although the tilting parameter ϵ creates robustness locally around the equilibrium, we cannot provide such guarantees around the switching plane in the remaining part of the state-space. In fact, we will demonstrate in Section 5.5.2 that in certain situations multiple consecutive switchings can occur. In order to prevent such undesired behavior from happening, a minimal dwell-time argument, see, e.g., Hespanha and Morse (1999); Solo (1994), is adopted in the switching function of the SPANI as in (5.4). This will be made more specific and precise in the next section.

5.3 Hybrid system modeling

In this section, we model the closed-loop system as discussed in Section 5.2.2, see Fig. 5.2, in the hybrid system formalism of Goebel et al. (2012), resulting in the description

$$\dot{\chi} = f(\chi, w), \quad \text{if } \chi \in \mathcal{F}, \tag{5.5a}$$

$$\chi^+ = g(\chi), \quad \text{if } \chi \in \mathcal{J}, \tag{5.5b}$$

where $\chi \in \mathbb{R}^{n_\chi}$ is the state, $w \in \mathbb{R}^{n_w}$ an exogenous input, $\mathcal{F} \subseteq \mathbb{R}^{n_\chi}$ and $\mathcal{J} \subseteq \mathbb{R}^{n_\chi}$ are the flow set and jump set, respectively, $f : \mathcal{F} \to \mathbb{R}^{n_\chi}$ and $g : \mathcal{J} \to \mathbb{R}^{n_\chi}$ are the flow and jump map, respectively, and χ^+ denotes the value of the state directly after the reset. For the analysis results in this chapter, the signals w are typically constant such that the standard notions related to the hybrid framework of Goebel et al. (2012), such as the concept of hybrid time domains and solutions of (5.5), are applicable. These are reported in Appendix A.4.1 for convenience of the reader. For more details on this hybrid modeling framework we refer to Goebel et al. (2012).

To obtain a complete closed-loop model of the feedback configuration in Fig. 5.2, we use the interconnections $e = r - y_p$ and $u = u_c + u_s$, combine (5.1), (5.2) and (5.4), and define the state-vector $x := [x_p^\top \;\; x_c^\top \;\; x_I^\top]^\top \in \mathbb{R}^n$, with $n = n_p + n_c + 1$. Moreover, we introduce a timer variable $\tau \in \mathbb{R}_{\geq 0}$ and Boolean $\ell \in \{0, 1\}$, and define the augmented state vector $\chi := [x^\top \; \tau \; \ell]^\top \in \Theta$, with $\Theta := \mathbb{R}^{n_x} \times \mathbb{R}_{\geq 0} \times \{0, 1\} \in \mathbb{R}^{n_x+2}$ and $w = [r \;\; d]^\top \in \mathbb{R}^2$. Then, the flow map f in (5.5a) is given by

$$f(\chi, w) = \begin{cases} \Big[(\bar{A}_1 x + \bar{B}_r r + \bar{B}_d d)^\top,\ 1,\ 0\Big]^\top, & \text{when } \ell = 0 \\ \Big[(\bar{A}_2 x + \bar{B}_r r + \bar{B}_d d)^\top,\ 1,\ 0\Big]^\top, & \text{when } \ell = 1 \end{cases} \tag{5.6a}$$

with

$$\bar{A}_1 := \begin{bmatrix} A_p - B_p D_c C_p & B_p C_c & +B_p \\ -B_c C_p & A_c & 0 \\ -\omega_i C_p & 0 & 0 \end{bmatrix}, \quad \bar{B}_r := \begin{bmatrix} B_p D_c \\ B_c \\ \omega_i \end{bmatrix}, \tag{5.6b}$$

$$\bar{A}_2 := \begin{bmatrix} A_p - B_p D_c C_p & B_p C_c & -B_p \\ -B_c C_p & A_c & 0 \\ -\omega_i C_p & 0 & 0 \end{bmatrix}, \quad \bar{B}_d := \begin{bmatrix} B_p \\ 0 \\ 0 \end{bmatrix}. \tag{5.6c}$$

We assume that, by proper design, the *linear* controller $\mathcal{C}_{nom}(s) + \mathcal{C}_I(s)$, see Fig. 5.2, is stabilizing and, as a result, the matrix $\bar{A}_1$ is Hurwitz. However, due to the 'wrong' sign of the integral action, $\bar{A}_2$ will in general not be Hurwitz. In (5.5), flow according to $\dot{\chi} = f(\chi, w)$, occurs when the state χ is in the flow set given by

$$\begin{aligned} \mathcal{F} := \big\{\chi \in \Theta \,|\, \big(\ell = 0 \wedge \big(x_I(\epsilon x_I + e) \geq 0 \,\vee \\ 0 \leq \tau \leq \tau_D\big)\big) \vee \big(\ell = 1 \wedge x_I(\epsilon x_I + e) \leq 0\big)\big\}, \end{aligned} \tag{5.6d}$$

in which $\tau_D \in \mathbb{R}_{\geq 0}$. Note that the state-dependent switching rule of the SPANI controller, see (5.4), is augmented with a minimal dwell-time argument, see, e.g., Hespanha and Morse (1999); Solo (1994). To be precise, we only include this time restriction in the first mode (when $\ell = 0$) in which the stable $\bar{A}_1$-dynamics is active and force the system to stay in this mode for at least $\tau_D \in \mathbb{R}_{\geq 0}$ time units. In the second mode (when $\ell = 1$), in which the unstable $\bar{A}_2$-dynamics is active, no time restrictions are imposed.

The jump map g in (5.5b) is given by

$$g(\chi) := \big[x^\top,\ 0,\ 1 - \ell\big]^\top, \tag{5.6e}$$

and the jump set is given by

$$\begin{aligned} \mathcal{J} := \big\{\chi \in \Theta \,|\, \big(\ell = 0 \wedge \big(x_I(\epsilon x_I + e) \leq 0 \wedge \tau \geq \tau_D\big)\big) \\ \vee \big(\ell = 1 \wedge x_I(\epsilon x_I + e) \geq 0\big)\big\}. \end{aligned} \tag{5.6f}$$

Note that $\tau_D > 0$ guarantees that there can be at most two consecutive jumps at one continuous time $t \in \mathbb{R}_{\geq 0}$. In particular, for any solution ϕ to the hybrid system $(\mathcal{F}, f, \mathcal{J}, g)$ and for any $(t, j) \in \operatorname{dom}\phi$, it holds that $(t', j+2) \in \operatorname{dom}\phi$ implies $t' \geq t + \tau_D$.

5.4 Stability analysis

In this section, we consider constant (step) references $r(t) = r_c$, $t \in \mathbb{R}_{\geq 0}$, and constant disturbances $d(t) = d_c$, $t \in \mathbb{R}_{\geq 0}$, and present LMI-based stability conditions for the hybrid system as in (5.5), (5.6). In order to do so, let us define the equilibrium set $\mathcal{A}$ of the hybrid system (5.5), (5.6), for which we would like to prove global exponential stability (GES), as follows

$$\mathcal{A} := \{\chi \in \mathcal{F} \cup \mathcal{J} \mid x = x^*\}, \tag{5.7}$$

in which x^* denotes the equilibrium point satisfying

$$\bar{A}_1 x^* + \bar{B}_r r_c + \bar{B}_d d_c = 0. \tag{5.8}$$

Note that, x^* (and thus $\mathcal{A}$) depends on the choice of r_c and d_c. Moreover, from (5.4) it follows that $e^* = 0$ in the equilibrium x^*, such that the equilibrium indeed conforms to the $\bar{A}_1$-dynamics for $\epsilon > 0$, and therefore satisfies (5.8). Note furthermore that since the system matrix $\bar{A}_1$ is Hurwitz, and thus invertible, (5.8) has one unique solution x^* for fixed $r_c \in \mathbb{R}$ and $d_c \in \mathbb{R}$.

Theorem 5.1 below poses sufficient conditions under which GES of the set $\mathcal{A}$ can be guaranteed for the hybrid system (5.5), (5.6). Consequently, under these conditions the exact tracking of the constant reference value r_c, and disturbance rejection of the constant disturbance value d_c, is guaranteed. Hereto, let us define what is meant by GES of the set $\mathcal{A}$ in this chapter, and introduce some notational conventions used in Theorem 5.1.

Definition 5.1. *The set $\mathcal{A}$ is said to be GES for the system* (5.5), (5.6) *with $r(t) = r_c$ and $d(t) = d_c$, $t \in \mathbb{R}_{\geq 0}$, if there exist a $\rho \in \mathbb{R}_{>0}$ and $\mu \in \mathbb{R}_{>0}$, such that for all $\chi(0,0) \in \mathcal{F} \cup \mathcal{J}$, it holds that the corresponding solutions $\chi(t,j)$ to* (5.5), (5.6) *satisfy $\|\chi(t,j)\|_{\mathcal{A}} \leq \rho e^{-\mu t} \|\chi(0,0)\|_{\mathcal{A}}$ for all $(t,j) \in dom\,\chi$.*

Remark 5.1. *Note that due to the dwell time condition with $\tau_D > 0$, Definition 5.1 is in fact equivalent to the definition of GES of $\mathcal{A}$ in Teel et al. (2013), see Appendix A.4.2 for a proof. This can be seen by using that for a solution ϕ to* (5.5), (5.6) *it holds that $j \leq 2\frac{t}{\tau_D} + 2$ for any $(t,j) \in dom\,\phi$. Nevertheless, we use Definition 5.1 as we are more interested in the evolution of the state χ over continuous time t.*

The matrix $Q \in \mathbb{R}^{(n+2)\times(n+2)}$ is defined by

$$Q := \begin{bmatrix} \bar{A}_2^\top P + P\bar{A}_2 & P\bar{A}_d\bar{A}_1^{-1}\bar{B}_r & P\bar{A}_d\bar{A}_1^{-1}\bar{B}_d \\ \star & 0 & 0 \\ \star & \star & 0 \end{bmatrix} \tag{5.9}$$

with $\bar{A}_d := \bar{A}_1 - \bar{A}_2$ and a free matrix $P \in \mathbb{R}^{n\times n}$. Furthermore, the matrix $\bar{R} \in \mathbb{R}^{(n+2)\times(n+2)}$ is defined by

$$\bar{R} := \left[\begin{array}{ccc|c|c} 0 & 0 & -\frac{1}{2}C_p^\top & -\frac{1}{2}\gamma_r C_p^\top & -\frac{1}{2}\gamma_d C_p^\top \\ \star & 0 & 0 & 0 & 0 \\ \star & \star & \epsilon & \epsilon\gamma_r & \epsilon\gamma_d \\ \hline \star & \star & \star & \epsilon\gamma_r^2 & \epsilon\gamma_r\gamma_d \\ \hline \star & \star & \star & \star & \epsilon\gamma_d^2 \end{array}\right], \tag{5.10}$$

for scalars

$$\gamma_r = -\begin{bmatrix} O_{1\times n_p} & O_{1\times n_c} & 1 \end{bmatrix} \bar{A}_1^{-1}\bar{B}_r \tag{5.11}$$

$$\gamma_d = -\begin{bmatrix} O_{1\times n_p} & O_{1\times n_c} & 1 \end{bmatrix} \bar{A}_1^{-1}\bar{B}_d, \tag{5.12}$$

related to the integral state in equilibrium

$$x_I^* = \gamma_r r_c + \gamma_d d_c. \tag{5.13}$$

Finally, let the matrix $M \in \mathbb{R}^{(n+2)\times(n+1)}$ be given by

$$M := \begin{bmatrix} I_{n\times n} & O_{n\times 1} \\ O_{2\times n} & \begin{bmatrix} \gamma_r \\ \gamma_d \end{bmatrix} \end{bmatrix}. \tag{5.14}$$

Theorem 5.1. *Consider the hybrid system given by* (5.5), (5.6), *in which* $\epsilon > 0$ *is fixed and* $\tau_D > 0$, *and the set* $\mathcal{A}$ *given by* (5.7). *If there exist a positive definite matrix* $P \in \mathbb{R}^{n\times n}$ *and a constant* $\alpha \in \mathbb{R}_{\geq 0}$ *satisfying*

$$\bar{A}_1^\top P + P\bar{A}_1 \prec 0 \tag{5.15}$$

$$M^\top \left(Q - \alpha\bar{R}\right) M \prec 0, \tag{5.16}$$

then the set $\mathcal{A}$, *with* $r(t) = r_c$ *and* $d(t) = d_c$, $t \in \mathbb{R}_{\geq 0}$, *is GES for the hybrid system* (5.5), (5.6).

Proof. The proof can be found in Appendix A.4.3. □

Remark 5.2. *Theorem 5.1 guarantees that solutions of the closed-loop system converge exponentially (as a function of continuous time t) to the set on which* $e = 0$ *for all* $\tau_D > 0$ *and* $r(t) = r_c$, $d(t) = d_c$, $t \in \mathbb{R}_{\geq 0}$. *In addition, for* $\tau_D = 0$

the closed-loop dynamics can be represented by a continuous-time switched linear system given by

$$\dot{x} = \begin{cases} \bar{A}_1 x + \bar{B}_r r + \bar{B}_d d \quad if \quad x_I(\epsilon x_I + e) \geq 0 & \text{(5.17a)} \\ \bar{A}_2 x + \bar{B}_r r + \bar{B}_d d \quad if \quad x_I(\epsilon x_I + e) < 0, & \text{(5.17b)} \end{cases}$$

with output $y_p = C_p x_p$. In such switched systems, sliding modes can occur when the vector fields on both sides of the switching surface point towards each other, see, e.g., Filippov (1988); Leine and Nijmeijer (2004). However, it can be shown that, based on a Lyapunov analysis of the convex combination between the dynamics on both sides of the switching plane, the occurrence of sliding modes (if they exist) does not change the GES of $\mathcal{A}$ under the hypothesis of Theorem 5.1. For details, see Hunnekens (2014).

5.5 Case study on a pick-and-place machine

In this section, we consider a simulation study based on an industrial pick-and-place machine used to place electrical components, such as resistors, capacitors, integrated circuits etc., with a high speed and high precision on a printed circuit board (PCB). The working principle of a pick-and-place machine is as follows: The first step is to place the PCB within the working area of the placement head, in the second step the placement head picks up an electrical component, and in the third step the placement head is navigated to a pre-described position on the PCB where it should place the component. Finally, in the fourth step, the component is placed on the PCB as soon as all positioning tolerances are met. In this case study, we focus particulary on the third step with the goal to enable the fourth step to start as soon as possible. Namely, the placement of the electrical component on the PCB in the fourth step can only be finalized when the closed-loop error e, related to step three, has converged within a pre-described error bound. Therefore, our objective is to study if we can increase the machine throughput by achieving a faster convergence of the closed-loop error to its specified error bound by replacing the linear integrator $\mathcal{C}_I(s)$ by a SPANI of the form (5.4) (with the same integrator gain ω_I).

5.5.1 Simulation model

A schematic representation of the simulation model is depicted in Fig. 5.4. In this figure, the plant $\mathcal{P}(s)$ is identified based on measured frequency response data, resulting in a 4^{th}-order model. The plant will be controlled by a proportional-integral-derivative (PID)-type controller $\mathcal{C}_{nom}(s) + \mathcal{C}_I(s)$, in which $\mathcal{C}_{nom}(s)$ consists of a PD-controller and a 2^{nd}-order low-pass filter. Additionally, as in many industrial motion controllers, acceleration feedforward is used, with gain m that represents the estimated plant mass, to compensate for the

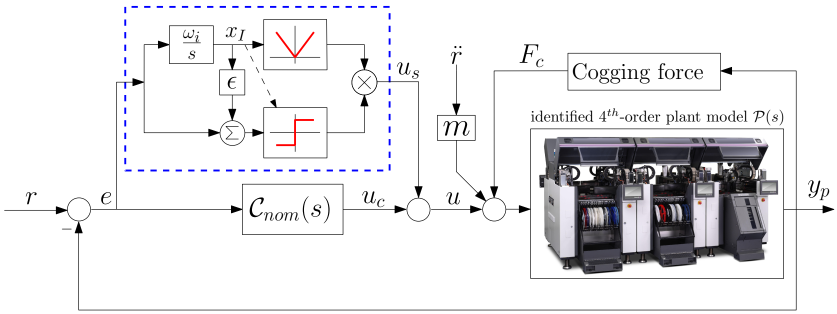

Fig. 5.4. Schematic representation of the simulation model.

low-frequency rigid-body plant dynamics. Cogging forces, which are position-dependent force disturbances caused by the magnetic interaction between the permanent magnets and the motor coils, are known to be the main disturbance source in this particular application. Based on identification experiments, we modeled this cogging disturbance force as a sinusoidal position-dependent force given by

$$F_c(y_p) = A_{F_c} \sin\left(\frac{\delta_p}{2\pi} y_p + \phi_{F_c}\right), \tag{5.18}$$

in which A_{F_c} denotes the maximum cogging force, δ_p the pitch between the magnets and ϕ_{F_c} a phase shift tuned on the basis of measurement data.

Remark 5.3. *Although there exist feedforward techniques that can compensate for such (repetitive) cogging force disturbances, for instance using iterative learning control, see e.g., Janssens et al. (2013); van Berkel et al. (2007), or look-up tables, these disturbances vary from machine to machine and often manufacturers do not have the resources to implement such techniques on each machine separately. Moreover, the vast majority of industrial applications will be subject to disturbances that cannot be easily identified, and thus perfectly compensated for by feedforward control. Hence, integral action in the controller is still necessary in order to achieve zero steady-state errors.*

In the following sections, we compare the transient performance of a linear controller with a controller in which the linear integrator is replaced by a SPANI. In Section 5.5.2, we consider the situation in which no dwell-time is included, i.e., $\tau_D = 0$. We show that the transient performance will increase by using a SPANI, but also that $\tau_D = 0$ might yield some undesired behavior in certain situations. In Section 5.5.3, we demonstrate that this undesired behavior can be prevented by including dwell-time restrictions as already introduced in Section 5.3.

5.5.2 Transient performance comparison with $\tau_D = 0$

In this section, we take $\tau_D = 0$ and study the response for two 4^{th}-order reference trajectories corresponding to two different positions on the PCB where the electrical component should be placed, i.e., the first reference trajectory has an end position of 200 mm and the second of 105 mm. Note that due to the position-dependent cogging forces, this results in two different disturbance situations that the SPANI controller will have to cope with.

Let us first consider the reference with an end position of 200 mm. Fig. 5.5 shows the error[1] profiles using; a linear controller (dash-dotted blue), and in solid black the error profile obtained if we replace the linear integrator $\mathcal{C}_I$ by a SPANI of the form (5.4) (with the same gain ω_I) and $\epsilon = 0.0115$. This value for ϵ is motivated by the conditions of Theorem 5.1 and Remark 5.2. In fact, by verifying these conditions we can guarantee that the equilibrium x^* of (5.17) is GES for all $\epsilon \geq 0.0115$. As indicated in Fig. 5.5, compared to the linear case, an improved, and asymptotically stable, response can be obtained using a SPANI. Note that with 'improved', we mean both a reduction in overshoot and a faster convergence to the error bound (depicted by the horizontal dotted lines). This is in correspondence with the two performance objectives previously defined in Section 5.5.1. Firstly, we observe a significant overshoot reduction of $\sim 20\%$ almost immediately after the pick-and-place robot reaches its end-position (~ 0.443 s in Fig. 5.5), while an even more significant overshoot reduction is achieved in the response around $t = 0.3$ s, see the smaller figure inside Fig. 5.5. Secondly, almost immediately after the pick-and-place robot reaches its end-position (~ 0.443 s in Fig. 5.5) the error signal of the system with SPANI has converged within the error bound, thereby again outperforming the linear controller. These performance improvements are achieved by only two switches (in the region of interest) of the SPANI filter, see Fig. 5.6 in which the total control signal $u = u_c + u_s$ is depicted.

Remark 5.4. *It is known that discontinuous control signals can excite high-frequency resonances typically present in motion systems and may result in actuator wear. One can therefore decide to 'smoothen' such signals by, for instance, using low-pass filters. This, however, will also inevitably lead to a decrease in potential performance benefits and, again a careful trade-off has to be made depending on the specifications at hand.*

Let us now consider the reference profile with an end position of 105 mm. The error profiles of the linear controller and the nominal controller with SPANI and $\epsilon = 0.0115$ are depicted in Fig. 5.7(a), which again indicates that the SPANI controller outperforms the linear controller with respect to overshoot (by $\sim 43\%$ in this case) and convergence within the error bound. However, it also reveals the following undesired behavior:

[1] To protect the interests of the manufacturer, all figures in this section have either been scaled or use blank axes in terms of units.

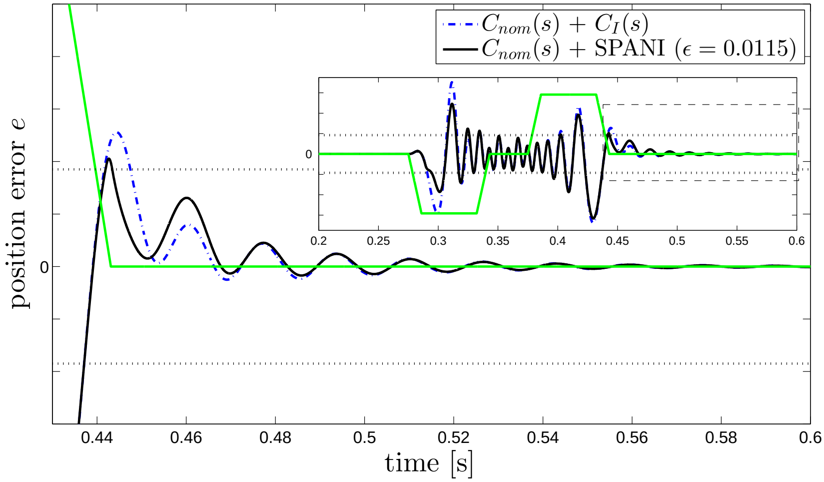

Fig. 5.5. Error profile for the region of interest using a 4^{th}-order reference trajectory with an end position of 200 mm. For the sake of clarity, a scaled acceleration profile is shown in green and a smaller figure is added showing the entire time span in which the region of interest is indicated by the dashed rectangle.

- For $t \in [0.43, 0.48]$: The error shows fast oscillatory behavior, resulting from a large number of switches;
- For $t \in [0.48, 0.52]$: An unexpected 'peak' in the error signal occurs while we expect to converge smoothly towards $e = 0$.

Both these phenomena are undesired and can be explained by considering Fig. 5.7(b-c), in which we consider the (e, x_I)-plot Fig. 5.7(b), and the integral action x_I and the output u_s of the SPANI versus time in Fig. 5.7(c). In these figures, the equilibrium point is depicted by point C, which, for this particular disturbance situation, requires positive integral action ($\sim x_I^* = 0.286$) to compensate for the cogging disturbance force at the setpoint. However, as indicated in Fig. 5.7(b-c), the integral action x_I has the wrong sign (up till point B). Still, up to point A in Fig. 5.7(b-c), the SPANI output u_s delivers, by means of many switches in the control signal u_s, *on average* enough integral action to approximately compensate for the cogging disturbance. However, after point A in the figure, $|x_I|$ is too small such that the SPANI cannot compensate for the cogging disturbance anymore. This results in a build-up of error, causing the peak in the error signal as depicted in Fig. 5.7(a) and Fig. 5.7(b-c). Eventually, after point B in Fig. 5.7, the integral state x_I becomes positive and converges to the equilibrium in point C.

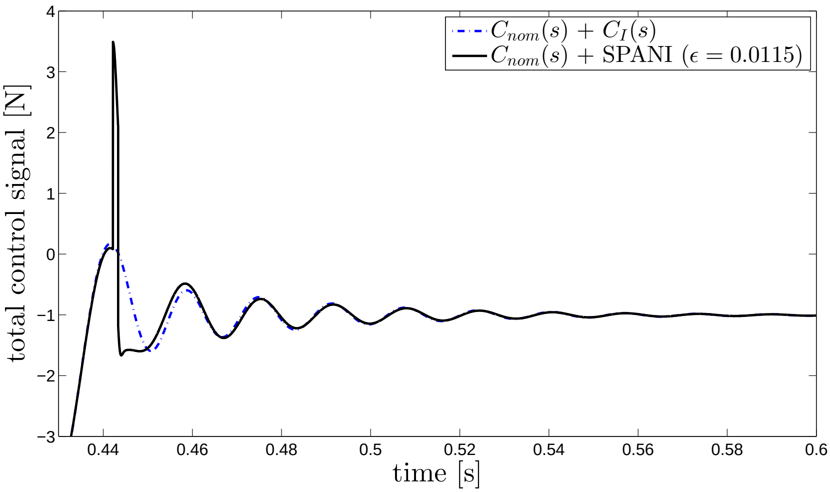

Fig. 5.6. Total control signal for the linear controller $\mathcal{C}_{nom} + \mathcal{C}_I$, and for $\mathcal{C}_{nom}$ + SPANI.

5.5.3 Transient performance comparison with $\tau_D > 0$

In this section, we show that adding a minimal dwell-time condition $\tau_D > 0$, as discussed in Section 5.3, can alleviate this undesired behavior. Including dwell-time logic in the switching condition of the SPANI filter requires the tuning of the new parameter τ_D, which according to Theorem 5.1 cannot cause instability of the set $\mathcal{A}$. Simulation results for such a SPANI filter with dwell-time restriction are depicted in Fig. 5.8 using $\tau_D = 0.0063$ s. The working principle of the new switching rule can be explained best by considering Fig. 5.8(b), in which the (e, x_I)-plane is shown. In point D, the response of the SPANI-controlled system reaches the switching plane for the first time and switches from mode 1 (red) to mode 2 (green) following the $\bar{A}_2$-dynamics. We stay in this mode until we reach the switching plane again at point E, where we switch back to mode 1. Apparently, the vector field of the $\bar{A}_1$-dynamics directs towards the switching plane but at the moment of crossing (point F) the dwell-time condition $\tau \geq \tau_D$ is not yet satisfied. Hence, no switch takes place and it takes until point G at which the dwell-time condition is satisfied. At that moment in time, we do not satisfy the condition $x_I(\epsilon x_I + e) \geq 0$, resulting in a switch to mode 2.

Let us now compare this result to the previous situation, i.e., as depicted in Fig. 5.7. Concentrating first on Figs. 5.7(b) and 5.8(b), we observe that up to point F the error profiles are identical[2]. As a result, the first peak in the error

[2]This applies in general for sufficiently small τ_D such that at point D in Fig. 5.8(b), we satisfy the dwell-time condition $\tau \geq \tau_D$.

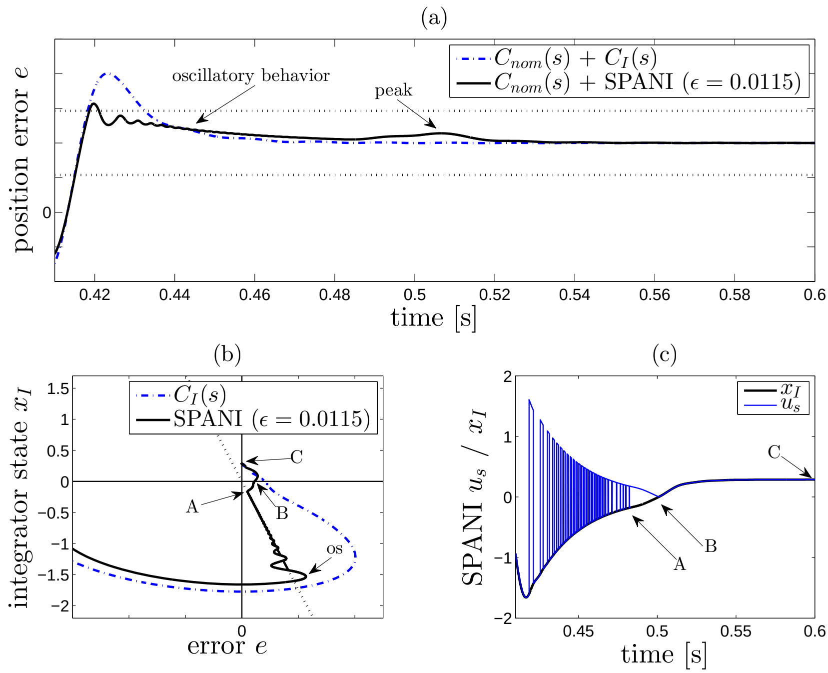

Fig. 5.7. **(a)** Error profile for the region of interest using a 4^{th}-order reference trajectory with an end position of 105 mm. **(b)** Error e versus integral action x_I. **(c)** Time versus output u_s of the SPANI and integral action x_I.

profiles (around ~ 0.42 s) of Figs. 5.7(a) and 5.8(a) is identical. However, for sufficiently large τ_D, this does not apply to the second peak (around ~ 0.43 s) in the error profile. This can be explained by considering point F; for the case $\tau_D = 0$ a switch to mode 2 takes place at point F causing an immediate change in the vector field. However, for the case with $\tau_D = 0.0063$, no switch takes place up till point G, thereby causing the system to reside longer in mode 1, which, in turn, causes the error to overshoot more in this particular situation. Therefore, including such dwell-time logic into the switching condition might result in a (slight) decrease of potential transient performance benefits. Nevertheless, it is clear from Fig. 5.8 that the dwell-time condition prevents the undesirably large number of switches in the control signal as in Fig. 5.7(c) for the case $\tau_D = 0$. Not only the number of switches has decreased, see Fig. 5.8(c), the error profile also now gradually converges to $e = 0$ without the occurrence of a sudden unwanted peak (compare Figs. 5.7(a) and 5.8(a)).

Remark 5.5. *By increasing the dwell-time parameter τ_D, the stable $\bar{A}_1$-dynamics*

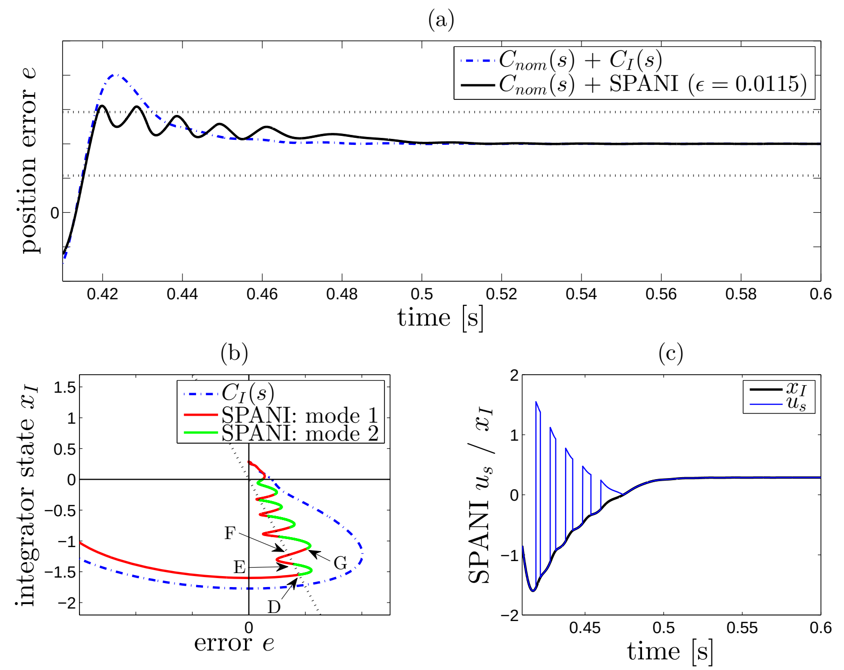

Fig. 5.8. **(a)** Error profile for the region of interest using a 4^{th}-order reference trajectory with an end position of 105 mm. **(b)** Error e versus integral action x_I. **(c)** Time versus output u_s of the SPANI and integral action x_I.

is active for a longer time. In fact, for $\tau_D = \infty$, the linear, and stabilizing, controller $\mathcal{C}_{nom}(s) + \mathcal{C}_I(s)$ is active for all times $t \in \mathbb{R}_{\geq 0}$. Hence, the undesired behavior as discussed in this section, see Fig. 5.7, can be prevented by selecting the dwell-time parameter τ_D sufficiently large. From an overshoot-reduction point of view, however, a small τ_D is favorable, leading to a design trade-off as before.

5.5.4 Final note

The main motivation for and the rationale behind the design of the SPANI is to improve the transient performance of linear systems by reducing overshoot, which is successfully demonstrated in this section. It is important to note that, in general, it is hard to give any guarantees on the settling behavior. In the benchmark study presented in this section, we satisfied both our objectives, i.e., reducing overshoot and a faster convergence to an error bound. The secondary objective can not always be guaranteed and it depends on the tuning of the dwell-time parameter τ_D and the disturbance situation at hand. However, the primary objective of reducing overshoot is satisfied in all (considered) cases.

5.6 Conclusions

In this chapter, we proposed the split-path nonlinear integrator (SPANI) as a novel variation/extension to a nonlinear filter that was originally introduced in the late 1960s. The SPANI is especially designed for transient performance improvement of linear systems. In particular, we focussed on the transient performance improvement in terms of overshoot to step responses, while being able to achieve zero steady-state errors in the presence of constant disturbances. By means of simulations it was demonstrated that, in particular situations, the SPANI controller can indeed outperform its linear counterpart. Moreover, a formal stability analysis was presented for this novel feedback control configuration with SPANI based on a hybrid dynamical system model for the closed-loop dynamics. Based on this hybrid modeling formalism, sufficient Lyapunov-based stability conditions have been provided in terms of linear matrix inequalities. These conditions proved to be useful in the design of the SPANI. A nice additional feature of the SPANI is that it is easy to apply in industrial practice as all the individual components of the proposed nonlinear controller can be synthesized using classical loop-shaping techniques. By presenting a fundamental modeling framework based on hybrid models and corresponding stability analysis tools, and also showing both the advantages and disadvantages of the SPANI controller, a complete design framework for SPANI controllers has been laid down. As such, we hope that this work inspires others to consider SPANI controllers for their specific control problems, and if needed, develop their own variations. This is particularly important as the design of nonlinear/hybrid controllers outperforming linear controllers remains to be a challenging problem of high industrial relevance.

Chapter 6

Improved $\mathcal{L}_2$-gain analysis for a class of hybrid systems

Abstract – In this chapter, we consider a special class of hybrid systems with periodic time-triggered jump conditions, and in which the jump map has a piecewise linear character. This hybrid systems class forms a relevant field of study as different control applications can be modeled in this hybrid system framework, including reset control, networked control and event-triggered control systems. After showing the unifying modeling character of this class of dynamical systems, we are interested in analyzing stability and $\mathcal{L}_2$-gain properties and we present novel conditions to do so which are significantly less conservative than the existing ones in literature. The effectiveness of the proposed modeling and analysis techniques is illustrated by means of a reset control example.

6.1 Introduction

Hybrid systems, see Goebel et al. (2012), combine continuous dynamics, often called flow dynamics and represented by ordinary differential equations on the one hand, and discrete dynamics, which are sometimes captured through jump dynamics and represented by instantaneous jumps/resets of states on the other hand. In this chapter, we are interested in a particular class of hybrid systems with periodic time-triggered jump conditions and piecewise linear (PWL) jump maps. This class of hybrid systems finds its use in a broad spectrum of control applications including reset control, see, e.g., Aangenent et al. (2010); Baños and Barreiro (2012); Beker et al. (2004); Guo et al. (2012); Loquen et al. (2008); Nešić et al. (2008); Zaccarian et al. (2011), event-triggered control, see, e.g., Heemels et al. (2013, 2012); Lunze and Lehmann (2010); Tabuada (2007), and

This chapter is based on van Loon et al. (2014).

a particular class of networked control systems Dačić and Nešić (2007); Donkers et al. (2011); Hespanha et al. (2007); Walsh et al. (2002), as we will highlight in this chapter. In particular, we show that all three application classes can be modeled in the considered hybrid modeling framework.

Besides showing the unifying modeling character of the studied class of hybrid systems, we are also interested in the stability and $\mathcal{L}_2$-gain analysis of these dynamical systems. The latter is an important performance measure for many situations, and has already attracted quite some attention in the literature, see, e.g., Dai et al. (2010); Goebel et al. (2009); Heemels et al. (2013) and Aangenent et al. (2010); Loquen et al. (2008); Nešić et al. (2008); Zaccarian et al. (2011) for related classes of hybrid systems. Especially the work in Dai et al. (2010); Heemels et al. (2013) focused on the hybrid systems class with periodic time-triggered jump conditions and exploited common quadratic timer-dependent Lyapunov/storage functions based on solutions to Riccati differential equations, i.e., Lyapunov/storage functions that depend on a timer state, see, e.g., van der Schaft (1999). This analysis led to conditions based on linear matrix inequalities (LMIs) for obtaining upper bounds on the $\mathcal{L}_2$-gain. In fact, in this chapter we employ a similar analysis but instead of using a *common quadratic* timer-dependent Lyapunov/storage function, we propose to use more versatile timer-dependent piecewise quadratic (PWQ) Lyapunov/storage functions, thereby providing improved conditions for $\mathcal{L}_2$-gain estimates compared to the existing ones in literature. In contrast to the standard use of PWQ Lyapunov functions, see, e.g., Johansson and Rantzer (1998), due to the presence of both flow and jump dynamics, and the timer dependence of the Lyapunov/storage function for the $\mathcal{L}_2$-gain analysis, new proof techniques are needed. In particular, the proof of our main result is based on using *trajectory-dependent* Lyapunov/storage functions in the sense that the functions do not only depend on the actual value of the state, but also on (future) disturbance values. In order to show that the realized conditions result in better estimates of the $\mathcal{L}_2$-gain than the existing ones in Heemels et al. (2013), we will provide a numerical example that indeed illustrates the realized improvements.

Summarizing, the contribution of this chapter is twofold. First, we will show that the presented hybrid systems framework covers a broad variety of control applications, thereby demonstrating the unifying character of the hybrid systems class under study. The second contribution is formed by providing improved $\mathcal{L}_2$-gain estimates compared to the existing ones in literature.

The remainder of the chapter is organized as follows. In Section 6.2, we introduce a general representation of the hybrid modeling framework that we study in this chapter, and provide the problem formulation. In Section 6.3, we show how two control applications can be modeled in this unifying framework. The main result on improved conditions to analyze the stability and $\mathcal{L}_2$-gain properties of the hybrid system under study is presented in Section 6.4, and the effectiveness of the conditions is demonstrated using a numerical example in

Section 6.5. Finally, we end with conclusions in Section 6.6.

6.1.1 Nomenclature

The following notational conventions will be used. Let $\mathbb{N}$, $\mathbb{R}$ denote the set of non-negative integers and real numbers, respectively. We call a matrix $P \in \mathbb{R}^{n\times n}$ positive definite and write $P \succ 0$, if $P = P^\top$ and $x^\top P x > 0$ for all $x \neq 0$. Similarly, we call $P \in \mathbb{R}^{n\times n}$ negative definite, and write $P \prec 0$, when $P = P^\top$ and $x^\top P x < 0$ for all $x \neq 0$. We use I_n to denote the identity matrix with dimensions $n \times n$. For brevity, we write symmetric matrices of the form $\begin{bmatrix} A & B \\ B^\top & C \end{bmatrix}$ sometimes as $\begin{bmatrix} A & B \\ \star & C \end{bmatrix}$. Furthermore, a function $\phi : \mathbb{R}_{\geq 0} \to \mathbb{R}_{\geq 0}$ is a class $\mathcal{K}_\infty$ function if it is zero at zero, continuous, strictly increasing and unbounded, i.e., $\lim_{s\to\infty} \phi(s) = \infty$.

6.2 Hybrid model class and problem formulation

In this chapter, we study the class of hybrid systems given by

$$\frac{\mathrm{d}}{\mathrm{d}t}\begin{bmatrix} \xi \\ \tau \end{bmatrix} = \begin{bmatrix} A\xi + Bw \\ 1 \end{bmatrix}, \text{ when } \tau \in [0, h] \tag{6.1a}$$

$$\begin{bmatrix} \xi^+ \\ \tau^+ \end{bmatrix} = \begin{cases} \begin{bmatrix} J_1\xi \\ 0 \end{bmatrix}, & \text{when } \tau = h \text{ and } \xi^\top Q \xi > 0 \\ \begin{bmatrix} J_2\xi \\ 0 \end{bmatrix}, & \text{when } \tau = h \text{ and } \xi^\top Q \xi \leq 0 \end{cases} \tag{6.1b}$$

$$z = C\xi + Dw. \tag{6.1c}$$

The states of this hybrid system consist of $\xi \in \mathbb{R}^{n_\xi}$ and a timer variable $\tau \in \mathbb{R}_{\geq 0}$. The variable $w \in \mathbb{R}^{n_w}$ denotes the disturbance input and z the performance output. Moreover, A, B, C, D, J_1, J_2, Q are constant real matrices of appropriate dimensions and $h \in \mathbb{R}_{>0}$ is a positive timer threshold.

Interpreting the dynamics of (6.1), which is done in the sense of Goebel et al. (2012), reveals that (6.1) has *periodic* time-triggered jump conditions, i.e., jumps take place at times kh, $k \in \mathbb{N}$. Note that this guarantees, amongst others, that the hybrid system (6.1) produces global solutions, i.e., defined on $t \in [0, \infty)$, and Zeno behavior, see, e.g., Goebel et al. (2012), does not occur. Moreover, the jump map is a (possibly discontinuous) piecewise linear (PWL) map given by (6.1b), and in between the jumps the system flows according to the differential equations in (6.1a). This class of systems includes the closed-loop systems arising from reset control systems in Guo et al. (2012), and periodic event-triggered control (PETC) for linear systems in Heemels et al. (2013), and many more. How the two mentioned applications can be modeled in this unifying framework is discussed in detail in Section 6.3 below.

Remark 6.1. *The hybrid system* (6.1) *can be seen as a sampled-data or time-regularized version of the hybrid system*

$$\dot{\xi} = A\xi + Bw, \qquad \text{when } \xi^\top Q\xi > 0 \tag{6.2a}$$

$$\xi^+ = J\xi, \qquad \text{when } \xi^\top Q\xi \leq 0. \tag{6.2b}$$

Indeed, if we take in (6.1) $J_1 = I_{n_\xi}$ *and* $J_2 = J$*, the resulting hybrid model can be seen as an implementation of the jump rule in* (6.2b) *but only verified at the times* $t_k = kh$, $k \in \mathbb{N}$*. Such regularizations are often used when* (6.2) *might exhibit Zeno behavior, see, e.g., Guo et al. (2012); Heemels et al. (2013); Nešić et al. (2008); Zaccarian et al. (2011) (the occurrence of Zeno behavior in systems as in* (6.2) *has been investigated in Borgers and Heemels (2014)). Clearly, its 'sampled-data' version of the form* (6.1) *has no such behavior, which therefore has analysis and implementation advantages.*

Remark 6.2. *Note that the hybrid system* (6.1) *has a PWL jump map with only two regions specified by* $\xi^\top Q\xi > 0$ *and* $\xi^\top Q\xi \leq 0$*, respectively. However, the modeling and analysis provided below can easily be extended to conewise linear jump maps with more than* 2 *regions.*

In this chapter, we are, besides showing the (unifying) modeling character of the class of systems described by (6.1), also interested in the stability and $\mathcal{L}_2$-gain analysis of these systems. These properties are formally defined below.

Definition 6.1. *The hybrid system* (6.1) *is said to be globally exponentially stable (GES), if there exist* $c > 0$ *and* $\rho > 0$ *such that for any initial condition* $\xi(0) = \xi_0 \in \mathbb{R}^{n_\xi}$ *all corresponding solutions to* (6.1) *with* $\tau(0) \in [0, h]$ *and* $w = 0$ *satisfy* $\|\xi(t)\| \leq ce^{-\rho t}\|\xi_0\|$ *for all* $t \in \mathbb{R}_{\geq 0}$*. In this case, we call* ρ *a (lower bound on the) decay rate.*

Definition 6.2. *The hybrid system* (6.1) *is said to have an* $\mathcal{L}_2$*-gain from* w *to* z *smaller than or equal to* γ*, if there is a* $\mathcal{K}_\infty$ *function* $\delta : \mathbb{R}^{n_\xi} \to \mathbb{R}_{\geq 0}$ *such that for any* $w \in \mathcal{L}_2$*, any initial state* $\xi(0) = \xi_0 \in \mathbb{R}^{n_\xi}$*, and* $\tau(0) \in [0, h]$*, the corresponding solution to* (6.1) *satisfies* $\|z\|_{\mathcal{L}_2} \leq \delta(\xi_0) + \gamma\|w\|_{\mathcal{L}_2}$*, where* $\mathcal{L}_2$ *denotes the set of square-integrable functions and* $\|\cdot\|_{\mathcal{L}_2}$ *the corresponding* $\mathcal{L}_2$*-norm.*

Before presenting new techniques to analyze GES and the $\mathcal{L}_2$-gain, we will first show the unifying modeling capabilities of the model class (6.1).

6.3 Unified modeling framework

In this section, we will consider three different control applications and show that they can be written in the hybrid system framework given by (6.1).

6.3.1 Periodic event-triggered control systems

The first domain of application is event-triggered control (ETC), see, e.g., Lunze and Lehmann (2010); Tabuada (2007), Heemels et al. (2013) for some recent approaches, and Heemels et al. (2012) for a recent overview. ETC is a control strategy that is designed to reduce the amount of computations and communications in a feedback control system by updating and communicating sensor and actuator data only when needed to guarantee stability or performance properties. The ETC strategy that we consider in this chapter is recently proposed in Heemels et al. (2013) as a novel ETC strategy for linear systems that combines ideas from periodic sampled-data control and ETC, leading to so-called periodic event-triggered control (PETC) systems. In PETC, the event-triggering condition is verified *periodically* in time instead of continuously as in standard ETC, see, e.g., Lunze and Lehmann (2010); Tabuada (2007). Hence, at every sampling interval it is decided whether or not new measurements and control signals need to be computed and transmitted.

In the PETC setting of Heemels et al. (2013) that we consider in this chapter, the plant is given by a continuous linear time-invariant (LTI) system of the form

$$\begin{cases} \dot{x}_p &= A_p x_p + B_{pu} u + B_{pw} w \\ y &= C_p x_p, \end{cases} \tag{6.3}$$

where $x_p \in \mathbb{R}^{n_p}$ denotes the state of the plant, $u \in \mathbb{R}^{n_u}$ the control input and $y \in \mathbb{R}^{n_y}$ the plant output. The plant in (6.3) is controlled in an event-triggered feedback fashion using the following state-feedback controller

$$u(t) = K\hat{x}_p(t), \quad \text{for } \ t \in \mathbb{R}_{\geq 0}, \tag{6.4}$$

where $\hat{x}_p \in \mathbb{R}^{n_p}$ is a left-continuous signal[1], given for $t \in (t_k, t_{k+1}]$, $k \in \mathbb{N}$, by

$$\hat{x}_p(t) = \begin{cases} x_p(t_k), & \text{when } \ \xi(t_k)^\top Q \xi(t_k) > 0, \\ \hat{x}_p(t_k), & \text{when } \ \xi(t_k)^\top Q \xi(t_k) \leq 0, \end{cases} \tag{6.5}$$

where $\xi := [x_p^\top \ \ \hat{x}_p^\top]^\top$ and t_k, $k \in \mathbb{N}$, are the sampling times, which are periodic in the sense that $t_k = kh$, $k \in \mathbb{N}$, with $h > 0$ the sampling interval. Fig. 6.1 shows a schematic representation of the PETC configuration that we consider in this chapter. In this figure, $\hat{x}_p(t)$ denotes the most recently transmitted measurement of the state $x_p(t)$ to the controller. Whether or not $x_p(t)$ is transmitted is based on an event-triggering condition. In particular, if at time t_k it holds that $\xi^\top(t_k)Q\xi(t_k) > 0$, the current state $x_p(t_k)$ is transmitted to the controller and $\hat{x}_p$, and as a consequence u, are updated accordingly. If, however, $\xi^\top(t_k)Q\xi(t_k) \leq 0$, the current state information is not sent to the controller and $\hat{x}_p$ and u are kept the same for (at least) another sampling interval. In Heemels

[1] A signal $x : \mathbb{R}_{\geq 0} \to \mathbb{R}^n$ is called left-continuous, if for all $t > 0$, $\lim_{s \uparrow t} x(s) = x(t)$.

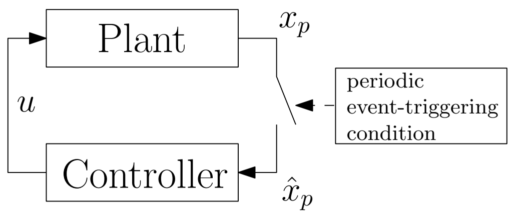

Fig. 6.1. Schematic representation of an event-triggered control system.

et al. (2013) it was shown that such quadratic event-triggering conditions form a relevant class of triggering conditions because many popular event triggering conditions can be written in this form. For instance, an event-triggering condition of the form

$$\|\hat{x}_p(t_k) - x_p(t_k)\| > \sigma\|x_p(t_k)\|, \tag{6.6}$$

with $\sigma > 0$, can be used to determine whether, at time t_k, it is required to transmit $x_p(t_k)$ to the controller, or that the latest sent value $\hat{x}_p(t_k)$ is still adequate. Clearly, condition (6.6) can be written in the quadratic form of (6.5) by taking

$$Q = \begin{bmatrix} (1-\sigma^2)I_{n_p} & -I_{n_p} \\ -I_{n_p} & I_{n_p} \end{bmatrix}. \tag{6.7}$$

The complete model of the PETC system can be captured in the hybrid system format of (6.1), by combining (6.3), (6.4) and (6.5), where we obtain

$$A = \begin{bmatrix} A_p & B_{pu}K \\ 0 & 0 \end{bmatrix}, \quad B = \begin{bmatrix} B_{pw} \\ 0 \end{bmatrix}, \quad J_1 = \begin{bmatrix} I_{n_p} & 0 \\ I_{n_p} & 0 \end{bmatrix},$$

and $J_2 = I_{n_\xi}$ with $n_\xi = 2n_p$. In addition to the state feedback controller in (6.4), one can also use dynamic output-feedback PETC controllers and output-based event-triggering conditions, see Heemels et al. (2013), in a straightforward fashion.

6.3.2 Reset control systems

A second domain of applications of the class of hybrid systems that we consider in this chapter is formed by reset control. Reset control is a discontinuous control strategy designed as a means to overcome the fundamental limitations of linear feedback by allowing to reset the controller state, or subset of states, whenever certain conditions on its input and output are satisfied, see, e.g., Aangenent et al. (2010); Beker et al. (2004); Nešić et al. (2008); Zaccarian et al. (2011). In all afore-cited papers the reset condition is monitored continuously, while in Guo et al. (2012) the authors proposed to verify the reset condition at discrete-time instances. In other words, at every sampling time $t_k = kh$, $k \in \mathbb{N}$, with sampling interval $h > 0$, it is decided whether or not a reset takes place. This periodic reset verification can be modeled in the hybrid systems class (6.1). In order to show this, we consider reset controllers, to control systems of the form (6.3), of the type

$$\frac{\mathrm{d}}{\mathrm{d}t}\begin{bmatrix} x_c \\ \tau \end{bmatrix} = \begin{bmatrix} A_c x_c + B_c e \\ 1 \end{bmatrix}, \text{ when } \tau \in [0, h] \tag{6.8a}$$

$$\begin{bmatrix} x_c^+ \\ \tau^+ \end{bmatrix} = \begin{cases} \begin{bmatrix} x_c \\ 0 \end{bmatrix}, & \text{when } \tau = h \text{ and } \xi^\top Q \xi > 0 \\ \begin{bmatrix} R_c x_c \\ 0 \end{bmatrix}, & \text{when } \tau = h \text{ and } \xi^\top Q \xi \leq 0 \end{cases} \tag{6.8b}$$

$$u = C_c x_c + D_c e, \tag{6.8c}$$

where $x_c \in \mathbb{R}^{n_c}$ denotes the continuous state of the controller and x_c^+ its value after a reset, $R_c \in \mathbb{R}^{n_c \times n_c}$ is the reset matrix and $e := r - y \in \mathbb{R}$ is the error between the reference signal r and the output of the plant y. Moreover, $\xi := [x_p^\top \ \ \hat{x}_c^\top]^\top$ is an augmented state vector containing plant and controller states. The reset condition that we employ in this chapter is based on the sign of the product between the error e and controller input $u \in \mathbb{R}$, which was originally proposed in Zaccarian et al. (2005)[2]. In particular, the reset controller (6.8) acts like a linear controller whenever its input e and output u have the same sign, i.e., $e^\top u > 0$, and it resets its output otherwise. This reset condition can be represented, for the case $r = 0$, in terms of a general quadratic relation as in (6.8b), with

$$Q = \begin{bmatrix} C_p & 0 \\ -D_c C_p & C_c \end{bmatrix}^\top \begin{bmatrix} 0 & -1 \\ -1 & 0 \end{bmatrix} \begin{bmatrix} C_p & 0 \\ -D_c C_p & C_c \end{bmatrix}. \tag{6.9}$$

Remark 6.3. *Note that two well-known reset controllers, namely, the Clegg integrator and the first-order reset element (FORE), see, e.g., Zaccarian et al. (2005) and the references therein, can be modeled as in* (6.8)*, if implemented in a periodic time-triggered manner, using*

$$\textit{Clegg integrator}: \left[\begin{array}{c|c} A_c & B_c \\ \hline C_c & D_c \end{array}\right] = \left[\begin{array}{c|c} 0 & 1 \\ \hline 1 & 0 \end{array}\right], \tag{6.10}$$

$$\textit{FORE}: \left[\begin{array}{c|c} A_c & B_c \\ \hline C_c & D_c \end{array}\right] = \left[\begin{array}{c|c} -\beta & 1 \\ \hline 1 & 0 \end{array}\right], \tag{6.11}$$

in which $\beta \in \mathbb{R}$ denotes the single pole of the FORE.

[2] In Zaccarian et al. (2005), the reset condition is verified in continuous time, so not at discrete times $t_k = kh$, $k \in \mathbb{N}$ for some $h > 0$.

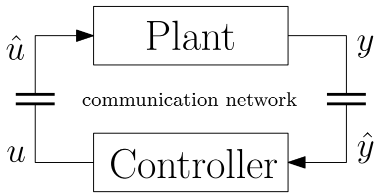

Fig. 6.2. Schematic representation of a networked control system.

The interconnection of the reset control system (6.8) and plant (6.3) can be written in the hybrid system format of (6.1), with augmented state vector $\xi = [x_p^\top \; x_c^\top]^\top$, in which

$$A = \begin{bmatrix} A_p - B_{pu}D_cC_p & B_{pu}C_c \\ -B_cC_p & A_c \end{bmatrix}, \;\; B = \begin{bmatrix} B_{pw} \\ 0 \end{bmatrix}, \;\; J_2 = \begin{bmatrix} I_{n_p} & 0 \\ 0 & R_c \end{bmatrix},$$

and $J_1 = I_{n_\xi}$ with $n_\xi = n_p + n_c$.

Remark 6.4. *By showing that the PETC applications in Heemels et al. (2013) and periodic reset control systems in Guo et al. (2012) fit in the same framework* (6.1)*, it is possible to use the stability conditions of Heemels et al. (2013) for PETC in the context of reset control in Guo et al. (2012), which actually provides less conservative stability conditions than used in Guo et al. (2012), cf. (Heemels et al., 2013, Theorem III.4) with (Guo et al., 2012, Proposition 4). Transforming results from one application domain to another is one particular advantage of using a unifying modeling framework.*

6.3.3 Networked control systems

The third domain of application that we consider in this chapter consist of networked control systems (NCSs), see, e.g, Hespanha et al. (2007) for an overview. An NCS is a control system in which the control loops are closed over a real-time communication network, which is schematically depicted in Fig. 6.2. In this figure, $y \in \mathbb{R}^{n_y}$ denotes the plant output and $\hat{y} \in \mathbb{R}^{n_y}$ its so-called 'networked' version, i.e., the most recent output measurements of the plant that are available at the controller. The control output is denoted by $u \in \mathbb{R}^{n_u}$ and the most recent control output available at the plant (actuators) is given by $\hat{u} \in \mathbb{R}^{n_u}$.

In the remainder of this section, we will show that the hybrid system model (6.1) also captures a specific class of NCSs with constant transmission intervals and a shared network with dynamic protocols, as, for instance, studied in Dačić and Nešić (2007); Donkers et al. (2011); Walsh et al. (2002). Such NCS configurations can be modeled in the framework (6.1) by considering plants of the form (6.3), in which the control input u is replaced by its networked version $\hat{u}$. The output-feedback controller with state $x_c \in \mathbb{R}^{n_c}$ is assumed to be given in either continuous-time by

$$\begin{cases} \dot{x}_c &= A_c x_c + B_c \hat{y} \\ u &= C_c x_c + D_c \hat{y}, \end{cases} \tag{6.12}$$

or in discrete time (with abuse of notation) by

$$\begin{cases} x_c(t_{k+1}) = A_c x_c(t_k) + B_c \hat{y}(t_k) \\ u(t) \qquad\;\; = C_c x_c(t_k) + D_c \hat{y}(t_{k-1}), \end{cases} \tag{6.13}$$

for all $t \in (t_k, t_{k+1}]$, where we adopt a zero-order-hold (ZOH) assumption. The network-induced errors are defined as follows:

$$e = \begin{bmatrix} e_y \\ e_u \end{bmatrix} := \begin{bmatrix} \hat{y} - y \\ \hat{u} - u \end{bmatrix}, \tag{6.14}$$

and describe the difference between the most recently received information at the controller/actuators and the current value of the plant/controller output, respectively. The network itself is assumed to operate in a ZOH fashion in between the updates of the values $\hat{y}$ and $\hat{u}$, i.e., $\dot{\hat{y}} = 0$ and $\dot{\hat{u}} = 0$ between update times. We consider the case where the plant is equipped with n_y sensors and n_u actuators that are grouped into N nodes. At the transmission/update times t_k, $k \in \mathbb{N}$, the updates satisfy

$$\begin{cases} \hat{y}(t_k^+) = \Gamma^y_{\sigma_k} y(t_k) + (I - \Gamma^y_{\sigma_k})\hat{y}(t_k) \\ \hat{u}(t_k^+) = \Gamma^u_{\sigma_k} u(t_k) + (I - \Gamma^u_{\sigma_k})\hat{u}(t_k). \end{cases} \tag{6.15}$$

In (6.15), $\Gamma_i := \mathrm{diag}(\Gamma^y_i, \Gamma^u_i)$, $i = \{1, \ldots, N\}$, are diagonal matrices given by $\Gamma_i = \mathrm{diag}(\gamma_{i,1}, \ldots, \gamma_{i,n_y+n_u})$, in which the elements $\gamma_{i,j}$, with $i \in \{1, \ldots, N\}$ and $j \in \{1, \ldots, n_y\}$, are equal to one, if plant output y^j is in node i and are zero elsewhere, and elements $\gamma_{i,j+n_y}$, with $i \in \{1, \ldots, N\}$ and $j \in \{1, \ldots, n_u\}$, are equal to one, if controller output u^j is in node i and are zero elsewhere. In the modeling framework, network protocols determine at a transmission/update time t_k, $k \in \mathbb{N}$, which node is allowed access to the network in order to update its values. This is exactly captured in (6.15) when node $\sigma_k \in \{1, \ldots, N\}$ gets access. The hybrid framework (6.1) especially allows one to study quadratic network protocols, see, e.g., Dačić and Nešić (2007); Donkers et al. (2011); Walsh et al. (2002), of the form

$$\sigma_k = \arg\min \, \xi^\top(t_k) R_i \xi(t_k), \tag{6.16}$$

for all $i \in \{1, \ldots, N\}$, in which R_i, $i \in \{1, \ldots, N\}$ are certain given matrices and $\xi = [x_p^\top \; x_c^\top \; e_y^\top \; e_u^\top]^\top$. In fact, the well-known try-once-discard (TOD) protocol, see Walsh et al. (2002), belongs to this particular class of protocols. In this protocol, the node with the largest network-induced error is granted access to the network in order to update its values, which is defined by

$$\sigma_k = \arg\max_{i\in\{1,\dots,N\}} \|\Gamma_i e(t_k)\|^2. \tag{6.17}$$

For simplicity, let us only consider two nodes (although the extension to $N > 2$ nodes can be done in a straightforward fashion, see also Remark 6.2) and continuous-time controllers of the type (6.12). The complete model of the NCS can be written in the hybrid system format of (6.1), by combining (6.3), (6.12), (6.14) and (6.16), in which the augmented state vector is defined as $\xi = [x_p^\top \; x_c^\top \; e_y^\top \; e_u^\top]^\top$, and the updates are according to

$$\begin{bmatrix}\xi^+\\ \tau^+\end{bmatrix} = \begin{cases}\begin{bmatrix}J_1\xi\\ 0\end{bmatrix}, & \text{when } \tau = h \text{ and } \xi^\top R_1\xi \le \xi^\top R_2\xi,\\[2ex] \begin{bmatrix}J_2\xi\\ 0\end{bmatrix}, & \text{when } \tau = h \text{ and } \xi^\top R_2\xi \le \xi^\top R_1\xi,\end{cases} \tag{6.18}$$

and the matrices in (6.1) are given by

$$A = \begin{bmatrix} A_p + B_{pu}D_cC_p & B_{pu}C_c & B_{pu}D_c & B_{pu}\\ B_cC_p & A_c & B_c & 0\\ -C_p(A_p + B_{pu}D_cC_p) & -C_pB_{pu}C_c & -C_pB_{pu}D_c & -C_pB_{pu}\\ -C_cB_cC_p & -C_cA_c & -C_cB_c & 0\end{bmatrix},$$

$$B = \begin{bmatrix} B_{pw}\\ 0\\ -C_pB_{pw}\\ 0\end{bmatrix} \quad \text{and} \quad J_i = \begin{bmatrix} I & 0\\ 0 & I-\Gamma_i\end{bmatrix}, \quad \text{for } i \in \{1,2\}.$$

6.4 Stability and $\mathcal{L}_2$-gain analysis of the hybrid system

In this section, we present improved conditions to analyze stability and performance of the hybrid system (6.1). As these conditions build upon results presented in (Heemels et al., 2013, Section III.A), we first briefly recall this analysis and refer to Heemels et al. (2013) for more details.

6.4.1 Riccati-based analysis

In Heemels et al. (2013), an $\mathcal{L}_2$-gain analysis is performed on systems of the form (6.1), which is based on a Lyapunov/storage function $V(\xi,\tau)$, see van der Schaft (1999), satisfying

$$\tfrac{\mathrm{d}}{\mathrm{d}t}V \le -2\rho V - \gamma^{-2}z^\top z + w^\top w, \tag{6.19}$$

during the flow (6.1a), and

$$V(J_1\xi, 0) \leq V(\xi, h), \quad \text{for all } \xi \text{ with } \xi^\top Q\xi > 0, \tag{6.20a}$$

$$V(J_2\xi, 0) \leq V(\xi, h), \quad \text{for all } \xi \text{ with } \xi^\top Q\xi \leq 0, \tag{6.20b}$$

during jumps (6.1b). From these conditions, we can guarantee that the $\mathcal{L}_2$-gain from w to z is smaller than or equal to γ. In Heemels et al. (2013), $V(\xi, \tau)$ was chosen of the form

$$V(\xi, \tau) = \xi^\top P(\tau)\xi, \tag{6.21}$$

where $P\colon [0, h] \to \mathbb{R}^{n_\xi \times n_\xi}$ with $P(\tau) \succ 0$ for $\tau \in [0, h]$, is selected to satisfy the Riccati differential equation (where we omitted τ for compactness of notation)

$$\begin{aligned}\tfrac{\mathrm{d}}{\mathrm{d}\tau}P = &-A^\top P - PA - 2\rho P - \gamma^{-2}C^\top C \\ &- (PB + \gamma^{-2}C^\top D)M(B^\top P + \gamma^{-2}D^\top C),\end{aligned} \tag{6.22}$$

provided the solution exists on $[0, h]$ for a desired convergence rate $\rho > 0$, in which $M := (I - \gamma^{-2}D^\top D)^{-1}$ is assumed to exist and to be positive definite, which means that $\gamma^2 > \lambda_{\max}(D^\top D)$. It is proven in Heemels et al. (2013) that this choice for the matrix function P guarantees satisfaction of the 'flow condition' (6.19). The 'jump condition' (6.20) is guaranteed by LMI-based conditions, which were obtained by relating $P_0 := P(0)$ to $P_h := P(h)$ and lead to a proper value of the boundary value P_h. This was done by introducing the Hamiltonian matrix

$$H := \begin{bmatrix} A + \rho I + \gamma^{-2}BMD^\top C & BMB^\top \\ -C^\top LC & -(A + \rho I + \gamma^{-2}BMD^\top C)^\top \end{bmatrix}, \tag{6.23}$$

in which $L := (\gamma^2 I - DD^\top)^{-1}$. Moreover, the matrix exponential

$$F(\tau) := e^{-H\tau} = \begin{bmatrix} F_{11}(\tau) & F_{12}(\tau) \\ F_{21}(\tau) & F_{22}(\tau) \end{bmatrix} \tag{6.24}$$

was defined, which enables the computation of the explicit solution to the Riccati differential equation (6.22), yielding

$$P_0 = (F_{21}(h) + F_{22}(h)P_h)\,(F_{11}(h) + F_{12}(h)P_h)^{-1}\,, \tag{6.25}$$

provided that the solution (6.25) is well defined on the interval $[0, h]$, see, e.g., Başar and Bernhard (1991). To guarantee this, in Heemels et al. (2013) the following assumption was adopted.

Assumption 6.1. *$F_{11}(\tau)$ is invertible for all $\tau \in [0, h]$.*

Let us also introduce the notation $\bar{F}_{11} := F_{11}(h)$, $\bar{F}_{12} := F_{12}(h)$, $\bar{F}_{21} := F_{21}(h)$ and $\bar{F}_{22} := F_{22}(h)$, and the matrix $\bar{S}$ that satisfies $\bar{S}\bar{S}^\top := -\bar{F}_{11}^{-1}\bar{F}_{12}$. The matrix $\bar{S}$ exists under Assumption 6.1, because this assumption will guarantee that the matrix $-\bar{F}_{11}^{-1}\bar{F}_{12}$ is positive semi-definite, see the proof of (Heemels et al., 2013, Theorem III.2). In Heemels et al. (2013), the following result was presented in which the LMIs were derived guaranteeing (6.20) by using (6.25) (note that compared to the LMIs in Heemels et al. (2013), here an additional Schur complement has been used).

Theorem 6.1. *(Heemels et al. (2013)) Consider the hybrid system* (6.1) *and let $\rho > 0$ and $\gamma > \sqrt{\lambda_{max}(D^\top D)}$ be given. Assume that Assumption 6.1 holds and that there exist a matrix $P_h \succ 0$, and scalars $\mu_i \geq 0$, $i \in \{1, 2\}$, such that*

$$\begin{bmatrix} P_h + (-1)^i \mu_i Q - J_i^\top \bar{F}_{21}\bar{F}_{11}^{-1} J_i - J_i^\top \bar{F}_{11}^{-\top} P_h \bar{F}_{11}^{-1} J_i & J_i^\top \bar{F}_{11}^{-\top} P_h S \\ \star & I - S^\top P_h S \end{bmatrix} \succ 0, \quad (6.26)$$

Then, the hybrid system (6.1) *is GES with convergence rate ρ (when $w = 0$) and has an $\mathcal{L}_2$-gain from w to z smaller than or equal to γ.*

The conditions (6.26) guarantee indeed that (6.20) holds, and (6.19) and (6.20) together can be used to establish GES and an $\mathcal{L}_2$-gain smaller than or equal to γ.

6.4.2 Main result on novel $\mathcal{L}_2$-gain conditions

The analysis in Heemels et al. (2013), as briefly recalled above, is based on the existence of a *common* quadratic timer-dependent Lyapunov/storage function as in (6.21). The novelty in our improved conditions lies in the fact that we will use a more versatile timer-dependent piecewise quadratic Lyapunov/storage function, see, e.g., Ferrari-Trecate et al. (2002); Johansson and Rantzer (1998), based on the regions

$$\Omega_i := \left\{ \xi \in \mathbb{R}^{n_\xi} \,\middle|\, \xi^\top X_i \xi \geq 0 \right\}, \quad (6.27)$$

where the symmetric matrices X_i, $i \in \{1, \dots, N\}$, are such that $\{\Omega_1, \Omega_2, \dots, \Omega_N\}$ forms a partition of $\mathbb{R}^{n_\xi}$, i.e., $\cup_{i=1}^N \Omega_i = \mathbb{R}^{n_\xi}$ and the intersection of Ω_i and Ω_j, $i, j \in \{1, \dots, N\}$, is of zero measure. We assume that $\{\xi \in \mathbb{R}^{n_\xi} \mid \xi^\top Q \xi \leq 0\} \subseteq \bigcup_{i=1}^{N_1} \Omega_i$ and $\{\xi \in \mathbb{R}^{n_\xi} \mid \xi^\top Q \xi \geq 0\} \subseteq \bigcup_{i=N_1+1}^{N} \Omega_i$.

Note that the construction of a Lyapunov/storage function for the hybrid system (6.1) is less straightforward if compared to the more classical case of discrete-time and continuous-time piecewise affine systems (see Ferrari-Trecate et al. (2002); Johansson and Rantzer (1998)). This is due to the presence of both flow and jump dynamics and the fact that the jumps do depend both on time and the state. To introduce the storage function, we need the following notation. We denote by $\bar{\xi}(t, \xi_0, w)$ the solution to $\dot{\xi} = A\xi + Bw$ at time t with $\xi(0) = \xi_0$ and input $w \in \mathcal{L}_2$. Given $w \in \mathcal{L}_2$ and some fixed $t \in \mathbb{R}_{\geq 0}$, we denote by w_t the time-shifted signal given by $w_t(s) = w(s+t)$ for $s \geq 0$. We propose now to use the timer-dependent PWQ storage function given by

$$W(\xi, \tau, w, t) = \xi^\top \bar{P}_i(\tau)\xi \quad \text{if} \quad \bar{\xi}(h-\tau, \xi, w_t) \in \Omega_i, \tag{6.28}$$

where $\bar{P}_i(\tau)$, for each $i \in \{1, \dots, N\}$, is a solution to the Riccati differential equation

$$\begin{aligned} \tfrac{\mathrm{d}}{\mathrm{d}\tau}\bar{P}_i = &-A^\top \bar{P}_i - \bar{P}_i A - 2\rho \bar{P}_i - \gamma^{-2} C^\top C \\ &- (\bar{P}_i B + \gamma^{-2} C^\top D) M (B^\top \bar{P}_i + \gamma^{-2} D^\top C), \end{aligned} \tag{6.29}$$

for a desired convergence rate $\rho > 0$, satisfying $\bar{P}_i(h) = P_i$, where the positive definite matrices P_i, $i \in \{1, \dots, N\}$, are chosen according to solutions of the LMIs presented in Theorem 6.2 below. Interestingly, note that the value of $W(\xi, \tau, w, t)$ at time t (given τ) depends on ξ and $w\,|_{[t,t+h-\tau]}$ and thus on *future* disturbance values. The state dependence is only at the present time, i.e., on $\xi(t)$, while the dependence on the future disturbance is only in selecting the index 'i' in (6.28). In particular, the sector Ω_i at the *next* sampling instant ($(k+1)h$, $k \in \mathbb{N}$) determines 'i', which remains constant in between two consecutive jump times, i.e., in the entire interval $[kh, (k+1)h)$. As such, we have a trajectory/disturbance-dependent Lyapunov/storage function. Thus the trajectory-dependency of the Lyapunov/storage function deviates from the common results in the literature on dissipativity or $\mathcal{L}_2$-gain analysis as there the Lyapunov/storage function typically depends only on the current state (or sometimes time), but not on future values of the disturbances/state. As a consequence, the interpretation of W as a genuine Lyapunov/storage function is less natural. We merely use it as a function (or functional) to establish the desired $\mathcal{L}_2$-gain properties in the mathematical proof, see also Remark 6.5 below.

Theorem 6.2. *Let $\gamma > \sqrt{\lambda_{\max}(D^\top D)}$, $N_1 < N$, and Assumption 6.1 hold. Suppose that there exist matrices $P_i = P_i^\top$, $i \in \{1, \dots, N\}$, and scalars $\mu_{i,j} \geq 0$, $i, j \in \{1, \dots, N\}$, satisfying*

$$\begin{bmatrix} P_i - \mu_{i,j} X_i & J_1^\top \bar{F}_{11}^{-\top} P_j \bar{S} & J_1^\top (\bar{F}_{21}\bar{F}_{11}^{-1} + \bar{F}_{11}^{-\top} P_j \bar{F}_{11}^{-1}) \\ \star & I - \bar{S}^\top P_j \bar{S} & 0 \\ \star & \star & \bar{F}_{21}\bar{F}_{11}^{-1} + \bar{F}_{11}^{-\top} P_j \bar{F}_{11}^{-1} \end{bmatrix} \succ 0 \tag{6.30a}$$

for all $i \in \{N_1+1, \dots, N\}$, $j \in \{1, \dots, N\}$, and

$$\begin{bmatrix} P_i - \mu_{i,j} X_i & J_2^\top \bar{F}_{11}^{-\top} P_j \bar{S} & J_2^\top (\bar{F}_{21}\bar{F}_{11}^{-1} + \bar{F}_{11}^{-\top} P_j \bar{F}_{11}^{-1}) \\ \star & I - \bar{S}^\top P_j \bar{S} & 0 \\ \star & \star & \bar{F}_{21}\bar{F}_{11}^{-1} + \bar{F}_{11}^{-\top} P_j \bar{F}_{11}^{-1} \end{bmatrix} \succ 0 \tag{6.30b}$$

for all $i \in \{1, \dots, N_1\}$, $j \in \{1, \dots, N\}$, and

$$P_i \succ 0, \quad \textit{for all } i \in \{1, \dots, N\}. \tag{6.30c}$$

Then, the hybrid system (6.1) *is GES with convergence rate* ρ *(when* $w = 0$*) and has an* $\mathcal{L}_2$*-gain from* w *to* z *smaller than or equal to* γ*.*

Proof. The proof can be found in Appendix A.5.1. □

Remark 6.5. *Let us provide some more intuition behind our main result in Theorem 6.2. In this respect, an important observation is that feasibility of* (6.26) *not only implies that the hybrid system* (6.1) *is* $\mathcal{L}_2$*-stable with an upper bound on the* $\mathcal{L}_2$*-gain given by* γ*, it is* ***equivalent*** *to a check of* ℓ_2*-stability with gain less than or equal to* 1*, for the following discrete-time PWL system*

$$\xi_{k+1} = \begin{cases} \bar{F}_{11}^{-1} J_1 \xi_k + S w_k & \text{if } \xi_k^\top Q \xi_k > 0 \\ \bar{F}_{11}^{-1} J_2 \xi_k + S w_k & \text{if } \xi_k^\top Q \xi_k \leq 0 \end{cases} \tag{6.31a}$$

$$z_k = \begin{cases} \tilde{C} J_1 \xi_k & \text{if } \xi_k^\top Q \xi_k > 0 \\ \tilde{C} J_2 \xi_k & \text{if } \xi_k^\top Q \xi_k \leq 0, \end{cases} \tag{6.31b}$$

in which $\tilde{C}$ *satisfies* $\tilde{C}^\top \tilde{C} := \bar{F}_{12} \bar{F}_{11}^{-1}$*, using a common quadratic Lyapunov/storage function and only one S-procedure relaxation (i.e., relaxation (ii) below).*

In general, we can obtain less conservative conditions for the ℓ_2*-gain for a discrete-time PWL system* (6.31) *than the conditions* (6.26) *only using a common quadratic storage function. This is mainly because the analysis for a discrete-time PWL system allows us to apply, instead of a common Lyapunov/storage function, a more versatile piecewise quadratic Lyapunov/storage function, see Ferrari-Trecate et al. (2002); Johansson and Rantzer (1998) of the form*

$$V(\xi) = \xi^\top P_i \xi \quad \text{if } \xi \in \Omega_i, \tag{6.32}$$

for $i \in \{1, \ldots, N\}$ *and* Ω_i *as in* (6.27)*, and in addition, regional information can be used to relax the analysis even more, i.e.,*

(i) : require that P_i *is only positive definite in its corresponding sector, i.e.,* $P_i - \kappa_i X_i \succ 0$ *for all* $i \in \{1, \ldots, N\}$ *and* $\kappa_i \geq 0$*;*

(ii) : relaxation related to the current time instant, i.e., if $V(\xi_k) = \xi_k^\top P_i \xi_k$ *it holds that* $\xi_k^\top X_i \xi_k \geq 0$*;*

(iii) : relaxation related to the next the time instant, i.e., if $V(\xi_{k+1}) = \xi_{k+1}^\top P_j \xi_{k+1}$ *it holds that* $\xi_{k+1}^\top X_j \xi_{k+1} \geq 0$*.*

The LMI conditions (6.30) *in Theorem correspond to an* ℓ_2*-gain analysis for the discrete-time PWL system* (6.31) *with gain less than or equal to* 1*, using a Lyapunov/storage function of the form* (6.32) *and one S-procedure relaxation based on (ii). We are able to connect this to an* $\mathcal{L}_2$*-gain analysis of* (6.1) *by using a trajectory/disturbance-dependent Lyapunov/storage function as in* (6.28)*, in* *which the dependence on the future disturbance is only in selecting the index 'i' in* (6.28) *(which remains constant in between two consecutive jump times, i.e., in the entire interval* $[kh, (k+1)h)$*) while the state dependence is only at the present time, i.e., on* $\xi(t)$*.*

Although in Theorem 6.2 above we were able to use the relaxation (ii), we could not prove the result using the other relaxations (i) and (iii). Inspired by this observation, in Heemels et al. (2015a,b) the authors show, by adopting lifting-based techniques, the ***complete equivalence*** *between the* $\mathcal{L}_2$*-gain determination of* (6.1) *and the* ℓ_2*-gain characterization through* (6.31)*. In such a case,* ***all*** *relaxations (i), (ii) and (iii) may be applied.*

6.5 Reset control example

In this section, we illustrate the improvement of the presented theory using a numerical example taken from Nešić et al. (2008). In this example, the plant consists of an integrator system of the form (6.3) with

$$\left[\, A_p \middle| B_{pu} \middle| B_{pw} \middle| C_p \,\right] = \left[\, 0 \middle| 1 \middle| 1 \middle| 1 \,\right], \tag{6.33}$$

and $t_k = kh$, $k \in \mathbb{N}$, with sampling interval $h = 0.1$, which is controlled by a FORE of the form (6.8) and (6.11). The partition we use of the state-space into N number of sectors as in (6.27) is inspired by Aangenent et al. (2010); Zaccarian et al. (2005) and based on defining the angles $\phi_i = [-\sin(\theta_i)\ \ \cos(\theta_i)]^\top$ for $\theta_i = \frac{i\pi}{N}$, $i \in \{0, 1, \ldots, N\}$, such that we can define the following sector matrices $S_i = \phi_i(-\phi_{i-1})^\top + \phi_{i-1}(-\phi_i)^\top$. This allows us to form the symmetric matrices X_i of (6.27) as follows:

$$X_i = \begin{bmatrix} C_p & 0 \\ -D_c C_p & C_c \end{bmatrix}^\top S_i \begin{bmatrix} C_p & 0 \\ -D_c C_p & C_c \end{bmatrix}, \tag{6.34}$$

for all $i \in \{1, \ldots, N\}$. In the remainder of this example, we select $N_1 = 5$ and $N = 10$.

In Fig. 6.3, the $\mathcal{L}_2$-gain is represented as a function of the pole β of the FORE. The dashed line is obtained by the existing conditions in Heemels et al. (2013), see Theorem 6.1 using a common Lyapunov/storage function as in (6.21). The solid curve is obtained using the conditions of Theorem 6.2. From these curves it can be concluded that the results of Theorem 6.2 provide a significant improvement compared to the existing approach based on a common quadratic Lyapunov/storage function. In fact, for $\beta > 0$ the existing approach could not even establish a finite $\mathcal{L}_2$-gain, while the new approach presented here leads to such guarantees.

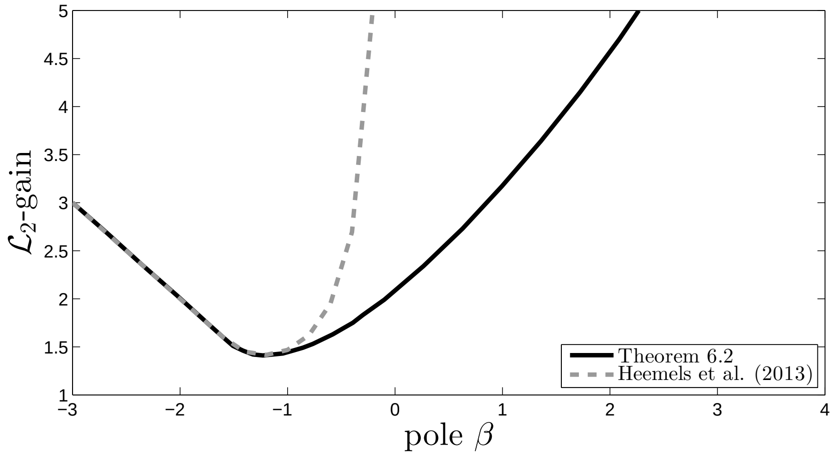

Fig. 6.3. $\mathcal{L}_2$-gain as function of the pole β of the FORE.

6.6 Conclusions

In this chapter, we have considered a particular class of hybrid systems with periodic time-triggered jump conditions and piecewise linear jump maps. The relevance of this framework is demonstrated by showing that a wide variety of control applications in the domains of reset control, event-triggered control, and networked control systems, can be captured in this framework. Interestingly, the unifying character of the framework can enable the transfer of results between the diverse application domains (see, e.g., Remark 6.4). In addition, we provided improved conditions to analyze the stability and the $\mathcal{L}_2$-performance of the hybrid systems under study using trajectory-dependent Lyapunov/storage functions as a technical novelty. The new conditions include the existing ones as a special case, and, hence, will never provide worse estimates of the $\mathcal{L}_2$-gain. In fact, using a numerical example it was shown that these new conditions result in (significantly) better estimates for the $\mathcal{L}_2$-gain compared to the existing ones in the literature.

Chapter 7

Conclusions and recommendations

7.1 Conclusions

In this thesis, hybrid control of linear (motion) systems has been considered. In the Introduction of this thesis (see Section 1.3), the general objectives of this thesis were stated as follows:

(I) *The development of novel hybrid/nonlinear controllers to improve the transient and/or steady-state performance of linear motion systems which are applicable to industrial high-tech systems;*

(II) *The development of novel techniques to analyze stability and performance of hybrid systems, preferably by exploiting frequency-domain design tools and non-parametric models;*

(III) *Experimental and industrial validation of the proposed controllers and techniques.*

The main contributions of this thesis can be summarized in terms of contributions on these three general objectives, which will be further detailed below.

Objective (I): Novel hybrid controller designs that connect to the industrial practice and result in an improved performance.

In Chapter 2, a novel scheduled controller architecture was proposed for dynamical systems with position-dependent switching sensor configurations. The proposed controller architecture has the favorable property that all individual components (except the time-varying gain) can be designed using classical frequency-domain loop-shaping techniques. Moreover, it was shown that, compared to the current state-of-practice linear control solutions, an improved transient and steady-state performance could be obtained.

In Chapter 3, a novel reference-dependent variable-gain control strategy was proposed that allows for a varying 'bandwidth' of the feedback controller in order to deal with reference-dependent conflicting control design trade-offs between low-frequency tracking and high-frequency noise suppression. All linear components of this controller can be designed using frequency-domain loop-shaping techniques for which easy-to-use tuning guidelines have been presented as well as a guideline to design the time-varying gain.

In Chapter 5, the concept of the split-path nonlinear filter was revisited and a novel variant was introduced, namely, the split-path nonlinear integrator (SPANI), which is especially designed for transient performance improvement of linear systems. The presented design tools for the SPANI connect to industrial practice in the sense that these allow the control engineer to design a linear integrator in parallel to a nominal linear controller, e.g., using classical frequency-domain loop-shaping techniques, and then to simply replace the linear integrator by a SPANI with the same gain.

Objective (II): Novel techniques to analyze stability and performance of hybrid systems.

The contributions on this topic can be categorized by 'data-based' conditions and 'LMI-based' conditions for stability and performance analysis.

The stability conditions in the Chapters 2, 3 and 4 are all data-based. In particular, the stability conditions for: The novel switched controller architecture in Chapter 2, the novel 'bandwidth-on-demand' controller in Chapter 3, and reset control systems (RCSs) in Chapter 4, are all graphically verifiable based on measured frequency response data of the (linear part of the) dynamical system.

In the Chapters 5 and 6, novel LMI-based conditions are presented to assess stability and/or $\mathcal{L}_2$-performance of two particular classes of hybrid systems. The LMI-based stability conditions presented in Chapter 5 are based on a hybrid dynamical system model for the closed-loop dynamics with SPANI, and also proved to be useful in the design of a SPANI. In Chapter 6, we focussed on a particular hybrid system class and showed the unifying modeling capabilities by modeling three different control application domains, namely, event-triggered control (ETC) systems, see, e.g., Heemels et al. (2012), reset control systems (RCS) and networked control systems (NCS), see, e.g., Bemporad et al. (2010); Hespanha et al. (2007), in this framework. Moreover, we provided novel LMI-based conditions to analyze the stability and characterize the $\mathcal{L}_2$-performance of the hybrid systems under study.

Objective (III): Validation on industrial benchmark systems.

Several industrial benchmark systems have been considered in this thesis in order to validate the proposed hybrid controllers and/or analysis techniques. In Chapter 2, the proposed switched controller has been experimentally validated on a motion system used in the lithography industry. In Chapter 3, the effectiveness of the proposed controller with a 'bandwidth-on-demand' characteristic has been experimentally demonstrated using an industrial nano-positioning motion system. In Chapter 4, the novel graphical data-based stability analysis conditions for reset control systems have been applied to an industrial piezo-actuated motion system used in the lithography industry. Finally in Chapter 5, a model-based case study of a positioning operation of an industrial pick-and-place machine has been used to validate our proposed split-path nonlinear integrator (SPANI).

Linear control techniques offer the control engineer a powerful, easy-to-use and insightful toolkit to design appropriate controllers for linear (motion) systems. Therefore, they are the logical first solution to try when feedback control is required. However, when the achievable performance of a linear control system is not meeting the requirements due to the inherent fundamental limitations, this thesis offers new solutions to overcome this situation. Indeed, in this thesis, we have shown that, depending on the specific (industrial) situation at hand, the use of nonlinear components may offer the necessary design freedom to overcome these fundamental limitations. In this respect, the three novel hybrid controllers that have been developed in this thesis, i.e., the scheduled controller in Chapter 2, the 'bandwidth-on-demand' controller in Chapter 3 and the SPANI in Chapter 5, together with their designs guidelines and analysis techniques, can be of great value. In fact, the analysis and design of these novel hybrid/nonlinear controllers is supported, to a great extend, on easy-to-obtain (measured) frequency response data. In addition, this thesis presents the first results on data-based stability conditions for reset control systems. We project that such, for industry, favorable aspects will contribute towards a greater (industrial) acceptance of hybrid/nonlinear control designs.

The obtained results in Chapters 2-5, are all 'application-driven' and meant for industrial use. In this respect, the results in Chapter 6 have a more generic nature. Firstly, the unifying modeling character of this chapter is instrumental in enabling the transfer of results between the diverse control application domains, such as event-triggered control systems, reset control systems and networked control systems. Secondly, new tools are presented for the analysis of stability and the $\mathcal{L}_2$-gain properties of these hybrid systems, which given the increasing popularity of these type of control systems, can be valuable contributions for control engineers.

Still, many of the existing hybrid/nonlinear controller designs in the literature, of which the three developed novel controller designs in this thesis form no exception, are rather specific. This is due to the fact that their designs often depend on the different performance objectives, disturbance situations and (industrial) applications at hand. Therefore, additional research is in order to develop systematic methods for the design and analysis of hybrid/nonlinear controllers, for instance by providing guidelines when to use which type of hybrid/noninear controller technique. Hopefully, such advancements, which are necessary in order to raise hybrid/nonlinear control towards a more generic level, can be supported by the results obtained in this thesis.

As a final note, the author expresses the wish that this thesis also provides awareness among control engineers about the high-potential that hybrid/nonlinear controller solutions may offer, *and* that the design and analysis of such controllers not necessarily implies a much more difficult design process, but that it might be even closely connected to techniques that (industrial) control engineers are accustomed to.

7.2 Recommendations

In this section, recommendations for future research are given, starting with thise that are based on each individual chapter.

Chapter 2. In this chapter, we constructed a switched controller on the basis of two plant descriptions in which we employed the standing assumption that the plants descriptions corresponding to the regions with sensor loss could be regarded as equal. However, in many practical situations those (four) plant descriptions will show differences. In order to improve the performance even further, it would be good to study if the proposed scheduled controller structure allows to deal with five plant descriptions as well, i.e., $\mathcal{P}_i(s)$, $s \in \mathbb{C}$, based on the regions Λ_i, $i = 1, 2, \ldots, 5$, as in Fig. 2.3(a). In this respect, the most challenging aspect is to preserve the favorable frequency-domain based design and analysis tools. It is expected that the design aspect can remain unchanged, i.e., frequency-domain loop-shaping techniques can still be used to design individual controllers based on the plant descriptions $\mathcal{P}_i(s)$, $i = 1, 2, \ldots, 5$. However, extending the graphical data-based stability conditions towards such a case is less trivial. Nevertheless, it is a fact that switches *always* take place when $\theta \in \Lambda_2$, i.e., within the area in which all four sensors are available, which allows us to construct four transfer functions $\mathcal{G}_i(s)$, $i = 1, 2, 3, 4$ as in (2.11). The question that should be answered is if it is possible to prove that closed-loop stability can be verified by checking four circle criterion-like conditions as in Theorem 2.2, hereby taking in mind that the four individual circle criterion-like conditions are based on the Kalman-Yakubovic-Popov criterion (i.e., we probably cannot guarantee the existence of a common Lyapunov function). In this respect, based on a dwell-time reasoning, see Hespanha and Morse (1999), it is interesting to study if we can prove that we always stay sufficiently long in the area in which all four sensors are available such that the transient effects caused by the switch have vanished (and we have reached a steady-state) before another switch takes place. Currently, this is a topic of ongoing research.

Chapter 3. The design and tuning of the shaping filter $\mathcal{F}(s)$, $s \in \mathbb{C}$, is crucial for both stability as well as for performance of the 'bandwidth-on-demand' controller. It is expected that the design of this filter, which in the current approach requires some heuristic tuning, becomes more involved when the high-bandwidth LTI controller is more complex compared to the low-bandwidth LTI controller, e.g., which can be the case for plants with high residual behavior. It is therefore recommended to study if it is possible to construct a more systematic design approach for the design of this filter.

Chapter 4. The most important recommendation is to include temporal regularization in the reset controller (4.1) with (4.2), see also Remark 4.3. It is in the line of expectation that this should be possible, as, according to Forni et al. (2011); Nešić et al. (2008), the input/output pair $(e, -u)$ of $\mathcal{R}$ as in (4.1) with (4.2) is still confined to a (slightly) larger region despite the presence of the time regularization. Additional research is required to verify this line of reasoning and transform it into a systematic design procedure. Currently, this is a topic of ongoing research.

A second recommendation concerns the possible level of conservatism of the presented data-based stability conditions. Compared to the LMI-based conditions proposed in Zaccarian et al. (2011), our conditions yield both advantages as well as disadvantages. The main advantage is clear, namely the demand from industry for easy-to-use data-based conditions for RCSs which do not require parametric models. Moreover, for systems with larger state dimensions, LMI-based conditions often require numerical 'tricks', such as balancing of matrices, in order to yield feasible results. The presented frequency-domain conditions do not suffer from these aspects, although one disadvantage can be the possible level of conservatism. The LMI-based conditions in Zaccarian et al. (2011) are based on piecewise-quadratic Lyapunov functions, thereby potentially offering more freedom compared to our conditions, which rely on the Kalman-Yakubovic-Popov criterion and thus the existence of a single Lyapunov function. Therefore, it would be interesting to study if our data-based stability conditions can be relaxed, while maintaining the (for industry) favorable verification method based on measured frequency response data.

Chapter 5. One modification to the SPANI filter could be the inclusion of a lead-filter in the phase-branch. This would allow to 'anticipate' on a switch in the integral action, i.e., a switch in the integral action happens prior to the error becoming zero, which possibly could lead to a further improvement in reducing the amount of overshoot. Additional research is required on how to appropriate tune such a lead filter, and on how to include such a filter in the current stability conditions.

Chapter 6. In many hybrid control applications, there is a need to prevent the occurrence of so-called 'Zeno behavior', i.e., infinitely many discrete-time events in a finite time interval, which can be realized by the inclusion of temporal regularization, see also Remark 6.1. Given the importance of several applications, such as reset control systems, event-triggered control systems, etc., there is a need for computing such a minimal inter-event time, i.e., the time period in between to consecutive discrete-time events guaranteeing unbounded (hybrid) solutions, while simultaneously guarantee certain stability and $\mathcal{L}_p$-gain properties from disturbance inputs to performance outputs. In the current literature, the closest results in this context are published in Nešić et al. (2008). However, in their examples the minimal inter-event time bounds are never concretely computed, and their techniques are merely used as tools for existence of such a positive threshold. The techniques/results of Chapter 6, and their extensions towards lifting in Heemels et al. (2015a,b), open the door to construct novel tools for *computing* minimal inter-event times for time-regularized hybrid systems as discussed in Remark 6.1, while simultaneously guaranteeing certain stability and $\mathcal{L}_p$-gain properties from disturbance inputs to performance outputs. Currently, this is a topic of ongoing research.

A final more generic recommendation, which has already briefly been mentioned in the conclusions, is to explore towards more general systematic design procedures for hybrid/nonlinear controllers. This is because many of the existing hybrid/nonlinear controller designs in the literature are based on *specific*: performance objectives, disturbance situations and (industrial) applications. For a control engineer searching for new solutions to overcome the fundamental limitations in LTI control, this requires extensive knowledge of the current literature. Therefore, the development of a so-called 'hybrid control recipe book' is recommended. This would provide the control engineer with easy-to-follow guidelines of which type of hybrid/nonlinear control solution would be suitable/preferable for the particular control design problem at hand. It is expected that such developments will further enhance the practical applicability of these high-potential control solutions.

Appendix A

Proofs and technical results

A.1 Appendices of Chapter 2

A.1.1 Proof of Proposition 2.1

Proof. The proof consists of two steps. In the first step, we will demonstrate that, under the hypothesis of the proposition, no unstable pole-zero cancelations occur in open-loop. In the second step, we show that no unstable pole-zero cancelations occur when closing the loop.

Step 1: Due to the proposed controller architecture, pole-zero cancelations only occur in $\mathcal{O}_1(s)$, which is given by

$$\begin{aligned}\mathcal{O}_1(s) &= \mathcal{P}_1(s)\mathcal{C}_2(s)\mathcal{C}_\Delta(s)\\ &= \mathcal{P}_1(s)\mathcal{H}(s)\underbrace{\Delta_{\mathcal{C}_2}(s)\Delta_{\mathcal{C}_2}^{-1}(s)}_{\text{cancelation}}\Delta_{\mathcal{C}_1}(s)\\ &= \mathcal{P}_1(s)\mathcal{C}_1(s).\end{aligned} \tag{A.1}$$

Note that this implies that we have to verify that no unstable pole-zero cancelations occur in:

1) $\Delta_{\mathcal{C}_2}^{-1}(s)\Delta_{\mathcal{C}_2}(s)$;

2) $\mathcal{C}_1(s)$, i.e., (2.6) with $i = 1$;

3) $\mathcal{P}_1(s)\mathcal{C}_1(s)$.

Conditions 1) and 2) are satisfied by (ii), i.e., by Design criterion 1, and condition 3) is true due to (iii). As a result, no unstable pole-zero cancelations occur in the open-loop (A.1).

Step 2: In this step, we will prove that no unstable pole-zero cancelations occur when closing the loop. In order to do so, let us first consider the (non-minimal) state-space realization of (A.1) is given by

$$\dot{x} = A_{\mathcal{O}_1}x + B_{\mathcal{O}_1}e_1 \tag{A.2a}$$
$$y_{\mathcal{P}_1} = C_{\mathcal{O}_1}x, \tag{A.2b}$$

and the similarity transformation $q = T^{-1}x$, for some nonsingular matrix T, that transforms (A.2) into its Kalman decomposition given by

$$\dot{q} = \bar{A}_{\mathcal{O}_1}q + \bar{B}_{\mathcal{O}_1}e_1 \tag{A.3a}$$
$$y_{\mathcal{P}_1} = \bar{C}_{\mathcal{O}_1}q, \tag{A.3b}$$

with $\bar{A}_{\mathcal{O}_1} = T^{-1}A_{\mathcal{O}_1}T$, $\bar{B}_{\mathcal{O}_1} = T^{-1}B_{\mathcal{O}_1}$ and $\bar{C}_{\mathcal{O}_1} = C_{\mathcal{O}_1}T$, in which

$$\left[\begin{array}{c|c}\bar{A}_{\mathcal{O}_1} & \bar{B}_{\mathcal{O}_1}\\ \hline \bar{C}_{\mathcal{O}_1} & \end{array}\right] = \left[\begin{array}{cccc|c} A_{11} & 0 & 0 & 0 & 0\\ A_{21} & A_{22} & 0 & 0 & B_2\\ A_{31} & 0 & A_{33} & 0 & 0\\ A_{41} & A_{42} & A_{43} & A_{44} & B_4\\ \hline C_1 & C_2 & 0 & 0 & \end{array}\right] \tag{A.4}$$

and $\mathcal{O}_1(s) = C_2(sI - A_{22})^{-1}B_2$. Due to the lower triangular structure of $\bar{A}_{\mathcal{O}_1}$, its eigenvalues are given by the eigenvalues of the diagonal matrices A_{11}, A_{22}, A_{33}, and A_{44}. Note that the eigenvalues related to pole-zero cancelations are related to the eigenvalues of A_{11}, A_{33}, and A_{44}, which are all Hurwitz because no unstable pole-zero cancelations occur in (A.1) (as was already concluded in *Step 1*). Let us close the loop and, therefore, focus on the complementary sensitivity function $\mathcal{T}$ (transfer from r to $y_{\mathcal{P}_1}$), which is given in state space description by

$$\begin{aligned} \dot{q} &= \bar{A}_{\mathcal{T}} q + \bar{B}_{\mathcal{T}} r \\ y_{\mathcal{P}_1} &= \bar{C}_{\mathcal{T}} q, \end{aligned} \tag{A.5}$$

in which

$$\left[\begin{array}{c|c} \bar{A}_{\mathcal{T}} & \bar{B}_{\mathcal{T}} \\ \hline \bar{C}_{\mathcal{T}} & \end{array}\right] = \left[\begin{array}{cccc|c} A_{11} & 0 & 0 & 0 & 0 \\ A_{21} - B_2C_1 & A_{22} - B_2C_2 & 0 & 0 & B_2 \\ A_{31} & 0 & A_{33} & 0 & 0 \\ A_{41} - B_4C_1 & A_{42} - B_4C_2 & A_{43} & A_{44} & B_4 \\ \hline C_1 & C_2 & 0 & 0 & \end{array}\right], \tag{A.6}$$

and $\mathcal{T}(s) = C_2(sI - (A_{22} - B_2C_2))^{-1}B_2$. By condition (i), $A_{22} - B_2C_2$ is a Hurwitz matrix. Using the lower triangular structure of $\bar{A}_{\mathcal{T}}$, and the previous observation that A_{11}, A_{33}, and A_{44} are Hurwitz, it follows that $\bar{A}_{\mathcal{T}}$ is a Hurwitz matrix. With the similarity transformation $q = T^{-1}x$, we know that (A.5) is algebraic equivalent to the realization of $\mathcal{T}$ resulting from Fig. 2.5, using (2.1) and (2.6) with $i = 1$ (or (2.6) with $i = 2$ and (2.7)), which is given by

$$\dot{x} = Ax + Br \tag{A.7}$$

$$y_{\mathcal{P}_1} = C_{\mathcal{T}} x, \tag{A.8}$$

with $C_{\mathcal{T}} := \begin{bmatrix} \mathcal{C}_{\mathcal{P}_1} & 0 & 0 \end{bmatrix}$, and A, B are given by (2.15). □

A.1.2 Proof of Theorem 2.2

Proof. Consider a similarity transformation $\xi = T^{-1}x$, using a nonsingular matrix T, that transforms (A, B, C) of system (2.14) into the Kalman decomposition

$$\dot{\xi}_1 = \tilde{A}_{11}\xi_1 + \tilde{F}_1 v \tag{A.9a}$$

$$\dot{\xi}_2 = \tilde{A}_{21}\xi_1 + \tilde{A}_{22}\xi_2 + \tilde{B}_2 w + \tilde{F}_2 v \tag{A.9b}$$

$$\dot{\xi}_3 = \tilde{A}_{31}\xi_1 + \tilde{A}_{33}\xi_3 + \tilde{F}_3 v \tag{A.9c}$$

$$\dot{\xi}_4 = \tilde{A}_{41}\xi_1 + \tilde{A}_{42}\xi_2 + \tilde{A}_{43}\xi_3 + \tilde{A}_{44}\xi_4 + \tilde{B}_4 w + \tilde{F}_4 v \tag{A.9d}$$

with output

$$\zeta = \tilde{C}_1\xi_1 + \tilde{C}_2\xi_2 + D_v v \tag{A.9e}$$

and input

$$w = -\alpha(\theta)\zeta. \tag{A.9f}$$

Note that by hypothesis (I), the matrices $\tilde{A}_{11}, \tilde{A}_{22}, \tilde{A}_{33}$ and $\tilde{A}_{44}$ (suppose they are present) are Hurwitz (due to the lower triangular structure).

In the remainder of the proof, we show that for each subsystem (A.9) there exists an ISS Lyapunov function (ISSLF) $V_i(\xi_i) = \xi_i^\top P_i \xi_i$, $P_i = P_i^\top \succ 0$, $i = 1, 2, 3, 4$. Clearly, V_i satisfies

$$\lambda_{min}(P_i)\|\xi_i\|^2 \leq V_i(\xi_i) \leq \lambda_{max}(P_i)\|\xi_i\|^2, \tag{A.10}$$

in which $\lambda_{min}(P_i)$, $\lambda_{max}(P_i)$ denotes the minimum eigenvalue and the maximum eigenvalue of P_i, $i = 1, 2, 3, 4$, respectively. Combining the existence of such ISSLF for each subsystem using a cascade-like argument, see Sontag (2008), implies that the complete system (A.9) is ISS with respect to v. In fact, we will construct an ISSLF for the overall system (2.14).

Subsystem 1: Since $\tilde{A}_{11}$ is Hurwitz, there exist a quadratic positive definite ISSLF satisfying (A.10) for $i = 1$, and

$$\dot{V}_1 \leq -c_1\|\xi_1\|^2 + \gamma_1\|v\|^2 \tag{A.11}$$

with $c_1, \gamma_1 > 0$.

Subsystem 2: Note that $\mathcal{G}(s) = \tilde{C}_2\left(sI - \tilde{A}_{22}\right)^{-1}\tilde{B}_2$ as subsystem 2 corresponds to the observable and controllable part of the system (2.14). Hence, using the Kalman-Yakubovich-Popov lemma, see Khalil (2000), and under hypothesis (II) of the theorem, there exist matrices L, $P_2 = P_2^\top \succ 0$, and a positive constant ε_2 such that

$$\tilde{A}_{22}^\top P_2 + P_2\tilde{A}_{22} = -L^\top L - \varepsilon_2 P_2 \tag{A.12a}$$

$$P_2\tilde{B}_2 = \tilde{C}_2^\top - \sqrt{\tfrac{2}{\rho}}L^\top. \tag{A.12b}$$

Let us take $V_2(\xi_2) = \xi_2^\top P_2 \xi_2$ as a candidate ISSLF, satisfying (A.10) for $i = 2$, and for which the time derivative yields

$$\dot{V}_2 = \xi_2^\top(\tilde{A}_{22}^\top P_2 + P_2\tilde{A}_{22})\xi_2 + 2\xi_2^\top P_2\tilde{B}_2 w + 2\xi_2^\top P_2\tilde{A}_{21}\xi_1 + 2\xi_2^\top P_2\tilde{F}_2 v \tag{A.13}$$

$$\overset{(A.12)}{=} -\varepsilon_2 V_2 - \xi_2^\top L^\top L\xi_2 + 2\xi_2^\top\left(\tilde{C}_2^\top - \sqrt{\tfrac{2}{\rho}}L^\top\right)w + 2\xi_2^\top P_2\tilde{A}_{21}\xi_1 + 2\xi_2^\top P_2\tilde{F}_2 v \tag{A.14}$$

$$\overset{(A.9e)}{=} -\varepsilon_2 V_2 - \xi_2^\top L^\top L\xi_2 + 2\zeta w - 2\xi_1^\top\tilde{C}_1^\top w - 2v^\top D_v^\top w + 2\sqrt{\tfrac{2}{\rho}}\xi_2^\top L^\top w + 2\xi_2^\top P_2\tilde{A}_{21}\xi_1 + 2\xi_2^\top P_2\tilde{F}_2 v. \tag{A.15}$$

Using $w = -\alpha(\theta)\zeta$, with $\alpha(\theta) \in [0,1]$, this yields

$$\begin{aligned}
\dot{V}_2 \leq & -\varepsilon_2 V_2 - \xi_2^\top L^\top L \xi_2 - 2w^2 - 2\xi_1^\top \tilde{C}_1^\top w - 2v^\top D_v^\top w + 2\sqrt{\tfrac{2}{\rho}}\xi_2^\top L^\top w \\
& + 2\xi_2^\top P_2 \tilde{A}_{21}\xi_1 + 2\xi_2^\top P_2 \tilde{F}_2 v \qquad \text{(A.16)} \\
= & -\varepsilon_2 V_2 - \left[L\xi_2 + \sqrt{\tfrac{2}{\rho}}w\right]^\top \left[L\xi_2 + \sqrt{\tfrac{2}{\rho}}w\right] - \underbrace{\left(2 - \tfrac{2}{\rho}\right)}_{=:\phi} w^2 - 2\xi_1^\top \tilde{C}_1^\top w \\
& - 2v^\top D_v^\top w + 2\xi_2^\top P_2 \tilde{A}_{21}\xi_1 + 2\xi_2^\top P_2 \tilde{F}_2 v \qquad \text{(A.17)} \\
\leq & -\varepsilon_2 V_2 - \phi w^2 - 2\xi_1^\top \tilde{C}_1^\top w - 2v^\top D_v^\top w + 2\xi_2^\top P_2 \tilde{A}_{21}\xi_1 + 2\xi_2^\top P_2 \tilde{F}_2 v \qquad \text{(A.18)} \\
\overset{(A.10)}{\leq} & -\kappa_2 \|\xi_2\|^2 - \phi w^2 - 2\xi_1^\top \tilde{C}_1^\top w - 2v^\top D_v^\top w + 2\xi_2^\top P_2 \tilde{A}_{21}\xi_1 + 2\xi_2^\top P_2 \tilde{F}_2 v \\
& \qquad \text{(A.19)}
\end{aligned}$$

for $\kappa_2 := \varepsilon_2 \lambda_{\min}(P_2) > 0$, and where we used that $-2w^2 = -\frac{2}{\rho}w^2 - \left(2 - \frac{2}{\rho}\right) w^2$ for $\rho \neq 0$. In fact, according to the hypothesis of the theorem, $\rho > 1$, which yields $\phi = \left(2 - \frac{2}{\rho}\right) > 0$. Using the relation $2ab \leq \delta a^2 + \frac{1}{\delta}b^2$, which holds for all $a, b \in \mathbb{R}$ and all $\delta > 0$, we obtain

$$\begin{aligned}
\dot{V}_2 \leq & -c_2\|\xi_2\|^2 - c_w\|w\|^2 + \hat{c}_2\|\xi_1\|^2 + \gamma_2\|v\|^2 && \text{(A.20)} \\
\leq & -c_2\|\xi_2\|^2 + \hat{c}_2\|\xi_1\|^2 + \gamma_2\|v\|^2 && \text{(A.21)}
\end{aligned}$$

for some $c_2, c_w, \hat{c}_2, \gamma_2 > 0$. Hence, V_2 is indeed an ISSLF for subsystem 2 with respect to v and ξ_1. Consequently, one can show based on (A.11) and (A.21) that $V_{12} := \mu_1 V_1 + V_2$, for $\mu_1 > 0$ sufficiently large, is an ISSLF for the cascaded system comprising of subsystems 1 and 2, the dynamics of which is given by

$$\begin{bmatrix} \dot{\xi}_1 \\ \dot{\xi}_2 \end{bmatrix} = \begin{bmatrix} \tilde{A}_{11}\xi_1 + \tilde{F}_1 v \\ \tilde{A}_{21}\xi_1 + \tilde{A}_{22}\xi_2 + \tilde{B}_2 w + \tilde{F}_2 v \end{bmatrix} \qquad \text{(A.22)}$$

and (A.9f), (A.9e). Indeed, for sufficiently large μ_1 we would obtain that

$$\dot{V}_{12} \leq -c_{12}\|\xi_1\|^2 - c_{12}\|\xi_2\|^2 + \gamma_{12}\|v\|^2, \qquad \text{(A.23)}$$

for some $c_{12}, \gamma_{12} > 0$.

Subsystem 3: Since $\tilde{A}_{33}$ is Hurwitz, there exists a quadratic positive definite ISSLF satisfying (A.10) for $i = 3$, and

$$\dot{V}_3 \leq -c_3\|\xi_3\|^2 + \hat{c}_3\|\xi_1\|^2 + \gamma_3\|v\|^2 \qquad \text{(A.24)}$$

with $c_3, \hat{c}_3, \gamma_3 > 0$. Based on (A.23) and (A.24) we can easily see that $V_{123} := \mu_2 V_{12} + V_3$, for sufficiently large $\mu_2 > 0$, satisfies

$$\dot{V}_{123} \leq -c_{123}\|\xi_1\|^2 - c_{123}\|\xi_2\|^2 - c_{123}\|\xi_3\|^2 + \gamma_{123}\|v\|^2, \qquad \text{(A.25)}$$

for some $c_{123}, \gamma_{123} > 0$, and hence is an ISSLF for the cascaded system consisting of subsystems $1, 2, 3$, the dynamics of which is given by

$$\begin{bmatrix} \dot{\xi}_1 \\ \dot{\xi}_2 \\ \dot{\xi}_3 \end{bmatrix} = \begin{bmatrix} \tilde{A}_{11}\xi_1 + \tilde{F}_1 v \\ \tilde{A}_{21}\xi_1 + \tilde{A}_{22}\xi_2 + \tilde{B}_2 w + \tilde{F}_2 v \\ \tilde{A}_{31}\xi_1 + \tilde{A}_{33}\xi_3 + \tilde{F}_3 v \end{bmatrix} \tag{A.26}$$

and (A.9f), (A.9e).

Subsystem 4: Since $\tilde{A}_{44}$ is Hurwitz, there exist a quadratic positive definite ISSLF satisfying (A.10) for $i = 4$, and

$$\dot{V}_4 \leq -c_4\|\xi_4\|^2 + \hat{c}_4\|\xi_1\|^2 + \bar{c}_4\|\xi_2\|^2 + \tilde{c}_4\|\xi_3\|^2 + \gamma_4\|v\|^2 \tag{A.27}$$

with $c_4, \hat{c}_4, \bar{c}_4, \tilde{c}_4, \gamma_4 > 0$. Based on (A.25) and (A.27), we can establish that $V_{1234} := \mu_3 V_{123} + V_4$, for sufficiently large $\mu_3 > 0$, satisfies

$$\dot{V}_{1234} \leq -c_{1234}\|\xi_1\|^2 - c_{1234}\|\xi_2\|^2 - c_{1234}\|\xi_3\|^2 - c_{1234}\|\xi_4\|^2 + \gamma_{1234}\|v\|^2, \tag{A.28}$$

for some $c_{1234}, \gamma_{1234} > 0$, and hence is an ISSLF for the cascaded systems consisting of subsystem $1, 2, 3, 4$, the dynamics of which is given by

$$\begin{bmatrix} \dot{\xi}_1 \\ \dot{\xi}_2 \\ \dot{\xi}_3 \\ \dot{\xi}_4 \end{bmatrix} = \begin{bmatrix} \tilde{A}_{11}\xi_1 + \tilde{F}_1 v \\ \tilde{A}_{21}\xi_1 + \tilde{A}_{22}\xi_2 + \tilde{B}_2 w + \tilde{F}_2 v \\ \tilde{A}_{31}\xi_1 + \tilde{A}_{33}\xi_3 + \tilde{F}_3 v \\ \tilde{A}_{41}\xi_1 + \tilde{A}_{42}\xi_2 + \tilde{A}_{43}\xi_3 + \tilde{A}_{44}\xi_4 + +\tilde{B}_4 w + \tilde{F}_4 v \end{bmatrix} \tag{A.29}$$

and (A.9f), (A.9e). According to Sontag (2008); Sontag and Wang (1995), this establishes ISS of the Lur'e system (A.29), (A.9f), (A.9e), with respect to v, which completes the proof. $\square$

A.2 Appendix of Chapter 3

A.2.1 Proof of Theorem 3.1

Proof. The proof basically follows the reasoning of the proof in Pavlov et al. (2006); van de Wouw et al. (2008); Yakubovich (1964), with the minor exception that in our system $\varphi(v, e)$ as in (3.8) depends on the scheduling variable $v(t)$, $t \in \mathbb{R}$. We note that a key step of the proof of Pavlov et al. (2006); van de Wouw et al. (2008); Yakubovich (1964) consists of proving incremental stability, i.e., showing that two solutions $x_1 : \mathbb{R} \to \mathbb{R}^{n_x}$ and $x_2 : \mathbb{R} \to \mathbb{R}^{n_x}$ subject to the same scheduling variable v and external inputs d, but with different initial conditions, converge to each other. It is essential for this part of the proof to observe that $\alpha(v(t))$, $t \in \mathbb{R}$, is exactly the same for both solutions given the external inputs (including r and thus v). $\square$

A.3 Appendix of Chapter 4

A.3.1 Hybrid systems notation

According to Goebel et al. (2012), solutions of (4.9), (4.2) are defined on hybrid time domains as follows. A *compact hybrid time domain* is a set $E = \bigcup_{j=0}^{J-1}[t_j, t_{j+1}] \times \{j\} \subset \mathbb{R}_{\geq 0} \times \mathbb{N}$ with $J \in \mathbb{N}_{>0}$ and $0 = t_0 \leq t_1 \leq \cdots \leq t_J$. A *hybrid time domain* is a set $E \subset \mathbb{R}_{\geq 0} \times \mathbb{N}$ such that $E \cap ([0,T] \times \{0,\dots,J\})$ is a compact hybrid time domain for each $(T,J) \in E$. A *hybrid signal* is a function defined on a hybrid time domain. A hybrid signal $w : \operatorname{dom} w \to \mathbb{R}^{n_w}$ is a *hybrid input* if $w(\cdot, j)$ is Lebesgue measurable and locally essentially bounded for each j (note that the class of disturbance signals $w(t,j)$ is in fact a larger class than we typically consider, namely $w(t)$). A hybrid signal $x : \operatorname{dom} x \to \mathbb{R}^{n_x}$ is a *hybrid arc* if $x(\cdot, j)$ is locally absolutely continuous for each j.

A hybrid arc $x : \operatorname{dom} x \to \mathcal{X}$ for an input $w : \operatorname{dom} w \to \mathcal{W}$ is a solution x to (4.9), (4.2) if $\operatorname{dom} x = \operatorname{dom} w$, $(x(0,0), w(0,0)) \in \mathcal{F} \cup \mathcal{J}$, and

1. for all $j \in \mathbb{N}$ and almost all $(t,j) \in \operatorname{dom} x$
$$\dot{x}(t,j) = \bar{A}x(t,j) + \bar{B}w(t), \text{ and } (x(t,j), w(t)) \in \mathcal{F}$$
2. for all $(t,j) \in \operatorname{dom} x$ such that $(t, j+1) \in \operatorname{dom} x$
$$x(t,j+1) = \bar{A}_r x(t,j), \text{ and } (x(t,j), w(t)) \in \mathcal{J}.$$

A.3.2 Proof of Theorem 4.1

Proof. A smooth function $W : \mathbb{R}^{n_\xi + n_r} \to \mathbb{R}$ is an ISS-Lyapunov (ISSLF) function, see Cai and Teel (2009), for the system (4.9) with (4.2), if it satisfies, for $\kappa_i > 0$, $i = 1, 2, \dots, 4$, the following conditions

$$\kappa_1\|x\|^2 \leq W(x) \leq \kappa_2\|x\|^2 \tag{A.30a}$$
$$\dot{W}(x) \leq -\kappa_3\|x\|^2 + \kappa_4\|w\|^2 \quad \text{for all } x \in \mathcal{F} \tag{A.30b}$$
$$W(x^+) \leq W(x) \qquad \text{for all } x \in \mathcal{J}. \tag{A.30c}$$

In the remainder of the proof, we demonstrate the existence of such a function W (under the hypothesis of the theorem) by the following four steps:

- Step 1: We disregard the internal dynamics of $\mathcal{R}$ and exploit the fact that the input/output pairs $(e, -u)$ of $\mathcal{R}$ satisfy the sector condition $eu \leq -\frac{1}{\alpha}u^2$ by the grace of the form of $\mathcal{F}$ and $\mathcal{J}$ in (4.2). Let us therefore introduce the following auxiliary (base nonlinear) system

$$\Sigma_{bns} : \begin{cases} \mathcal{H} : \begin{cases} \dot{\xi} = A\xi + Bu + B_w w \\ e = C\xi + D_w w \end{cases} \\ \quad\;\; u = -\phi(e) \end{cases} \tag{A.31}$$

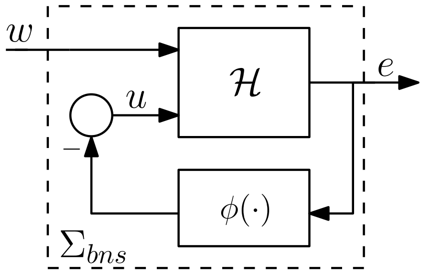

Fig. A.1. Lur'e-type system description of Σ_{bns} as in (A.31).

in which $\phi(e)$ satisfies the following sector condition

$$0 \leq \frac{\phi(e)}{e} \leq \alpha, \tag{A.32}$$

for all $e \in \mathbb{R}$, $e \neq 0$, see Fig. A.1 for a schematic representation. In the remainder of this first step, we use the circle criterion to prove that the system Σ_{bns} admits an ISS Lyapunov function (ISSLF) $V : \mathbb{R}^{n_\xi} \to \mathbb{R}$, see Sontag and Wang (1995);

- Step 2: We show that the detectability condition in Assumption 4.1 can be converted to a Lyapunov-like function $V_r : \mathbb{R}^{n_r} \to \mathbb{R}$;
- Step 3: We show that the resulting V of Step 1 and V_r of Step 2 can be combined into a function $W : \mathbb{R}^{n_\xi + n_r} \to \mathbb{R}$, and that we satisfy the ISSLF condition during flow, i.e., (A.30b);
- Step 4: We show that the ISSLF constructed in Step 3 does not increase during resets, thereby also satisfying the ISSLF condition during jumps, i.e., (A.30c). This allows us to construct a bound on the norm of the total state as in (4.10) (for ease of notation, we construct a bound on $x(t)$ dropping the 'j', see also Remark 4.3).

Step 1: We will show that there exists an ISSLF $V(\xi) = \frac{1}{2}\xi^\top P \xi$ with $P = P^\top \succ 0$ for the auxiliary system (A.31). Using the Kalman-Yakubovich-Popov lemma, see Khalil (2000), under hypothesis (I) and (II) of the theorem and minimality of (A, B, C), there exist matrices L, $P = P^\top \succ 0$, and a positive constant ε such that

$$A^\top P + PA = -L^\top L - \varepsilon P \tag{A.33a}$$

$$PB = C^\top - \sqrt{\tfrac{2}{\alpha}} L^\top . \tag{A.33b}$$

Let us take $V(\xi) = \frac{1}{2}\xi^\top P\xi$ as a candidate ISSLF, satisfying

$$\lambda_{min}(P)\|\xi\|^2 \leq V(\xi) \leq \lambda_{max}(P)\|\xi\|^2, \tag{A.34}$$

in which $\lambda_{min}(P)$ and $\lambda_{max}(P)$ denote the minimum eigenvalue and the maximum eigenvalue of P, respectively, and for which the time derivative along solutions of (4.5) satisfies

$$\begin{aligned}\dot{V} &= \tfrac{1}{2}\xi^\top(A^\top P + PA)\xi + \xi^\top PBu + \xi^\top PB_w w \\ &\overset{(A.33)}{=} -\tfrac{\varepsilon}{2}V - \tfrac{1}{2}\xi^\top L^\top L\xi + \xi^\top C^\top u - \xi^\top L^\top\sqrt{\tfrac{2}{\alpha}}u + \xi^\top PB_w w \\ &\overset{(4.5b)}{=} -\tfrac{\varepsilon}{2}V - \tfrac{1}{2}\xi^\top L^\top L\xi + e^\top u - w^\top D_w^\top u - \xi^\top L^\top\sqrt{\tfrac{2}{\alpha}}u + \xi^\top PB_w w.\end{aligned} \tag{A.35}$$

Using the sector condition $e^\top u \leq -\frac{1}{\alpha}u^2$ imposed on the flow by the form of $\mathcal{F}$ in (4.2a), this yields

$$\begin{aligned}\dot{V} &\leq -\tfrac{\varepsilon}{2}V - \tfrac{1}{2}\xi^\top L^\top L\xi - \tfrac{1}{\alpha}u^2 - w^\top D_w^\top u - \xi^\top L^\top\sqrt{\tfrac{2}{\alpha}}u + \xi^\top PB_w w \\ &= -\tfrac{\varepsilon}{2}V - \tfrac{1}{2}\left(L\xi + \sqrt{\tfrac{2}{\alpha}}u\right)^\top\left(L\xi + \sqrt{\tfrac{2}{\alpha}}u\right) + \left(\xi^\top PB_w - u^\top D_w\right)w \\ &\leq -\tfrac{\varepsilon}{2}V + \left(\xi^\top PB_w - u^\top D_w\right)w.\end{aligned} \tag{A.36}$$

Note that

$$\begin{aligned}\left(\xi^\top PB_w - u^\top D_w\right)w &\leq \|B_w w\|\|\xi^\top P\| + \|D_w\|\|uw\| \\ &\leq \lambda_{max}(P)\|B_w\|\|w\|\|\xi\| + \|D_w\|\|u\|\|w\| \\ &\leq \lambda_{max}(P)\|B_w\|\|w\|\|\xi\| + \alpha\|D_w\|\|C\xi + D_w w\|\|w\| \\ &\leq c_1\|w\|\|\xi\| + c_2\|w\|^2,\end{aligned} \tag{A.37}$$

where we explicitly used that $\|u\| \leq \alpha\|e\|$ which follows from $e^\top u \leq -\frac{1}{\alpha}u^2$, with $c_1 := \lambda_{max}(P)\|B_w\| + \alpha\|D_w\|\|C\| > 0$ and $c_2 := \alpha\|D_w\|^2 > 0$. Moreover, note that

$$c_1\|w\|\|\xi\| + c_2\|w\|^2 \leq c_1^2\delta_1\|w\|^2 + c_2\|w\|^2 + \tfrac{1}{\delta_1}\|\xi\|^2 \tag{A.38}$$

for any $\delta_1 > 0$. Using (A.37) and (A.38) in (A.36) yields

$$\dot{V} \leq -c_3\|\xi\|^2 + c_4\|w\|^2 \tag{A.39}$$

with $c_3 := \left(\frac{\varepsilon\lambda_{min}(P)}{2} - \frac{1}{\delta_1}\right)$ and $c_4 := (c_1^2\delta_1 + c_2)$, which implies that, for sufficiently large δ_1, V is indeed an ISSLF for system $\mathcal{H}$ in (4.5) with respect to the input w.

Step 2: Assumption 4.1 implies that there exist a matrix gain K such that $A_r + KC_r$ is Hurwitz, see, e.g., Hespanha (2009). Consequently, there exists a $P_r = P_r^\top \succ 0$ such that the following matrix equality holds

$$(A_r + KC_r)^\top P_r + P_r(A_r + KC_r) = -I. \tag{A.40}$$

Let us take $V_r(x_r) = x_r^\top P_r x_r$ with $P_r = P_r^\top \succ 0$ as a candidate Lyapunov function for the system (4.1) with input e during flow, satisfying

$$\lambda_{min}(P_r)\|x_r\|^2 \leq V_r(x_r) \leq \lambda_{max}(P_r)\|x_r\|^2. \tag{A.41}$$

The time-derivative of V_r along the flow dynamics of $\mathcal{R}$ satisfies

$$\dot{V}_r = x_r^\top \left(A_r^\top P_r + P_r A_r\right) x_r + 2x_r^\top P_r B_r e. \tag{A.42}$$

Note that (A.40) implies

$$\begin{aligned} x_r^\top \left(A_r^\top P_r + P_r A_r\right) x_r &= -\|x_r\|^2 - 2x_r^\top C_r^\top K^\top P_r x_r \\ &= -\|x_r\|^2 + 2u^\top K^\top P_r x_r \\ &\leq -\|x_r\|^2 + 2\|u\|\|K\|\lambda_{max}(P_r)\|x_r\| \\ &= -\|x_r\|^2 + c_5\|u\|\|x_r\| \\ &\leq -c_6\|x_r\|^2 + c_7\|u\|^2 \end{aligned} \tag{A.43}$$

with $c_5 := 2\lambda_{max}(P_r)\|K\| > 0$, $c_6 := (1 - \frac{1}{\delta_2}) > 0$ for $\delta_2 > 1$ and $c_7 := c_5^2\delta_2 > 0$. Using (A.43) in (A.42) yields

$$\begin{aligned} \dot{V}_r &\leq -c_6\|x_r\|^2 + c_7\|u\|^2 + 2x_r^\top P_r B_r e \\ &\leq -c_6\|x_r\|^2 + c_7\|u\|^2 + 2\lambda_{max}(P_r)\|x_r\|\|B_r\|\|e\| \\ &= -c_6\|x_r\|^2 + c_7\|u\|^2 + c_8\|e\|\|x_r\| \\ &\leq -c_9\|x_r\|^2 + c_7\|u\|^2 + c_{10}\|e\|^2 \end{aligned} \tag{A.44}$$

with $c_8 := 2\lambda_{max}(P_r)\|B_r\| > 0$, $c_9 := c_6 - \frac{1}{\delta_3}$, for $\delta_3 > 0$ and $c_{10} := c_8^2\delta_3 > 0$. Using $\|u\| \leq \alpha\|e\|$ which follows from $e^\top u \leq -\frac{1}{\alpha}u^2$, see (4.2a), this yields

$$\begin{aligned} \dot{V}_r &\leq -c_9\|x_r\|^2 + c_{11}\|e\|^2 \\ &\overset{(4.5b)}{\leq} -c_9\|x_r\|^2 + c_{12}\|\xi\|^2 + c_{13}\|w\|^2 \end{aligned} \tag{A.45}$$

with $c_{11} := \alpha^2 c_7 + c_{10} > 0$, $c_{12} := c_{11}(\|C\|^2 + \frac{1}{\delta_4}) > 0$ for $\delta_4 > 0$ and $c_{13} := c_{11}(4\delta_4\|C\|^2\|D_w\|^2 + \|D_w\|^2) > 0$.

Step 3: Let us construct the following candidate ISSLF

$$W(\xi, x_r) = V(\xi) + \mu V_r(x_r) = x^\top P_w x, \tag{A.46}$$

for some $\mu > 0$ and $P_w = \text{diag}(P, \mu P_r)$, satisfying

$$\lambda_{min}(P_w)\|x\|^2 \leq W(x) \leq \lambda_{max}(P_w)\|x\|^2, \tag{A.47}$$

thereby satisfying (A.30a) with $\kappa_1 = \lambda_{min}(P_w)$ and $\kappa_2 = \lambda_{max}(P_w)$. The time-derivative of W along flow of (4.9), (4.2) satisfies

$$\begin{aligned} \dot{W} &= \dot{V} + \mu \dot{V}_r \\ &\leq -(c_3 - \mu c_{12})\|\xi\|^2 - \mu c_9 \|x_r\|^2 + (c_4 + \mu c_{13})\|w\|^2 \\ &\leq -\kappa_3 \|x\|^2 + \kappa_4 \|w\|^2 \end{aligned} \tag{A.48}$$

with $\kappa_3 := \min((c_3 - \mu c_{12}), \mu c_9)$, $\kappa_4 := c_4 + \mu c_{13}$, and for sufficiently small μ such that $(c_3 - \mu c_{12}) > 0$. Hence, $W(\xi, x_r)$ satisfies (A.30b) and is an ISSLF for the hybrid system (4.9) during flow.

Step 4: Due to (4.1) the ISSLF constructed in *Step 3* satisfies

$$W(\xi^+, 0) \leq W(\xi, x_r) \tag{A.49}$$

during jumps of (4.9), (4.2). Consequently, for a solution x to (4.9), (4.2), with input disturbance w, that is unbounded in the t direction, and by combining (A.47), (A.48) and (A.49) (in which we take the conservative bound $W(\xi^+, 0) = W(\xi, x_r)$ at jumps), and using similar arguments as in Cai and Teel (2009); Sontag and Wang (1995), we have that

$$\begin{aligned} W(x(t)) &\leq -\sigma_1 W \quad \text{for } \|x\| \geq \sigma_2 \|w\|, \\ &\leq \max\left\{ e^{-\sigma_1 t} W(x(0)), \sigma_3 \|w_{[0,t]}\|_\infty \right\} \end{aligned} \tag{A.50}$$

with $\sigma_1 := \frac{1}{2\lambda_{max}(P_w)}\kappa_3$, $\sigma_2 := \sqrt{2\kappa_3\kappa_4}$, with $\sigma_3 := \lambda_{max}(P_w)\sigma_2$, for all $t \in \mathbb{R}_{\geq 0}$. Consequently,

$$\|x(t)\| \leq \sqrt{\tfrac{\lambda_{max}(P_w)}{\lambda_{min}(P_w)}} e^{-\frac{\sigma_1}{2}t} \|x(0)\| + \sqrt{\tfrac{\sigma_3}{\lambda_{min}(P_w)}} \sqrt{\|w_{[0,t]}\|_\infty}. \tag{A.51}$$

The latter inequality shows that the system (4.9), (4.2) is ISS according to Definition 4.1. This completes the proof. $\square$

A.4 Appendices of Chapter 5

A.4.1 Hybrid systems notation

According to Goebel et al. (2012), a set $E \subset \mathbb{R}_{\geq 0} \times \mathbb{N}$ is a compact hybrid time domain if $E = \cup_{j=0}^{J-1}([t_j, t_{j+1}], j)$ for some finite sequence of times $0 = t_0 \leq t_1 \leq t_2, \ldots \leq t_J$. It is a hybrid time domain if for all $(T, J) \in E$, $E \cap ([0, T] \times \{0, 1, \ldots, J\})$ is a compact hybrid time domain. A function $\phi : E \to \mathbb{R}^n$ is a hybrid arc if E is a hybrid time domain and if for each $j \in \mathbb{N}$, the function $t \to \phi(t, j)$ is locally absolutely continuous on the interval $I^j = \{t : (t, j)) \in E\}$. A hybrid arc ϕ is a solution to the hybrid system $(\mathcal{F}, f, \mathcal{J}, g)$ if $\phi(0, 0) \in \bar{\mathcal{F}} \cup \mathcal{J}$, and

1. for all $j \in \mathbb{N}$ such that $I^j = \{t : (t, j) \in \operatorname{dom} \phi\}$ has nonempty interior

$$\begin{aligned} &\phi(t, j) \in \mathcal{F} && \text{for all } t \in \operatorname{int} I^j \\ &\dot{\phi}(t, j) \in f(\phi(t, j), w(t)) && \text{for almost all } t \in I^j \end{aligned}$$

2. for all $(t, j) \in \operatorname{dom} \phi$ such that $(t, j + 1) \in \operatorname{dom} \phi$,

$$\begin{aligned} &\phi(t, j) \in \mathcal{J}, \\ &\phi(t, j + 1) \in g(\phi(t, j)). \end{aligned}$$

A.4.2 Proof of statement Remark 5.1

Proof. Due to the dwell time condition based on $\tau_D > 0$, the definition of GES of $\mathcal{A}$ that we employ in this chapter, i.e., the solution ϕ to the hybrid system satisfies

$$\|\chi(t, j)\|_{\mathcal{A}} \leq \rho e^{-\mu t} \|\chi(0, 0)\|_{\mathcal{A}} \tag{A.52}$$

for all $(t, j) \in \operatorname{dom} \chi$, is in fact equivalent to the definition of GES of $\mathcal{A}$ in Teel et al. (2013), i.e., the solution ϕ to the hybrid system satisfies

$$\|\chi(t, j)\|_{\mathcal{A}} \leq \hat{\rho} e^{-\hat{\mu}(t+j)} \|\chi(0, 0)\|_{\mathcal{A}} \tag{A.53}$$

for all $(t, j) \in \operatorname{dom} \chi$. Note that GES of $\mathcal{A}$ in the sense of Teel et al. (2013) obviously implies our notion of GES. To demonstrate the reverse, note that we can obtain the following relation

$$j \leq 2 \frac{t}{\tau_D} + 2, \tag{A.54}$$

and as a result

$$-t \leq \frac{\tau_D}{2}(2 - j), \tag{A.55}$$

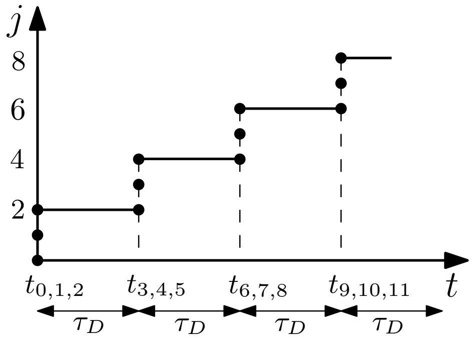

Fig. A.2. Schematic representation of a hybrid time domain for a worst case situation.

which holds for any $(t,j) \in \operatorname{dom} \chi$. In this respect, the hybrid time domain depicted in Fig. A.2 might be useful. This figure schematically represents the *worst case* situation, i.e., two consecutive jumps at t_0 and two consecutive jumps after τ_D time instances. Let us now consider (A.52)

$$\begin{aligned}\|\chi(t,j)\|_{\mathcal{A}} &\leq \rho e^{-\mu t}\|\chi(0,0)\|_{\mathcal{A}} \\ &= \rho e^{-\frac{\mu}{2}t} e^{-\frac{\mu}{2}t}\|\chi(0,0)\|_{\mathcal{A}} \\ &\overset{(A.55)}{\leq} \rho e^{\frac{\mu}{2}\frac{\tau_D}{2}(2-j)} e^{-\frac{\mu}{2}t}\|\chi(0,0)\|_{\mathcal{A}},\end{aligned}$$

which shows us that (A.53) is obtained with $\hat{\rho} := \rho e^{\frac{\mu\tau_D}{2}}$ and $\hat{\mu} := \min\{\frac{\mu\tau_D}{4}, \frac{\mu}{2}\}$ This completes the proof. □

A.4.3 Proof of Theorem 5.1

Proof. We start the proof by introducing the coordinate transformation $\tilde{x} := [\tilde{x}_p^\top \ \tilde{x}_c^\top \ \tilde{x}_I^\top]^\top = x - x^*$, and as a result $\|\chi\|_{\mathcal{A}} = \|\tilde{x}\|$.

Next, we will prove that $W(\chi) = V(\tilde{x}) = \tilde{x}^\top P \tilde{x}$, with $P = P^\top \succ 0$, satisfying (5.15)-(5.16), is a Lyapunov function for the hybrid system (5.5), (5.6). To do so, first observe that

$$c_1\|\tilde{x}\|^2 \leq W(\chi) \leq c_2\|\tilde{x}\|^2, \tag{A.56}$$

for some $c_2 \geq c_1 > 0$, since $P = P^\top \succ 0$. Second, we are going to show that during flow, we have that, along the solutions of (5.5), (5.6),

$$\begin{aligned}\langle \nabla W(\chi), f(\chi)\rangle &\leq -c_3\|\tilde{x}\|^2 \\ &\overset{(A.56)}{\leq} -c_4 W(\chi) \quad \text{for all } \chi \in \mathcal{F},\end{aligned} \tag{A.57}$$

for some $c_3 > 0$, $c_4 = \frac{c_3}{c_2} > 0$. To show this, we consider two cases. The first case is given by

$$\chi \in \Theta \;\text{ with } \ell = 0 \wedge (x_I(\epsilon x_I + e) \geq 0 \;\vee 0 \leq \tau \leq \tau_D), \tag{A.58}$$

in which

$$\dot{\tilde{x}} = \bar{A}_1 \tilde{x}. \tag{A.59}$$

Hence, we obtain that along solutions

$$\dot{V} = \tilde{x}^\top \left(\bar{A}_1^\top P + P\bar{A}_1\right) \tilde{x} \leq -c_5 \|\tilde{x}\|^2, \tag{A.60}$$

for some $c_5 > 0$, due to (5.15).

The second case is given by

$$\chi \in \Theta \;\text{ with } \ell = 1 \wedge x_I(\epsilon x_I + e) < 0, \tag{A.61}$$

in which

$$\dot{\tilde{x}} = \bar{A}_2 \tilde{x} - \bar{A}_d x^*, \tag{A.62}$$

where we used $\bar{A}_d := \bar{A}_1 - \bar{A}_2$, and (5.8). Note that we can express $x_I(\epsilon x_I + e)$ into the transformed coordinates as follows

$$\psi(\tilde{x}, x^*) := (\tilde{x}_I + x_I^*)(\epsilon \tilde{x}_I + \epsilon x_I^* - C_p \tilde{x}_p), \tag{A.63}$$

using $e = r_c - C_p x_p = r_c - C_p(\tilde{x}_p + x_p^*) = -C_p \tilde{x}_p$, since $r_c - C_p x_p^* = e^* = 0$. Let us introduce the augmented vector $\tilde{x}_a := [\tilde{x}^\top \;\; r_c \;\; d_c]^\top$, and use (5.11), (5.12) to express x_I^* in terms of r_c and d_c, as in (5.13). This allows us to write the switching function $\psi(\tilde{x}, x^*)$ in (A.63) in a quadratic form $\psi(\tilde{x}_a) = \tilde{x}_a^\top \bar{R} \tilde{x}_a$ (with some slight abuse of notation), where $\bar{R}$ is as defined in (5.10). Now we obtain

$$\begin{aligned} \dot{V} &= \tilde{x}^\top \left(\bar{A}_2^\top P + P\bar{A}_2\right) \tilde{x} - x^{*\top} \bar{A}_d^\top P \tilde{x} - \tilde{x}^\top P \bar{A}_d x^*, \\ &= \tilde{x}_a^\top Q \tilde{x}_a, \end{aligned} \tag{A.64}$$

for Q as defined in (5.9). Hence, we need to show that there exists a $c_6 > 0$ such that

$$\tilde{x}_a^\top Q \tilde{x}_a \leq -c_6 \|\tilde{x}\|^2, \;\text{ when } \ell = 1 \wedge \psi(\tilde{x}_a) < 0. \tag{A.65}$$

To prove this, observe that, for M defined in (5.14) and $\text{im}H \subseteq \ker Q$ with H defined as

$$H := \left[O_{1\times n} \;\; -\gamma_d \;\; \gamma_r\right]^\top, \tag{A.66}$$

in which $\gamma_d \neq 0$ and $\gamma_r \neq 0$, it holds that $\mathrm{im}M \oplus \mathrm{im}H = \mathbb{R}^n$. Hence, we can write $\tilde{x}_a = M\tilde{m} + h$ for some $\tilde{m} \in \mathbb{R}^{(n+1)\times 1}$ and $h \in \mathrm{im}H$. These facts lead to

$$\begin{aligned} \tilde{x}_a^\top Q \tilde{x}_a &= (M\tilde{m} + h)^\top Q (M\tilde{m} + h) \\ &= \tilde{m}^\top M^\top Q M \tilde{m} \end{aligned} \tag{A.67}$$

in which we used $\mathrm{im}H \subseteq \ker Q$ (and thus $Qh = 0$). In addition, note that, $\tilde{x}_a^\top \bar{R}\tilde{x}_a < 0$ implies that $\tilde{m}^\top M^\top \bar{R} M\tilde{m} < 0$, because $\mathrm{im}H \subseteq \ker\bar{R}$ (and thus $\bar{R}h = 0$). Hence, for the case where $\ell = 1$ and $\tilde{x}_a^\top \bar{R}\tilde{x}_a < 0$ we obtain

$$\begin{aligned} \tilde{m}^\top M^\top Q M\tilde{m} &\leq \tilde{m}^\top M^\top (Q - \alpha\bar{R}) M\tilde{m} \\ &\overset{(5.16)}{\leq} -c_7\|\tilde{m}\|^2, \end{aligned} \tag{A.68}$$

for some $c_7 > 0$, $\alpha \geq 0$. Using now that $\|\tilde{m}\| \geq c_8\|M\tilde{m}\|$ for some $c_8 > 0$, due to M having full column rank, and $\|M\tilde{m}\| \geq \|\tilde{x}\|$, in view of the form of M, we obtain (A.65) for $c_6 = c_7c_8 > 0$, as desired. This establishes (A.57) in which $c_3 = \min\{c_5, c_6\}$.

As a last step, we study the behavior during jumps, which leads to

$$W(g(\chi)) - W(\chi) = 0 \quad \text{for all } \chi \in \mathcal{J}, \tag{A.69}$$

due to (5.6e). This, together with the fact that $\tau_D > 0$ guarantees that there can be at most two consecutive jumps, and thus the hybrid time domain of solutions ϕ to (5.5), (5.6) are unbounded in the t-direction, i.e., $\sup\{t \,|\, (t,j) \in \mathrm{dom}\,\phi\} = \infty$. This implies that along a solution χ of the hybrid system (5.5), (5.6), the inequality in (A.57) and (A.69) combined imply

$$W(\chi(t,j)) \leq e^{-c_4 t} W(\chi(0,0)), \tag{A.70}$$

for all $(t,j) \in \mathrm{dom}\,\chi$ and all $t \in \mathbb{R}_{\geq 0}$. Hence, GES, in the sense of Definition 5.1, of the set $\mathcal{A}$ of the hybrid system (5.5), (5.6) for $r(t) = r_c$ and $d(t) = d_c$, $t \in \mathbb{R}_{\geq 0}$, is obtained with $\rho = \sqrt{\frac{c_2}{c_1}}$ and $\mu = \frac{1}{2}c_4$. This completes the proof. □

A.5 Appendix of Chapter 6

A.5.1 Proof of Theorem 6.2

Proof. The proof will exploit the Lyapunov/storage function as provided in (6.28) given a fixed initial state $\xi(0) = \xi_0 \in \mathbb{R}^{n_\xi}$, $w \in \mathcal{L}_2$ and $\tau(0) = 0$. Now we will prove three important facts.
(i) *Under Assumption 6.1, W as in* (6.28) *is a well-defined Lyapunov/storage function candidate for all $\tau \in [0, h]$.* Following the proof of Theorem III.2 of Heemels et al. (2013), and especially eqn. (63) of Heemels et al. (2013), we have that

$$\begin{aligned}\bar{P}_i(h-\tau) &= \bar{F}_{21}(\tau)\bar{F}_{11}^{-1}(\tau) + \bar{F}_{11}^{-\top}(\tau)\Big(\bar{P}_i(h) + \\ &\bar{P}_i(h)\bar{S}(\tau)\left(I - \bar{S}(\tau)^\top \bar{P}_i(h)\bar{S}(\tau)\right)^{-1}\bar{S}(\tau)^\top \bar{P}_i(h)\Big)\bar{F}_{11}^{-1}(\tau)\end{aligned} \tag{A.71}$$

for which we have that $\bar{P}_i(h) = P_i$, $i \in \{1, \dots, N\}$.

Requiring $\bar{P}_i(h-\tau)$ to be well defined for all $\tau \in [0, h]$ is equivalent to the existence of $\left(I - S(\tau)^\top \bar{P}_i(h) S(\tau)\right)^{-1}$ for all $\tau \in [0, h]$, as indicated by (A.71). This can be established by following the reasoning in (Heemels et al., 2013, Proof of Theorem III.2).

(ii) *During flow it holds that $\dot{W} \leq -2\rho W - \gamma^{-2} z^\top z + w^\top w$.* This is implied by the fact that each component storage function $\xi^\top \bar{P}_i(\tau)\xi$, $i \in \{1, \dots, N\}$, satisfies the Riccati differential equation (6.22) that implies the mentioned dissipation inequality during flow, see, e.g., Heemels et al. (2013). It is important to observe that due to the particular construction of W in (6.28) it holds that for each $k \in \mathbb{N}$ there exists an $i \in \{1, 2, \dots, N\}$ such that for all $t \in (kh, (k+1)h)$ $W(\xi, \tau, w, t) = \xi^\top \bar{P}_i(\tau)\xi$. Hence, the value of i in (6.28) changes only during jumps.

(iii) *During jumps the Lyapunov/storage function W does not increase i.e.,*

$$W(J_1\xi, 0, w, t) \leq W(\xi, h, w, t), \quad \textit{for all } \xi \in \Omega_i, \tag{A.72}$$

with $i \in \{N_1 + 1, \dots, N\}$, and

$$W(J_2\xi, 0, w, t) \leq W(\xi, h, w, t), \quad \textit{for all } \xi \in \Omega_i, \tag{A.73}$$

with $i \in \{1, \dots, N_1\}$. This is implied by feasibility of the conditions of Theorem 6.2, see (Heemels et al., 2013, Proof of Theorem III.2).

Combining the above three facts, and using $\mathcal{L}_2$-gain techniques as in van der Schaft (1999), we can guarantee GES of (6.1) (in case $w = 0$), and that the $\mathcal{L}_2$-gain of (6.1) is smaller than or equal to γ. Let $w \in \mathcal{L}_2$ be given. From item (i), and following the reasoning in (Heemels et al., 2013, Proof of Theorem III.2), we have that

$$c_1\|\xi\|^2 \leq W(\xi,\tau,w,t) \leq c_2\|\xi\|^2, \tag{A.74}$$

for some $0 < c_1 \leq c_2$ for all $\tau \in [0,h]$ and all $\xi \in \mathbb{R}^{n_\xi}$. Conditions (ii) and (iii) combined guarantee that

$$W(\xi(t),\tau(t),w,t) - W(\xi_0,0,w,0) \leq \int_0^t \Big[-\gamma^{-2}\|z\|^2 + \|w\|^2\Big]dt, \tag{A.75}$$

which by using that $W(\xi(t),\tau(t),w,t) \geq 0$ and letting $t \to \infty$ gives

$$-W(\xi_0,0,w,0) \leq \int_0^\infty \Big[-\gamma^{-2}\|z\|^2 + \|w\|^2\Big]dt. \tag{A.76}$$

Due to the inequality (A.74), we can bound $W(\xi_0,0,w,0) \leq c_2\|\xi_0\|^2$, and thus obtain

$$\int_0^\infty \|z\|^2 dt \leq c_2\gamma^2\|\xi_0\|^2 + \gamma^2\int_0^\infty \|w\|^2 dt. \tag{A.77}$$

Consequently, we have that $\|z\|_{\mathcal{L}_2} \leq \gamma\sqrt{c_2}\|\xi_0\| + \gamma\|w\|_{\mathcal{L}_2}$. This completes the proof. $\square$

Bibliography

Aangenent, W., van de Molengraft, M., and Steinbuch, M. (2005). Nonlinear control of a linear motion system. In *IFAC World Congress*, volume 16.

Aangenent, W. H. T. M., Witvoet, G., Heemels, W. P. M. H., van de Molengraft, M. J. G., and Steinbuch, M. (2010). Performance analysis of reset control systems. *Int. J. of Robust and Nonlinear Control*, 20(11):1213–1233.

Arcak, M. and Teel, A. R. (2002). Input-to-state stability for a class of Lurie systems. *Automatica*, 38(11):1945–1949.

Armstrong, B., Neevel, D., and Kusik, T. (2001). New results in N-PID control: Tracking, integral control, friction compensation and experimental results. *IEEE Trans. Contr. Syst. Technology*, 9(2):399–406.

Åström, K. J. and Hägglund, T. (2001). The future of PID control. *Contr. Eng. Practice*, 9(11):1163–1175.

Baños, A. and Barreiro, A. (2012). *Reset Control Systems.*

Başar, T. and Bernhard, P. (1991). *H_∞-Optimal Control and Related Minimax Design Problems: A Dynamic Game Approach.* Birkhäuser, Ed. Boston, M.A.

Beker, O., Hollot, C. V., Chait, Y., and Han, H. (2004). Fundamental properties of reset control systems. *Automatica*, 40(6):905–915.

Bemporad, A., Heemels, W. P. M. H., and Johansson, M. E. (2010). *Networked Control Systems*, volume 406. Springer "Lecture notes in control and information sciences".

Borgers, D. P. and Heemels, W. P. M. H. (Accepted, 2014). Event-separation properties of event-triggered control systems. *IEEE Trans. Autom. Control.*

Brogliato, B., Lozano, R., Maschke, B., and Egeland, O. (2007). *Dissipative Systems Analysis and Control.* Springer.

Butler, H. (2011). Position control in lithographic equipment. *Contr. Syst. Mag.*, 31(5):28–47.

Cai, C. and Teel, A. (2009). Characterizations of input-to-state stability for hybrid systems. *Syst. and Contr. Letters*, 58(1):47–53.

Carrasco, J., Baños, A., and van der Schaft, A. (2010). A passivity-based approach to reset control systems stability. *Syst. and Contr. Letters*, 59(1):18–24.

Clegg, J. (1958). A nonlinear integrator for servomechanisms. *Trans. of the A.I.E.E.*, 77(Part-II):41–42.

Dai, D., Hu, T., Teel, A. R., and Zaccarian, L. (2010). Output feedback synthesis for sampled-data system with input saturation. In *proc. American Control Conf.*, pages 1797 –1802.

Dačić, D. B. and Nešić, D. (2007). Quadratic stabilization of linear networked control systems via simultaneous protocol and controller design. *Automatica*, 43:1145–1155.

Deaecto, G. S., Geromel, J. C., and Daafouz, J. (2011). Dynamic output feedback H_∞ control of switched linear systems. *Automatica*, 47(8):1713 – 1720.

Demidovich, B. (1961). Dissipativity of a nonlinear system of differential equations. *Ser. Mat. Mekh.*, Part I-6:19–27.

Dinh, M., Scorletti, G., Fromion, V., and Magarotto, E. (2005). Parameter dependent H_∞ control by finite dimensional LMI optimization: application to trade-off dependent control. *Int. J. of Robust and Nonlinear Control*, 15(9):383–406.

Donkers, M. C. F., Heemels, W. P. M. H., van de Wouw, N., and Hetel, L. (2011). Stability analysis of networked control systems using a switched linear systems approach. *IEEE Trans. Autom. Control*, 56(9):2101–2115.

Eker, J. and Malmborg, J. (1999). Design and implementation of a hybrid control strategy. *IEEE Contr. Syst. Mag.*, 19(4):12–21.

Ferrari-Trecate, G., Cuzzola, F. A., Mignone, D., and Morari, M. (2002). Analysis of discrete-time piecewise affine and hybrid systems. *Automatica*, 38(12):2139 – 2146.

Feuer, A., Goodwin, G. C., and Salgado, M. (1997). Potential benefits of hybrid control for linear time invariant plants. In *Proc. American control conf.*, volume 5, pages 2790–2794.

Filippov, A. (1988). *Differential equations with discontinuous righthand sides*. Dordrecht, The Netherlands: Kluwer.

Fong, M. and Szeto, W. (1980). Application of a nonlinear filter to a conditionally stable system. *Int. J. of Control*, 32(6):963–981.

Forni, F., Nešić, D., and Zaccarian, L. (2011). Reset passivation of nonlinear controllers via a suitable time-regular reset map. *Automatica*, 47(9):2099–2106.

Foster, W., Gieseking, D., and Waymeyer, W. (1966). A nonlinear filter for independent gain and phase (with application). *Trans. ASME J. Basic Eng.*, 78:457–462.

Franklin, G. F., Powel, J. D., and Emami-Naeini, A. (2006). *Feedback control of dynamic systems*. Pearson Prentice Hall, 5th edition.

Freudenberg, J., Middleton, R., and Stefanpoulou, A. (2000). A survey of inherent design limitations. In *Proc. American control conf.*, volume 5, pages 2987–3001.

Goebel, R., Sanfelice, R. G., and Teel, A. R. (2009). Hybrid dynamical systems. *IEEE Contr. Syst. Mag.*, 29(2):28–93.

Goebel, R., Sanfelice, R. G., and Teel, A. R. (2012). *Hybrid dynamical systems: modeling, stability and robustness*. Princeton University Press.

Groot Wassink, M., van de Wal, M., Scherer, C., and Bosgra, O. H. (2005). LPV control for a wafer stage: Beyond the theoretical solution. *Contr. Eng. Practice*, 13(2):231–245.

Guo, Y., Gui, W., Yang, C., and Xie, L. (2012). Stability analysis and design of reset control systems with discrete-time triggering conditions. *Automatica*, 48(3):528–535.

Heemels, W. P. M. H., de Schutter, B., Lunze, J., and Lazar, M. (2010). Stability analysis and controller synthesis for hybrid dynamical systems. *Phil. Trans. R. Soc. A*, 368(1930):4937–4960.

Heemels, W. P. M. H., Donkers, M. C. F., and Teel, A. R. (2013). Periodic event-triggered control for linear systems. *IEEE Trans. Autom. Control*, 58(4):847–861.

Heemels, W. P. M. H., Dullerud, G., and Teel, A. R. (2015a). A lifting approach to $\mathcal{L}_2$-gain analysis of periodic event-triggered and switching sampled-data control systems. In *Accepted for the 54th IEEE Conf. Decision and Control*.

Heemels, W. P. M. H., Dullerud, G., and Teel, A. R. (2015b). $\mathcal{L}_2$-gain analysis for a class of hybrid systems with applications to reset and event-triggered control: A lifting approach. *accepted*.

Heemels, W. P. M. H., Johansson, K. H., and Tabuada, P. (2012). An introduction to event-triggered and self-triggered control. In *Proc. IEEE Conf. Decision and Control*, pages 3270–3285.

Heertjes, M., Gruntjens, K., van Loon, S., Kontaras, N., and Heemels, W. (2015). Design of a variable gain integrator with reset. In *Proc. American control conf.*, pages 2155–2160.

Heertjes, M. and Steinbuch, M. (2004). Stability and performance of a variable gain controller with application to a dvd storage drive. *Automatica*, 40(4):591–602.

Heertjes, M. and Vardar, Y. (2013). Self-tuning in sliding mode control of high-precision motion systems. In *IFAC Proceedings Volumes*, pages 13–19.

Heertjes, M. F., Cremers, F., Rieck, M., and Steinbuch, M. (2005). Nonlinear control of optical storage drives with improved shock performance. *Contr. Eng. Practice*, 13(10):1295–1305.

Heertjes, M. F. and Nijmeijer, H. (2012). Self-tuning of a switching controller for scanning motion systems. *Mechatronics*, 22(3):310 – 319.

Heertjes, M. F., Sahin, I. H., van de Wouw, N., and Heemels, W. P. M. H. (2013). Switching control in vibration isolation systems. *IEEE Trans. Contr. Syst. Technology*, 21(3):626–635.

Heertjes, M. F., Schuurbiers, X. G. P., and Nijmeijer, H. (2009). Performance-improved design of N-PID controlled motion systems with applications to wafer stages. *IEEE Trans. Indus. Electronics*, 56(5):1347–1355.

Hespanha, J. and Morse, A. (1999). Stability of switched systems with average dwell-time. In *Proc. 38th IEEE Conf. Decision and Control*, volume 3, pages 2655–2660 vol.3.

Hespanha, J. P. (2009). *Linear systems theory.* Princeton University Press.

Hespanha, J. P. and Morse, A. S. (2002). Switching between stabilizing controllers. *Automatica*, 38(11):1905–1917.

Hespanha, J. P., Naghshtabrizi, P., and Xu, Y. (2007). A survey of recent results in networked control systems. *Proc. IEEE*, 95(1):138–162.

Horowitz, I. and Rosenbaum, P. (1975). Nonlinear design for cost of feedback reduction in systems with large parameter uncertainty. *Int. J. of Control*, 21(6):977–1001.

Hunnekens, B. G. B. (2014). *Performance optimization of hybrid controllers for linear motion systems.* PhD thesis, Eindhoven University of Technology.

Hunnekens, B. G. B., Heertjes, M. F., van de Wouw, N., and Nijmeijer, H. (2015a). Performance optimization of piecewise affine variable-gain controllers for linear motion systems. *Mechatronics*, 24(6):648–660.

Hunnekens, B. G. B., van de Wouw, N., Heertjes, M. F., and Nijmeijer, H. (2015b). Synthesis of variable gain integral controllers for linear motion systems. *IEEE Trans. Contr. Syst. Technology*, 23(1):139–149.

Janssens, P., Pipeleers, G., and Swevers, J. (2013). A data-driven constrained norm-optimal iterative learning control framework for LTI systems. *IEEE Trans. Contr. Syst. Technology*, 21(2):546–551.

Johansson, M. and Rantzer, A. (1998). Computation of piecewise quadratic Lyapunov functions for hybrid systems. *IEEE Trans. Autom. Control*, 43(4):555–559.

Khalil, H. K. (2000). *Nonlinear Systems.* Prentice Hall.

Khargonekar, P. P. and Poolla, K. R. (1986). Uniformly optimal control of linear time-invariant plants: Nonlinear time-varying controllers. *Syst. Control Lett.*, 6(5):303–308.

Krishnan, K. R. and Horowitz, I. M. (1974). Synthesis of a non-linear feedback system with significant plant-ignorance for prescribed system tolerances. *Int. J. of Control*, 19(4):689–706.

Leine, R. and Nijmeijer, H. (2004). *Dynamics and Bifurcations of Non-Smooth Mechanical Systems.* Berlin, Germany: Springer.

Leith, D. J. and Leithead, W. E. (2000). Survey of gain-scheduling analysis and design. *Int. J. of Control*, 73(11):1001–1025.

Liberzon, D. (2003). *Switching in systems and control.* Birkhäuser.

Lin, Z., Pachter, M., and Banda, S. (1998). Toward improvement of tracking performance nonlinear feedback for linear systems. *Int. J. of Control*, 70(1):1–11.

Loquen, T., Tarbouriech, S., and Prieur, C. (2008). Stability of reset control systems with nonzero reference. In *Proc. IEEE Conf. Decision and Control*, pages 3386–3391.

Lunze, J. and Lehmann, D. (2010). A state-feedback approach to event-based control. *Automatica*, 46(1):211 – 215.

Martinez, V. M. and Edgar, T. F. (2006). Control of lithography in semiconductor manufacturing. *Contr. Syst. Mag.*, 26(6):46–55.

Narendra, K. S. and Balakrishnan, J. (1997). Adaptive control using multiple models. *IEEE Trans. Autom. Control*, 42(2):171–187.

Nešić, D., Teel, A. R., and Zaccarian, L. (2011). Stability and performance of SISO control systems with first-order reset elements. *IEEE Trans. Autom. Control*, 56(11):2567–2582.

Nešić, D., Zaccarian, L., and Teel, A. R. (2008). Stability properties of reset systems. *Automatica*, 44(8):2019–2026.

Panni, F., Waschl, H., Alberer, D., and Zaccarian, L. (2014). Position regulation of an EGR valve using reset control with adaptive feedforward. *IEEE Trans. Contr. Syst. Technology*, 22(6):2424–2431.

Pavlov, A., van de Wouw, N., and Nijmeijer, H. (2006). *Uniform Output Regulation of Nonlinear Systems: A Convergent Dynamics Approach*. Birkhäuser.

Prieur, C., Tarbouriech, S., and Zaccarian, L. (2013). Lyapunov-based hybrid loops for stability and performance of continuous-time control systems. *Automatica*, 49(2):577–584.

Rugh, W. J. and Shamma, J. S. (2000). Research on gain scheduling. *Automatica*, 36(10):1401–1425.

Scherer, C. W. (2001). LPV control and full block multipliers. *Automatica*, 37(3):361–375.

Seron, M. M., Braslavsky, J. H., and Goodwin, G. C. (1997). *Fundamental Limitations in Filtering and Control*. Berlin: Springer.

Shamma, J. S. and Athans, M. (1991). Guaranteed properties of gain scheduled control for linear parameter-varying plants. *Automatica*, 27(3):559–564.

Skogestad, S. and Postlethwaite, I. (2005). *Multivariable Feedback Control: Analysis and Design*. John Wiley & sons, Ltd.

Solo, V. (1994). On the stability of slowly time-varying linear systems. *Mathematics of Control, Signals and Systems*, 7(4):331–350.

Sontag, E. D. (2008). Input to state stability: Basic concepts and results. In *Nonlinear and Optimal Control Theory*, volume 1932 of *Lecture Notes in Mathematics*, pages 163–220. Springer Berlin Heidelberg.

Sontag, E. D. and Wang, Y. (1995). On characterizations of the input-to-state stability property. *Syst. Control Lett.*, 24(5):351–359.

Steinbuch, M., Helvoort, J. J. M., Aangenent, W. H. T. M., de Jager, A. G., and van de Molengraft, M. J. G. (2005). Data-based control of motion systems. In *Proc. IEEE Conf. on Control Applications*, pages 529–534.

Steinbuch, M. and Norg, M. L. (1998). Advanced motion control: An industrial perspective. *European J. of Control*, 4(4):278–293.

Stoorvogel, A. A. (1995). Nonlinear L_1 optimal controllers for linear systems. *IEEE Trans. Autom. Control*, 40(4):694–696.

Tabuada, P. (2007). Event-triggered real-time scheduling of stabilizing control tasks. *IEEE Trans. Autom. Control*, 52(9):1680–1685.

Teel, A., Forni, F., and Zaccarian, L. (2013). Lyapunov-based sufficient conditions for exponential stability in hybrid systems. *IEEE Trans. Autom. Control*, 58(6):1591–1596.

van Berkel, K., Rotariu, I., and Steinbuch, M. (2007). Cogging compensating piecewise iterative learning control with application to a motion system. In *Proc. American control conf.*, pages 1275–1280.

van de Wal, M., van Baars, G., Sperling, F., and Bosgra, O. H. (2002). Multivariable $\mathcal{H}_\infty/\mu$ feedback control design for high-precision wafer stage motion. *Contr. Engineering Practice*, 10:739–755.

van de Wouw, N., Pastink, H. A., Heertjes, M. F., Pavlov, A. V., and Nijmeijer, H. (2008). Performance of convergence-based variable-gain control of optical storage drives. *Automatica*, 44(1):15–27.

van der Schaft, A. (1999). *$\mathcal{L}_2$ Gain & Passivity techniques in nonlinear control.* 2nd edition.

van Herpen, R. M. A. (2014). *Identification for control of complex motion systems : optimal numerical conditioning using data-dependent polynomial bases.* PhD thesis, Eindhoven University of Technology.

van Loon, S. J. L. M., Gruntjes, K., Heertjes, M. F., van de Wouw, N., and Heemels, W. P. M. H. (2015a). Frequency-domain tools for stability of reset control systems. *in preparation for journal publication.*

van Loon, S. J. L. M., Heemels, W. P. M. H., and Teel, A. R. (2014). Improved $\mathcal{L}_2$-gain analysis for a class of hybrid systems with applications to reset and event-triggered control. In *Proc. 53rd IEEE Conf. Decision and Control*, pages 1221–1226.

van Loon, S. J. L. M., Hunnekens, B. G. B., Heemels, W. P. M. H., van de Wouw, N., and Nijmeijer, H. (2015b). Split-path nonlinear integral control for transient performance improvement. *Automatica*, under review.

van Loon, S. J. L. M., Hunnekens, B. G. B., Simon, A. S., van de Wouw, N., and Heemels, W. P. M. H. (2015c). Bandwidth-on-demand motion control with a nano-positioning application. *IEEE Contr. Syst. Technology*, submitted.

van Loon, S. J. L. M., van der Weijst, R., Heertjes, M. F., and Heemels, W. P. M. H. (2015d). Scheduled controller design for systems with two switching sensor configurations: A frequency-domain approach. Accepted for the 5th IFAC Conference on Analysis and Design of Hybrid Systems.

Walsh, G. C., Hong, Y., and Bushnell, L. G. (2002). Stability analysis of networked control systems. *IEEE Trans. Contr. Syst. Technology*, 10(3):438–446.

Yakubovich, V. A. (1964). The matrix inequalities method in the theory of the stability of nonlinear control systems - I. *Automation and Remote Control*, 7:905–917.

Yakubovich, V. A., Leonov, G. A., and Gelig, A. K. (2004). *Stability of Stationary Sets in Control Systems with Discontinuous Nonlinearities*. World Scientific (1978 original Russian version), Singapore.

Zaccarian, L., Nešić, D., and Teel, A. R. (2005). First order reset elements and the clegg integrator revisited. In *Proc. American control conf.*, volume 1, pages 563–568.

Zaccarian, L., Nešić, D., and Teel, A. R. (2011). Analytical and numerical Lyapunov functions for SISO linear control systems with first-order reset elements. *Int. J. of Robust and Nonlinear Control*, 21(10):1134–1158.

Zaccarian, L. and Teel, A. R. (2002). A common framework for anti-windup, bumpless transfer and reliable designs. *Automatica*, 38(10):1735 – 1744.

Zheng, J., Guo, G., and Wang, Y. (2005). Nonlinear PID control of linear plants for improved disturbance rejection. In *16th IFAC World Congress*, volume 16, pages 281–286.

Zheng, Y., Chait, Y., Hollot, C. V., Steinbuch, M., and Norg, M. L. (2000). Experimental demonstration of reset control design. *Contr. Eng. Practice*, 8(2):113–120.

Zhou, K., Doyle, J. C., and Glover, K. (1996). *Robust and optimal control*. Prentice-Hall, Inc. Upper Saddle River, NJ, USA.

Zoss, L., Witte, A., and Marsch, J. (1968). A nonlinear three response controller with two response adjustment. In *Proc. of the Advances in intrumentation*, pages 1–6.

Summary

This thesis considers the analysis and design of hybrid/nonlinear controllers with the aim to improve the performance of linear (motion) systems. The ever increasing performance demands on the speed and accuracy of industrial (motion) systems require essential control engineering innovations. Nevertheless, the vast majority of state-of-practice controller designs rely on classical linear control theory, which hampers the necessary improvements as linear controllers suffer from inherent fundamental performance limitations. These performance limitations will, especially in case of conflicting control goals, lead to a design compromise and thus result in a suboptimal control solution. In this thesis, we therefore consider a larger controller class consisting of hybrid/nonlinear controllers. Compared to linear controllers, these controllers provide more controller design freedom that enables the possibility to overcome the fundamental limitations in linear control. However, despite their potential, nonlinear/hybrid controllers are often not so easily embraced by control engineers in industry. Namely, many design and analysis techniques for such controllers do not connect to the current industrial control practice, in which frequency-domain design tools and non-parametric models are commonly exploited. As such, an important open problem is the design of hybrid/nonlinear controllers for linear (motion) systems, using frequency-domain loop-shaping techniques as a basis.

This thesis develops four novel hybrid/nonlinear controllers that all have the ability to outperform linear controllers, and all allow the user to employ measured frequency response data of the plant as a basis for the controller design.

First, we present a novel switched controller architecture for motion systems that exhibit, from a control point-of-view, position-dependent dynamics as a result of varying sensor configurations. All individual components (except the time-varying gain) of the resulting controller architecture can be designed using classical frequency-domain loop-shaping techniques. Moreover, the presented stability conditions are graphically verifiable based on measured frequency response data. Its effectiveness, in terms of improving both transient and

steady-state performance compared to the current state-of-the-art linear control solution, is demonstrated by means of real-time experiments on a high-precision industrial motion stage.

Second, we present a technique that allows for a reference-dependent varying 'bandwidth' of the feedback controller. By taking actual reference information into account, this novel design allows to automatically adapt the 'bandwidth' of the control system on-line, which is advantageous if the motion system is subject to time-varying, and reference-dependent, performance requirements. Namely, this feature allows us to balance trade-offs between low-frequency tracking performance and sensitivity to higher-frequency disturbances in a favorable manner when compared to (fixed bandwidth) linear control solutions. Easy-to-use design guidelines and stability analysis techniques are presented for the design of such a 'bandwidth-on-demand' controller, which are based on employing measured frequency response data of the plant. The effectiveness of this control strategy to outperform (fixed bandwidth) linear control solutions is demonstrated by means of experiments on an industrial nano-positioning motion setup.

Third, reset control is another nonlinear/hybrid control technique that is considered in this thesis. In the literature, many results exist that demonstrate the potential of a reset controller to improve the transient performance of linear (motion) systems. The vast majority of these results rely in their design and analysis on parametric models and on solving linear matrix inequalities (LMIs). In this thesis, we have established new conditions, based on measured frequency response data, to verify stability of the closed-loop reset control system. The practical applicability of these data-based stability conditions for reset control systems is demonstrated through experiments on an industrial piezo-actuated motion system used in the lithography industry.

Fourth, this thesis also presents a split-path nonlinear integrator (SPANI), which is a novel variant of the split-path nonlinear filter introduced in the late 1960s. The SPANI has been developed with the aim to improve the transient performance of linear systems by appropriate modulation of the magnitude and phase of the integral part of the controller, while still ensuring a zero steady-state error in the presence of constant external disturbances. In the basis, the design of the SPANI can be performed using classical frequency-domain loop-shaping techniques by designing a linear integrator in parallel to a nominal linear controller, and then replacing the linear integrator by a SPANI with the same gain. In addition, many situations require the tuning of an additional (scalar) parameter, for which the presented LMI-based stability conditions may serve as a guideline. The effectiveness of this control strategy, as a way to improve the transient performance, is demonstrated using a model-based benchmark study on an industrial pick-and-place machine.

Besides the above contributions on the development of new hybrid/nonlinear control techniques, this thesis also considers a particular class of hybrid systems with periodic time-triggered jump conditions. We demonstrate the relevance of this hybrid modeling framework by, firstly, modeling three application domains, consisting of event-triggered control systems, reset control systems and networked control systems, in this framework and, secondly, showing that the unifying modeling character is instrumental in enabling the transfer of results between the diverse application domains. Moreover, new LMI-based conditions are presented to analyze the stability and the $\mathcal{L}_2$-performance of the hybrid dynamical systems under study using trajectory-dependent Lyapunov/storage functions as a technical novelty. These conditions result in a tighter estimate on an important steady-state performance measure, the $\mathcal{L}_2$-gain between disturbance inputs and performance outputs, compared to the existing conditions found in the literature.

The contributions of this thesis support the design of hybrid/nonlinear controllers that have the ability to outperform linear controllers. By demonstrating their potential and by presenting analysis and design techniques that connect to the current industrial practice, this thesis aims to contribute to the industrial acceptance of such controllers.

Societal summary

High-tech mechatronic systems, such as wafer scanners, printers, pick-and-place machines, electron microscopes, et cetera, constitute an important economic value worldwide and especially for the Netherlands. Nowadays, these high-tech systems have to perform their (motion) tasks while complying with increasingly high performance demands on precision and throughput. In order to meet these stringent performance requirements, feedback controllers are essential in all of these high-tech applications. The vast majority of the current controller designs in industry rely on classical linear control theory. However, limiting the controller design space in this way obstructs achieving the required improvements due to the fact that linear controllers suffer from inherent fundamental performance limitations. These performance limitations will, especially in case of conflicting control goals, lead to a design compromise and thus a suboptimal control solution.

In this research, a larger controller class, consisting of hybrid/nonlinear controllers, is considered to overcome the fundamental limitations in linear control. In particular, four novel hybrid/nonlinear controllers are presented accompanied by systematic analysis and design methods that all have strong connections to the current industrial practice. By means of experimental results on industrial wafer stages and on a nano-positioning motion system, together with an extensive case study on an industrial pick-and-place machine, the practical feasibility of these controllers as well as their ability to outperform linear control solutions has been demonstrated. Therefore, this research may contribute to a wider spread of these high-potential hybrid/nonlinear controllers in industry.

Samenvatting

Dit proefschrift beschouwt het ontwerp en de analyse van hybride/niet-lineaire regelaars met als doel de prestatie van lineaire (positioneer)systemen te verbeteren. De alsmaar voortdurende eisen ten aanzien van snelheid en nauwkeurigheid van industriële (positioneer)systemen vraagt om essentiële innovaties ten aanzien van het actief regelen van deze systemen. Toch zijn de meeste regelsystemen in de huidige praktijk nog steeds gebaseerd op klassieke lineaire regeltheorie, wat de noodzakelijke verbeteringen hindert doordat deze lineaire regelaars onderhevig zijn aan fundamentele prestatie beperkingen. Deze beperkingen zullen, zeker in het geval van conflicterende regeldoelen, leiden tot compromis in het ontwerp, en als gevolg daarvan een suboptimale regeloplossing. Het is daarom dat dit proefschrift een grotere klasse regelaars beschouwt, bestaande uit hybride/niet-lineaire regelaars. Deze regelaars bieden meer ontwerp vrijheid ten opzichte van lineaire regelaars wat ons in staat stelt om de fundamentele beperkingen in lineaire regeltheorie te overwinnen. Echter, ondanks het grote potentieel dat deze klasse regelaars te bieden heeft worden ze nog niet veelvuldig toegepast door regeltechnici in de industrie. Een van de redenen hiervoor is dat de meeste ontwerp en analyse methoden voor deze regelaars gebruik maken van parametrische systeem modellen en het numeriek oplossen van lineaire matrix ongelijkheden (LMIs), wat niet aansluit bij de frequentiedomein gebaseerde technieken waar veel regeltechnici in de dagelijkse praktijk mee van doen hebben. Het is daarom belangrijk om hybride/niet-lineaire regelaars te ontwikkelen waarbij frequentiedomein loop-shaping technieken kunnen worden gebruikt als een basis voor het regelaarontwerp.

Dit proefschrift presenteert vier nieuwe hybride/niet-lineaire regelaars die ten opzichte van lineaire regelaars allemaal in staat zijn om een betere prestatie te behalen, en waarbij een groot deel van het regelaarontwerp uitgevoerd kan worden met behulp van gemeten frequentie response data van het systeem.

Als eerste presenteren we een nieuwe geschakelde regelaarstructuur voor systemen die, vanuit het oogpunt van de regelaar, onderhevig zijn aan positieafhan-

kelijke dynamica als gevolg van variërende sensor combinaties. Alle individuele componenten (behalve de tijdsvariërende gain) van de resulterende regelaarstructuur kunnen worden ontworpen met behulp van frequentiedomein loop-shaping regelaarontwerp technieken. Daarnaast kunnen de bijbehorende stabiliteitcondities geverifieerd worden door middel van gemeten frequentie response data. Door middel van experimentele resultaten, behaald op een industrieel positioneersysteem, demonstreren we dat de nieuw ontworpen hybride regelaar ons in staat stelt om zowel een betere transiënte als steady-state prestatie te behalen ten opzichte van het huidige lineaire regelaarontwerp.

Als tweede presenteren we een techniek die ons in staat stelt om de 'bandbreedte' van de regelaar online te laten variëren op basis van actuele referentie informatie. Dit is met name voordelig als het (positioneer)systeem onderhevig is aan tijdvariërende, en referentie afhankelijke, prestatie eisen. Namelijk, vergeleken met (vaste bandbreedte) lineaire regelaars stelt deze techniek ons in staat om op een gunstigere manier om te gaan met afwegingen tussen laagfrequent volggedrag en gevoeligheid voor hoogfrequente verstoringen. Zowel de ontwerptechnieken als de stabiliteitanalyse van deze 'bandwidth-on-demand' regelaar zijn gebaseerd op gemeten frequentie response data van het systeem, en sluiten daardoor aan op de wensen vanuit de praktijk. Door middel van experimentele resultaten op een industrieel positioneersysteem demonstreren we dat deze hybride regelaar in staat is de prestatie van een lineair regelsysteem te overtreffen.

Dit proefschrift beschouwt ook zogenaamde 'reset' regelaars. In de literatuur bestaat een veelvoud aan resultaten waarin wordt aangetoond dat reset regelaars in staan zijn om de transiënte prestatie van lineaire (positioneer)systemen te verbeteren. Echter, in al deze resultaten is het ontwerp en analyse van deze regelaars gebaseerd op parametrische modellen en het oplossen van LMIs. In dit proefschrift presenteren wij nieuwe technieken, gebaseerd op gemeten frequentie response data, om de stabiliteit van (positioneer)systemen met reset regelaar te verifiëren. Daarnaast kunnen deze data-gebaseerde technieken ook waardevol zijn voor het ontwerp van deze regelaars. De praktische toepasbaarheid van deze technieken is gedemonstreerd door middel van experimentele resultaten op een industrieel positioneersysteem dat gebruikt wordt in de lithografie industrie.

In dit proefschrift is ook een nieuwe variant op een 'split-path' niet-lineair filter ontwikkeld, namelijk de 'split-path' niet-lineaire integrator (SPANI). De SPANI is ontwikkeld om de transiënte prestatie van lineaire (positioneer)systemen te verbeteren door middel van passende modulatie van de magnitude- en tekeninformatie van het integrerende deel van de regelaar. Het ontwerp van de SPANI kan voor een groot deel worden uitgevoerd met behulp van frequentiedomein loop-shaping technieken door een lineaire integrator parallel aan een nominale regelaar te ontwerpen. Vervolgens kan de lineaire integrator worden vervangen door de SPANI met behoudt van gain. Echter, in de meeste gevallen zal er een additionele papameter getuned moeten worden waarvoor de door ons gepresenteerde stabiliteitcondities kunnen dienen als handleiding. De effectiviteit van deze regelstrategie wordt gedemonstreerd op een simulatievoorbeeld van een industriële 'pick-and-place' machine.

Naast de contributies op het gebied van de ontwikkeling van nieuwe hybride/niet-lineaire regelaars, draagt dit proefschrift ook bij aan een modelleer- en analyse-raamwerk voor een bepaalde klasse van hybride systemen met periodieke tijd-getriggerde reset condities. Allereerst demonstreren we de relevatie van dit modelleer-raamwerk door drie applicatie domeinen, bestaande uit event-triggered control systemen, reset control systemen en networked control systemen, hierin te modeleren. Daarnaast demonstreren we dat het verenigende modelleer karakter ons in staat stelt om resultaten van een afzonderlijk applicatie domein naar de andere over te dragen. Verder presenteren we ook nieuwe LMI gebaseerde technieken om de stabiliteit en prestatie in termen van $\mathcal{L}_2$-gain (tusssen verstorings ingangen en prestatie uitgangen) te verifiëren. Door middel van een simulatievoorbeeld van een reset regelsysteem demonstreren we dat deze nieuwe condities ons in staat stellen om striktere afschattingen van de $\mathcal{L}_2$-gain te verkrijgen ten opzichte van de bestaande condities in de literatuur.

Samenvattend, de contributies van dit proefschrift dragen bij aan het ontwerp en de analyse van hybride/niet-lineaire regelaars voor lineaire (positioneer)systemen. Het is aangetoond dat deze regelaars de potentie bieden om een betere prestatie te behalen ten opzichte van lineaire regelaars. Daarnaast presenteert dit proefschrift verschillende analyse en ontwerp methodieken die aansluiten met de hedendaagse praktijk in de industrie. Hopelijk kan dit proefschrift daardoor de acceptatie van dergelijke regelaars in industriële toepassingen bespoedigen.

Dankwoord

JFK Airport New York, wachtend op mijn vliegtuig naar Amsterdam en nog nagenietend van een fantastische ‘confekantie’. Er kan geen beter moment zijn om het dankwoord van dit proefschrift te schrijven. Terugblikkend op de afgelopen jaren kan ik niet anders concluderen dat ik het zeker heb getroffen om een promotieopdracht te mogen uitvoeren binnen een zeer prettige en stimulerende werkomgeving. En ook al draagt dit proefschrift alleen mijn naam, ik had dit niet kunnen schrijven zonder de bijdragen en steun die ik van anderen heb ontvangen.

Op de eerste plaats wil ik mijn beide promotoren Maurice en Nathan, en mijn co-promotor Marcel bedanken.

Maurice, bedankt dat je mij de kans hebt gegeven om een promotieonderzoek uit te voeren binnen jouw groep, en Nathan, bedankt dat jij hier als tweede promotor bij betrokken wilde zijn. Voor jullie beiden geldt dat we elkaar al sinds mijn afstuderen kennen. Ik ben jullie dan ook dankbaar voor alle fijne discussies, jullie grenzeloze inzet en kritische, maar altijd eerlijke en constructieve feedback. In al deze jaren heb ik zo veel van jullie mogen leren, en dan heb ik het niet alleen over werk gerelateerde zaken zoals het uitvoeren van onderzoek en het schrijven van wetenschappelijke artikelen, maar juist ook op persoonlijk vlak. Nathan, ik wil jou nog speciaal bedanken voor de gezellige avonden tijdens conferenties, en dan in het bijzonder onze reis naar Wenen. Maurice, jij nog extra bedankt voor de ontspannende mini road trip door America en de gezelligheid tijdens onze hikes door de Smoky Mountains! Gelukkig waren de beren meer geïnteresseerd in het vinden van plantaardig voedsel dan in ons.

Marcel, jouw vrolijke karakter, ongekende enthousiasme voor ons vakgebied, en je inhoudelijke scherpte hebben er voor gezorgd dat ik altijd enorm graag met je heb samengewerkt. Ik ben dan ook dankbaar dat jij als co-promotor bij mijn promotieonderzoek betrokken wilde zijn.

Henk, officieel was ik geen student binnen jouw groep maar toch zagen we elkaar geregeld tijdens onze HyPerMotion meetings. Ondanks dat ik (2 keer!) op jouw stoel ben gaan zitten heb ik mij altijd erg welkom gevoeld in jouw kamer. Daarnaast heb ik jouw oprechte betrokkenheid bij mijn project, feedback op mijn werk en steun tijdens mijn 'twijfel momentjes' altijd enorm gewaardeerd.

Furthermore, I would like to thank Luca Zaccarian, Arjan van der Schaft and Siep Weiland for taking part in the reading committee that approved this thesis as well as for taking part in the defense committee. Ook wil ik op deze plaats de gebruikers binnen het STW HyPerMotion project bedanken voor de prettige meetings, positieve feedback en fijne samenwerking. Daarnaast heb ik in de afgelopen jaren met verschillende studenten mogen werken. Stijn, Robert, Andrei, Koen en Carel, hartstikke bedankt voor de prettige samenwerking gedurende deze periode. Hopelijk heb ik jullie iets bij kunnen brengen, ik heb in ieder geval erg veel van jullie geleerd!

Ik wil ook mijn kamergenoten Thomas en Bram bedanken. Bram, jij als kamergenoot en projectpartner verdient een hele prominente plaats in dit dankwoord. We hebben meer dan drie jaar bij elkaar op de kamer gezeten en ik kan me niet herinneren dat er ook maar een dag voorbij is gegaan waarop we niet hebben gelachen. Maar naast de prettige omgang op persoonlijk vlak hebben we ook goed samengewerkt binnen het gezamenlijke project, wat tot een paar hele mooie onderzoekslijnen heeft geleidt. Deze bijzonder prettige en stimulerende werkomgeving, die daarnaast ook zeker niet beperkt bleef tot kamer -1.123, heeft er voor gezorgd dat ik de afgelopen jaren met veel plezier naar mijn werk gegaan ben. Dit gezegd hebbende, ik vraag me af of ik ooit nog in een vergelijkbare werkomgeving mag werken als die op de vloeren '-1' en '0'. Ik denk dat het uniek is voor 'onze gang' dat de 'scheidslijn' tussen collega's en vrienden in veel gevallen flinterdun is of zelfs in zijn geheel is verdwenen. Daarom aan alle collega's: Bedankt voor de (vele) gezellige koffie pauzes, conferenties/confekanties, en alle andere uitjes zoals borrels, uit eten gaan en concerten bezoeken. Speciale dank gaat uit naar: Tom voor zijn hulp bij het ontwerpen van de cover, Thijs, Dennis en Joost voor het altijd open staan voor een praatje, Joris en Michael voor de gezellige lunches, Geertje, Robert, Elise en Jan voor de lunchwandelingen, Frank, Niek, Michiel and Sava for the nice road trip through the USA, and to Menno, Nick, Matthijs, and Behnam for the frequent dinners & drinks. Naast al deze gezellige bezigheden/uitjes is fietsen ook erg belangrijk voor mij om te ontspannen. Tom vd S., Dennis, Niek, Tom O., Gillis, Robert, Benjamin, Lennart, Michiel, Elise en Emile, bedankt voor de vele gezellige race/MTB ritjes en de fietsvakanties naar Mallorca, de Vogezen, en de Eifel. Sorry voor het (lange) wachten als het weer eens bergop ging...

Het gezegde 'de laatste loodjes wegen het zwaarst' is mij niet vreemd geweest in de laatste fase van het schrijven van dit proefschrift. Echter, als ik heel eerlijk ben heb ik eigenlijk nooit veel redenen gehad tot klagen, toch heeft mij dit er niet van weerhouden dat veelvuldig te doen. Thijs, Geertje, Elise en Menno, super bedankt voor jullie luisterend oor en steun!

Verder wil ik ook nog mijn vrienden bedanken, en daarnaast mag mijn familie zeker niet ontbreken in dit dankwoord. Het is fijn om te weten dat ik altijd op jullie kan rekenen, bedankt daarvoor!

Als laatste wil ik de twee belangrijkste mensen in mijn leven bedanken. Pa, moemske, jullie hebben mij gevormd tot de persoon die ik nu ben. Heel mijn leven heb ik van jullie alle vrijheid gehad om mijn eigen weg te bepalen en hebben jullie altijd voor de volledige honderd procent achter mij gestaan. Ik ben dankbaar dat jullie mij te allen tijde een veilige thuishaven bieden. Dit gegeven is voor vele zaken, waaronder dit proefschrift, onmisbaar.

List of publications

Peer-reviewed journal articles

- S.J.L.M. van Loon, B.G.B. Hunnekens, A.S. Simon, N. van de Wouw, W.P.M.H. Heemels, *Bandwidth-on-demand motion control: A nano-positioning application*, submitted for publication in IEEE Control Systems Technology, 2015, under review
- S.J.L.M. van Loon, B.G.B. Hunnekens, W.P.M.H. Heemels, N. van de Wouw, H. Nijmeijer, *Transient performance improvement of linear systems using a split-path nonlinear integrator*, accepted for publication in Automatica, 2015
- N.W. Bauer, S.J.L.M. van Loon, N. van de Wouw, W.P.M.H. Heemels, *Exploring the boundaries of robust stability under uncertain communication: An NCS toolbox applied to a wireless control setup*, IEEE Control Systems Magazine, vol. 34(4), pp. 65-86, 2014
- S.J.L.M. van Loon, M.C.F. Donkers, N. van de Wouw, W.P.M.H. Heemels, *Stability analysis of networked and quantized linear control systems*, Nonlinear Analysis: Hybrid Systems, vol. 10(C), pp. 111-125, 2013

Peer-reviewed articles in conference proceedings

- S.J.L.M. van Loon, R. van der Weijst, M.F. Heertjes, W.P.M.H. Heemels, *Scheduled controller design for systems with two switching sensor configurations: A frequency-domain approach*, Proceedings of the 5th IFAC Conference on Analysis and Design of Hybrid Systems (ADHS), pp. 99-104, 14-16 October 2015, Atlanta, Georgia, USA
- M.F. Heertjes, K.G.J. Gruntjens, S.J.L.M. van Loon, N. Kontaras, W.P.M.H. Heemels, *Design of a variable gain integrator with reset*, Proceedings of the 2015 American Control Conference (ACC 2015), pp. 2155-2160, 1-3 July 2015, Chicago, Illinois, USA

- S.J.L.M. van Loon, W.P.M.H. Heemels, A.R. Teel, *Improved $\mathcal{L}_2$-gain analysis for a class of hybrid systems with applications to reset and event-triggered control*, Proceedings of the 53rd IEEE Conference on Decision and Control (CDC 2014), pp. 1221-1226, 15-17 December 2014, Los Angeles, California, USA
- B.G.B. Hunnekens, S.J.L.M. van Loon, N. van de Wouw, W.P.M.H. Heemels, H. Nijmeijer, *Analyzing the non-smooth dynamics induced by a split-path nonlinear integral controller*, Proceedings of the 8th European Nonlinear Dynamics Conference (ENOC 2014), 6-11 July 2014, Vienna, Austria
- S.J.L.M. van Loon, B.G.B. Hunnekens, W.P.M.H. Heemels, N. van de Wouw, H. Nijmeijer, *Transient performance improvement of linear systems using a split-path nonlinear integrator*, Proceedings of the 2014 American Control Conference (ACC 2014), pp. 341-346, 4-6 June 2014, Portland, USA
- N.W. Bauer, S.J.L.M. van Loon, M.C.F. Donkers, N. van de Wouw, W.P.M.H. Heemels, *Networked control systems toolbox: Robust stability analysis made easy*, Proceedings of the 3rd IFAC Workshop on Distributed Estimation and Control in Networked Systems (NECSYS), pp. 55-60, 14-15 September 2012, Santa Barbara, USA
- S.J.L.M. van Loon, M.C.F. Donkers, N. van de Wouw, W.P.M.H. Heemels, *Stability analysis of networked control systems with periodic protocols and uniform quantizers*, Proceedings of the 4th IFAC Conference on Analysis and Design of Hybrid Systems (ADHS), pp. 186-191, 6-8 June 2012, Eindhoven, The Netherlands
- D.J. Rijlaarsdam, S.J.L.M. van Loon, P.W.J.M. Nuij, M. Steinbuch, *Nonlinearities in industrial motion stages - detection and classification*, Proceedings of the American Control Conference (ACC), pp. 186-191, June 30 - July 2, 2010, Baltimore, USA

Journal articles in preparation

- R. van der Weijst, S.J.L.M. van Loon, M.F. Heertjes, W.P.M.H. Heemels, *Scheduled controller design for systems with varying sensor configurations: A frequency-domain approach*
- M.F. Heertjes, K.G.J. Gruntjens, S.J.L.M. van Loon, N. van de Wouw, W.P.M.H. Heemels, *Stability and performance of a switching integral control design with reset*
- S.J.L.M. van Loon, K.G.J. Gruntjens, M.F. Heertjes, N. van de Wouw, W.P.M.H. Heemels, *Frequency-domain tools for stability analysis of reset control systems*

Curriculum vitae

Bas van Loon was born on September 19, 1983 in Tilburg, the Netherlands. In 2002 he finished his secondary education at the St. Odulphus Lyceum in Tilburg. Subsequently, he received his Bachelor's degree in Automotive Engineering from the HAN University in Arnhem, the Netherlands, in 2006, and his Master's degree in Mechanical Engineering from the Eindhoven University of Technology, in 2011. His master's thesis was entitled "Stability analysis of networked and quantized control systems: Theory and matlab implementation" and was carried out under the supervision of Tijs Donkers, Nathan van de Wouw and Maurice Heemels.

Since October 2011, Bas has been working as a Ph.D. student in the Control Systems Technology Group of Maurice Heemels, at the Eindhoven University of Technology. The research is part of the STW project "HyPerMotion: Hybrid control for performance improvement of linear motion systems", a joint project together with the Dynamics and Control Group, in cooperation with Bram Hunnekens, Nathan van de Wouw and Henk Nijmeijer, and in cooperation with various industrial partners. Extensive collaboration with project partner Bram Hunnekens, and several industrial partners, was undertaken throughout the project.

The research focus of the HyPerMotion project is on the design and tuning of hybrid controllers for linear motions systems, with the goal to improve the performance of these systems. The main results of this research are presented in this thesis.